



National Library
of Canada

Bibliothèque nationale
du Canada

Canadian Theses Service

Service des thèses canadiennes

Ottawa, Canada
K1A 0N4

NOTICE

The quality of this microform is heavily dependent upon the quality of the original thesis submitted for microfilming. Every effort has been made to ensure the highest quality of reproduction possible.

If pages are missing, contact the university which granted the degree.

Some pages may have indistinct print especially if the original pages were typed with a poor typewriter ribbon or if the university sent us an inferior photocopy.

Reproduction in full or in part of this microform is governed by the Canadian Copyright Act, R.S.C. 1970, c. C-30, and subsequent amendments.

AVIS

La qualité de cette microforme dépend grandement de la qualité de la thèse soumise au microfilmage. Nous avons tout fait pour assurer une qualité supérieure de reproduction.

S'il manque des pages, veuillez communiquer avec l'université qui a conféré le grade.

La qualité d'impression de certaines pages peut laisser à désirer, surtout si les pages originales ont été dactylographiées à l'aide d'un ruban usé ou si l'université nous a fait parvenir une photocopie de qualité inférieure.

La reproduction, même partielle, de cette microforme est soumise à la Loi canadienne sur le droit d'auteur, SRC 1970, c. C-30, et ses amendements subséquents.

UNIVERSITY OF ALBERTA

PERFORMANCE OF GEOGRID REINFORCED CLAY SLOPES

BY

LIU YIXIN



**A thesis submitted to the Faculty of Graduate Studies and Research
in partial fulfillment of the requirements for
the degree of Doctor of Philosophy**

DEPARTMENT OF CIVIL ENGINEERING

Edmonton, Alberta

Spring 1992



National Library
of Canada

Bibliothèque nationale
du Canada

Canadian Theses Service Service des thèses canadiennes

Ottawa, Canada
K1A 0N4

The author has granted an irrevocable non-exclusive licence allowing the National Library of Canada to reproduce, loan, distribute or sell copies of his/her thesis by any means and in any form or format, making this thesis available to interested persons.

The author retains ownership of the copyright in his/her thesis. Neither the thesis nor substantial extracts from it may be printed or otherwise reproduced without his/her permission.

L'auteur a accordé une licence irrévocable et non exclusive permettant à la Bibliothèque nationale du Canada de reproduire, prêter, distribuer ou vendre des copies de sa thèse de quelque manière et sous quelque forme que ce soit pour mettre des exemplaires de cette thèse à la disposition des personnes intéressées.

L'auteur conserve la propriété du droit d'auteur qui protège sa thèse. Ni la thèse ni des extraits substantiels de celle-ci ne doivent être imprimés ou autrement reproduits sans son autorisation.

ISBN 0-315-73259-8

UNIVERSITY OF ALBERTA

RELEASE FORM

NAME OF AUTHOR: Liu Yixin

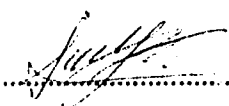
TITLE OF THESIS: Performance of Geogrid Reinforced Clay Slopes

DEGREE: Doctor of Philosophy

YEAR THIS DEGREE GRANTED: Spring 1992

Permission is hereby granted to the University of Alberta Library to reproduce single copies of this thesis and to lend or sell such copies for private, scholarly or scientific research purposes only.

The author reserves all other publication and other rights in association with the copyright in the thesis, and except as hereinbefore provided neither the thesis nor any substantial portion thereof may be printed or otherwise reproduced in any material form whatever without the author's prior written permission.

(SIGNED) 

PERMANENT ADDRESS:

7414 - 111 Street

Edmonton, Alberta

T6G 1H1

DATE April 24, 1992

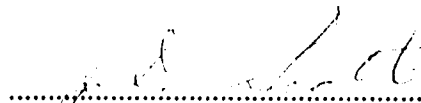
UNIVERSITY OF ALBERTA

FACULTY OF GRADUATE STUDIES AND RESEARCH

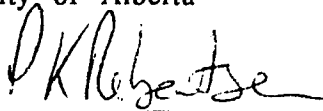
The undersigned certify that they have read, and recommend to the Faculty of Graduate Studies and Research for acceptance, a thesis entitled **Performance of Geogrid Reinforced Clay Slopes** submitted by **Liu Yixin** in partial fulfillment of the requirements for the degree of Doctor of Philosophy in Geotechnical Engineering.



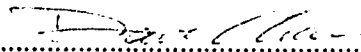
.....
Dr. D.C. Sego, Professor, Chairman
Department of Civil Engineering
University of Alberta



.....
Dr. J.D. Scott, Professor, Supervisor
Department of Civil Engineering
University of Alberta



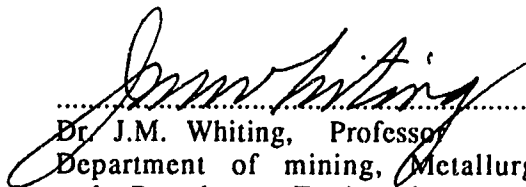
.....
Dr. P.K. Robertson, Professor
Department of Civil Engineering
University of Alberta



.....
Dr. D.H.K. Chan, Associate Professor
Department of Civil Engineering
University of Alberta



.....
Mr. K.O. Anderson, Professor
Department of Civil Engineering
University of Alberta



.....
Dr. J.M. Whiting, Professor
Department of mining, Metallurgical
and Petroleum Engineering
University of Alberta



.....
Dr. R.J. Fannin, Assistant Professor
Department of Civil Engineering
The University of British Columbia

Date..... April 3, 1992.....

To my mother, with love and respect

ABSTRACT

Slope reinforcement using geosynthetics is a relatively new technology in geotechnical engineering. Most of the research work in the literature is focused on reinforced slopes constructed with granular materials. To achieve a better understanding of the reinforcement mechanism of cohesive soil slopes and to provide guidelines for design and construction of reinforced cohesive soil slopes, a test fill was built near Devon, Alberta.

The test fill, 12 m high with 1:1 side slopes, was constructed in three stages. There are four sections in the test fill. Three sections were reinforced with different geogrid materials, namely Tensar SR2, Signode TNX5001 and Paragrid 50S, and the fourth section was unreinforced for the purpose of comparison. The test fill was monitored using extensive field instrumentation, including electrical wire resistance strain gauges, inductance coils, horizontal and vertical extensometers and inclinometers, and piezometers. Field measurements were taken during and after the fill construction and were interpreted as tensile strains in the geogrids, horizontal and vertical deformations of the fill and the foundation soils and pore pressures in the fill and the foundation soils.

Stability analyses of the reinforced slopes were conducted using limit equilibrium methods. The modified Bishop's method, modified Spencer's method and the two-part wedge method were used. Calculated factors of safety and predicted failure surfaces were compared with the field measurements and observations. It was concluded that the failure modes of reinforced cohesive soil slopes are rotational shear surfaces and that the modified Bishop's method is the most appropriate method for stability analysis in practice.

Based on the field measurements, the reinforcement mechanisms of cohesive soil slopes were analyzed in aspects of horizontal and vertical load transfer. It was found that the geogrids stabilize the soil by allowing horizontal load transfer from overstressed zones to understressed zones of soil and by reducing the vertical transfer of horizontal loads from the soil above a reinforcement layer to the soil below the layer. The interaction between the soil and the geogrids in both the resistant and active zones was also analyzed.

Implications of the analyses and recommendations on design methods are discussed as the practical significance of the research.

ACKNOWLEDGEMENTS

The research project on the Devon Test Fill was funded by Alberta Transportation and Utilities. The assistance from the Geotechnical Section and the Research and Development Branch and District 7 of Alberta Transportation and Utilities are appreciated.

This research was conducted under the supervision of Dr. J.D. Scott and Dr. D.C. Sego. I would like to thank them for their most valuable guidance and support during the past few years.

R.J. Chalaturnyk helped to prepare the initial proposal for this research project. B.A. Hofmann assisted in developing the design of the test fill and supervised the fill construction in 1986. The author started this research in May 1989 when the fill construction had been completed. Field readings after this date were taken by the author. The contributions made by Chalaturnyk and Hofmann, and by other fellow students who worked on this project, are sincerely appreciated.

I wish to acknowledge the technical assistance from Gerry Cyre and other technologists in the Department of Civil Engineering, University of Alberta, during the field instrumentation.

A special appreciation to my wife, Ting. Her love, patience and continuous support made the academic learning easier and the life more enjoyable to me.

I would also like to thank my best friends, the Brooks family, for their understanding and encouragement.

To my mother, I dedicate this thesis. Without her love and encouragement for a further education, my achievement so far would not have been possible.

Table of Contents

Chapter	Page
1. Introduction	1
1.1 General.....	1
1.2 Objectives of Thesis.....	3
1.3 Scope and Organization.....	4
2. Literature Review.....	6
2.1 Introduction.....	6
2.2 Properties of Reinforced Soils.....	6
2.2.1 Stress-Strain Behavior of Reinforced Soils.....	6
2.2.2 Interfacial Properties between Soil and Reinforcement.....	9
2.3 Soil Reinforcement Using Geosynthetics.....	12
2.4 Limit Equilibrium Analysis and Design Method on Reinforced Slopes.....	15
2.4.1 Failure Modes and General Design Methodology of Reinforced Slopes.....	16
2.4.2 Factor of Safety.....	18
2.4.3 Soil and Reinforcement Properties and Strain Compatibility....	21
2.4.4 Limit Equilibrium Stability Analysis Methods.....	24
2.5 Finite Element Analysis on Reinforced Slopes.....	32
2.6 Full Scale Tests on Reinforced Slopes.....	37
2.7 Summary.....	51
2.7.1 Soil Reinforcement Mechanisms.....	52
2.7.2 Properties of Soil and Reinforcement and Interaction.....	52
2.7.3 Limit Equilibrium Analyses and Factor of Safety.....	52
2.7.4 Performance of Full Scale Model Reinforced Slopes.....	54
3. Devon Geogrid Test Fill.....	56
3.1 Introduction.....	56
3.2 Properties of Soils.....	56
3.2.1 Properties of Foundation Soils.....	57
3.2.2 Properties of Fill Soil.....	59
3.3 Properties of Geogrids.....	63
3.4 Interaction between Soil and Geogrid.....	64
3.4.1 Direct Shear Tests.....	65
3.4.2 Pullout Tests.....	70
3.5 Construction of Test Fill.....	77

3.6	Instrumentation of Test Fill.....	80
3.6.1	Electrical Wire Resistance (EWR) Strain Gauges.....	81
3.6.2	Inductance Co's.....	82
3.6.3	Inclinometers.....	83
3.6.4	Magnetic Extensometers.....	84
3.6.5	Piezometers.....	85
4.	Interpretation of Field Measurements.....	105
4.1	Introduction.....	105
4.2	Strains in Longitudinal Members of Geogrids.....	105
4.2.1	Tensar Bottom Layer.....	106
4.2.2	Tensar Middle Layer.....	109
4.2.3	Tensar Top Layer.....	110
4.2.4	Signode Bottom Layer.....	111
4.2.5	Signode Middle Layer.....	112
4.2.6	Signode Top Layer.....	113
4.2.7	Paragrid Bottom Layer.....	114
4.2.8	Paragrid Middle Layer.....	114
4.2.9	Paragrid Top Layer.....	115
4.3	Strain between Adjacent Transverse Members of Geogrids.....	116
4.3.1	Tensar Bottom Layer.....	116
4.3.2	Tensar Middle Layer.....	118
4.3.3	Tensar Top Layer.....	120
4.3.4	Signode Bottom Layer.....	120
4.3.5	Signode Middle Layer.....	121
4.3.6	Signode Top Layer.....	122
4.3.7	Paragrid Bottom Layer.....	123
4.3.8	Paragrid Middle Layer.....	124
4.3.9	Paragrid Top Layer.....	125
4.4	Horizontal Movement of Fill and Foundation Soils.....	125
4.4.1	0 m Level in Tensar Section.....	127
4.4.2	2 m Level in Tensar Section.....	128
4.4.3	4 m Level in Tensar Section.....	129
4.4.4	6 m Level in Tensar Section.....	130
4.4.5	Vertical Alignment beneath Toe in Tensar Section.....	130
4.4.6	Vertical Alignment beneath Crest in Tensar Section.....	131
4.4.7	0 m Level in Signode Section.....	132
4.4.8	2 m Level in Signode Section.....	133
4.4.9	4 m Level in Signode Section.....	134
4.4.10	6 m Level in Signode Section.....	134
4.4.11	Vertical Alignment beneath Toe in Signode Section.....	135
4.4.12	Vertical Alignment beneath Crest in Signode Section.....	136
4.4.13	0 m Level in Paragrid Section.....	136
4.4.14	2 m Level in Paragrid Section.....	137
4.4.15	4 m Level in Paragrid Section.....	138
4.4.16	6 m Level in Paragrid Section.....	138
4.4.17	Vertical Alignment beneath Toe in Paragrid Section.....	138
4.4.18	Vertical Alignment beneath Crest in Paragrid Section.....	139

4.4.19	0 m Level in Unreinforced Section.....	140
4.4.20	2 m Level in Unreinforced Section.....	140
4.4.21	4 m Level in Unreinforced Section.....	141
4.4.22	6 m Level in Unreinforced Section.....	141
4.4.23	Vertical Alignment beneath Toe in Unreinforced Section.....	142
4.4.24	Vertical Alignment beneath Crest in Unreinforced Section...	142
4.5	Vertical Movement of Fill and Foundation Soils.....	143
4.5.1	0 m Level in Tensar Section.....	146
4.5.2	2 m Level in Tensar Section.....	147
4.5.3	4 m Level in Tensar Section.....	147
4.5.4	6 m Level in Tensar Section.....	148
4.5.5	Vertical Alignment beneath Crest in Tensar Section.....	149
4.5.6	Vertical Alignment beneath Toe in Tensar Section.....	150
4.5.7	0 m Level in Signode Section.....	150
4.5.8	2 m Level in Signode Section.....	151
4.5.9	4 m Level in Signode Section.....	152
4.5.10	6 m Level in Signode Section.....	152
4.5.11	Vertical Alignment beneath Crest in Signode Section.....	153
4.5.12	Vertical Alignment beneath Toe in Signode Section.....	154
4.5.13	0 m Level in Paragrid Section.....	154
4.5.14	2 m Level in Paragrid Section.....	155
4.5.15	4 m Level in Paragrid Section.....	155
4.5.16	6 m Level in Paragrid Section.....	156
4.5.17	Vertical Alignment beneath Crest in Paragrid Section.....	156
4.5.18	Vertical Alignment beneath Toe in Paragrid Section.....	157
4.5.19	0 m Level in Unreinforced Section.....	157
4.5.20	2 m Level in Unreinforced Section.....	158
4.5.21	4 m Level in Unreinforced Section.....	159
4.5.22	6 m Level in Unreinforced Section.....	159
4.5.23	Vertical Alignment beneath Crest in Unreinforced Section...	160
4.5.24	Vertical Alignment beneath Toe in Unreinforced Section.....	160
4.6	Pore Pressures.....	160
4.6.1	Fill Soil in Tensar Section.....	161
4.6.2	Foundation Soils in Tensar Section.....	162
4.6.3	Signode Section.....	162
4.6.4	Paragrid Section.....	163
4.6.5	Unreinforced Section.....	163
5.	Summary of Field Measurements.....	215
5.1	Introduction.....	215
5.2	Strains in Geogrids.....	215
5.2.1	Strains in Tensar Geogrid.....	216
5.2.2	Strains in Signode Geogrid.....	216
5.2.3	Strains in Paragrid Geogrid.....	217
5.2.4	Comparison of Strains in Geogrids.....	218
5.3	Horizontal Movements of Soils.....	219
5.3.1	Movements of Fill Soil.....	219
5.3.2	Movements of Foundation Soils.....	221

5.4	Vertical Movements of Soils.....	222
5.5	Pore Pressures.....	224
6.	Limit Equilibrium Analyses.....	239
6.1	Introduction.....	239
6.2	Bishop's Modified Methods.....	242
6.2.1	Introduction.....	242
6.2.2	Incorporation of Reinforcement Forces.....	243
6.2.3	Results of Stability Analyses by Bishop's Modified Method.....	245
6.3	Spencer's Modified Method.....	249
6.3.1	Formulation.....	249
6.3.2	Results of Stability Analyses by Spencer's Modified Method...	250
6.4	Two-Part Wedge Method.....	252
6.4.1	Formulation.....	252
6.4.2	Uncertainties in Two-Part Wedge Method.....	254
6.4.3	Results of Two-Part Wedge Analysis.....	254
6.5	Summary and Discussion on Results of Limit Equilibrium Analyses.....	259
7.	Analyses of Field Measurements.....	289
7.1	Introduction.....	289
7.2	Failure Modes of Reinforced Slopes.....	289
7.3	Deformation within Slopes.....	293
7.4	Reinforcement Mechanisms.....	298
7.4.1	Horizontal Load Transfer.....	298
7.4.2	Vertical Load Transfer.....	300
7.5	Interaction between Soil and Geogrid and Strain Compatibility.....	304
7.5.1	Interaction Mechanism.....	304
7.5.2	Strain Compatibility and Reinforcement Force Mobilization....	306
7.6	Summary.....	313
8.	Implication and Recommendations to Design Methods.....	327
8.1	Introduction.....	327
8.2	General Procedures in Design of Reinforced Slopes.....	327
8.3	External Loads and Pore Water Pressures.....	330
8.4	Properties of Fill.....	331
8.5	Performance Requirements of Reinforcement and Factors of Safety.....	332

8.6	Failure Modes and Methods of Internal Stability Analysis.....	333
8.7	Number and Layout of Reinforcement Layers.....	334
8.8	Reinforcement Force Incorporation.....	335
8.9	Pullout and Interfacial Shear Resistance.....	336
8.10	External Stability.....	337
8.11	Secondary Reinforcement, Drainage and Surface Control.....	338
9.	Summary and Conclusions.....	340
9.1	General.....	340
9.2	Summary of Field Measurements.....	341
9.3	Conclusions.....	343
9.3.1	Stability Analyses.....	343
9.3.2	Reinforcement Mechanisms and Deformation Characteristics.....	345
9.4	Recommendations for Future Studies.....	346
	REFERENCES.....	348
	Appendix A. Additional Figures for Devon Test Fill.....	358
	Appendix B. Description and Source Code of RSSABM.....	372
	Appendix C. Description and Source Code of RSSASM.....	381
	Appendix D. Description and Source Code of RSSAWM.....	393

List of Tables

Table	Page
3.1 Results of Consolidation Tests on Upper Foundation Soil (from Hofmann, 1989).....	87
3.2 Summary of CU Test Results on Upper Foundation Soil (from Hofmann, 1989).....	87
3.3 Atterberg Limits and Grain Size Distribution of Fill Soil (from Hofmann, 1989).....	88
3.4 Comparison of UU Triaxial Test Results on Shelby Tube Samples of Fill Soil (from Hofmann, 1989).....	88
3.5 Summary of CU Triaxial Test Results on Fill Soil (from Hofmann, 1989).....	89
3.6 Physical Properties of Geogrids (from Bobey, 1988).....	90
3.7 Values of Interfacial Stress Factor from Direct Shear Tests (from Costalonga, 1988).....	90
3.8 Summary of Pullout Test Results (modified from Costalonga, 1988).....	91
3.9 Parameters and Some Results of Load Transfer Analyses on Pullout Tests (modified from Costalonga, 1988).....	92
4.1 Summary of Field Measurements.....	164
5.1 Summary of Peak Strains in Geogrids.....	226
5.2 Summary of Peak Horizontal Strains in Fill Soil.....	227
5.3 Summary of Localized Vertical Displacements in Fill Soil.....	228
6.1 Soil Properties in Devon Test Fill.....	263
6.2 Factor of Safety of Model Slope (Unreinforced) from BMM.....	263
6.3 Factor of Safety of Model Slope (Reinforced) from BMM.....	264
6.4 Factor of Safety of Slopes in Test Fill (Unreinforced) from BMM.....	265
6.5 Results of Stability Analysis in Tensar Reinforced Slope from BMM..	266
6.6 Results of Stability Analysis in Signode Reinforced Slope from BMM.	267
6.7 Results of Stability Analysis in Paragrid Reinforced Slope from BMM	268
6.8 Effect of Cohesion on Factor of Safety of Slopes in Test Fill (BMM).....	269
6.9 Factor of Safety of Model Slope from SMM.....	269
6.10 Results of Stability Analysis in Tensar Reinforced Slope from SMM...	270
6.11 Results of Stability Analysis in Signode Reinforced Slope from SMM.	271
6.12 Results of Stability Analysis in Paragrid Reinforced Slope from SMM	272
6.13 Factor of Safety of Model Slope from Wedge Method for $C_b=0$	273
6.14 Factor of Safety of Model Slope from Wedge Method for $C_b=C'/2F_s$	274
6.15 Factor of Safety of Model Slope from Wedge Method for $C_b=C'/F_s$	275

6.16	Factor of Safety of Tensar Reinforced Slope from Wedge Method.....	276
6.17	Factor of Safety of Signode Reinforced Slope from Wedge Method.....	277
6.18	Factor of Safety of Paragrid Reinforced Slope from Wedge Method....	278
6.19	Results of Stability Analysis in Reinforced Slopes of Devon Test Fill from Wedge Method.....	279
6.20	Summary of Factor of Safety of Model Slope from BMM, SMM and Wedge Method.....	280
6.21	Summary of Factor of Safety of Slopes in Devon Test Fill from BMM, SMM and Wedge Method.....	281
7.1	Maximum Tensile Force and Equivalent Pullout Displacement in Resistant Zone.....	316
7.2	Summary of Undrained Pullout Analyses in Resistant Zones.....	316
7.3	Summary of Drained Pullout Analyses in Resistant Zones.....	317

List of Figures

Figure	Page
3.1 Plan View of Devon Test Fill.....	93
3.2 Cross Section and Geogrid Layout of Reinforced Slope.....	94
3.3 Typical Borehole Log of Foundation Soils.....	94
3.4 Grain Size Distribution of Fill Soil (modified from Hofmann, 1989)....	94
3.5 Compaction Curve of Fill Soil (modified from Bobey, 1988).....	94
3.6 Variation of Undrained Shear Strength versus Water Content of Fill Soil (modified from Hofmann, 1989).....	96
3.7 Results of Wide Strip Tensile Tests on Geogrids (from Scott et al., 1988).....	96
3.8 Direct Shear Box Apparatus (modified from Bobey, 1988).....	97
3.9 Strength Envelopes from Direct Shear Tests (modified from Bobey, 1988).....	97
3.10 Efficiency of Interfacial Shear Resistance (modified from Bobey, 1988).....	98
3.11 Typical Configuration and Basic Mechanisms of Pullout Tests.....	98
3.12 Pullout Curves of Tensar SR2 Grid (modified from Costalonga, 1988)...	98
3.13 Pullout Curves of Signode TNX5001 Grid (modified from Costalonga, 1988).....	98
3.14 Progressive Displacements versus Pullout Displacements for Tensar SR2 Grid (modified from Costalonga, 1988).....	100
3.15 Progressive Displacements versus Pullout Displacements for Signode TNX5001 Grid (modified from Costalonga, 1988).....	100
3.16 Progressive Displacements versus Pullout Forces for Tensar SR2 Grid (modified from Costalonga, 1988).....	101
3.17 Progressive Displacements versus Pullout Forces for Signode TNX5001 Grid (modified from Costalonga, 1988).....	101
3.18 Construction Schedule of Devon Test Fill.....	102
3.19 Layout of Soil Instrumentation in Devon Test Fill.....	102
3.20 Layout of Geogrid Instrumentation in Devon Test Fill.....	103
3.21 Calibration Curve of Inductance Coils (range 2).....	103
3.22 Calibration Curve of Inductance Coils (range 3).....	104
4.1 EWR Gauge Measurements in 5 m location in Tensar Bottom Layer...	165
4.2 Strain (EWR) in Tensar Bottom Layer (before adjustment).....	165
4.3 Strain Distribution (EWR) in Tensar Bottom Layer.....	166
4.4 Strain Development (EWR) in Tensar Bottom Layer.....	166
4.5 Strain Distribution (EWR) in Tensar Middle Layer.....	167

4.6	Strain Development (EWR) in Tensar Middle Layer.....	167
4.7	Strain Distribution (EWR) in Tensar Top Layer.....	168
4.8	Strain Development (EWR) in Tensar Top Layer.....	168
4.9	Strain Distribution (EWR) in Signode Bottom Layer.....	169
4.10	Strain Distribution (EWR) in Signode Middle Layer.....	169
4.11	Strain Distribution (EWR) in Signode Top Layer.....	170
4.12	Strain Distribution (EWR) in Paragrid Bottom Layer.....	170
4.13	Strain Distribution (EWR) in Paragrid Middle Layer.....	171
4.14	Strain Distribution (EWR) in Paragrid Top Layer.....	171
4.15	Strain Distribution (coil) in Tensar Bottom Layer.....	172
4.16	Strain Development (coil) in Tensar Bottom Layer.....	172
4.17	Strain Distribution (Coil) in Tensar Middle Layer.....	173
4.18	Strain Development (Coil) in Tensar Middle Layer.....	173
4.19	Strain Distribution (Coil) in Tensar Top Layer.....	174
4.20	Strain Development (Coil) in Tensar Top Layer.....	174
4.21	Strain Distribution (Coil) in Signode Bottom Layer.....	175
4.22	Strain Distribution (Coil) in Signode Middle Layer.....	175
4.23	Strain Distribution (Coil) in Signode Top Layer.....	176
4.24	Strain Distribution (Coil) in Paragrid Bottom Layer.....	176
4.25	Strain Distribution (Coil) in Paragrid Middle Layer.....	177
4.26	Strain Distribution (Coil) in Paragrid Top Layer.....	177
4.27	Distribution of Horizontal Strain of Soil at 0 m Level in Tensar Section.....	178
4.28	Development of Horizontal Strain of Soil at 0 m Level in Tensar Section.....	178
4.29	Distribution of Horizontal Strain of Soil at 2 m Level in Tensar Section.....	179
4.30	Development of Horizontal Strain of Soil at 2 m Level in Tensar Section.....	170
4.31	Distribution of Horizontal Strain of Soil at 4 m Level in Tensar Section.....	180
4.32	Horizontal Deflection (A) of Soils beneath Toe of Slope in Tensar Section.....	180
4.33	Horizontal Deflection (B) of Soils beneath Toe of Slope in Tensar Section.....	181
4.34	Development of Horizontal Deflection (A) of Soils beneath Toe of Slope in Tensar Section.....	181
4.35	Horizontal Deflection (A) of Soils beneath Crest of Slope in Tensar Section.....	182

4.36 Horizontal Deflection (B) of Soils beneath Crest of Slope in Tensar Section.....	182
4.37 Distribution of Horizontal Strain of Soil at 0 m Level in Signode Section.....	183
4.38 Distribution of Horizontal Strain of Soil at 2 m Level in Signode Section.....	183
4.39 Distribution of Horizontal Strain of Soil at 4 m Level in Signode Section.....	184
4.40 Horizontal Deflection (A) of Soils beneath Toe of Slope in Signode Section.....	184
4.41 Horizontal Deflection (B) of Soils beneath Toe of Slope in Signode Section.....	185
4.42 Horizontal Deflection (A) of Soils beneath Crest of Slope in Signode Section (before adjustment).....	185
4.43 Horizontal Deflection (A) of Soils beneath Crest of Slope in Signode Section.....	186
4.44 Horizontal Deflection (B) of Soils beneath Crest of Slope in Signode Section.....	186
4.45 Distribution of Horizontal Strain of Soil at 0 m Level in Paragrid Section.....	187
4.46 Distribution of Horizontal Strain of Soil at 2 m Level in Paragrid Section.....	187
4.47 Distribution of Horizontal Strain of Soil at 4 m Level in Paragrid Section.....	188
4.48 Horizontal Deflection (A) of Soils beneath Toe of Slope in Paragrid Section.....	188
4.49 Horizontal Deflection (B) of Soils beneath Toe of Slope in Paragrid Section.....	189
4.50 Horizontal Deflection (A) of Soils beneath Crest of Slope in Paragrid Section.....	189
4.51 Horizontal Deflection (B) of Soils beneath Crest of Slope in Paragrid Section.....	190
4.52 Distribution of Horizontal Strain of Soil at 0 m Level in Unreinforced Section.....	190
4.53 Distribution of Horizontal Strain of Soil at 2 m Level in Unreinforced Section.....	191
4.54 Distribution of Horizontal Strain of Soil at 4 m Level in Unreinforced Section.....	191
4.55 Horizontal Deflection (A) of Soils beneath Toe of Slope in Unreinforced Section.....	192
4.56 Horizontal Deflection (B) of Soils beneath Toe of Slope in Unreinforced Section.....	192
4.57 Horizontal Deflection (A) of Soils beneath Crest of Slope	

in Unreinforced Section.....	193
4.58 Horizontal Deflection (B) of Soils beneath Crest of Slope in Unreinforced Section.....	193
4.59 Settlement at Ground Level in Tensar Section.....	194
4.60 Development of Settlement at Ground Level in Tensar Section.....	194
4.61 Settlement at 2 m Level in Tensar Section.....	195
4.62 Development of Settlement at 2 m Level in Tensar Section.....	195
4.63 Settlement at 4 m Level in Tensar Section.....	196
4.64 Development of Settlement at 4 m Level in Tensar Section.....	196
4.65 Vertical Deflection at 6 m Level in Tensar Section.....	197
4.66 Settlement beneath Crest of Slope in Tensar Section (before adjustment).....	197
4.67 Settlement beneath Crest of Slope in Tensar Section (after adjustment).....	198
4.68 Development of Settlement beneath Crest of Slope in Tensar Section..	198
4.69 Development of Settlement beneath Toe of Slope in Tensar Section....	199
4.70 Settlement at Ground Level in Signode Section.....	199
4.71 Settlement at 2 m Level in Signode Section.....	200
4.72 Settlement at 4 m Level in Signode Section.....	200
4.73 Vertical Deflection at 6 m Level in Signode Section.....	201
4.74 Settlement beneath Crest of Slope in Signode Section.....	201
4.75 Development of Settlement beneath Toe of Slope in Signode Section...	202
4.76 Settlement at Ground Level in Paragrid Section.....	202
4.77 Settlement at 2 m Level in Paragrid Section.....	203
4.78 Settlement at 4 m Level in Paragrid Section.....	203
4.79 Vertical Deflection at 6 m Level in Paragrid Section.....	204
4.80 Settlement beneath Crest of Slope in Paragrid Section.....	204
4.81 Development of Settlement beneath Toe of Slope in Paragrid Section.	205
4.82 Settlement at Ground Level in Unreinforced Section.....	205
4.83 Settlement at 2 m Level in Unreinforced Section.....	206
4.84 Settlement at 4 m Level in Unreinforced Section.....	206
4.85 Vertical Deflection at 6 m Level in Unreinforced Section.....	207
4.86 Settlement beneath Crest of Slope in Unreinforced Section.....	207
4.87 Development of Settlement beneath Toe of Slope in Unreinforced Section.....	208
4.88 Development of Pore Pressure at 1 m Level in Tensar Section.....	208
4.89 Development of Pore Pressure at 3 m Level in Tensar Section.....	209

4.90 Development of Pore Pressure at 5 m Level in Tensar Section.....	209
4.91 Development of Pore Pressure in Foundation Soil in Tensar Section...	210
4.92 Development of Pore Pressure in Fill Soil in Signode Section.....	210
4.93 Development of Pore Pressure in Foundation Soil in Signode Section.	211
4.94 Development of Pore Pressure in Fill Soil in Paragrid Section.....	211
4.95 Development of Pore Pressure in Fill Soil in Paragrid Section.....	212
4.96 Development of Pore Pressure in Foundation Soil in Paragrid Section	212
4.97 Development of Pore Pressure in Fill Soil in Unreinforced Section....	213
4.98 Development of Pore Pressure in Fill Soil in Unreinforced Section....	213
4.99 Development of Pore Pressure in Foundation Soils in Unreinforced Section.....	214
5.1 Strain Distribution (EWR) in Tensar Geogrid.....	229
5.2 Strain Distribution (coil) in Tensar Geogrid.....	229
5.3 Strain Distribution (EWR) in Signode Geogrid.....	230
5.4 Strain Distribution (coil) in Signode Geogrid.....	230
5.5 Strain Distribution (EWR) in Paragrid Geogrid.....	231
5.6 Strain Distribution (coil) in Paragrid Geogrid.....	231
5.7 Distribution of Horizontal Strain of Fill Soil in Tensar Section.....	232
5.8 Distribution of Horizontal Strain of Fill Soil in Signode Section.....	232
5.9 Distribution of Horizontal Strain of Fill Soil in Paragrid Section.....	233
5.10 Distribution of Horizontal Strain of Fill Soil in Unreinforced Section.	233
5.11 Settlement in Tensar Section.....	234
5.12 Settlement in Signode Section.....	234
5.13 Settlement in Paragrid Section.....	235
5.14 Settlement in Unreinforced Section.....	235
5.15 Pore Pressure and Pore Pressure Ratio in Fill Soil at End of 1987 Construction Season.....	236
5.16 Pore Pressure and Pore Pressure Ratio in Fill Soil at End of 1988 Construction Season.....	237
5.17 Pore Pressure and Pore Pressure Ratio in Fill Soil One Year after Completion of Test Embankment.....	238
6.1 Coordinates, Soil Profile and Reinforcement Layout of Slopes in Devon Test Fill.....	282
6.2 Forces Acting on An Individual Slice in BMM.....	282
6.3 Forces Acting on An Individual Slice in SMM.....	283
6.4 Forces Acting on the Two-part Wedge.....	284
6.5 Variation of Factor of Safety against Interwedge Force Inclination in Model Slope (unreinforced).....	285

6.6	Variation of Factor of Safety against Interwedge Force Inclination in Model Slope (horizontal reinforcement forces).....	285
6.7	Variation of Factor of Safety against Pore Pressure Ratio in Unreinforced Section in Test Fill.....	286
6.8	Variation of Factor of Safety against Interwedge Force Inclination in Slopes (unreinforced) in Test Fill.....	286
6.9	Variation of Factor of Safety against Interwedge Force Inclination in Tensar Reinforced Slope (1988, $r_u=0.29$).....	287
6.10	Variation of Factor of Safety against Interwedge Force Inclination in Paragrid Reinforced Slope (measured forces).....	287
6.11	Variation of Factor of Safety against Interwedge Force Inclination in Signode Reinforced Slope (1989, $r_u=0.2$).....	288
7.1	Failure Mechanism in Unreinforced Slope.....	318
7.2	Failure Mechanism in Tensar Reinforced Slope.....	319
7.3	Failure Mechanism in Signode Reinforced Slope.....	320
7.4	Failure Mechanism in Paragrid Reinforced Slope.....	321
7.5	Increment of Settlement at 2 m Level from November 1986 to November 1987.....	322
7.6	Increment of Settlement at 2 m Level from November 1987 to May 1989.....	322
7.7	Increment of Settlement at 4 m Level from November 1987 to May 1989.....	323
7.8	Mobilization of Tensile Forces in Reinforcing Layers.....	323
7.9	Horizontal Displacement in Tensar Section in November 1988.....	324
7.10	Horizontal Displacement in Signode Section in November 1988.....	324
7.11	Increment of Horizontal Displacement in Tensar Section from November 1987 to November 1988.....	325
7.12	Increment of Horizontal Displacement in Signode Section from November 1987 to November 1988.....	325
7.13	Relative Displacements between Soil and Geogrid and Interaction Mechanism in Resistant Zone and Active Zone.....	326
7.14	Shear Stress-Displacement Curves from Direct Shear Tests (modified from Bobey, 1988).....	326
8.1	Force Equilibrium in Active Zone.....	339
8.2	Mechanisms of External Instability.....	339
A1	Strain Development (EWR) in Signode Bottom Layer.....	358
A2	Strain Development (EWR) in Signode Middle Layer.....	358
A3	Strain Development (EWR) in Signode Top Layer.....	359
A4	Strain Development (EWR) in Paragrid Bottom Layer.....	359
A5	Strain Development (EWR) in Paragrid Middle Layer.....	360

A6	Strain Development (EWR) in Paragrid Top Layer.....	360
A7	Strain Development (coil) in Signode Bottom Layer.....	361
A8	Strain Development (coil) in Signode Middle Layer.....	361
A9	Strain Development (coil) in Signode Top Layer.....	362
A10	Strain Development (coil) in Paragrid Bottom Layer.....	362
A11	Strain Development (coil) in Paragrid Middle Layer.....	363
A12	Strain Development (coil) in Paragrid Top Layer.....	363
A13	Development of Horizontal Deflection (B) of Soils beneath Toe of Slope in Tensar Section.....	364
A14	Development of Horizontal Strain of Soil at 0 m Level in Signode Section.....	364
A15	Development of Horizontal Strain of Soil at 2 m Level in Signode Section.....	365
A16	Development of Horizontal Strain of Soil at 4 m Level in Signode Section.....	365
A17	Development of Horizontal Deflection (A) of Soils beneath Toe of Slope in Signode Section.....	366
A18	Development of Horizontal Deflection (B) of Soils beneath Toe of Slope in Signode Section.....	366
A19	Development of Horizontal Strain of Soil at 0 m Level in Paragrid Section.....	367
A20	Development of Horizontal Strain of Soil at 2 m Level in Paragrid Section.....	367
A21	Development of Horizontal Strain of Soil at 0 m Level in Unreinforced Section.....	368
A22	Development of Horizontal Strain of Soil at 2 m Level in Unreinforced Section.....	368
A23	Development of Settlement at 0 m Level in Signode Section.....	369
A24	Development of Settlement at 2 m Level in Signode Section.....	369
A25	Development of Settlement at 0 m Level in Paragrid Section.....	370
A26	Development of Settlement at 2 m Level in Paragrid Section.....	370
A27	Development of Settlement at 0 m Level in Unreinforced Section.....	371
A28	Development of Settlement at 2 m Level in Unreinforced Section.....	371

List of Symbols

A_i	cross section area of element i (pullout tests)
A_{pi}	plan area of element i (pullout tests)
C_b	total cohesion along interwedge boundary
C_{b1}	total interwedge boundary cohesion acting on wedge I
C_{b2}	total interwedge boundary cohesion acting on wedge II
E	overall interfacial efficiency
E_ϕ	interfacial frictional efficiency
E_c	interfacial cohesive efficiency
F_i	pullout force at the beginning of element i (pullout tests)
F_s	factor of safety
F_t	target factor of safety
F_u	factor of safety of unreinforced slope
H	height of slope
K_d	design coefficient of earth pressure
L_1	length of slip surface of wedge I
L_2	length of slip surface of wedge II
L_e	effective embedded length of reinforcement
M_d	disturbing moment of soil
M_r	resisting moment of soil
M_t	resisting moment provided by reinforcement
N'	effective normal stress on base of slice
N_1'	effective normal force on base of wedge I
N_2'	effective normal force on base of wedge II
N_c	undrained bearing capacity factor
P	total pullout force or pullout capacity
Q	resultant interslice force
Q_1	interwedge force acting on wedge I
Q_2	interwedge force acting on wedge II
R	radius of potential slip circle
S	shear resistance along base of slice
S_1	shear resistance along base of wedge I
S_2	shear resistance along base of wedge II
S_v	vertical spacing between reinforcement layers
S_x	space between two consecutive anchor members

T	tensile reinforcement force at base of slice
T_{1h}	horizontal component of total reinforcement force at base of wedge I
T_{2h}	horizontal component of total reinforcement force at base of wedge II
T_{1v}	vertical component of total reinforcement force at base of wedge I
T_{2v}	vertical component of total reinforcement force at base of wedge II
U_1	total pore water pressure at base of wedge I
U_2	total pore water pressure at base of wedge II
U_{b1}	total pore water pressure acting on boundary of wedge I
U_{b2}	total pore water pressure acting on boundary of wedge II
W_1	weight of wedge I
W_2	weight of wedge II
X_i	displacement of element i (pullout tests)
W	weight of slice
a	area of solid (members) in a unit area of geogrid material
a_b	fraction of geogrid width over which bearing surface extends
b	width of reinforcement
b	width of slice
c'	effective cohesion of soil
c_G	Interfacial adhesion between soil and solid geogrid material
c_T	total cohesion or adhesion along interface
c_u	undrained cohesion of soil
c_1'	average cohesion along base of wedge I
c_2'	average cohesion along base of wedge II
f^*	coefficient of bond
f_d	mechanical damage factor of reinforcement
f_{env}	environmental deterioration factor of reinforcement
f_m	material uncertainty factor of reinforcement
f_δ	interwedge roughness factor
k	horizontal earth pressure coefficient
r_u	pore pressure ratio
t	thickness of anchor member
z	depth of embedded reinforcement
α	inclination angle at base of slice
α	adhesion factor between soil and solid geogrid material
β	interfacial stress factor
δ	inclination angle of interwedge force

δ_G	interfacial friction angle between soil and solid geogrid material
δ_T	effective overall interfacial friction angle between soil and geogrid
γ	unit weight of soil
ϕ'	effective angle of internal friction of soil
ϕ_u	undrained internal friction angle of soil
ϕ_1'	average internal friction angle along base of wedge I
ϕ_2'	average internal friction angle along base of wedge II
θ	inclination angle of interslice force
θ_1	inclination angle slip surface in wedge I
θ_2	inclination angle slip surface in wedge II
σ_b'	bearing effective stress on anchor members
σ_n'	effective normal stress
τ	shear strength of soil
τ_T	total interfacial shear strength

Chapter 1. Introduction

1.1 General

The concept of earth reinforcement can be traced back to ancient history. The Great Wall in northern China and the Ziguratt near Baghdad are typical and remarkable examples of early reinforced soil structures. The former was completed circa 210 B.C., using tamarisk branches as reinforcement materials; the later, constructed in the period 1595 - 1171 B.C., was built with bricks of clay mixed with straw or dry reed and reinforced with horizontally placed mats woven from river reed. These reinforced soil structures are still standing today.

As a modern method of construction in geotechnical engineering, earth reinforcement has substantially advanced since the 1960's. A great milestone of the new development was the concept of "reinforced earth" developed by Henri Vidal in the 1960's. It refers to a mass of frictional soil which incorporates horizontally placed long, thin metal strips of a constant length. In the past two decades, however, the application of soil reinforcement has been significantly broadened as new geosynthetic materials were developed.

The use of reinforcement typically reduces cost of construction, increases tolerance of the soil structures to ground movement and increases the feasibility of soil structures which are difficult to construct using conventional methods due to poor soil conditions or limited right of way. Various types of reinforcing materials, metal strips or meshes and polymeric materials such as geotextiles and geogrids, have been used and different design methods have been developed for different types of reinforced soil structures.

There are three types of reinforced soil structures in geotechnical engineering: reinforced retaining walls, slopes, and embankments on soft foundations. For a reinforced embankment on a soft foundation, a layer of reinforcement is usually placed at the base of the embankment to carry part of the horizontal load from the embankment and to prevent failure in the foundation. For a reinforced wall or a slope, reinforcement layers are placed within the backfill materials. Other than the geometrical difference, these two types of reinforced soil structures (walls and slopes) can be distinguished

by the tensile force distribution in the reinforcement. For a typical reinforced wall, the reinforcement is attached to rigid facing units and, therefore, the maximum tensile force in the reinforcement occurs at the surface of the wall. For a reinforced slope, the reinforcement is usually unconnected at the face and the tensile force in the reinforcement is zero at the slope surface (Fannin and Hermann, 1990). In addition to these two types of structures, there is another type of reinforced soil structure which has characteristics of both reinforced walls and slopes. In this type of structure, which can be vertical or sloped, the reinforcement is either connected to flexible facing units, such as metal meshes, or wrapped around the compacted backfill. The location of the maximum tensile force in a reinforcement layer depends on the rigidity of the facing units and the horizontal movement of the backfill. When the facing units are not sufficiently tensioned, the maximum tensile force may occur at a distance from the surface of the structure; otherwise, the maximum tensile force may occur at or near the surface.

In the category of reinforced slopes, deformation and stability are the two main concerns. An accurate assessment of deformation in a reinforced slope can be achieved only through a stress-deformation analysis, such as a finite element analysis. Stability of a reinforced slope, on the other hand, can be evaluated using either a limit equilibrium or a stress-deformation analysis. Limit equilibrium methods are still the most common analytical approaches in recent design practices for reinforced slopes. Worldwide case records of reinforced soil structures indicate that the current design methods are conservative (Mitchell, 1987). The conservatism comes from uncertainties in the following:

1. stress-deformation characteristics of reinforced slopes and load distributions within the soil and the reinforcement;
2. failure modes of reinforced slopes and suitable corresponding limit equilibrium methods;
3. reinforcement mechanisms in slopes reinforced with geosynthetics;
4. mobilization of the shear strength in the soil and the definition of the factor of safety in a reinforced slope;

5. mobilization of the tensile strength in the reinforcement and performance criteria of reinforcing materials;
6. reinforcement force orientation and its incorporation in the stability analysis;
7. interaction between the soil and the reinforcement and the strain compatibility;
8. deformation patterns of reinforced soil slopes.

To obtain rational and economical designs of reinforced slopes, a good understanding of the above aspects is required. Well instrumented full scale tests are the most appropriate approaches to fulfil this requirement. In order to achieve a better understanding of the reinforcement mechanism in a geogrid reinforced cohesive soil slope and accumulate experience for both analytical and practical purposes, a test fill, 12 m high with 1:1 side slopes, was built near Devon, Alberta. The test fill has four sections, three reinforced with different types of geogrids and one unreinforced section. Locally available silty clay was used as the fill material and three layers of geogrids at a 2 m vertical spacing were installed in each test section as the primary reinforcement. The reinforced slopes were designed with a low factor of safety in order that sufficient lateral strains in the fill would occur to mobilize the tensile resistance of the geogrids while the overall stability of the slopes would be maintained.

1.2 Objectives of Thesis

The main objectives of this research are to determine how individual geogrid layers reinforce a mass of cohesive soil and to measure the stress transfer from the soil to the geogrids within the fill. The studies have been carried out through the comparison between the strain distribution in the soil and in the reinforcement and the comparison between the strain profiles in the unreinforced slope and in the reinforced slopes. Load distributions, which are associated with strain distributions, within the fill and the reinforcing layers will provide valuable information for design of reinforcement location, spacing and layout.

The secondary objective of the research is to investigate the failure mechanism of reinforced slopes. Limit equilibrium analyses incorporating measured tensile forces in the reinforcement and pore pressures within the fill have been conducted and the predicted failure surfaces compared to the strain localization measured in the soil and the reinforcement. Favorable agreement between the prediction and the field measurements will help to develop confidence in the methods of stability analyses. As well, it will aid in assessing technical details such as the reinforcement force orientation and its incorporation into the stability analysis, the shear strength parameters of the soil, the definition of the overall or partial factors of safety and the estimation of the working tensile force in the reinforcement.

Another objective of this thesis is to document this extensively instrumented case record for the geotechnical engineering literature.

1.3 Scope and Organization of Thesis

Few areas in geotechnical engineering have developed as rapidly as soil reinforcement. The greatly increasing literature on slope reinforcement is summarized in chapter 2. The literature review is organized into aspects of the properties of reinforced soils, soil reinforcement mechanisms, limit equilibrium analyses and design methods, finite element analyses and full scale tests of reinforced slopes.

Chapter 3 gives the background of the research on the Devon test fill. Properties of the fill and the geogrids used in the test embankment and characteristics of the interaction between the soil and the geogrids for both the pullout and direct shear mechanisms are summarized. Details of the fill construction and the instrumentation are also described in this chapter.

Chapter 4 documents the details of field data interpretation, including the measurements from electric wire resistance strain gauges, inductance coils, extensometers, inclinometers and piezometers. The results of the measurements are presented following the construction and consolidation stages of the test fill. Problems associated with the interpretation are also documented. The performance of the test fill is summarized in chapter 5.

Limit equilibrium analyses are carried out on the slopes in the test fill. Bishop's modified method, Spencer's modified method and the two-part wedge method are used and the reinforcement forces are incorporated in several ways in the stability analyses. Details of the stability analyses are described in chapter 6. Chapter 7 presents the analyses of the field measurements. The analyses are carried out to determine the likely failure modes and deformation patterns within the reinforced slopes, the load transfer between the soil and the reinforcement, and the interaction between these two materials in both the resistant and active zones of the reinforced slopes.

Based on the theoretical analyses and the field measurements, some recommendations are made for the design of geogrid reinforced cohesive soil slopes. General design procedures are summarized and technical details for each procedure are described in chapter 8. Finally, the entire thesis is summarized and concluded in chapter 9.

Chapter 2. LITERATURE REVIEW

2.1 Introduction

In the past two decades, design and construction procedures for soil reinforcement using geosynthetics have progressed considerably. A large number of research projects and case histories have been published in the literature. This chapter presents a summary of the publications related to: reinforced soil properties, reinforcement mechanisms, limit equilibrium methods of stability analysis on reinforced slopes, finite element analysis methods and full scale model tests of reinforced structures. The literature review in this chapter will lead to a better understanding of research topics related to slope reinforcement and provide valuable guidance for the research carried out on the Devon test fill.

2.2 Properties of Reinforced Soils

The inclusion of reinforcing members changes the stress state in a soil body. Hence, the stress-strain behavior of reinforced soils is different from the behavior of soils without reinforcement. The change of the stress state in reinforced soils, in terms of magnitude and orientation, is predominantly controlled by the interfacial properties between the soil and the reinforcement.

Other than full scale model tests and finite element analyses, the stress-strain behavior of reinforced soils and the interfacial properties are studied mainly using laboratory tests, such as small scale model tests, triaxial tests, shear box tests and pullout tests.

2.2.1 Stress-Strain Behavior of Reinforced Soils

Plane strain compression tests on reinforced sand were conducted by McGown et al (1978). When reinforcing materials were placed along the major principal stress plane, it was found that the strength of the sand with reinforcing fabrics apparently increased and the strains required to attain the peak strength increased as well. When the orientation of the reinforcement inclusion was changed, however, the effect of the reinforcement decreased, even weakening the sand. It was concluded that the fabrics should be placed

along the direction of the principal tensile strain in order to optimize the reinforcement efficiency. It was found that the effect of the reinforcement also depended upon the physical, geometrical, mechanical and surface characteristics of the reinforcing materials.

McGown et al. (1982) also conducted model tests on reinforced embankments over compressible rubber foundations. By comparing the measured strains and displacements in the reinforced slope with the strains and displacements in the unreinforced slope, it was found that the inclusion of the reinforcing materials reduced the horizontal displacements and the differential settlements at the base of the embankment.

Jewell (1980) carried out a series of direct shear test on reinforced sand. Lead markers were placed in layers in samples and an X-ray machine was used to identify particle movements and failure zone development when the samples were deformed. He confirmed that the reinforcement inclusion increases the strength of the sand when it is favorably oriented and weakened the sand otherwise. He also confirmed that the shear displacement to the peak strength for the reinforced sand is always greater than that for the unreinforced sand when the inclusion is favorable. The displacement required to mobilize the peak strength in the reinforced sand increased as the strength of the reinforced sand increased. From observations on displacements of specimens undergoing direct shear, Jewell found that the reinforcement significantly affected the displacement of the sand in the reinforcement direction. On the center plane through the sand close to the reinforcement, the strains were very small; the reinforcement had inhibited the formation of the failure plane which would otherwise have occurred. In contrast, with continued shearing, the vertical displacement in the reinforced samples was always greater than for the unreinforced sand; the reinforced samples continued to experience volume change over a more extended range of shear displacement. He also found that there was a significant rotation of principal axes in the sand close to the reinforcement.

In the same research, Jewell examined the influences of the material properties and the spacing and layout of the reinforcement on the behavior of the reinforced sand. He pointed out that the longitudinal stiffness of the reinforcement has a significant effect on the stress-strain properties of

reinforced sand, whereas the bending stiffness does not have an important influence. Reinforcement materials with different longitudinal stiffnesses lead to various strain patterns and sizes of strained zones. When the spacing of the reinforcing layers was considered, Jewell indicated that spacing not only affects the efficiency and the friction angle between the sand and the reinforcement, but also alters the failure mechanism. When the sand was heavily reinforced, the failure did not occur in a well defined and consistent pattern, but rather with many local and discontinuous zones of rupture. Sand which contained a relatively large amount of reinforcement deformed under conditions of extreme kinematical constraint; discrete zones of concentrated strain were seen to appear at different orientations throughout the sand samples. It was possible that these zones of preferential strain in the sand represented fractures, rather than simple rupture. Jewell also discussed the influence of mean stress and sand density. Increasing either the mean stress level or the initial void ratio in the sand led to smaller overall peak strength and greater pre-failure deformation in the reinforced sand.

In attempting to draw conclusions on the behavior of reinforced sand, Jewell described a load and deformation sequence which might happen in reinforced sand. Under an applied loading, an increment of shear load is applied to the reinforced sand and the sand undergoes strains. The strains cause displacement in the sand adjacent to and in the direction of the reinforcement which, due to compatibility between the reinforcement and sand, induces strains in the reinforcement itself. A direct feedback occurs between the reinforcement and the sand, with the reinforcement experiencing strain and developing axial force and, in turn, modifying the developing strain (and stress) field within the sand.

Jewell (1980) also carried out direct shear tests on reinforced clay (kaolin). It was found that for reinforced clay, the maximum increase in strength was mobilized early in the test before the stage at which the peak shear strength for the unreinforced kaolin was mobilized. Reinforcement appeared not to have a significant effect on the overall volume change behavior of kaolin during shear. Preferential failure could occur in kaolin itself, along bands inclined to the reinforcement, before the limiting reinforcement force could be generated. Close to the reinforcement, a greater zone of kaolin deformed

than in an unreinforced test, and a series of approximately linear rupture bands formed, on either side and inclined to the direction of the reinforcement.

2.2.2 Interfacial Properties between Soil and Reinforcement

Jewell et al. (1984) conceptually identified three main mechanisms of soil-reinforcement (geogrid) interaction: (a) soil shearing on plane surfaces of the reinforcement which are parallel to the direction of relative movement of the soil; (b) soil bearing on surfaces of the reinforcement which are substantially normal to the direction of relative movement of the soil; (c) soil shearing over soil through the apertures in a reinforcement grid. Analytical expressions for direct sliding resistance were derived and the bearing stresses of the anchorage members were estimated based on bearing capacity theory for deep footings. Thus, the expressions for overall bond strength between soil and reinforcement were obtained in terms of bond coefficient. The influences of soil particle size and pore pressures were discussed as well.

Interfacial properties between soil and reinforcement were studied mainly using laboratory shear box tests and pullout tests. Five commonly used modified direct shear box test methods were summarized by Richards and Scott (1985) and further discussed by Bobey (1988). (Bobey's work will be discussed in detail in the next chapter.) The reinforcement inclusions either coincided with the intended shear plane (Bobey, 1988) or were inclined at various angles to the intended shear plane (Jewell, 1980, Ingold, 1980). Although the detailed stress-strain behavior of the reinforced soil cannot be directly determined from the boundary measurements of force and displacement (Jewell, 1980), the shear box test does provide a valuable estimate of the overall bond strength between soil and reinforcement.

In direct shear tests of reinforced soils, shear stresses in the intended shear plane are plotted against horizontal displacements. The test results are further interpreted to show the relationship between the normal stress and the peak shear stress and then the interfacial bond strengths are obtained in terms of soil strength parameters and bond coefficient (Jewell, 1980). It is important to note that the bond strengths depend on soil properties, reinforcement properties, normal stress levels and the strain rate used during the test.

Pullout tests have been used extensively to evaluate the interfacial bond between soil and reinforcement. Mowafy (1986) suggested that two mechanisms are involved in the interaction between soil and grid (mesh) reinforcement in pullout tests. The primary mechanism is that the tensile strength within the reinforcement is mobilized by the mesh-soil interlock and the soil confinement within the mesh openings; the secondary mechanism is the interfacial friction between the reinforcing material and the soil. For drained conditions, the transfer of stress between soil and reinforcement is by two components: friction and bearing resistance, as shown in the expression derived by Jewell et al. (1984). For undrained conditions, Ingold (1984) used a simple expression, indicating two mechanisms: adhesion and bearing force, to describe the interaction between the soil and reinforcement in pullout.

Typical configurations and boundary conditions for pullout tests were summarized by Costalonga (1988). The pullout force and displacement of the reinforcement (and tensile strains in the reinforcement) are two basic measurements in pullout tests. Based on a load transfer method which was originally derived for pile analysis, Beech (1987) developed an analytical approach to predict the tensile force distribution along the reinforcement according to the shear strength properties of the soil, the mechanical and geometrical properties of the reinforcement material and the pullout test results.

In attempting to compare pullout test mechanisms with the direct shear box tests, Jewell (1980) carried out a series of pullout tests. From his observations, Jewell pointed out that in a pullout test, strain in the sand develops in two thin bands immediately adjacent to and parallel to the reinforcement. In contrast, when a grid is placed in sand undergoing shear, strain develops in the sand in zones which are inclined to the reinforcement and extend a significant distance into the sand away from the reinforcement. In a pullout test, the body of sand is "at rest" and, therefore, experiences a relatively low stress ratio. As the pullout force is applied to displace the reinforcement, the sand immediately adjacent to the reinforcement experiences a rapidly increasing stress ratio. Once this stress ratio exceeds the critical state value, significant strains occur in the sand immediately adjacent to the reinforcement. These strains are contained within a mass of unyielding sand. Hence, he concluded that the

pullout test does not model the action of reinforcement placed in sand undergoing shear deformation. He also concluded that the apparent coefficient of friction between sand and reinforcement derived from a pullout test is not a fundamental parameter since it depends upon the stress level.

Ingold (1980) conducted pullout tests on both sand and clay reinforced with different types of materials. He compared the interfacial shear stress and normal stress behavior of reinforced soils in pullout tests with those in direct shear tests and found that results from the two types of tests are similar to each other at a low normal stress level but different at a high normal stress level. He also compared test results from both drained and undrained tests and concluded that for undrained conditions, pullout tests in clay give a much lower adhesion factor than direct shear tests likely due to the relative stiffnesses of the clay and the reinforcement.

Rowe et al. (1985) studied interfacial strength using both direct shear tests and pullout tests. The apparent interfacial friction angle obtained from the two types of tests on a natural fill ($\phi=31^\circ$) was nearly identical for the six types of geotextiles. For Tensar SR2 geogrid, however, the friction angle from the pullout test (18°) was much smaller than the angle from the direct shear test (30°) for the same soil, due to the different mechanisms involved in the two different tests.

Costalonga (1988) carried out a series of pullout tests on a cohesive soil. (Her work will be discussed in detail in the next chapter.) Geogrids, namely Tensar SR2 and Signode TNX5001, were tested. (Those geogrids were used in the Devon test fill.) The load transfer method was employed to calculate the force distribution and the results were compared with the actual test measurements. She concluded that the load transfer method is suitable for predicting the pullout mechanism of a soil-geosynthetic reinforcement systems. The tensile modulus of a reinforcement material influences the pullout characteristics; the higher the tensile modulus, the more efficiently the reinforcement develops pullout resistance. The bond strength of the geogrid junctions appeared not to affect the results of the tensile force distribution in the geogrids with the cohesive soil used in the research.

Katagiri et al (1990) conducted pullout tests in a large scale shear apparatus.

Pullout shear stress versus shear deformation were plotted for different normal stresses. A linear relationship between normal stress and pullout shear stress was obtained. The inclination of the line from the origin to 1/2 the maximum shear stress in the pullout test was assumed to be the shear stiffness of interaction, which varied with normal stress. A linear relationship between shear stiffness and normal stress was obtained for use in a finite element analysis.

2.3 Soil Reinforcement Mechanism using Geosynthetics

Geosynthetics are used for soil reinforcement in two main categories: reinforcing backfill materials and strengthening foundation soils. The objectives of reinforcement are achieved by providing stabilizing forces and improving soil strength through favorably altering the stress state in reinforced soils. Ingold (1980) summarized some aspects of the changing stress state. The friction between the reinforcement and soil due to lateral movement provides a confining stress which decreases the diameter of the Mohr circle. Within horizontally reinforced soil structures (the most common situation), the assumption of vertical and horizontal stresses being principal stresses is not correct. The horizontal reinforcement induces shear stresses along the horizontal plane which then can no longer be a principal plane. The strength increase can be expressed either as a pseudo cohesion, in the case of tensile failure of the reinforcement, or as an apparent increase in internal angle of shearing resistance of the soil when bond failure prevails. More realistically, both of these modes of failure can be explained by an enhanced internal confining stress developing in the soil.

The inclusion of reinforcement in soil masses also changes the deformation pattern and failure mode. From the observation of the performance of geogrid reinforced trial embankments in London clay, Irvin (1988) pointed out that it was apparent that the geogrid reinforcement reduced the transfer of horizontal stress from upper reinforcing levels to lower levels and modified the mode of deformation. Edgar (1984) mentioned that the use of a rigid geogrid mattress alters the direction of the normal slip circle failure surface by forcing it to pass vertically through the mattress and, as a result, the slip surface is forced into the deeper layers.

Bonaparte et al (1987) performed extensive research on the mechanism of soil reinforcement using geosynthetics. Different mechanisms were summarized and discussed. For slopes and retaining walls, the reinforcement strengthens the structures by adding tensile resistance to the soil mass and by increasing soil strength as a result of increased soil confinement. For sloped soil layers, such as clay liners and earth covers, the reinforcement reduces or prevents cracking and down slope movement of soil layers due to insufficient frictional resistance. For cases of embankments over uniform weak foundations, reinforcement increases the bearing capacity factor of safety, by lowering the horizontal load on the base of the embankment, and reduces lateral spreading and cracking of the embankment. For cases of embankments over locally weak foundations, the reinforcement bridges weak spots in order to reduce the risk of localized failure and to reduce differential settlements. For non-uniform foundation soil layers, the reinforcement transfers stress away from zones of weakness, assists in soil arching and redistributes the load within the soil mass. When placed at the base of a soil structure, reinforcement reduces tensile strain at the bottom of the compacted fill layer and, through stress transfer to the foundation soil, mobilizes the shear strength of a large volume of the foundation soil. It also reduces lateral and vertical aggregate and subgrade movements under highways and railways.

Rowe and Mylleville (1990) studied the strain behavior of reinforced granular fills over soft clay foundations using a finite element method. It was found that for a soft plastic clay deposit, the failure height varies with the allowable geotextile strain. Initially the strain of the geotextile increases slowly with increasing applied load. However, once continuous plastic failure occurs in the underlying foundation soil, the reinforcement must carry any additional applied load which must be resisted along the potential failure surface and, hence, the geotextile strains increase rapidly. It is obvious that reinforcement reduces or prevents the expansion and progress of the yielding zones in weak foundation soils, especially in soils showing brittle stress-strain characteristics. Similarly, Jewell (1986) pointed out that when reinforcement materials are placed at the base of embankments over weak foundations, they improve the bearing capacity of the foundation soil. Reinforcement forces reduce shear loading and increase the normal effective stresses on the shear

surface.

Milligan and La Rochelle (1984) explained in detail the effect of reinforcement on fills over weak soils. The reinforcement reduces splitting of the fill and causes beneficial changes in the stress distribution in soft foundation soils. Lateral movements of the fill and foundation soil mobilize a tensile force in the reinforcement, which reduces the displacement and consequently results in a lower shear stress at the interface. The inclusion of reinforcement prevents the rotation of the principal stress directions and may influence the vertical stress distribution by the high rigidity of the reinforcement. For reinforcement with low rigidity (conventional geotextiles), the vertical stress distribution may remain practically unchanged.

Chalaturnyk (1988) carried out a finite element analysis on a reinforced cohesive soil embankment. The model embankment was built on a rigid foundation. The geogrid, Tensar SR2, and the fill soil selected for the model embankment are exactly the same as used in the Devon test fill and the properties had been studied in detail by Hofmann (1988) and Bobey (1988). The model embankment was 18 m high with 1:1 side slopes. The reinforcement layers were placed horizontally with vertical spacings of 1 m. The stresses in the foundation soil were initiated using the "turn on gravity" method and the successive loads of the embankment were applied sequentially at 1 m lifts of the fill soil and the reinforcement.

By comparing the stress field in a reinforced slope with that in an unreinforced slope, Chalaturnyk found that a significant reduction of the shear stress in the soil occurs due to the presence of the reinforcement. It was further discussed that the major principal stress in the unreinforced and reinforced slopes effectively remains the same. The minor principal stress, however, is a much larger in the reinforced slope. The tensile stiffness of the reinforcement allows the soil to sustain a higher confining stress, which reduces the diameter of the Mohr circle, and consequently increases the soil strength and safety margin in comparison with the unreinforced slope. It was also mentioned that the presence of the reinforcement near the slope surface provides an increased horizontal stiffness thereby eliminating the development of tensile stress in the soil. It was concluded that the major

contribution of the reinforcement in improving the behavior of a soil slope is the addition of horizontal stiffness. Through increased confining stresses within the reinforced slope, the soil strength required to maintain equilibrium is reduced. Moreover, the horizontal stiffness of the reinforcement reduces the horizontal strains in the soil although it does not significantly affect the location of the peak horizontal strain. The reinforcement produces a considerable reduction in the maximum tensile strains but no appreciable change in the rotation of the strain axes in comparison with the unreinforced slope.

Geosynthetics have also been used to reinforce foundation soils in road design. Koerner (1990) outlined the mechanisms involved in the design of paved and unpaved roads using reinforcement materials. Reinforcement is used to increase the initial stiffness, provide confinement and increase strength, reduce cracking, spread loads and prevent loss of aggregates. Detailed discussion is beyond the scope of this thesis.

Increases in resistance to failure of soil masses from earthquake forces using geosynthetic reinforcement is another important aspect of reinforcement with a great potential for development. Unfortunately, only a few research projects have been published in the literature, Bonaparte et al. (1987) and Fukuoka et al. (1990), for example.

2.4 Limit Equilibrium Analysis and Design Methods for Reinforced Slopes

Limit equilibrium methods are the most commonly used approaches in stability analysis and design of slopes, reinforced and unreinforced, because of their simplicity. For unreinforced slopes, limit equilibrium methods are well accepted after having been used to design safe slopes for several decades. Safety margins have been reasonably established through engineering case histories. Engineers have gained confidence in the methods in spite of the well-known disadvantage that the deformation of the slopes cannot be assessed by these methods. For reinforced slopes, however, the situation is different. First of all, two types of materials, soil and reinforcement, are involved, leading to substantially higher complexities. Failure modes are more variable in reinforced slopes and, therefore, more assumptions have to be made in the stability analyses. Moreover, in slopes containing two types of materials,

strain compatibility and the degree of strength mobilization must be considered and the safety margin for the two separate materials must be properly defined. These difficulties in the design of reinforced slopes have been discussed extensively in the literature but remain unresolved.

2.4.1 Failure Modes and General Design Methodology of Reinforced Slopes

Bonaparte et al. (1987) divided the stability analysis of reinforced slopes into two categories: internal and external stability. Internal stability refers to the situation that potential failure surfaces intersect the reinforced soil body. Internal failure may result from either reinforcement rupture due to insufficient tensile strength of the reinforcing materials, or from pullout due to insufficient friction or passive resistance in the resistant or active zones. External stability refers to the situation where potential failure surfaces pass around the reinforced soil mass which is considered as an equivalent continuum having definable mechanical properties.

External stability of reinforced slopes can be analyzed using classic limit equilibrium methods. The potential failure surfaces to be investigated include those passing behind the reinforced soil mass, through the foundation soil and along the interface between the reinforced soil mass and the foundation soil (Bonaparte et al., 1987). In the analysis of internal stability, to account for the interaction between soil and reinforcement, some assumptions have to be made as to failure modes and slip surfaces of reinforced slopes, effects of reinforcement forces on stability, mobilization of soil strength, the tensile strength of reinforcing materials, and stress distribution within the reinforced soil mass. Different limit equilibrium analysis methods have been developed based on various assumptions, but there are some general procedures which most design methods follow.

For a slope with a single reinforcing layer, a general approach is summarized, from Fowler (1982), Jewell (1986), Ingold and Miller (1986) and so on, with the following steps:

- 1) Assume a failure mode (circular slip surface, bilinear surface, etc.), establish equilibrium equations and calculate the reinforcement force required to maintain equilibrium for a specified factor of safety. Analyze a

series of potential slip surfaces and find the maximum required reinforcement force.

2) According to the slope geometry and soil properties, estimate the working strain of the reinforcement.

3) Based on the maximum required reinforcement force and estimated working strain, choose a reinforcing material with such properties that the short term and long term stability of the slope can be achieved.

4) Check the soil-reinforcement bonding and determine the minimum embedded length of the reinforcing layer.

5) Check the external stability (or overall stability) for the slope configuration and the reinforcement layout and check the bearing capacity of the foundation soil if necessary.

For the situation of multi-layer reinforcement, Jewell et al. (1984) and Schmertmann et al. (1987) suggested that the tensile force in the reinforcing material should balance the horizontal force in the soil. The value of the horizontal force in the soil can be locally estimated by assuming the product of the horizontal stress in the soil, which is assumed to have a triangular distribution with depth below the slope crest, and the vertical area of the soil which the reinforcement layer has to stabilize. The spacings and properties of the reinforcing materials are determined according to the calculated horizontal reinforcement force. The factor of safety is then calculated using a relevant limit equilibrium method for the proposed reinforcement layout. A trial and error method is employed to achieve the desired factor of safety. The embedded length of the reinforcement and the overall stability are checked in the same manner as outlined above.

Rowe and Soderman (1985) proposed another approach for the limit equilibrium stability design of geotextile reinforced embankments which also employs finite element methods. The maximum height of an unreinforced embankment before collapse for a certain condition is defined as the collapse height. At the collapse height, the maximum strain occurring in a geotextile is referred to as the allowable compatible strain, which is determined by finite element methods. After the collapse height and the allowable compatible

strain are determined, the factor of safety for the reinforced embankment is calculated for a reinforcing material with a certain tensile modulus. A trial and error method is used to vary the modulus in order to achieve the specified factor of safety.

Bonaparte et al. (1987) also examined stability design approaches for reinforced walls using limit equilibrium methods. Similar to the methods for reinforced slopes, the stability problems of reinforced walls were divided into two categories: internal and external stability. The wall and the reinforced soil mass are assumed to behave as a rigid body in the external stability analysis. Four failure mechanisms have to be investigated: 1) sliding along the base of the reinforced soil mass or along any plane above or below the base; 2) overturning about the toe of the reinforced soil mass; 3) a bearing capacity failure in the foundation soil; and 4) a general slope failure. For the internal stability analysis, the two most common approaches are the semiempirical coherent gravity and the tieback wedge design methods. The coherent gravity procedure refers to the kinematic mechanism for wall movement being rotated about a hinged crest. The locus of the maximum reinforcement tensile force is assumed to be a two-part surface and the assumed earth pressure distribution along the two-part surface ranges from an at-rest condition at the top of the wall to an active condition in the lower portion of the structure. The tieback wedge procedure is related to the kinematic mechanism of rotation about a hinged toe. It is assumed that the shear strength of the reinforced fill is fully mobilized and the active earth pressure is generated along the potential failure surface. The classical Rankine failure surface is assumed to be the locus of maximum reinforcement tensile forces. Two failure mechanisms, rupture of the reinforcing material and pullout of the reinforcement from both active and passive zones, must be investigated in the internal stability analysis. Further detailed discussion on the stability design methods for reinforced walls is beyond the scope of this thesis.

2.4.2 Factor of Safety

The concept of factor of safety for unreinforced slopes has been well established and widely accepted in geotechnical engineering practice. "The factor of safety is defined as the factor by which the shear strength

parameters in terms of effective stress, c' and ϕ' , can be reduced before the slope is brought into a state of limiting equilibrium." (Bishop and Morgenstern, 1960). For reinforced slopes, however, this definition of the factor of safety cannot simply be applied directly because two substantially different types of materials, soil and reinforcement, are involved. The uncertainties, which the factor of safety mainly accounts for, are different for the two types of materials. Hence, how to establish the safety margin for the two types of materials becomes an important consideration in the stability assessment of reinforced slopes.

Jewell et al. (1984) suggested that the conventional definition of the factor of safety can be adopted. The soil shear strength available to provide equilibrium equals the peak strength for the soil divided by the overall factor of safety; the reinforcement force for equilibrium equals the maximum design value, which is determined from either strength of reinforcement or bonding properties, divided by the overall factor of safety. A conventional overall factor of safety in the order 1.3 to 1.5 is considered appropriate. Jewell et al. also suggested that the safety margin may equally well be expressed in terms of partial factors, that is, load factor and resistance factor. An additional residual factor may be used to allow for the consequences of failure, uncertainties in analyses, etc..

McGown et al. (1984) recommended that partial factors of safety should be employed at each part of the stability calculation process in order to account for factors such as variability of loads and materials, durability of materials, lack of accuracy of the design model and influence of construction methods. They further explained that for strain compatibility of the soil-reinforcement system, partial factors of safety need to be considered for both the strength of the reinforcement and the soil-reinforcement interaction coefficient used in the design. The strength of the reinforcement is the product of the operational strain and the isochronous stiffness of the material. The value of isochronous stiffness should take account of not only the operational temperature and design life of the structure but also the variability of the materials and the variability caused by site damage during transportation and field construction. Thus, partial factors of safety should be applied to the material properties provided by the manufacturer.

Christopher et al. (1990) discussed the safety of reinforcement materials. The allowable tensile force per unit width of reinforcement, T_a , should be determined by considerations of the allowable elongation, creep potential and possible strength degradation. For simplification, T_a can be expressed as

$$T_a = T_{ult} \cdot (CRF) / (FD \cdot FC \cdot FS) \leq T_s \quad (2.1)$$

where,

T_{ult} = ultimate tensile strength from wide strip tensile tests (ASTM D - 4595)

T_s = long term tension capability of the geosynthetic at a selected design strain (usually 5% or less)

FD = durability factor of safety (range from 1.1 to 2.0)

FC = construction damage factor of safety (range from 1.1 to 3.0)

FS = overall factor of safety to account for uncertainties in the geometry of the structure, fill and reinforcement properties, and external loads (should be a minimum of 1.5)

CRF = creep reduction factor (recommended 0.4 for polyester and 0.2 for polyethylene)

Bonaparte et al. (1987) pointed out that since the soil and reinforcement often exhibit markedly different stress-strain behavior, no meaningful overall factor of safety can be defined for reinforced soil structures. An approach that can be used is to apply partial factors of safety to each design variable. Partial load factors can be applied to the soil weight, surcharge loads, seepage forces and other load effects. Partial resistance factors can be applied to the soil strength and reinforcement tensile force. However, in applying partial factors in the stability design of reinforced slopes, there are several drawbacks: 1) the procedure is not extensively used in geotechnical practice; 2) it is more complex than using an overall factor of safety; and 3) it is not yet well correlated with case histories and experience. Therefore, they provided the following recommendations for incorporating an overall factor of safety into reinforced soil design analyses:

1. Do not factor the allowable tensile strength of the reinforcement with an additional factor of safety.
2. For the evaluation of external stability, define the overall factor of safety as the ratio of resisting forces or moments to the applied forces or moments.
3. For the evaluation of internal stability, apply the factor of safety to the soil shear strength parameters, c' and $\tan \phi'$.

Cheng and Christopher (1991) conducted a probabilistic study on the stability of two geotextile reinforced slopes. The probabilistic techniques were introduced to serve as supplements or complements to the existing deterministic procedures of stability analysis. The input variables for the analysis are treated as random variates represented by a mean value, a standard deviation and a probability density function. Variables are correlated to each other based on theoretical analysis. Factor of safety or required reinforcement tensile strength, being a function of these random variables, also become a random variable with a mean, standard deviation and probability density function. The coefficient of variation for each variable, such as soil and reinforcement properties, is evaluated based on the variability of the properties, laboratory testing techniques and experience. The coefficients of variation, together with correlations between variables, are incorporated into stability analysis equations and the probabilistic factors of safety are obtained. It was found that when unreinforced and reinforced slopes are set to the same safety margin, that is, the same factor of safety with different geometry and reinforcement layout, the estimated mean values of the probabilistic factors of safety are almost identical to each other. However, the unreinforced slope has a higher variability, while the reinforced slopes have a much higher reliability index. In other words, if designed with the same factor of safety, the reinforced slopes would actually be safer than the unreinforced and flatter slope. Therefore, it was concluded that the practice of assuming a reinforced slope is as safe as a flatter unreinforced slope with the same factor of safety is correct and conservative.

2.4.3 Soil and Reinforcement Properties and Strain Compatibility

After problems are defined and the analytical method is determined in the

design of reinforced slopes, the next key step is to choose parameters representing properties of the soil, the reinforcement and the interaction between the two types of materials. Since the mobilization of the tensile strength in reinforcement members is predominantly controlled by the movement of the soil, the strain compatibility (or displacement compatibility) becomes the main concern. Long term behavior of reinforcement materials is another factor to be considered.

Beech (1987) argued that displacement compatibility must be accounted for in two zones: at the intersection of the soil failure surface and reinforcement, and along the embedded length of reinforcement beyond the failure surface. The material properties of the reinforcement should be determined in such a way that the tension in the reinforcement, which is required to maintain equilibrium, is obtained when the shear displacement of the soil matches the tensile displacement of the reinforcement. Similarly, McGown (1984) pointed out that strain compatibility of soil and reinforcement has to be checked. He added that in most possible situations, strain at peak strength of reinforced granular material (lateral tensile strain) is 8% at most, usually less than 6%. So the reinforcement force, lying in or close to the direction of the principal tensile strain, must be limited to the corresponding strain level.

McGown (1984) stated that the strength of the soil under various drainage conditions is most commonly measured using triaxial or shear box apparatuses, although many other methods are available. For compacted granular materials, when the soil strains and its strength reduces from its peak value to that at constant volume, the reinforcement mobilizes more force and the whole system may remain in equilibrium. Hence for designs employing limit equilibrium methods for soil-reinforcement systems, the mobilized strength of compacted granular soils should be taken as their angle of friction at constant volume. Bonaparte et al. (1987) and Schmertmann et al. (1987) argued that both peak strength and strength at large strain can be used in limit equilibrium analysis depending upon the anticipated strain level in reinforced slopes.

McGown et al. (1986) mentioned that it is accepted that the interaction parameters between the various materials be taken as their peak values. However, there are substantial discrepancies in determining reinforcement

properties. Reinforcement materials which are relatively inextensible and do not creep are usually represented by the yield stress. The values are obtained by tensile testing at constant rates of stress or strain. Relatively extensible materials which do not creep can be tested in the same manner but there is no agreement on the strain at which the limiting stress for the material should be taken. For relatively extensible materials which do creep, the problems of deciding upon the limiting stress is even more difficult as they possess a complex stress-strain-time behavior. The methods of testing them need to provide data on their behavior under sustained loading conditions as occur in the field.

A simplified approach of accounting for strain compatibility is to specify the tensile strain of reinforcement according to the relative stiffness of soil and reinforcement and the working load of the reinforced structure. Jewell (1986) suggested that it usually needs 3 to 5% tensile strain for a polymer grid to mobilize working force in soil reinforcement. Fowler (1982) argued that an average fabric elongation of 5% is desired, but 10% fabric elongation would be acceptable. Wallace and Fluet (1987) pointed out that the short term strains that are appropriate for the purpose of developing tensile force in geogrids are in the order of 2%. Long term strains under working load, considering creep, would be about 5 to 10%. Rowe (1989) compared the results from a finite element analysis with a limit equilibrium analysis of a reinforced embankment on a soft foundation with 2% or 5% specified reinforcement strains. He concluded that the limit equilibrium analysis with 2% or 5% specified strains was conservative. Due to the fact that the working strain of reinforcement depends on the relative stiffness of the two types of materials, it is difficult to directly compare different recommendations on the working strains of reinforcement. Nevertheless, 5% is the value which seems to be relatively well accepted.

The mobilized reinforcement force is a product of the working tensile strain and the stiffness of the inclusion material. The stiffness of reinforcement obtained from unconfined wide strip laboratory tensile tests is often used in design. McGown et al. (1982) conducted in-soil tensile tests, at a strain rate of 2% per minute and a temperature of 20°C, on different types of geotextiles confined in a uniform sand. It was concluded that highly

structured non-woven and composite geotextiles significantly change the shape of their load-strain curves when tested in-soil, while the woven geotextiles with a simpler structural arrangement did not exhibit such a change. Fannin and Hermann (1990) measured both loads and strains in geogrid reinforcement layers in a reinforced steep slope of uniformly graded sand. From measurements of forces and strains in the embedded reinforcing layers, they found that the moduli of stiffness are compatible with data from isochronous load-strain curves reported for laboratory tests on unconfined samples. Such curves appear well-suited for interpretation of tensile strength tests on polymeric reinforcement. From the limited literature, it seems appropriate to use in design the load-strain relationship for geogrid reinforcement based on isochronous load-strain curves from laboratory unconfined tests.

Creep of polymeric materials is a well know phenomenon. McGown et al. (1984) conducted a series of creep tests on polymeric geogrids and derived isochronous load-strain curves to evaluate the time-dependent behavior of the materials. Fannin and Hermann (1991) also studied the time-dependent behavior of polymer grids based on the geogrid forces and strains measured in two instrumented reinforced test slopes. The measured increases of the strain under a constant load were found to match well with the values predicted according to the isochronous load-strain curves established from laboratory creep tensile tests. It was then concluded that the isochronous load-strain curves are well suited for design criteria for long term creep if the creep tensile tests are conducted under representative working conditions of load and temperature. In design practice, the creep phenomenon is eliminated by specifying a limit on the design strain of the reinforcement materials. McGown et al. (1984) and Bonaparte et al. (1987) agreed that polymeric materials do not tend to approach creep rupture when the strain is less than 10%. The value of 10% strain appears to be well accepted as a performance limit strain.

2.4.4 Limit Equilibrium Stability Analysis Methods

As discussed before, the external stability of reinforced slopes is analyzed using conventional limit equilibrium methods. The reinforced soil mass is usually considered as an equivalent continuum with definable material

properties. In the analysis of internal stability, however, some additional assumptions have to be made to account for the effect of the reinforcement layers.

Murray (1982) proposed an analytical approach of stability analysis on reinforced embankments and cuttings using limit equilibrium methods. A simple bilinear slip failure mechanism was assumed. A hyperbolic load-deformation relationship for the reinforcing fabric was adopted and the elongation of the fabric was specified to account for the strain compatibility between soil and reinforcement. The maximum force developed in the fabric equals the horizontal force of the soil within the spacing of adjacent fabric layers. The factor of safety is expressed in terms of the resistance forces, which include the contribution of reinforcement layers, divided by the disturbance forces. A comprehensive series of analytical equations were provided and their implications were illustrated. No attempt was made to account for long term stability. Murray's work was modified and expanded by Schneider and Holtz (1986). The contribution of the adherence resistance provided by the reinforcement was accounted for differently. The interfacial friction angle between soil and reinforcement ranges from half of the angle of internal friction for granular soils up to the full value of the angle. The initial stress parameter K and other design parameters were also discussed. To facilitate the complex stability analysis equations, design charts were developed and the procedures for using the charts were presented.

Jewell et al. (1984) carried out a comprehensive study on design methods for steep reinforced embankments on relatively stiff foundations. A computer program WAGGLE had been developed. Polymer grid reinforced uniform cohesionless soil embankments with horizontal crests and slope angles in the range of 30° to 80° were investigated. Internal failure and external failure (sliding along an interface) mechanisms were examined. The two-part wedge surfaces, which were suitable to check both mechanisms, were assumed. This mechanism is simple because only force equilibrium needs to be satisfied. It was argued that the current lack of knowledge about interslice forces in reinforced soil makes a simple mechanism attractive. A conventional factor of safety was applied to the peak strength of the soil. The reinforcement force in each grid layer similarly equals the maximum value

divided by the overall factor of safety. The design of a reinforcement layout to give a desired overall factor of safety for a slope proceeds by trial and error. The total number of reinforcement layers and their spacing can be arranged to give more or less equal factors of safety for the two failure mechanisms, internal and external failure, and their combination and to keep the total quantity of reinforcement required to a minimum.

Design charts for steep slopes reinforced with polymer grids were developed by Jewell et al. (1984) to provide quick solutions for preliminary design purposes. There are three main steps to use the design charts. Firstly, based on the force equilibrium of trial wedges, the maximum horizontal reinforcement force required to hold the slope in equilibrium for a desired safety margin is determined. Secondly, the minimum length for reinforcement layers is determined according to the bonding characteristics between the soil and the reinforcing inclusions. It was found that parallel truncation generally yields a more efficient use of reinforcement and a smaller quantity of materials to provide the desired factor of safety against all potential failure mechanisms. Thirdly, a practical spacing arrangement is derived to prevent any local overstressing in reinforcement layers. In other words, the horizontal stress which needs to be balanced by each reinforcement layer must not exceed either the tensile strength of the reinforcement or the bonding strength between soil and reinforcement. (The bond angle of friction was assumed conservatively to equal half the design friction angle for the soil.) These three procedural steps satisfy basic concerns in the design of reinforced slopes.

Jewell (1991) extended the previous work and provided revised design charts for steep reinforced slopes. A wider range of slope angles from 30° to 90° is allowed. It was considered that the critical equilibrium for steep reinforced slopes is usually governed by long term stability conditions, so the soil strength is described in terms of an effective frictional shearing resistance, (ϕ' , $c'=0$). The large strain or critical state shearing resistance of fill soils is recommended. It was found that for a compact fill reinforced with polymer materials, the mobilized shearing resistance in the equilibrium condition is almost certain to exceed the critical state value. The mobilized reinforcement force, however, is almost certain to be less than the force

calculated for equilibrium using the critical state friction angle of the soil. It was also recommended that it is prudent in most cases to allow for some pore water pressure arising during the life of the slope and long term equilibrium pore pressures as high as $r_u=0.25$ are possible in clay fill slopes. For polymer reinforcement materials, the maximum tensile strain is limited to 3% or 5% during the design life to ensure satisfactory serviceability. Reference properties provided by manufacturers (if only the mean or average values are quoted, they should be reduced by a factor of 1.15 to make them comparable to the characteristic values) should be factored for mechanical damage, environmental effects and material uncertainties and then used for design purposes. Interaction parameters between soil and reinforcement were discussed and steps for applying the design charts were described in detail.

Schmertmann et al. (1987) extended the work by Jewell et al. (1984). The main effort was to obtain a general truncation of reinforcement layers rather than the parallel truncation by Jewell et al. (1984). Two-part wedge, or bilinear, models were employed for reinforced slope stability analyses. The soil was modelled as a purely frictional material. All failure surfaces were assumed to start behind the slope crest and pass through the toe. The interfacial friction angle was assumed to be equal to 90% of the internal friction angle of the soil and the interwedge friction angle equal to the factored soil friction angle, rather than zero interwedge friction as assumed by Jewell et al. (1984). A conventional factor of safety was applied to the soil shear strength and interfacial bonding strength.

Design charts have been developed by Schmertmann et al. (1987) with the goal of providing practical, yet conservative, design guidelines for geogrid slope reinforcement. Three major output parameters, total reinforcement force and reinforcement lengths for the bottom and top layers, can be determined from the design charts. The total reinforcement force was determined based on force equilibrium in the two-part wedge and expressed non-dimensionally as a horizontal reinforcement force coefficient K . The ratio between the magnitudes of the two free-body reinforcement forces in the two-part wedge was determined based on an assumed triangular reinforcement tension distribution which increased proportionally with depth below the slope crest. A search was required to find the critical

combination of node location and wedge angle and to obtain the largest total reinforcement force. The length of the bottom reinforcement layer was assumed to be controlled by external stability requirements. The length of the top reinforcement layer would be controlled by internal stability requirements, that is, the embedded length beyond the critical slip surface had to provide sufficient bonding. The influence of assumptions regarding interwedge friction, reinforcement force distribution and interfacial friction was investigated and it was concluded that they do not have a significant effect on the total reinforcement force for steep slopes but do have an effect on reinforcement length.

Schmertmann et al. (1987) compared the results of the two-part wedge analyses with results of other limit equilibrium methods, such as the Bishop Modified Method with a circular slip surface and Spencer's Methods with non-circular surfaces. They concluded that the variation in the total reinforcement force determined by the different methods is within 10%, but the lengths of the reinforcement layers from the various methods differ significantly. This disagreement can be attributed to the different assumptions on the shape of the failure surfaces and to the different methods of including the reinforcement forces in the equilibrium analyses.

Jewell (1982) analyzed stability problems of reinforced embankments on soft foundations using a limit equilibrium method. He examined three principal failure mechanisms: internal, overall and foundation stability. Circular slip surfaces and tension cracks in the embankment fill were assumed. It was also assumed that the reinforcement force acts in the direction along which the reinforcement was originally placed and it only reduces the overall shear stresses carried by the soil without increasing the overall normal stress in the soil. The factor of safety is given by the ratio of restoring moments, including additional moments from the reinforcement, to disturbing moments. For a specified factor of safety, the reinforcement force, required to hold the slope in equilibrium for the critical slip circle, is calculated using a trial and error technique. The material properties of the reinforcement are then determined from considerations of strain compatibility and of bonding characteristics between soil and reinforcement for the limit state and the working state.

Ingold (1982) conducted an analytical study on the stability of reinforced embankments. Infinite slope failure and circular failure surface mechanisms were examined. The former was to investigate the possibility of surface planar slips. An analytical expression of the factor of safety is derived by incorporating the reinforcement force into the well established infinite slope analysis method. The circular failure surface was to analyze the large scale stability of the reinforced fill and the foundation. Bishop's method was chosen as the basis for this analysis. First, the unreinforced embankment is analyzed to determine the deficit between the obtained factor of safety and the desired factor of safety. Reinforcement is then included to compensate for the deficit. The reinforcement force, which was partially factored against tensile failure and assumed to act horizontally instead of tangentially, provides an additional resisting moment. The magnitude of the reinforcement force is assessed on a trial and error basis to obtain the desired factor of safety. Design charts were given for some simplified cases.

Similarly, Duncan et al. (1985) developed a computer program, STABGM, to analyze the stability of reinforced slopes. Bishop's method was taken as the basis of the analysis. The reinforcement force, which acts either horizontally or tangentially, provides an additional resisting moment against the circular slip failure. The program is capable of accounting for various factors such as pore pressure distribution, tension cracks, a rigid layer of foundation soil at a certain depth, etc..

Ingold and Miller (1986) examined the short, intermediate and long term stability of geotextile reinforced embankments on soft foundations. Immediately after an embankment is built, only the undrained shear strength of the foundation soil is mobilized to resist the embankment loading. The factor of safety could be considerably below the desired value and reinforcement may be required to provide additional stabilization. Bishop's method, taking the undrained shear strength of the foundation soil, is used to calculate the reinforcement force required to maintain short term equilibrium with the desired factor of safety. In the process of consolidation, the soil gains strength. On the other hand, the available tensile force in the reinforcement may decrease due to creep-related behavior. These two phenomena both develop with time. Therefore, it was suggested that the

required reinforcement force, for a desired factor of safety after construction, should be calculated using Bishop's method in terms of effective stresses. The decreased required tensile force, due to the decrease of the pore pressure ratio (Bishop and Morgenstern, 1960) during consolidation, is compared with the decreased available tensile force in the reinforcement creep curves to ensure that the former is always less than the latter at any time during consolidation. Since the strength of geotextile polymers decreases with time, the long term stability of the embankment and the foundation should be designed based on effective shear strength parameters, without reinforcement inclusions, such that an adequate factor of safety is maintained against both shallow and deep seated slips.

Leshchinsky and Volk (1986) proposed an analytical approach for the stability analysis of reinforced earth structures. A variational limit equilibrium method was used for the analysis and all global equilibrium requirements are satisfied. A rotational failure mechanism and a log-spiral failure surface were assumed. It was claimed that the collapse mechanism defined by the log-spiral surface is identical to the admissible mechanism used in the upper-bound theorem of plasticity. The objective of the analysis was to determine the minimum value of the factor of safety for a given reinforced earth structure in which the tensile forces in the reinforcement are known or specified. The reinforcement forces were assumed to be inclined so as to contribute the most resistance, that is, orthogonal to the radius of the log-spiral at their intersection when failure of the composite structure occurs. A number of non-linear equations were derived based on equilibrium and geometric conditions. Unknowns were determined by solving the equations and the result of the analysis is expressed as a stability number for a given reinforced structure. After a series of trial calculations, the stability number is expressed as a polynomial function of soil strength and reinforcement force for a given slope configuration. It was additionally concluded that the inclination of the reinforcement force influences the result of stability analyses on reinforced cohesive soils, but it has little effect on cohesionless soils.

The analytical approach for the stability analysis of reinforced earth structures was extended by Leshchinsky and Boedeker (1989). Both internal

and external stability were considered. It was assumed that the internal failure occurs along a log-spiral surface. Only the pullout mode of failure was considered for the internal stability and, therefore, the tensile forces in the reinforcement were defined by the available pullout resistance of each reinforcing layer. A bilinear slip surface was assumed for external stability. Only force equilibrium was considered for the two failure mechanisms. Closed form solutions were obtained and design charts were provided. If a multi-layer system is used in a reinforced structure, a triangular distribution, that is, zero at the crest and a maximum at the toe, was chosen to determine the tensile force in each layer. It was suggested that the triangular distribution might result in a conservative selection of geosynthetics for the bottom half. For the upper half, an uniform distribution also should be used in the design analysis to check that the upper reinforcement layers are firmly anchored against potentially higher pullout forces.

Jewell (1990) examined different limit equilibrium methods for stability analysis of reinforced slopes and pointed out that, for a conventional limit equilibrium analysis, the logarithmic spiral and the two part wedge analysis are satisfactory rigid body mechanisms because no assumptions are required for their solutions. He further stated that, to maintain equilibrium of reinforced soil slopes, the required forces calculated by a logarithmic spiral analysis, which can be considered as an upper bound solution, on cohesionless soil slopes are almost identical to the forces calculated by stress field analysis, which can be considered as a lower bound solution. For cohesive soils, the agreement between different limit equilibrium analyses, such as two part wedge and logarithmic spiral mechanisms, provides confidence for the stability analysis of reinforced clay soil slopes. Additionally, the length of reinforcement layers required to satisfy overall equilibrium was discussed and some suggestive comments on design charts for reinforced soil slopes were made.

Sawicki and Lesniewska (1991) studied the stability of reinforced soil slopes using a limiting plasticity approach. Reinforced soils are treated as macroscopically homogeneous and anisotropic materials with the gross behavior depending on the mechanical properties and interactive contributions of the soil and the reinforcement. The yield condition for

reinforced soils is expressed as a function of property parameters and stress components. Governing equations, representing the yield conditions, the flow rule and the equilibrium requirements, can be solved with the help of the method of characteristics for a given geometry of the slope and respective boundary conditions. From the numerical solutions, which are the so-called lower bound estimates according to plastic limit theorems, the stress characteristics, the slip surfaces and the applied external load under which the slope would fail are determined for a given condition of slope geometry, soil properties and reinforcement layout. The influences of the soil and reinforcement properties on the shape of slip surface were examined. It was found that the amount of reinforcement strongly affects the location of the slip lines. The active zone expands with increasing values of reinforcement force. The shape of slip lines for weak reinforcement may be approximated by bilinear surfaces. For stronger reinforcement, however, the shape becomes more and more curvilinear. After summarizing and evaluating a few typical limit equilibrium methods for analyzing the stability of reinforced slopes, the authors claimed that the advantage of their approach is that the slip surface is part of the solution rather than being assumed. They also claimed that this approach is rigorous and provides a framework for evaluating existing limit equilibrium models.

2.5 Finite Element Analysis on Reinforced Slopes

Finite element methods have been used by a number of authors to analyze reinforced soil structures, such as reinforced slopes and walls. The main advantage of these methods is that they provide a general view of the stress and strain distribution within the reinforced soil mass. Another advantage of the finite element method is that it can model incremental construction procedures which is essential because soil behavior depends on stress history and stress path. Other than the constitutive relationship of the soil, the modelling of the interaction between soil and reinforcement is a key concern in the finite element analysis. Finite element solutions are able to answer questions such as mobilization of tensile force in reinforcing materials, deformation of the reinforced soil structure, strain compatibility between soil and reinforcement, failure modes, stress and strain localization within the reinforced soil mass, etc..

Andrewes et al. (1982) carried out a finite element analysis on soil-geotextile systems. The soils were represented by triangular and quadrilateral elements. A non-linear elastic hyperbolic model was used to represent the soil behavior. Geotextiles were represented by straight line elements which had no bending stiffness. Polynomial functions were chosen to simulate the non-linear load extension relationships of the geotextiles. Soil-geotextile and soil boundary interactions were assumed to be purely frictional and simulated by spring elements of zero length connecting the nodes of soil elements to those of inclusion elements. A hyperbolic model was adopted to represent the interface friction behavior. The finite element solutions were compared with the measurements from a model strip footing test on sand reinforced with a non-woven melt-bonded geotextile. It was found that the finite element procedure provided a good prediction of the behavior of the reinforced soil mass before any locally developed failure occurred.

Rowe (1984), Rowe and Soderman (1985), Rowe and Mylleville (1990), and Mylleville and Rowe (1991) carried out comprehensive finite element studies of reinforced granular soil embankments on soft foundations. The soil was idealized as a small strain nonlinear elastoplastic material with a Mohr-Coulomb failure criterion and a nonassociated flow rule. The reinforcement material was treated as a structural membrane with an axial stiffness and negligible flexural rigidity. In the interface between soil and reinforcement, the displacements were assumed to be compatible until the shear stress reached the interfacial shear strength defined by Mohr-Coulomb criterion. The fill material was modelled to be placed in layers as different load steps. The geotextile reinforcement was assumed to be placed on the top of the foundation soil over the entire width of the embankment. The soil-reinforcement interface shear strength was assumed to be purely cohesive when in contact with a clayey foundation soil and purely frictional when in contact with a granular fill. Stress and strain distribution in the reinforced embankment were obtained from the analyses and illustrated in terms of velocity fields and strain contours, clearly showing deformation patterns, stress localizations and the mobilization of the shear strength of the fill. The results from the finite element analyses were compared with field experiments and plastic solutions and the accuracy was found to be reasonable. From the finite element analyses, the allowable compatible strain, that is, the strain in

the soil when the unreinforced embankment approaches collapse, was estimated. This strain could be used in evaluating the available tensile force in the reinforcement which then would be incorporated into limit equilibrium stability analyses. Design charts were obtained from the finite element analyses. Moreover, the influence of the tensile stiffness of the reinforcement on the stability of reinforced structures was discussed. It was found that the use of high modulus reinforcement changes the deformation pattern and failure mode (bearing capacity type failure rather than failure based on consideration of deformations), allows an increase in fill height and significantly reduces the shear strains in soft foundation soils. This latter change is especially important for soils susceptible to strain softening. From their research, it is suggested that a limiting strain as low as 0.5%, rather than 2% as recommended in the literature for sensitive brittle soils, may be necessary for high modulus geosynthetics to reduce shear strains in the soils to an acceptable level.

Karpurapu et al. (1991) carried out a finite element analysis on an incrementally constructed soil wall which is reinforced with Tensar Geogrid BX1100 (SS1). The wall was constructed using four rows of 0.75 m high panels and filled with uniformly graded washed sand. In the finite element analysis, the soil was simulated using a modified hyperbolic constitutive model characterized by a tangent Young's modulus, a bulk modulus and a dilation angle. Bar elements were used to simulate the reinforcement layers and the isochronous load-strain-time characteristics of the reinforcement were used to develop a nonlinear force-strain model. The interface between the soil and the geogrid was modelled using joint elements of zero thickness. The maximum shear stresses in the joint elements were controlled by a Mohr-Coulomb failure criteria and a perfect bond was assumed between the soil and the grid when the shear stresses were within the failure envelope. The results of the finite element analysis were compared with the measurements of the wall and it was concluded that the numerical simulation correctly predicted the general location and magnitude of peak grid strains. The simulation over-predicted the distance of significant reinforcement strain propagation into the reinforced soil zone. Hence, it is conservative in estimating embedment length. The failure surface predicted by the finite element analysis was observed to be in good agreement with the excavated

surface and was also consistent with the geometry of failure predicted by the Coulomb wedge method.

Matsui and San (1988) conducted a finite element stability analysis on reinforced slope cuttings. An elastoplastic joint element was derived based on the Coulomb yield criterion to account for the slippage between soil and reinforcement. Along a trial slip surface, the local factor of safety, which is defined in terms of principal stresses and shear strength parameters of the soil, can be calculated at different points and the average factor of safety of the slip surface is determined from the results of the finite element analysis. The overall stability of the reinforced slope cutting is then evaluated by comparing the results for possible potential slip surfaces. In addition, the shear strength parameters of the component materials are incrementally reduced by dividing them with a common reduction ratio to trace the development of the failure slip surface in the slope.

Taki et al. (1988) performed finite element analyses on cohesive soil slopes reinforced with a biaxially stretched polymer grid. An elastoplastic model was used assuming that the integrated mass of grid and soil forms a complete elastoplastic body. The Drucker-Prager constitutive relationship was adopted for the soil and the grids, laid horizontally in layers in the fill, were modelled as spring elements of the elastoplastic type. The results of finite element analyses were shown as: deformation patterns, vector diagrams of principal stresses and contours of local factors of safety. The results were compared with measurements of large scale model tests and it was found that the conformity of calculated displacements and grid strains with measured values were satisfactory. The development of elasto-plastic zones in the finite element analysis were also confirmed by the model observations. It was, therefore, concluded that the finite element analysis is a useful tool to solve the reinforcing mechanism of grids in an embankment.

Chalaturnyk (1988) carried out a comprehensive study on a reinforced cohesive soil (silty clay) embankment using a total stress, plane strain finite element method. The model embankment with a height of 18 m and side slopes of 1:1 was built on a rigid foundation and reinforced with a polymer grid material, Tensar SR2. Seventeen layers of geogrid were laid horizontally at a vertical spacing of 1 m. The finite element analysis was conducted

incrementally with each load step representing the placement of a 1 m lift of soil. A hyperbolic elastic model was adopted to simulate the constitutive relationship of the soil. A nonlinear quadratic reinforcement model was used to represent the load-strain behavior of the geogrid. No interface elements were provided to allow relative movements between the soil and the reinforcement. The results from the finite element analysis were presented as: velocity fields and contours of strength mobilization, maximum shear strains and displacements. Profiles of the reinforcement loads in reinforcing layers at various fill heights were also illustrated. The stress and strain fields in a reinforced slope were compared with the fields in an unreinforced slope and it was found that the beneficial effects provided by the presence of reinforcement in the soil slope were obvious. By providing a horizontal tensile stiffness within the soil mass, the reinforcement not only reduced the mobilized deviatoric stress by allowing the soil to sustain a higher confining stress, but also reduced strains in the soil mass, especially the horizontal strain.

Chalaturnyk also conducted limit equilibrium analyses on the geogrid reinforced embankment using the Bishop Modified Method. The results were compared with the results from the finite element method and the following conclusions were drawn:

- 1) The differences in how the reinforcement force was incorporated into the limit equilibrium analysis and how the force was oriented significantly affected both the overall factor of safety and the location of the critical potential failure surface.

- 2) By ignoring the favorable change of stress state due to the higher confining stress provided by the reinforcement tensile stiffness, the Bishop Modified Method (and other limit equilibrium methods) calculates a conservative factor of safety for the reinforced soil slope.

- 3) For reinforced slopes with uniformly spaced reinforcement, the conventional constant load distribution will provide satisfactory values for the factor of safety.

- 4) The choice of a circular slip surface as a failure mechanism within

reinforced soil slopes is reasonable. The points of maximum load in each layer of reinforcement follow a circular arc pattern within the slope and correspond very closely with the shape and location of the critical slip surface predicted by the Bishop Modified Method.

5) The maximum reinforcement load does not occur in the lowest reinforcing layer.

It is important to note that the above conclusions were obtained from a finite element analysis on a specific slope with a certain configuration, reinforcement layout and material properties. One should be cautious in applying these conclusions to other cases.

2.6 Full Scale Tests on Reinforced Slopes

Limit equilibrium and finite element methods analyze the behavior of reinforced soil slopes from different perspectives, providing useful tools for design purposes. However, these analyses are based on assumptions dealing with failure modes, strain compatibility, deformation patterns, constitutive relationships of materials, interaction between soil and reinforcement, and so on. It is essential that these assumptions be justified in engineering practice, especially by well instrumented full scale field tests.

Barsvary et al. (1982) reported on the instrumented field behavior of two reinforced embankments on soft foundations. Geotextiles were used as separation and reinforcement members at the base of two highway embankments. Details about design considerations, material properties and construction procedures were discussed. Elongation of geotextiles, settlements and pore pressures were measured and trenches were excavated through the fill one year after the construction to examine the geotextile materials and to evaluate the performance. From the field observations and measurements, it was found that geotextiles functioned well in both separating the fill materials from the soft foundation soils and reinforcing the embankments by providing a resisting moment against a rotational failure and restraining the fill from lateral sliding.

Bassett and Yeo (1988) described the performance of the Stanstead Abbots trial reinforced embankment. The instrumented trial embankment was a

London clay fill founded on soft alluvial clay deposits and reinforced with a layer of polymer grid, Tensar SR2, placed at the base of the embankment. Load cells and Bison strain gauges were used to measure loads and strains in the geogrids. Soil deformations and the pore pressure response were monitored using inclinometers, horizontal profile gauges and piezometers. The measured loads in the geogrid developed rapidly during construction but surprisingly continued to increase with time under the subsequent constant load condition. A dilemma occurred when the strain increased from 2% to 3% while the load in the geogrid at the same position increased from 14 KN/m to 16 KN/m. The measured strains were compared with the strains interpreted from the measured load at the same point and the isochronous curves of the geogrid material. It was found that the correspondence was good. The strains in the geogrid were also compared with the strains in the foundation soil and a close relationship was found which implied little or no slippage between the reinforcing layer and the underlying foundation soil. From the comparison of field measurements in the trial embankment with predicted reinforcement forces using different conventional and numerical approaches, it was concluded that the slip circle analysis was not satisfactory for the case of a wide load on a shallow foundation. It was also concluded that the accuracy of numerical predictions depended on suitable parameters rather than on the sophistication of the computing model and the worst part of the predictions was the drainage behavior.

Humphrey and Holtz (1986) summarized 37 case histories of reinforced embankments on soft foundations. The embankments were typically constructed of granular materials; only a few embankments were built using fine grained soils. In many cases, geotextiles, woven or nonwoven, were used to provide an additional separating effect, other than the reinforcing function, to reduce intrusion of fill materials into the soft foundation soil. Geogrids were used as reinforcement only in a few cases. In field construction, when the foundation soils were very soft, the fill was usually placed starting at the outside edge and then working inwards in order to fully mobilize fabric tension. For stronger foundations, fill placement proceeding outwards from the center was successful. Measured strains in the reinforcement varied over a wide range. After the end of construction, the strains were observed to increase with time in some cases and decrease in

others, due to consolidation or lateral creep deformation of the foundation soils. The strength of reinforcement samples excavated from embankments some time after construction was found to be 0 to 50% less than the original values. Three types of failures were observed: 1) excessive deformations because of a too low reinforcement modulus; 2) slope failure or excessive deformations due to tensile failure of the reinforcement; and 3) excessive deformations caused by geotextiles pulling apart at overlapped points or sewn seams.

Based on the 37 case histories, Humphrey and Holtz discussed the effect of reinforcement on stability of embankments. Except in two cases, the majority of the embankments were stabilized by the inclusion of reinforcement (in one case the reinforcement showed no effect and in the other the reinforced slope even failed at a lower height). The calculated increase in the factor of safety ranged from 5% to 34% for different undrained shear strengths of foundation soils. Finite element analyses indicated that reinforcement is more effective for lower strength soils. From the plot of the embankment height against the undrained shear strength of the foundation soils, it was found that the three examples of unreinforced embankments which failed fitted a straight line defined by conventional bearing capacity theory. The stable unreinforced embankments plotted below the line. Five reinforced embankments that failed fell on another straight line, which is above the line for the unreinforced cases. The stable reinforced embankments plotted below the second line. This comparison appears to indicate that reinforced embankments can, under some circumstances, be constructed up to 2 m higher than predicted by conventional bearing capacity theory. This conclusion is supported by four cases in which reinforced embankments were constructed 0.9 to 2 m higher than companion unreinforced embankments which failed.

Miki et al. (1988) conducted large scale experimental studies on polymer grid reinforced embankments. Test embankments, 3 m high with 1:0.7 side slopes, were constructed of silty and clayey sand and reinforced with a polymer grid, Tensar SS2. The length and the number of geogrid layers were varied to evaluate the mechanism of reinforcement. The model embankments were tested under artificial heavy rainfall conditions to study the effect of the reinforcement. Strains in the geogrid layers and settlements of the

embankments were measured and field observations were continued with time as the amount of rainfall accumulated. Finite element analyses with a Drucker-Prager soil model and elastoplastic spring geogrid elements were also carried out for the purpose of comparison. From the field observations, measurements and numerical analyses, some conclusions were drawn. When the length of reinforcing layers is small compared with the height of the embankment, internal stability is the governing factor; otherwise, internal stability becomes the controlling factor. Horizontally laid multi-layer geogrids significantly reduce the deformation in the reinforced zone. The results of the finite element analyses were in close agreement with the field observations and measurements. Surface erosion was a common problem for slopes with different reinforcement layouts.

Taki et al. (1988) carried out a full scale test on a polymer grid reinforced embankment. The test embankment, 14 m high and founded on a relatively rigid foundation, was constructed of sandy or silty clay and reinforced with biaxial polymer grids. There are five sections in the embankment. Three sections are reinforced respectively with one, two and four grid layers in a continuous pattern and one section is reinforced with five grid layers in a checkered pattern. The remain section of the embankment is unreinforced. Each reinforced section of the embankment is 10 m wide and the width of the unreinforced section is 15 m. The test embankment was constructed to the designed 14 m height with an initial side slope of 1:1.2 and then cut to a finished slope of 1:0.5 for the lower 6 m and 1:0.8 for the upper 8 m. Reinforcement layers were only placed in the lower 6 m of the fill soil and the upper 8 m of fill was constructed as a surcharge. The test embankment was monitored using strain gauges, displacement bars, settlement plates, inclinometers and extensometers. Strain gauges attached to the geogrids showed that the grid strain became higher as it approached the slope surface. When grids were laid in several rows, the upper ones had higher strain values than the lower ones. The measured horizontal displacements of both the slope and the internal earth decreased as the number of reinforcement layers was increased. When the lower 4 m of the fill was cut to vertical, failures were observed in the test embankment. It was found that the larger the number of the reinforcing layers, the deeper and more severe was the sliding. Grids were observed to break near the sliding surface. Just before sliding, the

horizontal displacement increased to 10 cm and the maximum grid strain to 2 to 3% which was the limit of the strain measurement. The strain at 1.5 m from the inner end of the grid was found to be as small as 0.1 to 0.3% indicating that the length of the grids was sufficient. The test section reinforced with five layers of grids in a checkered pattern was the only section which did not fail. This result indicates that an embankment with the reinforcing grids laid in a checkered pattern is effective from the structural point of view.

Hayden et al. (1991) presented a case history of a high clay embankment with geogrid reinforcement. The embankment, 244 m long with a side slope of 2:1 and a maximum fill height of 23.2 to 24.4 m, was part of a highway. The borrow soils were highly plastic clays with plasticity indices of 20% to 40% and a potential for expansion or swelling. The undrained shear strength of the fill was determined from laboratory tests on compacted samples and effective shear strength parameters were estimated based on literature data and back analyses of existing slopes in the area. The long term stability was considered as the most critical situation and the minimum factor of safety for all slope stability analyses of the critical sections was taken to be 1.3. The embankment was reinforced with different geogrid materials placed in continuous horizontal layers. Design strengths of the reinforcing materials took into account the potential for site damage, material deterioration and creep. The shear strength efficiency factor along the interface between the fill and the geogrids was assumed not smaller than 0.7.

Limit equilibrium methods were used for the stability analysis of the reinforced embankment. An extended version of Bishop's modified method of slices for circular potential failure surfaces was used for the analysis of internal stability while the Janbu method of slices was used for the external stability with non-circular, compound failure surfaces. The main goal of the reinforcement design process was to achieve an optimal layout of reinforcing layers with a minimized reinforcement cost for the required minimum factor of safety. For the final design of the geogrid reinforcement within the full-height of the clay fill, the project was successful with a savings of about \$1.1 million (US) over conventional options.

The embankment was monitored during construction. The instrumentation included extensometers, inclinometers, settlement stakes,

strain gauges and piezometers. Extension strains in the soil, ranging between 0 and 0.8% were in good agreement with the tensile strains, which were less than 0.5% at most locations, in the geogrids. Strains near the slope surface were larger than at locations deep in the embankment. This fact was believed to be related to the expansive nature of the clay soils which had access to moisture at the slope face. The locations of high lateral displacement, measured by vertical inclinometers, happened to fall fairly close to the critical circle predicted by the limit equilibrium method. Even though the implications of this interesting comparison were not clear, it appears to be potentially useful and might eventually reveal something about the relationship between field behavior and limit equilibrium design procedures for reinforced soil structures. From the field measurements and analyses, it was concluded that the small deformations in the soil and the geogrids indicated satisfactory overall performance of the embankment and relatively low levels of load in the geogrid reinforcement. The performance data indicated that deformation has not ceased and it was expected that this large plastic clay embankment would continue to deform as a fully drained soil loading condition gradually developed.

Irvin (1988) presented comprehensive studies on the field behavior of geogrid reinforced soil embankments. A 3 m high instrumented trial embankment, which was founded on and constructed from silty clay (London clay), was built and tested to failure. The trial embankment consisted of four sections: 1:1.5 side slope and unreinforced, 1:1.5 slope and reinforced with 2 layers of Tensar SR2 grid, 1:0.5 slope and reinforced with 3 layers of SR2 grid, and 1:1 slope and reinforced with 3 layers of SR2 grid. The sections were paired back to back and separated by sheet pile cut-off walls to reduce construction costs. Geogrid layers in each reinforced section were placed horizontally and wrapped around the slope surface to form envelopes. The construction of the embankment was completed in four weeks and compaction problems were experienced on the steeper, geogrid reinforced slope faces where it proved impossible to achieve effective compaction to the edge. Various instruments, magnetic extensometers, hydrostatic profile gauges, piezometers and survey points, were used to monitor the performance of the embankment. The instrumentation was designed to provide data on the stability of both reinforced and unreinforced slopes, the deformations and

failure modes of geogrid reinforced embankments, the pore pressure distribution and the influence zones of geogrid layers. Unfortunately, the strains of the geogrids were not measured.

Hydraulic surcharge loading was applied to different sections of the trial embankment. The loading was divided into two phases, pre-critical loading and post-critical loading, in 0.2 to 0.5 MN increments. The response of the slopes to the pre-critical loading was characterized by small quasi-elastic deformations, small internal deformations and profile changes and limited time dependent deformation under constant load. The response to the post-critical loading was characterized by significant elastic and plastic deformations per increment of applied load, high non-linear stress-deformation response, large internal and surface deformations, significant time dependent deformation and development of shear planes. Failure of the test slopes was characterized by rapid increases in the internal deformations, in the horizontal movements of the embankment face and by a residual load appreciably lower than the peak.

From the comparison of field observations and measurements between reinforced and unreinforced slopes, Irvin summarized these common features:

- 1) During dismantling of the trial embankment, it was found that the inclusion of geogrid layers modified the orientation of induced shear planes. Two shear planes, one deep seated and passing through the toe of the slope and the other encountering the face of the slope at approximately mid-height, were identified in the unreinforced slope. In reinforced slopes, induced shear surfaces generally formed adjacent to the base of each geogrid envelope and were confined within individual geogrid envelopes. There was no indication of the shear planes intersecting the geogrid or of shear planes between adjacent geogrid layers.

- 2) Examination of measured displacements indicated that both unreinforced and reinforced slopes deformed by similar amounts under approximately equal applied loads. The inclusion of geogrid envelopes increases the ultimate load, under which the slopes fail, by reducing the transfer of horizontal stresses and displacements from one envelope to another. The inclusion of geogrid reinforcement layers does not contribute

much to the overall strength of slopes until the soil had sheared sufficiently to tension the geogrid.

3) Two distinct phases of displacement were apparent for the unreinforced slopes. All movements are relatively small up to an applied critical load after which the displacement increases rapidly and distinct shear planes develop. The behavior of the reinforced slopes is characterized by three phases of deformation. Small internal and surface displacements up to the critical load are followed by large horizontal displacements of the fill and the formation of shear planes adjacent to the base of the upper geogrid envelope. The soil then moves outwards along the induced shear planes and tensions the geogrid on the face of the upper envelope, which experienced the greatest displacement under loading. These effects occur sequentially down the embankment from one grid envelope to another. The large displacements in the lower geogrid envelopes occur only when the fill within the upper envelope has sheared, the geogrid on the slope surface has been tensioned and the fill material within it has been constrained. It is apparent that the geogrid has less effect if it is placed only in horizontal layers rather than in the form of envelopes which constrain the face of the slope.

4) According to the field observations during testing it is apparent that shear of the fill material occurs above and adjacent to the base of the top geogrid envelope. There was no evidence to suggest shear between the base of the upper geogrid and the top of the lower geogrid.

5) In the reinforced sections with steeper side slopes (1:0.5, for example), the initial movement, before the critical loading, was essentially uniform throughout the embankment and was followed by rapid sequential deformation in each of the geogrid envelopes. In other words, the large displacements in the upper geogrid envelopes were closely followed by large displacements in the lower envelope. This action can probably be explained by the stress distribution induced in the embankment. The dispersal of the vertical stress in the steeper reinforced slopes is likely not as much as in the flatter ones. Consequently, the lower geogrid envelopes reach their critical load under a lower applied load and develop significant movements more closely following that in the upper envelopes.

6) Large post-critical deformation occurred when the vertical stress, acting on each geogrid layer, corresponded to the undrained shear strength of the clay fill, indicating that the inclusion of geogrids does not inhibit the onset of large displacements but does contain these after the geogrid material at the face becomes tensioned. Hence, the overall critical load for a reinforced slope depends on the number of geogrid envelopes and the slope geometry.

7) Geogrid layers do not provide preferential drainage paths by which porewater pressures are more readily dissipated.

After testing, the trial embankment was sectioned to examine induced shear planes, check the integrity of the geogrid fabric and retrieve samples of the geogrid for testing. It was found that bonding between the geogrid and the clay fill was good and damage to the geogrid during construction was minimal. The geogrid showed little evidence of deformation, even in the zones of excessively large horizontal displacements.

Fannin and Hermann (1988, 1990) reported on an instrumented steep sloped reinforced soil wall in Norway. The reinforced wall (2V:1H) with a height of 4.8 m was built of uniformly graded medium to fine sand and founded on gravelly sand. It was reinforced with Tensar grid SR55 as primary reinforcement and Tensar grid SS1 as intermediate reinforcement. The test wall consisted of two sections with different geogrid layouts to examine the influence of reinforcement length and spacing (0.6 to 1.2 m) on stability. The geogrid layers were placed horizontally and fixed to lightweight facing units of steel mesh at the surface of the slope to retain the soil and prevent surface erosion. Load cells, coil gauges and earth pressure cells were used to measure forces induced in the geogrid layers, strains in the geogrid layers and in the adjacent soil and earth pressures in the reinforced soil mass. Displacements at the slope surface were monitored to define the movement of the slope in qualitative terms. The field instrumentation was operated in three stages of testing: self-weight loading, a single load-unload cycle of surcharge of 29 kPa and a permanent surcharge composed of a 3 m high berm of soil on the crest.

Profiles of strains measured in the geogrid layers showed that larger

strains occurred near the slope surface where the grid was connected to the facing units, and the strains decreased to zero at the embedded ends. The magnitude of the strain was typically small and did not exceed 0.8% for self-weight loading and 1.3% for permanent surcharge loading. During the permanent surcharge loading, the largest increases in the reinforcement force were recorded in the uppermost layers and the smallest increases in the base layer. From the field observations and the measurements of strains and forces in the reinforcement and the soil, Fannin and Hermann summarized the following features of the reinforced wall:

- 1) A comparison of measured strains in the geogrid with the strains in the soil shows a good agreement, indicating a good interlock between the geogrid and the surrounding soil.

- 2) A non-uniform spacing of primary reinforcement, in which the spacing between geogrid layers near the base of the slope is smaller, is observed to promote a uniform distribution of force in the layers of reinforcement. In contrast, a uniform spacing of reinforcement mobilizes greater forces in the lower/middle layers than in the middle/upper layers of reinforcement. It implies that there is no significant movement in translation of the reinforced zones; rather each layer of reinforcement accepts the lateral stresses acting above and below it.

- 3) The in-situ modulus of stiffness of a geogrid, which is confined in the soil, can be calculated based on the measurements of forces and strains in the embedded reinforcement. The calculated modulus of stiffness appears to be compatible with the value from isochronous load-strain curves reported for laboratory tests on unconfined samples.

- 4) Creep is observed to take place in the reinforcement.

Fannin and Hermann (1988) described another instrumented test embankment with a height of 6 m and a side slope of 2:1. Four layers of Tensar SR2 grid were used as primary reinforcement, arranged and spaced based on the limit equilibrium design method of Jewell et al. (1984). Tensar grid SS1 was used as secondary reinforcement to provide additional local stability. Primary reinforcement layers were placed horizontally and wrapped around

the slope surface to form discrete envelopes of enclosed soil layers. The comparison of measured grid strains with strains expected in the reinforcement (from the Jewell et al. design method) shows that this limit equilibrium approach makes a significant overprediction of the strains actually mobilized in the reinforcement.

Considerable research has been performed on instrumented reinforced walls. Berg et al. (1986) presented two case histories of reinforced soil retaining walls. Design, construction and performance of the walls were discussed. The walls, up to 6 m high, were built using granular back fill reinforced with a polymer grid, Tensar SR2, and precast full or incremental height concrete facing panels which were set and bolted on to leveling pads. Reinforcing layers were placed horizontally with vertical spacing varying between 0.3 m and 0.9 m and pretensioned. The technique of connecting reinforcing layers to the facing panels was described in detail. Different factors of safety were chosen in the design against rupture, pullout of reinforcement and sliding, bearing capacity, overturning and global failure of the walls. Facing panel movements of the two walls were monitored and it was found that the observed movement, a rotation about a hinged toe, was consistent with the assumed kinematic mechanism of the tie-back wedge analysis. Horizontal soil stresses were measured using load cells to evaluate the magnitude of pressures exerted on the facing panels and on the pinned geogrid connections. It was found that near the toe of the walls, the measured values approached the values predicted with the tie-back wedge analysis; elsewhere, the measured lateral pressures were substantially less than the predicted maximums. Strains, measured using resistance gauges, indicated a distribution of peak geogrid strains that defined an approximate wedge. The measured geogrid strains, less than 1% at all levels, were smaller than those corresponding to the reinforcement tensile forces predicted with the tie-back wedge analysis. Deformations measured using inductance coils at three levels also indicated a line of maximum strains at an angle from the vertical. It was suggested that the use of the tie-back wedge method with a trapezoidal vertical pressure distribution, conventional factors of safety, well compacted granular fills and polymer strengths based on pure creep loading criterion, might be conservative.

Thamm et al. (1990) described a full scale test on a reinforced retaining wall. The trial 3.6 m high wall was backfilled with gravely sand and reinforced with geogrid Tensar SR2. The geogrid layers were laid horizontally and wrapped around the wall surface. After construction the wall was loaded stepwise to failure. Limit equilibrium methods with wedge failure and slip circle failure mechanisms and a plane strain finite element method were used to analyze the stability of the reinforced wall. Various instruments were installed to measure the strains in the geogrid layers and the earth pressure within the reinforced soil mass. The horizontal and vertical deformations of the wall face were monitored by inductive displacement transducers. From the measurements up to the failure load, it was found that the maximum displacement occurred at the middle height of the wall and the failure appeared to be rotational, along a circular or spiral surface. When the wall was loaded near failure, measured horizontal earth pressures showed that the influence of the applied load was mainly restricted to the upper part of the wall. Similarly, the uppermost layer of geogrid developed the largest strain while the bottom layer had the least. From the comparison of the analytical analysis results with the field observations and measurements, it was found that the wedge mechanism reasonably predicted the failure load for reinforced structures subjected to high surface loads. The slip circle analysis overestimated the failure load by around 20% but the failure surface seemed to fit field data well. The two dimensional elastoplastic finite element analysis suitably predicted the load-deformation behavior at load levels up to 80% of the failure load but the prediction of strains in the reinforcement was not satisfactory.

Simac et al. (1990) carried out a full scale test on a 6.1 m high reinforced wall. The wall was built of well graded sand and gravel and reinforced with layers of the biaxial geogrid, Miragrid 5T. The wall was designed with a low factor of safety (1.1 without surcharge loading) to maximize strains and loads in individual reinforcing layers. After construction, the wall was tested by applying an inclined 2.1 m high surcharge. The performance of the wall was monitored using various instruments: strains gauges, earth pressure cells, inclinometers and extensometers. Measurements by the vertical inclinometers and the external survey showed that the maximum horizontal movement occurred on the top of the wall and that a strain magnitude greater

than 1.0% was enough to create an active state of stress in the soil mass. This implies that reinforced soil walls may be designed based on the limit equilibrium model of a tie-back wedge. The strains in the geogrid layers, measured by both strain gauges and extensometers, indicated that the maximum strain occurred at the middle lower height of the wall. The measurements of grid strains appeared to fit the typical behavior for extensible type reinforcement. The reinforcement tension mobilized along a log spiral at low strains and degenerated to a Rankine failure mode as the strains increased and limit equilibrium was approached. Comparison of the predicted magnitude and location of the maximum geogrid force with the field measurements indicated that the Rankine stress distribution appears to be most appropriate for the magnitude and location of the maximum reinforcement force.

Kutara et al. (1990) conducted full scale tests on two reinforced embankments and a reinforced wall. The embankments, 6 m high with 1:1 side slopes, were constructed with silty sand and reinforced with a biaxial polymer grid, Tensar SS2, laid horizontally at different vertical spacings. The wall, 6 m high with a 1:0.2 slope, was constructed using the same fill material and reinforced with a uniaxial polymer grid, Tensar SR55. After the construction of the wall and embankments was completed, they were tested at three stages. A 3 m high vertical embankment was built on top of each reinforced structure as a surcharge. The structures were then submerged in water up to 5.25 m above the base. Finally, the water level was suddenly lowered after several days of submergence. Settlements at the crest and strains in the geogrid layers were measured during the three stages of testing. It was found that the reinforced structures responded to the rapid drawdown of the water table more than to the surcharge and submergence. The maximum settlement increased from 130 mm after submergence to 400 mm at the end of the drawdown. The maximum strain in the geogrids was 0.3% for the embankments and 1.0% for the wall after submergence. It then increased rapidly and exceeded 2%, which was the measuring limit for the strain gauges, during the drawdown. It is interesting to note that, for all three reinforced structures, the maximum strain appeared to occur at the third geogrid layer from the top, while the strain in the bottom grid layer was always significantly smaller than in the layers above.

Field observations and measurements were compared with results of analytical analysis: rotational slip method for the embankments and two-wedge limit equilibrium method for the wall. Kutara et al. summarized their discoveries. For a reinforced embankment, if it is designed by a rotational slip method, with a factor of safety above 1.3 and a design tensile strength for the reinforcement of 40% of the breaking strength, the strain in the reinforcing material would be minimized. If it is designed with a factor of safety of about 1.2, the strain in the reinforcement could exceed 1%. Thus, when a rotational slip method is used in a stability design for a reinforced embankment, assuming 40% of the breaking strength as the design tensile strength of the reinforcing material, it is desirable to assure a factor of safety of 1.2 to 1.3. For the design of reinforced walls, the two-wedge method with a factor of safety of about 1.5 appears to be appropriate. The rotational slip method provides conservative results. When cohesive soils are used as fill materials, the assumption $c=0$ leads to a considerable conservative design and, therefore, is inappropriate. In all cases, the rapid drawdown of the water table significantly decreases the factor of safety and increases the strain in the reinforcing materials.

Burwash and Frost (1991) reported a 9 m high reinforced retaining wall constructed on very stiff low plastic clay till and backfilled with low plastic cohesive soil similar to the foundation soil. The wall had a facade of H-pile and timber lagging and was reinforced with up to 10 layers of Tensar SR2 geogrid with lengths up to 6.8 m. Signs of distress in the wall, such as settlement and cracking of the ground surface, were first observed in one section of the wall 16 months after the wall was completed. Slope indicators placed on the outside face of the wall showed that the facade continued rotating about the toe. It was found through boreholes that the clay backfill in that section had softened to a depth of about 3 m. The water content of the clay fill measured 30 months after completion of the wall was 1.5 to 3% above the optimum or 5.5 to 7% above the placement water content. The saturation of the clay fill occurred by ponding of surface runoff near the face of the wall. The other section of the wall performed satisfactorily. It was postulated that the clay fill behaved as cohesionless backfill until saturated when its strength was significantly reduced. The geogrids were then subjected to excessive strains to compensate for the resulting loss in strength.

Rimoldi (1988) summarized nine instrumented case histories of reinforced soil structures, two steep slopes, one embankment on a weak foundation and six vertical walls. Most of these structures were constructed with granular soils and reinforced with a polymer grid, mainly Tensar SR2. The performances of the reinforced structures were monitored using various instruments, such as strain gauges, extensometers and profile gauges, load cells, and piezometers. The objective was to evaluate some major concerns in design practice, such as stress distribution in the reinforced soil mass, kinematic mechanisms, tensile force distributions along each geogrid layer and long term performance of reinforcing materials. From the review of these case histories, suggestions were made on several aspects:

1) Anticipated geogrid strains, estimated according to design charts, are usually significantly greater than measured values, for overall factor of safety ranging from 1.1 to 1.7. This overestimation occurs especially for cohesive soils where the cohesion is generally ignored for long term stability analysis.

2) If high line loads are applied on the top of reinforced structures, it is better to have more geogrid layers near the top than required by current design methods.

3) For reinforced slopes, the tensile force has a smooth distribution along the geogrids. The maximum value is not at the base but in one of the middle or lower layers. The larger the slope angle, the closer the peak strain location is to the slope surface.

4) For vertical walls with a low magnitude of surface surcharge, the tensile force smoothly increases from the top layer to the bottom one and the locus of the maximum tensile force is a line coinciding with the Rankine failure surface.

5) For vertical walls with a large surcharge, the tensile force diagram has a pronounced peak and the upper layers are in more tension than the lower ones; the locus of maximum tensile force is a line close to vertical.

2.7 Summary

Based on the discussion in the previous sections of this chapter, some major

findings are summarized from the literature review.

2.7.1 Soil Reinforcement Mechanisms

1) The effect of the reinforcement depends upon the orientation of the reinforcement inclusion. The reinforcement increases the strength of the reinforced soil when placed along or close to the direction of the principal tensile strain and weakens the soil otherwise.

2) The friction between the soil and reinforcement due to lateral movement provides a confining stress in the soil.

3) For slopes and retaining walls, the reinforcement strengthens the structures by adding tensile resistance to the soil mass and by increasing soil strength as a result of increased soil confinement. The reinforcement also reduces the transfer of horizontal stress from upper levels to lower levels and modifies the mode of deformation.

4) For an embankment on a soft foundation, the reinforcement increases the factor of safety for bearing capacity, by lowering the horizontal load on the base of the embankment, and reduces lateral spreading and cracking of the embankment. Even though the reinforcement may not reduce the total settlement of the embankment, it bridges weak spots, transfers stresses away from locally weak zones in the foundation and assists soil arching to reduce the risk of localized failure and reduce differential settlements.

2.7.2 Properties of Soil and Reinforcement and Their Interaction

1) Strain compatibility between the soil and the reinforcement must be considered. A simplified approach of accounting for strain compatibility is to specify the tensile strain in the reinforcement according to the relative stiffness of the soil and the reinforcement and the working load of the reinforced structure. A range of 2% to 5% tensile strain in the reinforcement is widely accepted.

2) For geogrid materials, it is appropriate to determine the tensile force in the reinforcement using the load-strain relationship based on isochronous load-strain curves from laboratory unconfined tests.

3) The isochronous load-strain curves are well suited for use in design against long term creep provided the tensile creep tests are conducted under representative working conditions of load and temperature.

4) For fill materials, both peak strength and strength at large strain can be used in limit equilibrium analysis depending on the anticipated strain level in reinforced slopes. For long term stability consideration, the strength at large strain should be used in design.

5) The longitudinal stiffness of the reinforcement has a significant effect on the stress-strain properties of a reinforced soil mass, whereas the bending stiffness does not have an important influence.

6) There are three main mechanisms of soil-geogrid interaction: (a) soil shearing on plane surfaces of the geogrid which are parallel to the direction of relative movement of the soil; (b) soil bearing on surfaces of the geogrid which are substantially normal to the direction of relative movement of the soil; and (c) soil shearing over soil through the aperture in the geogrid.

7) The apparent interfacial friction angles (between soil and geogrid) obtained from direct shear tests are different from those obtained from pullout tests.

2.7.3 Limit Equilibrium Analyses and Factor of Safety

1) The stability problems of reinforced slopes can be divided into two categories: internal and external stability. Internal failure may result from either reinforcement rupture or pullout of reinforcement due to insufficient friction in the resistant or active zones. External stability of reinforced slopes can be analyzed using classical limit equilibrium methods.

2) Circular and bilinear slip surfaces are the two common failure mechanisms assumed in internal stability analyses of reinforced slopes using limit equilibrium methods. A variational limit equilibrium method with a log-spiral failure surface has also been proposed. The variation in the total reinforcement force (required to maintain a desired factor of safety) determined by the different methods is usually small, but the lengths of the reinforcement layers predicted by the various methods differ significantly.

3) According to finite element analyses, the choice of a circular slip surface as a failure mechanism within reinforced soil slopes is reasonable. However, by ignoring the favorable change of stress state due to the higher confining stress provided by the reinforcement tensile stiffness, limit equilibrium methods calculate conservative factors of safety for reinforced soil slopes.

4) The value of the horizontal force in the soil can be locally estimated by assuming the product of the horizontal stress in the soil, which is assumed to have a triangular distribution with depth below the slope crest, and the vertical area of the soil which the reinforcement layer has to maintain.

5) The conventional definition of the factor of safety can be used in stability analyses of reinforced slopes. Both the soil shear strength and the allowable design reinforcement force, which is determined from either the tensile strength of reinforcement or bonding properties, are divided by an overall factor of safety. A conventional overall factor of safety in the order 1.3 to 1.5 is considered appropriate. Partial factors of safety are also recommended to account for variations in the two different types of materials and for strain compatibility.

6) According to a probabilistic study, if designed with the same factor of safety, a reinforced slope would actually be safer than an unreinforced and flatter slope. Therefore, the practice of assuming a reinforced slope is equally safe as a flatter unreinforced slope with the same factor of safety is appropriate but somewhat conservative.

2.7.4 Performance of Full Scale Reinforced Slopes

1) The magnitude of the tensile strain developed in the reinforcement depends on the geometry of a reinforced slope, layout of reinforcement layers and properties of the soil and the reinforcement. For slopes constructed with cohesive soils, the measured maximum tensile strains in the reinforcement are less than 2% to 3% at failure; for granular soil slopes, the maximum strains are generally less than 1%. Anticipated geogrid strains, estimated according to design charts, are usually significantly greater than measured values for factors of safety ranging from 1.1 to 1.7.

2) Reinforced embankments can, under some circumstances, be constructed up to 2 m higher than predicted by conventional bearing capacity theory for unreinforced slopes. The reinforcement is more effective for lower strength soils.

3) The inclusion of geogrid layers in a reinforced slope modifies the orientation of induced shear surfaces.

4) For a case of a reinforced slope constructed with silty clay (London clay), both unreinforced and reinforced slopes deformed a similar amounts under equal loads. The inclusion of geogrid increases the ultimate load by reducing the transfer of horizontal stresses and displacements from upper levels to lower levels.

5) When high external loads are applied on the top of reinforced soil structures, it is better to have more geogrids layers near the top than required by current design methods.

6) The maximum value of tensile strains in reinforcement layers in a slope is not at the base but in one of the medium-low layers. The larger the slope angle, the closer the peak strain location is to the slope surface.

7) Measured tensile strains in geogrids are in good correspondence with the strains interpreted from the measured loads and the isochronous curves of the geogrid material. In other words, the insitu modulus of stiffness of a geogrid, which is confined in the soil, is compatible with the value from isochronous load-strain curves reported for laboratory tests on unconfined samples.

8) Interlock between geogrids and the surrounding granular soil is good.

9) When an expansive soil is used as the fill material, strains near the slope surface are larger than at locations deep in the embankment.

10) The strength of reinforcement samples excavated from embankments some time after construction could be 0 to 50% less than the original values.

11) Geogrid layers do not provide preferential drainage paths by which pore water pressures are more readily dissipated.

Chapter 3. Devon Geogrid Test Fill

3.1 Introduction

Slope reinforcement using geosynthetics is a relatively new construction technique developed during the past two decades. In order to achieve a better understanding of the reinforcement mechanism in cohesive soil slopes and to provide guidance for future design practices, the Devon geogrid test fill was constructed beginning in 1986. The test fill, 12 m high with 1:1 side slopes, is located near Devon, Alberta, approximately 30 km south west of Edmonton. There are four sections in the test embankment (Fig. 3.1), three are reinforced with different types of geogrids, namely Tensar SR2, Signode TNX5001 and Paragrid 50S, and the fourth slope is unreinforced. This chapter summarizes the properties of the fill, the foundation soils and the geogrids. Then, the properties of interaction between the two types of materials are presented. Finally, the details of the construction and the field instrumentation of the test fill are described.

Since the primary objectives of the test fill were to determine how individual layers of geogrid reinforced a mass of cohesive soil and to measure the stress transfer between the soil and the geogrids during the construction of the embankment, the slopes were designed with a low factor of safety so that lateral strains in the soil would develop thus mobilizing the tensile resistance of the geogrids. To ensure that lateral strains occurred and to ensure that each reinforcing layer acted independent of the others, only three primary reinforcing layers spaced at 2 m were installed in the 12 m high fill (Fig. 3.2). This low number of geogrid layers was chosen so that both the local and overall stability of the slope was maintained while allowing the soil to deform.

3.2 Properties of Soils

The properties of the fill and foundation soils were studied by Hofmann (1989). Drained and undrained triaxial compression tests were carried out on compacted samples of the soil used to construct the fill and Shelby tube and block samples of the foundation soils. The main results of Hofmann's studies are summarized in the following sections and details of the laboratory testing are given by Hofmann (1989).

3.2.1 Properties of Foundation Soils

Details of the bedrock and surficial geology in the Devon area are given by Gabert (1968). The bedrock in the area is the lowest member of the Upper Cretaceous Edmonton Formation with alternating bentonitic carbonaceous shales and light grey sandstones containing coal seams. The deposits above the bedrock consist of three major geological units. The soil immediately above the bedrock is sands and gravels, deposits of the North Saskatchewan River. It was overlain by glacial basal till. This till is composed of materials from large granite boulders to fine silty clay and is heavily overconsolidated. A glaciofluvial deposit, well-bedded silts, sands and gravels, was sandwiched into the till as the glacier retreated and advanced again. This was then overlain by the glaciolacustrine sediments of Lake Edmonton. These sediments range from well-bedded sand, silt and clay to till-like materials deposited by melting of ice floating in Lake Edmonton. The geological history of the glaciolacustrine deposit suggests that the soil is normally consolidated. This layer of sediment at the location of the test fill, however, may have become overconsolidated as sand dunes formed and moved across the area.

Boreholes were drilled at the test fill site using a wet rotary drill rig which allowed Shelby tube samples, 73 mm in diameter by 610 mm long, to be taken. A typical borehole profile of the foundation soils is shown in Figure 3.3. The upper most 4.6 m of soil consists of a brown sandy silt to silty clay with some grey pockets. Block samples were taken from this layer of soil at a depth 4.5 m below the ground surface. The average SPT (standard penetration test) blow count in the upper soil indicates that the material is of medium consistency. The variation of water content with depth suggests the presence of a desiccated crust near the surface. The groundwater table is 5 m below the ground surface. This upper soil is underlain by a stiff to very stiff clay till which is heavily overconsolidated. The till is then underlain by a very dense sand beyond a depth of between 9 and 10 m from the ground surface. From the geological profile of the surficial sediments, it was obvious that the deformation of the foundation soils due to the construction of the test embankment would mainly occur in the glaciolacustrine deposits. Therefore, the studies focused on the upper most silt or silty clay.

The upper soil has an average water content of 32%, liquid limit of 37.2% and plastic limit of 23.9%. The dominant particle size of the soil is silt while the clay sizes are only 10 to 20%. According to the results of X-ray diffraction tests, the clay fraction contains up to 50% illite and up to 60% montmorillonite. Field observation in two test pits indicated vertical fissures at a spacing of 10 to 15 cm and horizontal fissures at a spacing of about 15 cm. The former seems to be related to some degree of stress relief and the latter associated with the nature of the lacustrine deposit.

Consolidation tests on the foundation soil were conducted using a floating-ring oedometer, 25.4 mm high by 63.5 mm in diameter. The test were carried out on both block and Shelby tube samples. The specimens were subject to a load sequence which was carefully chosen such that the estimated preconsolidation stress of approximately 350 to 500 kPa could be well defined. A seating load of 5 kPa was applied to each specimen before the dial gauge was set to zero and the specimen was then loaded to the in-situ vertical effective stress. The specimens were allowed to consolidate or swell for 24 hours under each load increment. The vertical strains of each specimen versus time were plotted as log-time and square-root-time consolidation curves and the time to complete 90% of the primary consolidation was obtained. Due to the fact that the immediate deformation and the primary consolidation of the specimens took place within several minutes after each load, the log-time consolidation curves were essentially straight lines which indicated secondary consolidation. Thus, it was only possible to determine the coefficient of consolidation, c_v , from the square-root-time plots for each load step. Moreover, it was difficult to calculate c_v from the consolidation curves at low normal stresses and the accuracy of the calculated c_v is questionable.

The results of the consolidation tests of the upper foundation soil are summarized in Table 3.1. It was observed that the primary consolidation was complete within several minutes. Even though the drainage paths in the field are much longer than in the laboratory, the consolidation of the foundation soil would occur as the embankment was constructed slowly. In other words, high excessive pore water pressures would not be expected to develop in the foundation soil.

Based on the above consolidation characteristics, consolidated undrained triaxial tests with pore pressure measurements were conducted on saturated soil specimens 76 mm long by 38 mm in diameter, obtained from both block and Shelby tube samples. Back pressures of 300 kPa and 400 kPa were used respectively for the block samples and the tube samples and the specimens were sheared at a displacement rate which gave a strain rate of 5.5% per hour. The specimens showed either a hyperbolic or an elastic-perfectly plastic stress-strain behavior. Therefore, the failure was defined by the maximum principal effective stress ratio. The pore pressure during shearing were positive indicating compression of the soil throughout the test. Skempton's pore pressure parameter at failure A_f tended to increase from 0.1 under a low confining stress to 0.83 under a stress of 275 kPa. A summary of the results of the consolidated undrained triaxial test are presented in Table 3.2.

3.2.2 Properties of the Fill Soil

To meet the design requirement that the fill soil deforms sufficiently to induce strain in the geogrids, the upper most foundation soil, silty clay which is relatively soft, in the test site area was selected as the material to construct the embankment. In order to characterize the physical properties and the stress-strain behavior of the fill material, large bag samples were removed from the borrow area. During the construction of the embankment, Shelby tube samples, 25.4 mm in diameter, and a large bag sample were removed from the compacted lifts of fill to determine the properties of the soil actually placed during the construction.

The Atterberg limits and grain size distribution for the fill soil are shown in Table 3.3 and the grain size distribution curves are given in Figure 3.4. Even though the plastic index and the percentage of clay sized particles of the soil from the borrow site are higher than the values of the soil from the test fill, both soils are classified as inorganic clays or silty clays of low to medium plasticity, according to the Unified Soil Classification System. Compaction tests of the fill material were conducted by Bobey (1988) using both the kneading and the dynamic methods. The two compaction methods resulted in essentially the same relationship between dry density and water content. The compaction curves of the fill material were established using the kneading

method and are shown in Figure 3.5. The optimum water content is 20.5% and the maximum dry density is 1.68 g/cm³.

In order to determine how the strength and stress-strain behavior of the fill soil varies with changes in water content and density, unconfined compression tests of compacted fill soil samples were conducted on specimens with a water content ranging between 14% and 22% and a dry density between 1.49 and 1.68 g/cm³. The specimens were prepared using kneading compaction technique. Two 39 mm outer diameter Shelby tubes were pushed into each compaction sample mould and specimens were extruded. The stress-strain curves from the unconfined compression tests vary from one specimen to others as the water content changes. The specimens compacted at water contents less than 18% exhibited brittle stress-strain curves, while the specimens compacted at water contents greater than 18% showed a slightly plastic stress-strain behavior until the maximum shear stress was reached at larger strains and then gradually dropped off. Again, to satisfy the design requirement that the fill deforms extensively without undergoing shear failure, the fill soil had to be compacted wet of its optimum water content of 20.5%.

The variation of the maximum undrained shear strength with changes of water content is illustrated in Figure 3.6. The maximum shear strength of the soil increases with increasing water content up to about 16.5% and then decreases rapidly with further increase in water content. According to the variation in the undrained shear strength, the water content for field compaction was specified at between 22% and 24% (dry density ranging from 1.66 to 1.59 g/cm³) such that the corresponding undrained shear strength would be between 60 and 40 kPa yielding a factor of safety against a shear failure in the 12 m high embankment, immediately after construction, of slightly greater than 1.0.

Unconsolidated undrained triaxial compression tests were conducted on Shelby tube specimens obtained from the compacted fill in the field to determine the variability of the actual shear strength throughout the embankment. The specimens were taken from the bottom 3 m of the compacted fill soil at different locations and elevation levels. Some specimens were saturated using a back pressure to examine the effect of the saturation on

the undrained shear strength of the fill soil. The specimens were sheared at a rate of 0.76 mm/min. The results of the unconsolidated undrained triaxial tests are compared in Table 3.4. The undrained shear strengths of the unsaturated specimens, subject to the same confining stress, showed a considerable amount of scatter, indicating the importance of moisture control in the fill construction to maintain a homogeneous shear strength within the test embankment. The tests conducted on the back pressure saturated specimens showed that neither the undrained shear strength nor the stress-strain behavior was affected by saturation, most likely due to the fact that the average degree of saturation of the soil compacted in the field is 92%.

Unconsolidated undrained triaxial tests were also conducted on laboratory compacted samples prepared from the fill soil. The soil was compacted using the standard kneading method at water contents between 22% and 24% and test specimens were extruded from 38 mm diameter Shelby tubes which had been pushed into the compaction sample mould. The specimens were saturated under a back pressure of 600 kPa and were sheared at a displacement rate of 0.76 mm/min. The specimens tested under confining stresses of 80, 160 and 240 kPa showed approximately the same stress-strain behavior, deviator stresses increasing with strain to large strain values. This stress-strain behavior of the fill soil indicates that the test fill slopes may deform considerably in their undrained state before consolidation commences.

Consolidated undrained triaxial compression tests with pore pressure measurements were conducted on the fill soil to evaluate the pore pressure response during shear. The specimens were prepared, at an average water content of 24%, in the same manner as those prepared for the unconfined compression tests. The specimens were allowed to saturate under a back pressure of 400 kPa for 24 hours prior to consolidation. The consolidation phase under a predetermined stress gave an average t_{90} of 55 minutes and an average coefficient of consolidation of $4.14 \times 10^{-3} \text{ cm}^2/\text{s}$. Once primary consolidation was complete the specimens were sheared at a displacement rate of 0.15 mm/min. without allowing drainage while the internal pore pressures were recorded. Failure of the specimens was defined by the maximum principal effective stress ratio. (The strains at failure defined by the

maximum principal effective stress ratio are about 6% smaller than the failure strains defined by the maximum deviator stress.)

Table 3.5 summarizes the results of the consolidated undrained tests. The stress-strain curves generally show a strain-hardening behavior. There is an initial steep portion in each stress-strain curve which gives a high tangent modulus; beyond about 2% strain, the stress rises slowly with increasing strain to failure. Peaks in the deviator stress of the specimens consolidated above 150 kPa can be observed in the stress-strains curves. The stress-strain curves of the samples consolidated at stresses less than 150 kPa, however, do not exhibit a peak in the deviator stress even up to 24% strain. Corresponding to the stress-strain curves, the pore pressures in the specimens rise sharply below 5% strain and then slowly decrease with increasing strain throughout the rest of the test. The pore pressures developed during shearing increase with increases in confining stresses. Skempton's pore pressure parameter at failure, A_f , increases approximately linearly from about 0.02 to 0.5 with increasing confining pressure.

The results of the consolidated undrained tests were interpreted using the total and effective stress p - q plots and the strength parameters were obtained. The total and effective stress friction angles calculated from the slope of the K_f lines were 17.6° and 28° respectively; the cohesive strength ranges from 23 to 24 kPa in terms of total stress and from 8 to 14 kPa in terms of effective stress.

To evaluate the long term stress-strain behavior of the fill soil, consolidated drained triaxial tests were carried out. The soil was compacted at an average water content of 21% which was 2% lower than that used for the consolidated undrained tests but close to the placement water content of the bottom 3 m of soil in the embankment. The specimens were prepared in the same manner as those prepared for the unconfined compression tests, saturated with a back pressure of 600 kPa, consolidated under different cell pressures and then sheared slowly under drained conditions while volume change measurements were recorded. The stress-strain curves of the consolidated drained tests appear to be hyperbolic, again indicating a strain-hardening behavior. The curves of volume change versus axial strain show that the specimens first contracted and then dilated at high strains. This behavior agrees well with the pore pressure response in the consolidated undrained tests. The results of

the drained tests were represented in the total/effective stress p - q plot and the strength parameters were obtained from the K_f line. The effective stress friction angle ranges from 27° to 28° and the cohesive strength varies from 23 to 27 kPa.

3.3 Properties of Geogrids

Three types of high tensile strength geogrids, Tensar SR2, Signode TNX5001 and Paragrid 50S, were used as reinforcing materials in the test fill. Their physical properties provided by the manufacturers are summarized in Table 3.6. Before the geogrids were used in the test fill, wide strip tensile tests were conducted on the materials and the results are given in Figure 3.7.

Tensar SR2 grids, uniaxially oriented and made by Tensar Corp., are probably the most widely used geogrids for soil reinforcement. The grids begin as a sheet with uniformly pre-punched holes. The sheet is then stressed in the longitudinal direction and, consequently, the holes are elongated in the longitudinal direction. The final draw ratio of about 8:1 causes the high density polyethylene to go into a post-yield state: its molecular structure is highly elongated and in a preferential state so that the strength, modulus and resistance to creep are increased dramatically over the original non-deformed material. This product has desirable properties for applications in which the major principal stress direction is known, such as reinforced slopes and walls.

Signode TNX5001, rectangle grids and a product of ITW-Signode Corp., is made from polyester strips. The longitudinal and transverse strips are ultrasonically bonded to one another forming the junctions. Similar to the Tensar SR2 grids, Signode TNX5001 grids are used when the major principal stress direction is known. Unfortunately, the production of this material was halted by the manufacturer after it was incorporated in the test fill.

Paragrid 50S, square grids and marketed by Mirafi Inc., consists of high-tenacity polyester filaments held together by a polypropylene sheath. At the joints between the longitudinal and transverse ribs, the contacting polypropylene sheaths are melt-bonded to one another. There were defects in the Paragrid material supplied and placed in the test fill. It was found during laboratory tests that some of the high strength fibers in the tension members

were weakened or damaged at the intersections of the grids. This damage was most likely caused by overheating of the polypropylene sheath during the welding process. Because of the defects, the strains developed in the geogrids are highly localized as will be discussed in more detail in subsequent chapters.

Other than the primary reinforcing materials mentioned above, Tensar SR1 and SS1, Signode TNX250 and Paragrid 5T grids were used in the three reinforced sections of the test fill as secondary reinforcing materials to provide additional reinforcement against shallow slope failures and failures of the steep soil slopes caused by the heavy equipment during the construction process. Those geogrids were not instrumented and, hence, detailed discussions on the properties of the secondary reinforcing materials are beyond the scope of this thesis.

3.4 Interaction between Soil and Geogrid

When a soil structure is reinforced with a geosynthetic material, the force in the reinforcement is mobilized by the soil movement through shearing along the interface between the soil and the reinforcement. Therefore, the interaction between the two materials becomes a key factor to understand how the reinforced structure behaves. There are three mechanisms involved when relative movements occur along the interface between soil and geogrid. They include interfacial shearing between the soil and geogrid, shearing between soil and soil in the open areas and bearing resistance of the soil against the anchor (transverse) members of the geogrid. These three mechanisms do not occur simultaneously at all locations along the interface. Different mechanisms are involved at different locations, such as within the active zone or resistant zone, of a reinforced soil structure. More details of the various mechanisms and their involvement within reinforced slopes will be discussed in later chapters.

There are mainly two types of laboratory tests, the direct shear test and pullout test, used for studying the interfacial characteristics between soil and geogrid. Direct shear tests evaluate the overall interfacial shearing while pullout tests examine shearing between soil and geogrid and the bearing of the soil against anchor members. These two types of tests were conducted by Bobey (1988) and Costalonga (1988) to study the interaction between the fill

soil and the geogrids used in the Devon test fill and the results of the studies are summarized in the following sections.

3.4.1 Direct Shear Tests

The direct shear test is a well known and widely accepted method to study interface behavior of soils. A Wykeham Farrance large capacity direct shear machine was modified by Bobey (1988) to study the interface characteristics between the fill soil and the geogrids used in the Devon test fill. The major mechanical details of the shear apparatus are shown in Figure 3.8. A sample dimension of $30 \times 30 \text{ cm}^2$ was chosen to minimize the size effect and to accommodate large open area and aperture size. Vertical load was exerted by a diaphragm air cylinder which is extremely sensitive to small pressure variations. The vertical loads applied from the diaphragm air cylinder to the shear box were measured using a load cell able to monitor the vertical stress to an accuracy of $\pm 0.1 \text{ kPa}$. Shear loads were applied to the apparatus by an electrical motor driving a mechanical screw jack via a 42 speed gearbox which can provide shear displacement rates varying from 0.00012 to 6.1 mm per minute. The loads were applied through a displacement control device and measured by a proving ring which has a capacity of 100 kN and an accuracy of $\pm 10 \text{ N}$ of the shear force. The shear displacements of the two halves of the box were measured by a Linear Variable Differential Transformer (LVDT) which has 50 mm of travel and can measure the horizontal displacement to the nearest 0.005 mm. All measuring devices, load cell, LVDT and proving ring, were calibrated prior to the tests.

Normal stresses of 50, 100, 175 and 250 kPa was chosen to consolidate the testing specimens. These stresses were selected to represent the vertical stresses experienced by a 2.5 m, 5 m, 8.75 m and 12.5 m high embankment, at the foundation interface. A displacement rate of 3.05 mm/min. was chosen to represent the most critical situation of an undrained shear failure at the end of the fill construction. During the early stage of the test program, trial tests were performed to study the influence of sample thickness and numbers of compacted layers. From the comparison of the trial test results, a thickness of approximately 10 cm and three layers of compaction were specified for each sample. A series of preliminary tests demonstrated that to obtain a dry density of 1.68 g/cm^3 , 64 blows per layer had to be applied to the soil using a

4.5 kg manual compaction hammer attached with a 10.2 cm² steel plate. The geogrids were clamped in the shear box such that the tension members were placed in the direction parallel to the shearing while the anchor members were placed transversely to the shearing direction.

The specimens were prepared and the tests were conducted based on the specifications mentioned above. A fresh bag of soil was prepared for each test at a water content of 23.0%. After mixing with tap water, the soil was cured in a moisture room for at least 18 hours to allow moisture content equalization and then sifted through a 12 mm sieve to break up any clumps. The soil was compacted in three layers by applying the blows in four series of 16 blows for each layer. (More details of the sample preparation are presented in Bobey (1988).) The geogrids were placed in the compacted soil along a plane between the top and bottom halves of the shear box, as shown in Figure 3.8. Once the compaction was completed, filter papers, saturated porous stones and loading plates were placed on both sides of the specimen and the shear box was positioned inside the direct shear apparatus. After the load transducer and LVDTs were placed and initialized, the required normal load was gradually applied to the specimen by the diaphragm air cylinder and the vertical compression was measured continuously by the LVDTs until the primary consolidation was complete. The specimen was then set to shear after the normal pressure was checked, the initial readings of the LVDTs and the proving ring were taken and a 2.5 mm spacing between the two halves of the box was achieved by loosening the locating pins and adjusting the spacer screws. The samples were sheared at a rate of 3.05 mm/min. and readings of the horizontal displacements, changes of sample height and shear forces were recorded by a datalogger at specified time intervals. Shearing was ceased when the shear force became constant, or passed beyond a peak and decreased to a constant residual value. The normal load and the measuring devices were removed from the shear apparatus and the relative position of the soil-reinforcement interface and the intended shear plane were checked visually after the test was finished.

The consolidated undrained direct shear tests were first conducted on silty clay samples without reinforcement. The samples were consolidated under stresses varying from 140 to 175 kPa. The dynamically compacted soil showed

either an elastic-perfectly plastic or a strain-hardening stress-displacement type of behavior. The shear strength increased rapidly with increasing shear displacement before it leveled off to achieve a peak value; or it kept increasing slightly after the "peak" strength. Only a few samples which were sheared under normal stresses less than 50 kPa showed a strain-softening type of behavior. The results of the direct shear tests on the compacted soil without reinforcement were compared with the results of the soil with reinforcement to obtain the interfacial shearing efficiency.

The direct shear tests were also conducted on the compacted silty clay samples with reinforcement placed along the shearing surface. Strain-hardening was found to be the typical stress-displacement behavior of the reinforced samples. Similar to the unreinforced samples, the deformations required to mobilize the peak undrained strength increased with increasing normal stresses. The magnitudes of the shear displacements to the peak strength (8 to 17 mm) were also similar to those of the unreinforced samples (8 to 15 mm).

The result of a direct shear test is usually interpreted by Mohr-Coulomb theory:

$$\tau = c + \sigma_n \tan \phi \quad (3.1)$$

where τ is the shear strength, σ_n is the normal stress, and c and ϕ are the strength parameters. Accordingly, the total interfacial shear strength of a reinforced sample in undrained conditions should be expressed as:

$$\tau_T = a (c_G + \sigma_n \tan \delta_G) + (1-a) (c_u + \sigma_n \tan \phi_u) \quad (3.2)$$

where,

τ_T = total interfacial shear strength

a = area of the solid grid (members) in a unit area of the geogrid material

c_G = interfacial adhesion between the solid and the soil

δ_G = angle of interfacial friction between the solid grid and the soil

c_u = undrained cohesion of the soil

ϕ_u = undrained angle of internal friction of the soil

In other words, the total interfacial strength along the shearing plane consists of the adhesion and friction resistance between the soil and the solid reinforcement and the cohesion and friction resistance of the soil in the open area. Due to the lack of published results for large shear box tests on reinforced clays and the lack of knowledge on the contributions of the different components to the total interfacial shear strength, it was impossible to interpret the undrained direct shear tests in the form of equation 3.2. Thus, the results of the direct shear tests on the reinforced silty clay were compared in terms of total interfacial shear strength or the Mohr-Coulomb failure envelope.

The Mohr-Coulomb failure envelopes of the unreinforced and reinforced (with Tensar SR2 or Signode TNX5001) samples are shown in Figure 3.9. The interfacial shear strength of the reinforced clay is less than the unreinforced clay. All failure envelopes are gently curved indicating the nonlinear relationship between the normal stress and the shear strength. It is seen from the figure that the interfacial shear resistances of the Signode reinforced samples are slightly higher than that of the Tensar geogrid. Since the open areas of the two materials are similar to each other (58% or $a=0.42$ for TNX5001 and 55% or $a=0.45$ for SR2), the difference in the interfacial behavior may be attributed to the difference in their aperture sizes. The higher cross-machine-direction aperture size of the Signode material allows more soil-soil shearing to develop than could occur with the Tensar grid. Consequently, a larger overall shear strength developed along the interface. (The adhesion and friction parameters between the soil and the solid reinforcement members, c_G and δ_G , are generally smaller than the cohesion and internal friction parameters, c_u and ϕ_u .)

The interfacial shear strength is generally expressed in terms of efficiency, E_c and E_ϕ , which are defined as:

$$E_\phi = \tan \delta_T / \tan \phi \quad (3.3)$$

$$E_c = c_T / c_u \quad (3.4)$$

where,

E_{ϕ} , E_c = efficiency in terms of friction and cohesion

δ_T = overall friction angle along interface between geogrid and soil

ϕ = internal friction angle of the soil.

c_T = total cohesion or adhesion along interface

c_u = cohesion of the soil

Data in the literature show that E_{ϕ} ranges from 0.4 to 1.0 and E_c from 0.1 to 0.9 and vary with the applied normal stress, particle size and geometry of the reinforcement. Hence, for simplicity, the efficiency is expressed in terms of total interfacial shear strength:

$$E = \tau_T / \tau \quad (3.5)$$

where τ_T and τ are the total (overall) interfacial shear strength and the shear strength of the soil respectively. The efficiency of the interfacial shear resistance for each reinforced test is shown in Figure 3.10. It ranges from 0.74 to 1.0 and appears to decrease with increasing normal stress. The efficiency of the Paragrid 50S material is greater than the other geogrids most likely due to its larger open area and aperture size. When the area of the solid grid is small, there is more soil to soil interaction. As a result, the interfacial shear strength approaches that of the unreinforced soil and the efficiency approaches unity. If this area becomes large, the shear strength is dominated by the friction between the soil and the reinforcement material and the interfacial behavior is characterized by the parameters of c_G and δ_G .

The consolidated undrained direct shear tests on compacted fill samples with and without reinforcement provided a way of evaluating the interfacial behavior between the soil and the geogrids. The tests determined the interfacial shear strength in terms of efficiency. The efficiency of the three reinforcing materials ranges between 0.74 and 1.0 varying with the normal stress and the geometry of the materials. The presence of the reinforcement seems not to significantly affect the strain-hardening behavior of the soil nor the amount of the horizontal shear displacement required to mobilize the peak strength. Other than the soil properties, the geometry of the geogrid material

seems to have the most important influence while other factors, such as the surface roughness and the thickness of the anchor members, have only minor effects on the measured interfacial behavior.

3.4.2 Pullout Tests

Pullout test is another important method of evaluating the interaction between soil and reinforcement. In the category of internal stability problem, of geogrid reinforced slopes, there are three possibilities of failure: sliding of a soil mass along the geogrid surface, tearing or rupture of the reinforcing materials and pullout of the geogrid from either the active zone or the resistant zone. In the last mode of failure, the reinforcement functions to bond together the resistant and active zones. Therefore, it must have an adequate capacity to resist pullout from the surrounding soil. The pull-out test seems to be the most appropriate test to model this type of interaction between soil and reinforcement.

The typical configuration and the basic mechanisms of a pullout test are shown in Figure 3.11. There are two mechanisms of interaction involved in the test: shearing between the soil and the solid grid members and bearing of the soil against the anchor members which is similar to the interaction at the base of a deep foundation in soil. The total pull-out resistance mainly depends upon the properties of the soil, the geometry of the reinforcing material and the normal stress acting along the reinforcement plane.

The pullout force and the corresponding displacement are the two major measurements made during the pullout tests. The results of the tests can be interpreted in several ways. They are often used to determine the bonding between soil and reinforcement, but they are also used to estimate the distribution of the tensile force along the reinforcement. In drained conditions, the total pullout force (particularly for Tensar geogrid) can be expressed as (Mitchell, 1987):

$$P = L_e \cdot b \cdot \gamma \cdot z [2a \cdot \tan \delta_G + t \cdot a_b \cdot \sigma'_b / (\sigma'_n \cdot S_x)] \quad (3.6)$$

$$\text{for } 5 < \sigma'_b / \sigma'_n < 100$$

where,

P = total pullout force or pullout capacity

L_e = effective embedded length of reinforcement

b = width of reinforcement

γ = unit weight of soil

z = depth

σ'_b = bearing effective stress on anchor members

σ'_n = normal effective stress on reinforcement

S_x = space between two consecutive anchor members

a_b = fraction of geogrid width over which bearing surface extends

t = thickness of anchor member

The first term of the equation ($L_e \cdot b \cdot \gamma \cdot z \cdot 2a \cdot \tan \delta_G$) represents the shear resistance between soil and solid reinforcement members while the second term represents the bearing resistance of the soil against the anchor members. Bearing capacity theory gives the lower and upper bound for σ'_b/σ'_n . The values of σ'_b/σ'_n can be obtained from pullout tests and the bonding between the two materials is estimated in terms of coefficient of bond f^* :

$$f^* = a (\tan \delta_G / \tan \phi) + t \cdot a_b \cdot \sigma'_b / (\sigma'_n \cdot S_x \cdot 2 \tan \phi) \quad (3.7)$$

By knowing the values of δ_G and σ'_b/σ'_n from pullout tests and other tests, such as direct shear tests, not only the pullout capacity can be determined, the contributions of the two components to the pullout capacity can also be estimated.

In undrained conditions, the total pullout force can be similarly expressed as (Ingold, 1980):

$$P = N_c \cdot c_u \cdot \Sigma a_b + \beta \cdot c_u \cdot \Sigma a \quad (3.8)$$

where,

N_c = undrained bearing capacity factor

β = interfacial stress factor

The first term of equation 3.8 represents the undrained bearing resistance of the anchor members while the second term relates to the surface adhesion, βc_u , generated on the surface area parallel to the direction of pullout. The values of N_c and β can be determined based on pullout or other tests and the undrained pullout capacity can be estimated using equation 3.8. Table 3.7 shows the values of the interfacial stress factor from consolidated undrained direct shear tests reported by Costalonga (1988).

To study the interaction behavior between the fill soil and the geogrids used in the Devon test fill, a series of pull-out tests were conducted by Costalonga (1988) using a modified large direct shear test apparatus. The pullout box is 106 cm long, 36 cm wide and 20 cm deep. The front and back plates of the pullout box are 1.27 cm thick each with a 2 cm high slot that runs the full width of the box. The middle height of the slots coincides with the middle height of the soil sample. Vertical loads were applied to the pullout box using two symmetric lever systems and weights through a flexible loading system which consists of a series of prismatic elements forming a pyramid shaped loading head. This loading system allows differential settlement and ensures a uniform distribution of the normal stress on the sample. Horizontal pullout forces were applied by an electric motor and measured using a load cell (capacity of 4500 kg) mounted between the travel arm of the motor and the jaws which grab the geogrid. In order to prevent slippage of the geogrid and to minimize stress concentration at the grabbing point of the geogrid, different steel jaws were designed to fit different geogrids.

The geogrids and the entire pullout box were well instrumented during the tests. LVDTs were used to measure displacements of the geogrids at different locations outside the box. They were also used to monitor the consolidation settlements of the soil samples and the changes in height during a pullout test. The deformations of the geogrids inside the sample box were measured using LVDTs attached to prestressed wires which passed through the soil sample and were attached through holes drilled at the center of the anchor members. In addition, four load cells were installed inside the front end of the pullout box to

measure the soil pressure acting on the front end and to evaluate the passive force developed in the soil.

Before the pullout tests were carried out, calibration tests were conducted to examine the performance of the apparatus and the instrumentations as well as to check the consistency of the strain rate. A strain rate of 3%/min. (12 mm/min.) was selected to ensure undrained test condition. Due to the limitation of the capacity of the pullout reaction frame, confining stresses of only 20, 50 and 100 kPa were used during all tests.

The silty clay taken from the borrow site of the Devon test fill was used in the pullout tests. The soil was air dried, crushed and mixed with water to the final moisture content which ranged from 24% to 25%. It was then kept in a moisture room for water content equalization before it was compacted in the pullout box. Immediately after approximately 1.15 kg of soil was placed in the box, the soil was compacted dynamically using a 4.5 kg hammer with a steel plate (12 x 12 cm²) attached to one end at a drop height of 17.5 cm. 440 blows were applied to each compaction layer and the dry density ranged from 1.49 g/cm³ to 1.58 g/cm³. When the compaction of the first layer was finished, the layer was leveled. After half of the second layer was placed, the geogrid sample was placed on the top of the loose soil and the horizontal loading system was assembled. The other half of the soil was then placed and the layer was compacted. The third layer of soil was placed and compacted following the same procedures as the first layer and the finished sample had a final thickness of about 10 cm. A polyethylene sheet was placed on the top of the sample and wax was used in both the front and back slots in the test apparatus to prevent loss of water from the soil during the test.

The vertical load was applied immediately after the completion of the compaction and leveling and the sample was consolidated under the preselected normal stress. When consolidation was complete, the horizontal load was applied and the geogrid was pulled out of the soil at the designated displacement rate. The pullout force, the deformations of the geogrids inside and outside of the box and the vertical displacement of the sample were monitored by the instrumentations and recorded continuously using a datalogging system. When the test was finished, the sample was unloaded, all instrumentations were removed and the soil in the box was removed for post-

test observation. Evidence of slippage and bearing failure of the soil against the anchor members of the grids were clearly observed.

The three types of geogrids, Tensar SR2, Signode TNX5001 and Paragrid 50S, used in the Devon test fill were tested by Costalonga (1988) and the results of the pullout tests on the silty clay with SR2 and TNX5001 were analyzed. The results of the samples with Paragrid 50S were not analyzed since the grids failed prematurely because of the damage at the junctions which resulted during the geogrid manufacture. A summary of the laboratory pullout test data is presented in Table 3.8. The average initial water content of the test soil is 24.9% and the average dry unit weight is 15.1 kN/m^3 . The samples had an average saturation of 89.6%. Consolidation of the specimens under the normal stress was small, averaging around 3.8% vertical strain.

The load - displacement curves of the specimens with SR2 and TNX5001 are shown in Figure 3.12 and 3.13. It is seen from the figures that the failure occurred by pullout rather than rupture of the geogrids. Comparing the curves using SR2 with the curves using TNX5001, it was found that the pullout resistance develops faster for the geogrid with higher modulus (Signode TNX5001). The pullout curves of TNX5001 show a nearly elastic perfectly plastic shape with the peak pullout resistance mobilized at a pullout displacement (outside the box) less than 20 mm. The curves of SR2 show a hyperbolic shape: the pullout resistance increases with increasing displacement until it reaches a peak value at a displacement which varies between 40 and 60 mm.

Horizontal displacements of the anchor members inside the pullout box were measured by LVDTs and designated as progressive displacements (implying that the displacements of the anchor members near the end of the geogrid layer are smaller than the anchor members closer to the front of the pullout box). The progressive displacements versus the pullout displacements are shown in Figure 3.14 and 3.15 for Tensar SR2 and Signode TNX5001 geogrids respectively. Figure 3.16 and 3.17 show the progressive displacements developed in the two geogrids versus the pullout force. It is obvious that the anchor members close to the front of the pullout box displace more than the anchor members within the soil mass. The differences in the displacements between adjacent anchor members give the elongations of the grid which are

directly related to the tensile force developed in the grid. It was found from the measured data that the progressive displacement curves of the SR2 grid are more varied than the curves of the TNX5001 grid. This indicates that the SR2 grid underwent larger tensile deformations than the TNX5001 grid during the pullout experiments. The parallel and nearly straight lines in Figure 3.15 show that the Signode geogrid behaves during the pullout tests like a rigid mesh. Even though the TNX5001 grid has a larger open area and cross-machine-direction aperture size and, consequently, a larger interfacial bonding efficiency (Bobey, 1988), the pullout capacities of the two geogrids are similar to each other, because the larger deformation in the SR2 grid mobilizes the shear resistance in a larger volume of soil and a higher interfacial resistance since more geogrid participated. This feature has an important implication in design practices, as will be discussed in subsequent chapters.

The results of the pullout tests, performed on the soil and the geogrids used in the Devon test fill, were further interpreted by Costalonga (1988) using a load transfer approach. The entire length of the embedded geogrid was divided into a number of elements. The total pullout force was expressed by equation 3.8 for the undrained test conditions. The interfacial stress factor, β , between soil and geogrid was assumed to be 0.5 and the bearing capacity coefficient, N_c , to be 7.5 based on data previously reported in the literature. The soil shear strength was assumed to be a function of the displacement of the geogrid and a hyperbolic relationship $y=ax/(b+x)$ was used to model the mobilization of the soil shear strength. The behavior of the tensile force versus deformation of the geogrid was also assumed to be hyperbolic, i.e.,

$$F_i = a \cdot \epsilon / (b + \epsilon) = A_i (a(X_i - X_{i+1})/L) / (b + (X_i - X_{i+1})/L) \quad (3.9)$$

where,

F_i = pullout force at the beginning of element i (from the pullout test)

a, b = curve fitting parameters from tensile test of the geogrid alone

A_i = cross section area of element i

X_i = displacement of element i (from the pullout test)

X_{i+1} = displacement of element $i+1$, unknown

From equation 3.9, the value of X_{i+1} is calculated. For the soil:

$F_i - F_{i+1}$ = mobilized shear force along element i

$$F_i - F_{i+1} = 2\beta \cdot A_{pi} \cdot A \cdot X_{i+1} / (B + X_{i+1}) \quad (3.10)$$

where,

F_{i+1} = tensile force at the beginning of element $i+1$

A, B = curve fitting parameters of soil shear strength

A_{pi} = plan area of element i

At junctions, the shear resistance in the soil includes two components:

$$F_i - F_{i+1} = (2\beta \cdot A_{pi} + A_{bi} \cdot N_c) A \cdot X_{i+1} / (B + X_{i+1}) \quad (3.11)$$

where A_{bi} = bearing area of element i .

From either equation 3.10 or 3.11, the value of F_{i+1} is obtained. Substituting the axial force transferred, F_{i+1} , into equation 3.9, the displacement X_{i+2} is calculated. The process is carried on until the last element. If the calculated force in this element (at the end of the geogrid length) is not zero, the calculation is repeated using different values of F_i and X_i from the original pullout test results. When convergence is achieved, the displacements and the tensile forces along the length of the geogrid are estimated.

The parameters used in the analyses of the load transfer approach and some results of the calculation are summarized in Table 3.9. The predicted displacements along the embedded length of the geogrids were compared with the measurements from the pullout tests and the agreement was favorable. It was, therefore, concluded that the load transfer method can be used to predict the pullout mechanism of a soil-geosynthetic reinforcement system and to assist in the design of the required embedded length of a geogrid. The contribution of each interaction mechanism between the soil and the geogrid to the total pullout force was also evaluated assuming that the values of $\beta=0.5$

and $N_c=7.5$ were reasonable. It was found that for the Tensar SR2 grid, 79% of the maximum pullout force was due to shear along the surface of the grid while the same mechanism represented 88% for the Signode TNX5001. In other words, for the types of soil and geogrids used in the pullout tests, the mechanism of shearing along the planar surface of the grids prevails over the mechanism of bearing of the soil against the anchor members.

3.5 Construction of the Test Fill

The construction of the Devon test fill was commenced in the summer of 1986. Prior to the fill construction, a number of boreholes were drilled in the foundation soils and Shelby tube samples and auger samples were taken for soil identification and laboratory testing purposes. Soil block samples were also taken from the foundation. The foundation instrumentation was then installed to establish the zero reference values. Four concrete monuments, one at each test section, and a bedrock benchmark for survey purposes were installed and field survey was carried out. In addition to the field work, wide strip laboratory tensile tests were carried out on the three types of geogrids, Tensar SR2, Signode TNX5001 and Paragrid 50S, to obtain the force-displacement curves.

As shown in Figure 3.18, the construction of the test fill was carried out in three stages. The site and foundation preparation was started on June 8, 1986 with grading of the site to a foundation elevation of 702 m. The horizontal instrumentation pipes were installed on the ground level prior to the placement of the fill soil. On September 4, 1986 (day 0) placement of the embankment fill began. The fill soil was hauled from the borrow area by dozer pulled scrapers and dumped on the fill site. The soil was then spread using dozers and compacted by a four wheel compactor. A small dozer and a small compactor were used along the edge of the slopes and near the locations of the vertical instrumentation. The fill was usually placed and compacted in lifts varying between 0.15 m and 0.4 m. Field density tests (nuclear and in-situ methods) were conducted and the water content of the fill was monitored for quality control purposes during the construction. Due to the rainy weather during the summer, the fill placed was often wet of the designed water content range. Thus, the soil was spread and left for a period of time to reduce the water content before it was compacted. When the fill height reached 1 m, the

fill was leveled using a dozer. The leveling was carried out under the supervision of surveyors to ensure the elevation control. The bottom primary reinforcement geogrid layer was then laid on the top of the soil and the cables were attached to the strain gauges, which had been previously bonded to the geogrids in laboratory before the instrumented geogrid sections were shipped to the fill site. A set of field readings were taken as the initial measurements immediately after the instrumented geogrids were laid out. More fill soil was placed and compacted on the top of the first primary reinforcing layer and the embankment was constructed to a height of 3 m on October 23, 1986, when construction stopped due to the onset of freezing air temperatures. The horizontal soil instrumentation and one layer of secondary reinforcement geogrids were placed at the 2 m level during the first construction season.

The construction of the test fill was resumed on August 30, 1987. The top sandy soil was removed with a bull dozer and new fill was placed and compacted. The fill was then leveled at the 705 m elevation. The second or middle primary reinforcement layer of geogrids was placed at the 3 m level and all cables were connected to the strain gauges. Fill soil was then placed and compacted on the top of this reinforcing layer, following the same procedures mentioned above, after the initial strain gauge readings had been taken. When the fill height reached 5 m, the fill soil was again leveled to allow the placement of the top primary reinforcement layer. The same procedures were carried out and the fill height reached 6 m at the end of the second construction season on November 3, 1987. The horizontal soil instrumentation and one layer of secondary reinforcing geogrid was placed at the 4 m level during the second construction season.

The construction of the test fill continued in the summer of 1988. The additional 6 m of soil was filled to reach the 12 m design height on October 29, 1988. Six layers of secondary reinforcing geogrids were placed during the 1988 construction season. Due to rainy weather and the limitation of available construction time, the top 6 m of the fill soil was placed and compacted considerably wet of the design water content and at larger lifts than used in the bottom 6 m of the fill. No quality control tests were conducted during the summer of 1988 and the construction was not closely inspected. The water

content of the top 6 m of the fill was estimated at about 3 to 5 % higher than the bottom 6 m of the fill.

There were several problems during the construction of the test fill. Firstly, due to rain, the water content of the fill varied significantly from one location to another in the fill. Secondly, when the fill was too wet, some drier soils were added and mixed with the wet soil. Finally, because of the steep side slopes, the compaction of the fill along the edge of the slopes was poor compared to the soil in the fill center. All the above problems reduced the consistency and uniformity of the properties throughout the test fill.

After the fill construction was completed, surface protection and erosion control materials were placed on the surface of the test fill during the fall of 1988 and the spring of 1989. During the rainy season in the early summer of 1989, some surface movements of the soil occurred, especially at the instrumented sections. The soil movements occurred mainly in the bottom 6 m of the fill and were about 0.5 m deep and parallel to the slope surface. Horizontal extensometer and inclinometer tubes at the ground level and the 2 m level were covered by the debris requiring some repair work to be carried out. The instrumentation was recovered by hand-digging and the field measurements were carried on. During the summer of 1990, similar but more severe surface soil movements occurred. Although the depth of the movements remained about 0.5 m, the movements migrated along the surface soil to the 8 or 9 m level and more soil was involved on the slope surface. A great effort, including hand and machine work, was required to finally recover the instrumentation. The surface movements again occurred during the summer of 1991 and more debris accumulated at the toe of the slopes.

These surface movements were most likely related to the weakness within the surface soil caused by cyclic freeze-thaw of the surface soils. When freezing penetrated into the soil, ice lenses likely formed parallel to the slope surface. Upon thaw, the shear strength of the soil decreased while the permeability of the soil parallel to the slope surface increased, which provided conduits for water infiltrated during the rainy periods. As a result, the surface soil moved down the slopes. Both the primary and secondary reinforcing geogrids were unable to prevent this type of soil movements. Also the surface protection and erosion control materials were ineffective.

Some possible minor instabilities in the unreinforced slope were observed. In the summer of 1989, tension cracks were found near the crest of the unreinforced slope. The cracks were several centimeters wide and several meters long parallel to the crest. Tension cracks were also observed on the slope surface about 1 to 2 m below the crest. In July 1989, the extensometer access tube at the 4 m level became blocked at a location about 4 to 5 m from the slope surface in the unreinforced section following a heavy rainfall. During the summer of 1990, the tension cracks near the crest of the unreinforced slope became wider and more cracks developed on the surface beyond the crest. At the same time, the tension cracks on the slope surface became longer and more obvious. In May of 1991, after a heavy rain fall, a shallow soil movement occurred in the unreinforced slope. A back scarp could be seen on the slope surface about 1 to 2 m below the crest. A series of tension cracks parallel to the crest were observed on the top of the fill beyond the crest. The maximum width of the cracks was about 10 cm and the crack closest to the center line of the test fill was about 2 to 3 m beyond the crest of the slope. There was no such obvious instability observed in the reinforced sections.

3.6 Field Instrumentation of The Test Fill

Extensive instrumentation was installed to monitor the performance of the foundation, the fill soil and the geogrids. The instrumentation includes electrical wire resistance strain gauges, inductance coils, multipoint magnetic extensometers, inclinometers and pneumatic piezometers. Field surveys were carried out during and after the fill construction as a part of the field instrumentation to assist in understanding the readings from the instrumentation. The layout of the instrumentation in the test fill is illustrated in Figure 3.19 and 3.20. The main goal of the instrumentation was to record the overall deformation of the fill and the foundation soils, the interaction between soil and geogrids, and the pore pressure response within the test fill. The following sections discuss the details of the field instrumentation.

3.6.1 Electrical Wire Resistance (EWR) Strain Gauges

Electrical wire resistance strain gauges, code number CEA-13-250UN-350, made by Micro Measurements Group Inc., were used on the longitudinal members of the geogrids placed in the test fill. This type of general purpose strain gauge has a wide range of operating temperature (-75°C to $+205^{\circ}\text{C}$) and a large range of strain (up to 5%). They are less expensive than other types of EWR strain gauges with specified features. The readout system is based on the principle of the Wheatstone Bridge; a quarter bridge system with a minimum reading of ten microstrain units was adopted in this program.

Each strain gauge was bonded to the longitudinal member of geogrids using epoxy (AE 10/15 adhesive, made by Micro Measurements Group Inc.) after pretreating the surface by sanding, cleaning, degreasing and neutralizing (Soderberg, 1990). The gauge was then sealed with a waterproof rubber coating after the electrical leads had been soldered. A pair of aluminum splints were installed to protect the gauge from damage during transportation and installation of the geogrids in the test fill. The splints were removed during installation and the gauges were covered with a piece of styrofoam to protect them from damage during fill placement. At each instrumented location, a pair of strain gauges were installed on the top and the bottom of the longitudinal member to monitor the elongation as well as bending of the geogrid. Since the mechanical properties of the geogrids are temperature dependent, a thermocouple was placed with each pair of strain gauges. Dummy electrical strain gauges were also installed in the test fill at 0.5, 1 and 5 m distances from slope surface to account for temperature influences in the strain gauges.

Figure 3.20 shows the locations of the EWR strain gauges. The instrumentation positions began at 0.5 m and then were spaced at 1 m intervals beyond 1 m from the slope surface. The strains were measured, in units of 10 microstrains, by a readout box, model P-3500, made by Measurements Group, with a gauge factor of 2.12 and balance setting of 0.979. In order to overcome systematic errors, the same readout box was used in the majority of the field measurements. On occasions when a different readout box had to be used, the

field readings were adjusted using the readings obtained from the dummy field strain gauges.

Initial or zero field readings were taken for each gauge immediately after the layer of geogrid was laid out on the test fill. The differences between the initial readings and the subsequent readings gave the strains which developed in the geogrids due to loading applied by the embankment soil. The apparent strains, which were calculated from the measured temperature increments and the coefficient of thermal expansion of the geogrid-gauge system, were subtracted from the measured strains. At each location, an average grid strain was obtained from the measurements of the top and bottom gauges. When one of the two gauges failed, the representative strain was determined from the sum of the average before failure and the increments of strain measured in the remaining gauge. In a total of 96 strain gauge locations, there were only 8 locations where both EWR strain gauges failed to work.

4.1.2 Inductance coils

Inductance coils, model 4101A, made by Bison Instruments Inc., were used to monitor strains across adjacent transverse members of the geogrids. The coils measure the electromagnetic coupling between two sensors of 5.3 cm in diameter and 0.68 cm in thickness. The coupling is extremely sensitive to axial distance between the sensors; it is capable of measuring strains from 0.01% to as large as 50%. This range is greater than the working range of the EWR strain gauges and is not influenced by moisture content and temperature variation within the soil, as claimed by the manufacturer. The coils have other advantages, such as a durability, low costs and ease of installation and operation. The readout indicator is hand-portable and completely self-contained.

The inductance coils installed were designed to measure axial strains between two sensors. In other words, the pair of disk shaped sensors are designed to be placed in parallel and coaxial orientation separated by a distance over which the strain is averaged. In the case of monitoring the strain in a layer of geogrid, however, the relative transverse movement between the sensors is measured, i.e., the pair of sensors have to be placed

approximately in the same plane. To evaluate the accuracy and sensitivity of the inductance coils to the transverse movement, a series of calibration tests were conducted before installing the coils. Figure 3.21 and Figure 3.22 show calibration curves indicating the relationships between the amplitudes in the readout indicator and central distances of two sensors. The calibration tests were conducted on two sets of inductance coils and the results were consistent and repeatable. From calibration tests, it is found that the minimum detectable strain is between 0.02% to 0.05% within the range of working distance between sensors in the test fill.

Inductance coils were attached to the geogrids by plastic bolts placed through the center of adjacent transverse members. They were placed at the same depth, several centimeters from the EWR gauges. Electrical leads were connected after the geogrids were placed in the field. The coils were protected in the field using plywood and styrofoam. Initial readings were taken immediately after the completion of field installation. Measured amplitudes from the readout indicator were converted into distances between sensors according to the calibration curves. The distances measured thereafter were compared with the initial distances and displacements and strains, developed in the geogrids due to construction and load transfer within the test fill, were calculated. Between August 1986 to September 1990, only 10 from a total of 87 inductance coils failed.

4.1.3 Inclinerometers

Two types of inclinometers were used in the test fill. A horizontal digital uniaxial inclinometer, model P/N 50329, made by Sinco Slope Indicator Co. and operated in a 7.2 cm inner diameter casing which was installed during the construction, was employed to measure vertical deflections between two pairs of supporting wheels (61.0 cm apart). Measurements were taken from one side of the embankment to the other with the wheels of the sensor running along a set of grooves nearly vertically oriented over the entire length of casing. A vertical digital biaxial inclinometer, model P/N 50325, made by Sinco Slope Indicator Co. and operated in a 5.9 cm inner diameter casing, was used to monitor horizontal deflections between two pairs of wheels (61.0 cm apart), in directions parallel and perpendicular to the axis of the embankment. Measurements were taken from the top of casings to the bottom

with wheels of the sensors running along a set of grooves oriented either parallel or perpendicular to the axis of the embankment.

The layout of inclinometer casings is shown in Figure 3.19. The horizontal inclinometer casings, model 51103, were installed at levels 0, 2, 4 and 6 m above the ground surface, i.e., at levels 1 m below and above the geogrid layers, continuously from one side of the fill to the another. The vertical casings, model 51111, were placed beneath the toe and the crest of the slope in each instrumented section. Each vertical casing was installed to a depth 12 m below ground surface to ensure that it was founded in the stiff soil and its bottom would not be displaced laterally by the test fill.

Deflections in both the horizontal and vertical casings were detected by accelerometers contained within the sensors and the output signals were recorded using a digital indicator read at the surface of the fill. Field readings were taken for opposite directions, in which the accelerometers were facing, to eliminate zero errors caused by either the sensors or the indicator. Field records from the digital indicator were interpreted into deflections according to calibration test results obtained in the laboratory. Initial deflections were subtracted from the measurements and therefore, the soil deflections due to the embankment were obtained. From calibration tests, it was found that accelerometers and the indicator are capable of detecting an angular deflection of 0.003 degree, or 0.03 mm relative displacement over a 61.0 cm distance.

4.1.4 Magnetic Extensometer

Magnetic probe extensometers were used to monitor horizontal and vertical movements of the fill and foundation soils. During construction of the test embankment, ring magnets, made by the Department of Civil Engineering, were placed in the foundation soils (through a borehole) and in the fill soil at locations where soil movement was to be monitored. A PVC central access tube was then placed in each installation. A sensing probe incorporating a reed switch traveled within the access tube and sensed the position of magnets along the outside of the tube. The reed switch closed on entering the magnet field, activating a buzzer at the surface. A steel measuring tape used to suspend the probe measured the distance from the

collar of the access tube to each magnet. The accuracy of the steel measuring tape is ± 1.0 mm.

The layout of extensometer access tubes is the same as the inclinometer casings as shown in Figure 3.19. Along the vertical access tube, the bottom magnet, used as a datum to measure the relative vertical displacements of the magnets placed above, was placed 11 m below the ground surface in the stiff till. During the 1988 construction season, the horizontal access tubes at the 6 m level and the vertical access tubes beneath the crest of all test sections were damaged. The access tube at the 4 m level in the south part of the test fill was blocked during the summer 1989 at a location 2 to 4 m from its west end due to localized excessive vertical soil displacements within the test embankment.

The magnetic extensometers measured the distances between magnets and the collar of the access tube. When the horizontal displacements of the fill were measured, the probe was pulled through an access tube from one side of the embankment to the other and the distances between magnets and one end of the access tube were measured. A tension of 45 to 60 Newtons was applied onto the steel measuring tape. To eliminate systematic errors, the horizontal and vertical measurements were taken with the probe approaching the magnets from the same direction during all field measurements. Measured distances between the magnets and the collar of the access tube were converted into distances between a reference magnet and the other magnets allowing the soil displacement to be calculated when the initial distances the measured distances were subtracted from the measured distances.

4.1.5 Piezometers

Pore pressures within the fill and foundation soils were monitored by pneumatic piezometers. Pore pressure transducers, model 51417 and made by Sinco Slope Indicator Co., were placed at locations where pore pressures were to be measured. The reading station was coupled to the pore pressure transducers by means of twin nylon tubing covered by a common water-proof polyethylene jacket. A readout indicator, model C-6300 and made by Terra Technology Corp., was employed as the readout terminal. The indicator is hand-portable with a self-contained air-pressure tank and a resolution of ± 1 kPa.

Figure 3.19 shows the layout of piezometers in the four sections of the test fill. Measurements were taken during, immediately after the construction as well as at regular time intervals after completion of the test fill. To eliminate pressure loss in the access tube, a low flow rate was maintained during the field measurements. The piezometers performed well: only 4 in a total number of 55 piezometers failed during the research program.

Parameters	Stress Range (kPa)	Block Sample	Tube Sample
Pc' (kPa)	-----	458	417
Cc	800 - 1600	0.535	0.344
Cr	20 - 500	0.053	0.015
t90 (min.)	500	1.96	0.84
	800	2.43	1.24
Cv (cm /s)	500	0.01	0.024
	800	0.008	0.018
Mv (m /kN)	500	1.61E-4	8.36E-5
	800	1.41E-4	9.23E-5
K (cm/s)	500	1.57E-7	1.98E-7
	800	1.03E-7	1.55E-7

Table 3.1 Results of Consolidation Tests on Upper Foundation Soil
(from Hofmann, 1989)

Specimen type		c (kPa)	ϕ (°)	c' (kPa)	ϕ' (°)
Block	range	25.0 - 26.7	13.0 - 13.0	23.0 - 25.3	24.0 - 24.8
	design	25.0	13.0	23.0	24.0
Tube	range	10.0 - 11.6	15.0 - 18.0	6.0 - 16.5	24.4 - 33.0
	design	10.0	15.0	6.0	33.0

Table 3.2 Summary of CU Triaxial Test Results on Upper Foundation Soil
(from Hofmann, 1989)

Soil Sample	W (%)	W _L (%)	W _p (%)	I _p (%)	%sand	%silt	%clay
Borrow site	----	42.3	20.7	21.6	28	44	28
	----	40.0	19.6	20.4	25	43	32
	----	40.0	19.2	20.8	----	----	----
Test fill	----	33.3	18.1	15.2	22	60	18
	----	----	----	----	23	57	20
	20.0	37.4	20.9	16.5	5	73	22
	19.1	34.5	23.0	11.5	20	62	18
	----	----	----	----	20	61	19

Table 3.3 Atterberg Limits and Grain Size Distribution of Fill Soil (from Hofmann, 1989)

σ_3 (kPa)	$S_r < 100\%$		$S_r = 100\%$	
	$(\sigma_1 - \sigma_3)$ (kPa)	ϵ_f (%)	$(\sigma_1 - \sigma_3)$ (kPa)	ϵ_f (%)
0	166	12.7	---	---
80	182	15.0	235	20.7
160	178	15.0	244	16.4
240	244	14.0	274	15.0
	271	21.7	---	---

Table 3.4 Comparison of UU Triaxial Test Results on Shelby Tube Samples of Fill Soil (from Hofmann, 1989)

cell pressure (kPa)	W (%)	Sr (%)	$(\sigma_1 - \sigma_3)_f$ (kPa)	$(\sigma'_1 / \sigma_3)_f$	U _f (kPa)	ϵ_f (%)	A
25	21.3	94.7	100	5.46	2.4	3.0	0.024
50	25.1	92.7	104	3.81	12.6	6.1	0.121
75	24.3	94.5	125	3.60	27.0	7.0	0.216
100	23.6	90.6	143	6.02	71.7	4.4	0.501
125	23.7	87.7	165	3.40	56.0	13.7	0.339
150	23.0	99.1	187	3.37	71.0	7.0	0.380
175	22.9	92.9	211	4.26	110.3	5.2	0.523
200	23.1	90.9	230	3.36	102.7	10.1	0.446
203	22.5	94.9	258	2.30	91.0	11.0	0.353

Table 3.5 Summary of CU Triaxial Test Results on Fill Soil
(from Hofmann, 1989)

Geogrid		Tensar SR2	Signode TNX5001	Paragrid 50S
Type of Polymer		high density polyethylene	polyester	polyester polypropylene
Structure		uniaxial grid	rectangular grid	square grid
Junction		planar	welded	welded
Weight (g/m)		930	544	530
Open Area (%)		55	58	78
Aperture Size (mm)	*MD	99.1	89.7	66.2
	CMD	15.2	26.2	66.2
Thickness (mm)		#T 1.27	T 0.75	T 2.50
		A 4.57	J 1.50	J 3.75
Color		black	black	yellow

* MD: machine direction; CMD: cross machine direction

T: tension member; A: anchor member; J: joint

Table 3.6 Physical Properties of Geogrids (from Bobcy, 1988)

Normal Stress (kPa)	Undrained Shear Strength (kPa)	Efficiency		Interfacial Stress Factor	
		SR2	TNX5001	SR2	TNX5001
20	40	0.75	0.97	0.44	0.93
50	60	0.76	0.92	0.47	0.81
100	90	0.77	0.87	0.49	0.69

Table 3.7 Values of Interfacial Stress Factor from Direct Shear Tests (from Costalonga, 1988)

Geogrid	Normal Stress (kPa)	Wi (%)	Dry Unit Weight (kN/m)	Peak Pullout Force (kN/m)	Displ. at Peak Pull-out Force (mm)	Residual Pullout Force (kN/m)	Displ. at Residual Pullout Force (mm)
SR2	20	23.4	15.1	30.1	43.2	25.3	50.0
SR2	50	25.4	15.1	22.9	58.6	22.3	70.0
SR2	51	25.3	15.3	26.8	42.0	26.7	60.0
SR2	102.5	24.4	15.1	41.5	58.2	39.5	70.0
TNX5001	20	25.2	15.0	21.4	25.0	19.6	70.0
TNX5001	50	24.7	14.6	30.2	22.0	29.2	70.0
TNX5001	51.7	25.6	15.5	30.8	19.0	30.2	70.0
TNX5001	100.7	25.5	15.4	38.0	17.0	34.5	70.0

Table 3.8 Summary of Pullout Test Results (modified from Costalonga, 1988)

Geogrid		SR2	SR2	SR2	SR2	TNX5001	TNX5001	TNX5001	TNX5001
Normal Stress (kPa)		20	50	51	102.5	20	50	51.7	100.7
Geogrid Tensile Parameters	a	115500	105000	100000	190000	102.1	102.1	102.1	102.1
	b	3.95	7.0	4.37	9.5	4.29	4.29	4.29	4.29
Soil Shear Strength Parameters	A	47.25	35.94	42.1	65.0	43.0	60.5	61.6	75.0
	B	0.20	0.25	0.20	0.15	0.15	0.10	0.075	0.085
Pullout Force (kN)		9.82	7.46	8.75	13.53	7.08	10.0	10.2	12.25
Pa* (kN)		7.78	5.91	6.93	10.70	6.24	8.78	8.94	10.89
Pb (kN)		2.04	1.55	1.82	2.81	0.77	1.08	1.10	1.34

* Pa: resisting force due to adhesion; Pb: resisting force due to bearing

Table 3.9 Parameters and Some Results of Load Transfer Analyses on Pullout Tests (modified from Costalonga, 1988)

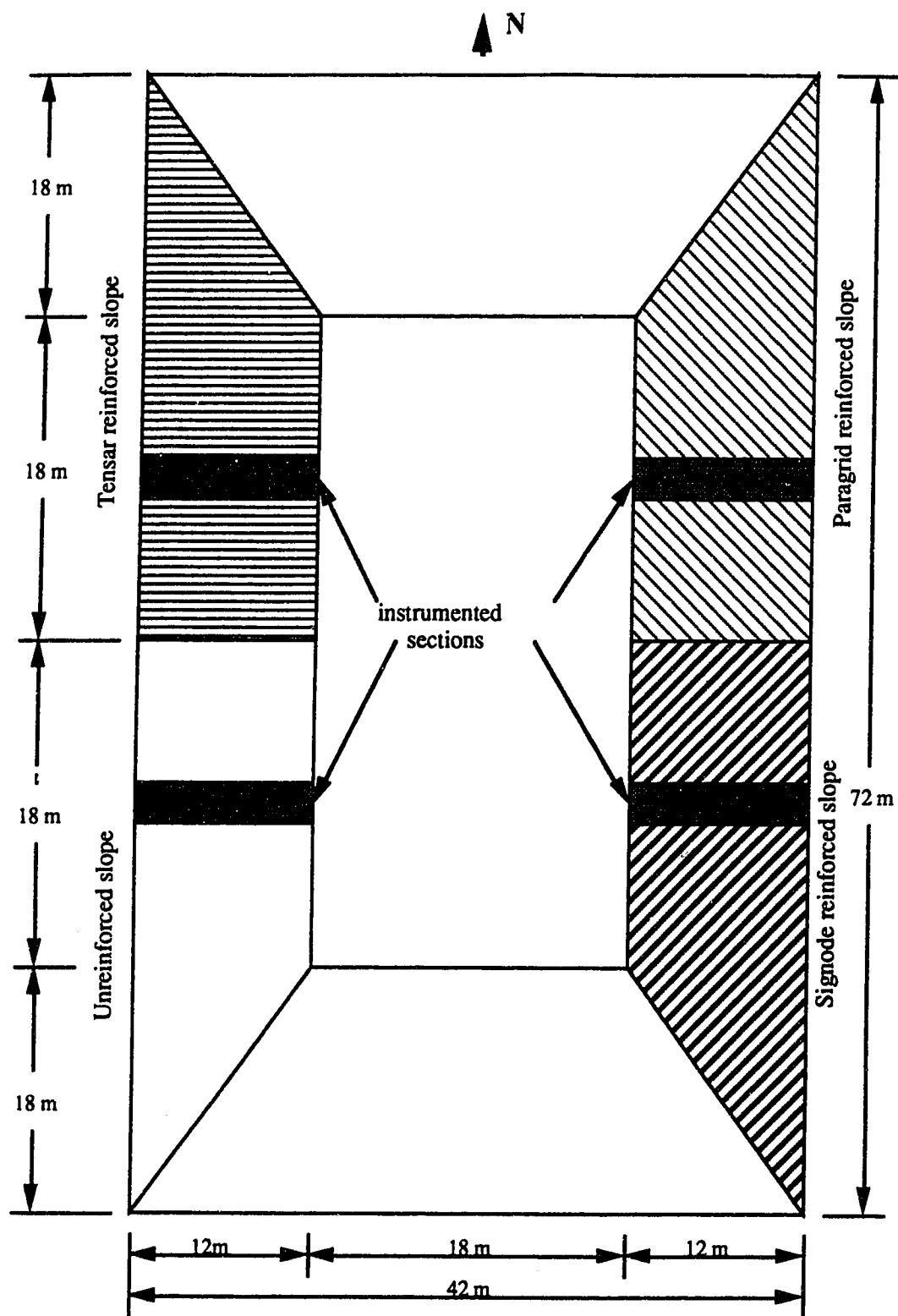


Figure 3.1 Plan View of Devon Test Fill

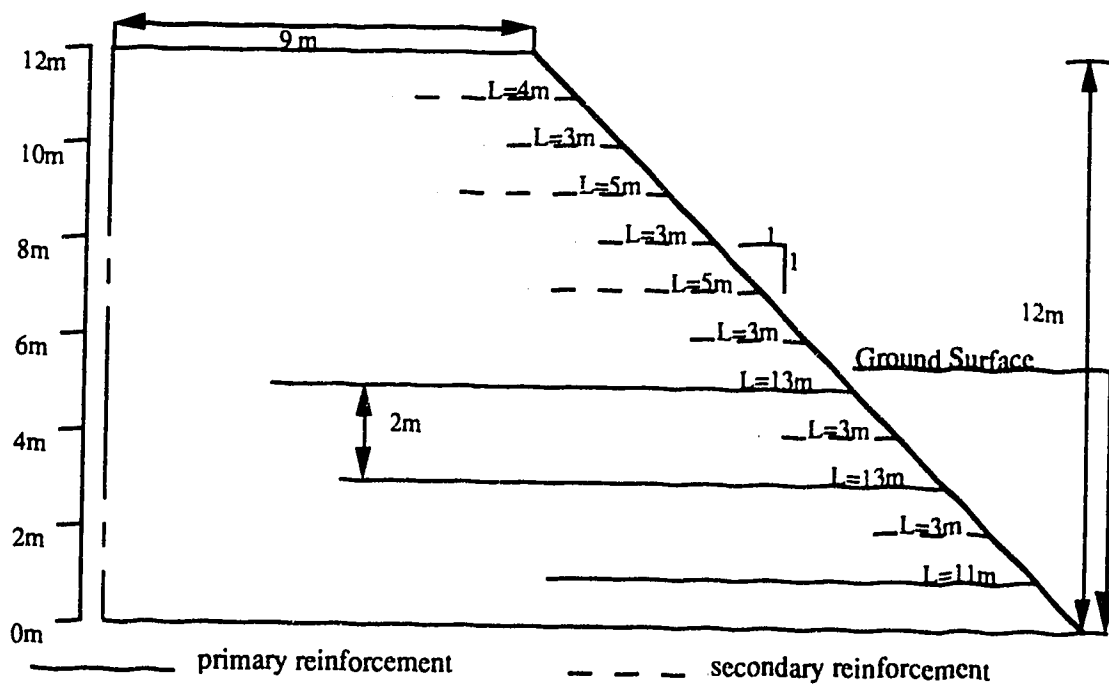


Figure 3.2 Cross Section and Geogrid Layout of Reinforced Slope

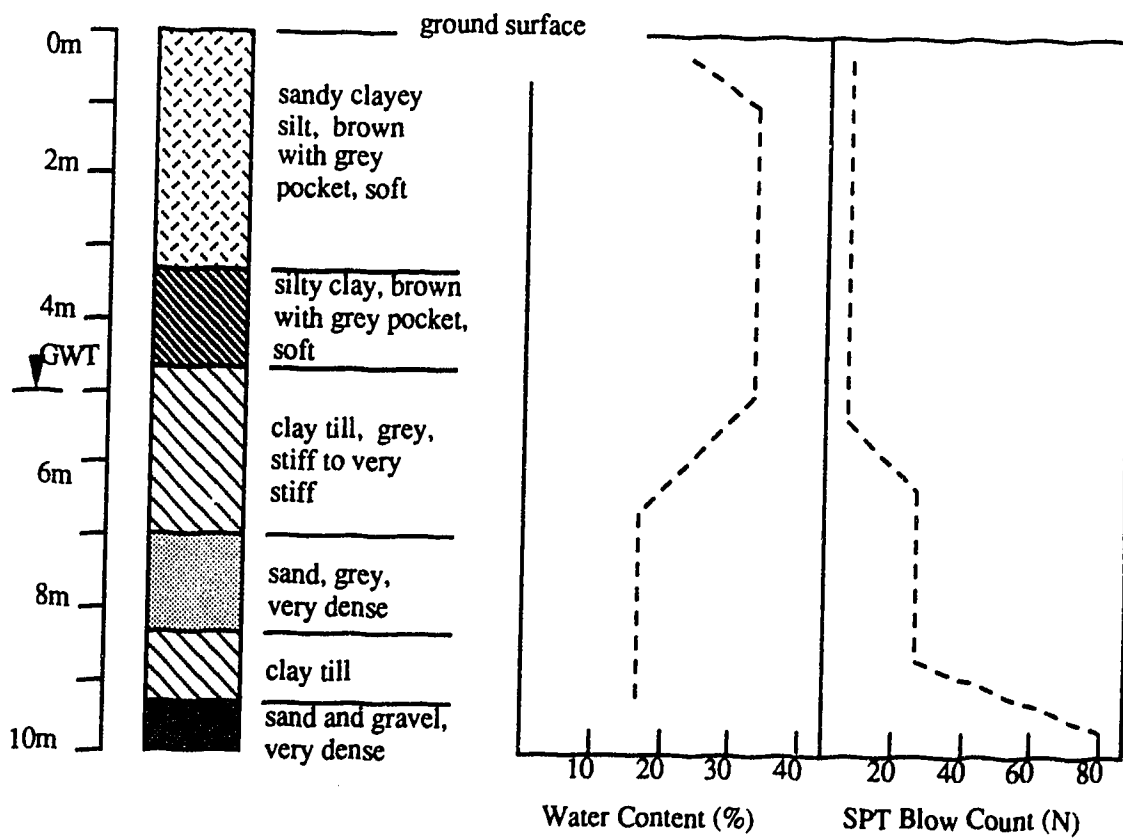


Figure 3.3 Typical Borehole Log of Foundation Soil
(modified from Hofmann, 1989)

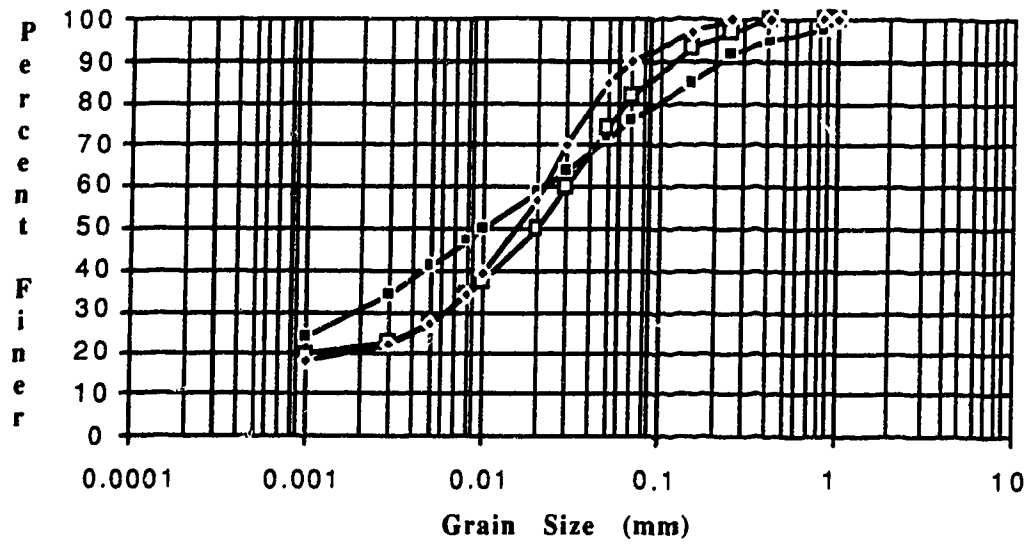


Figure 3.4 Grain Size Distribution of Fill Soil (modified from Hofmann, 1989)

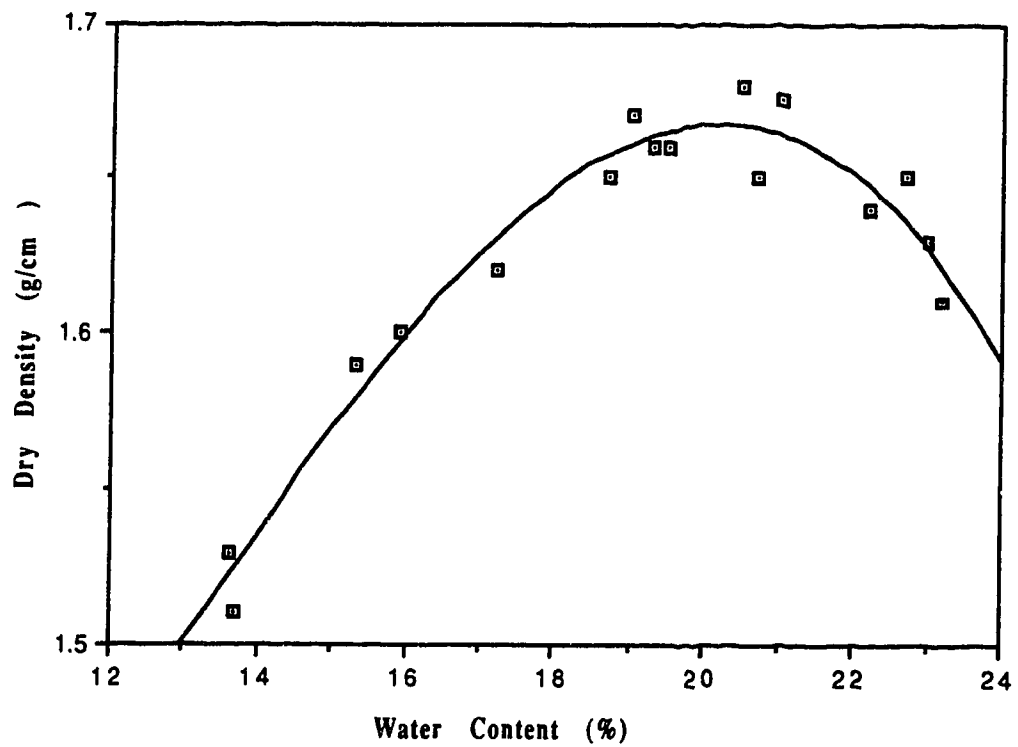


Figure 3.5 Compaction Curve of Fill Soil (modified from Bobey, 1988)

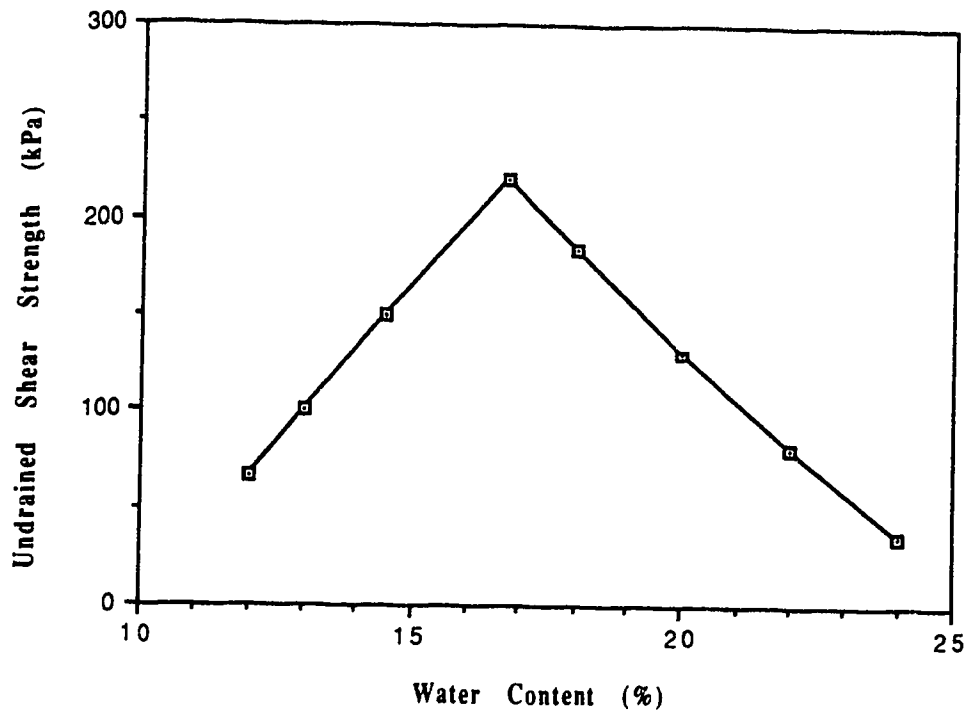


Figure 3.6 Variation of Undrained Shear Strength versus Water Content of Fill Soil (modified from Hofmann, 1989)

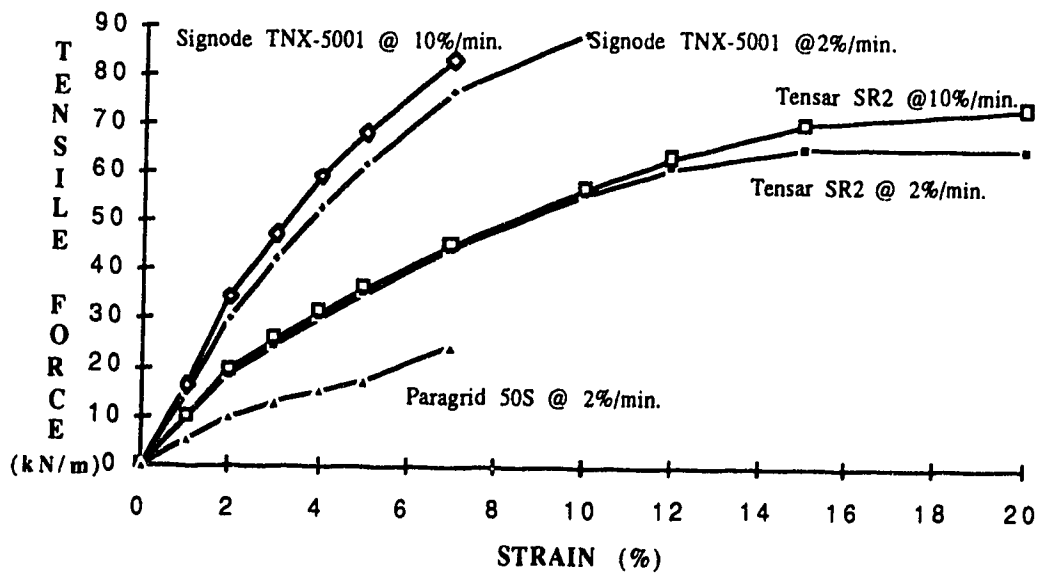


Figure 3.7 Results of Wide Strip Tensile Tests on Geogrids (from Scott et al., 1988)

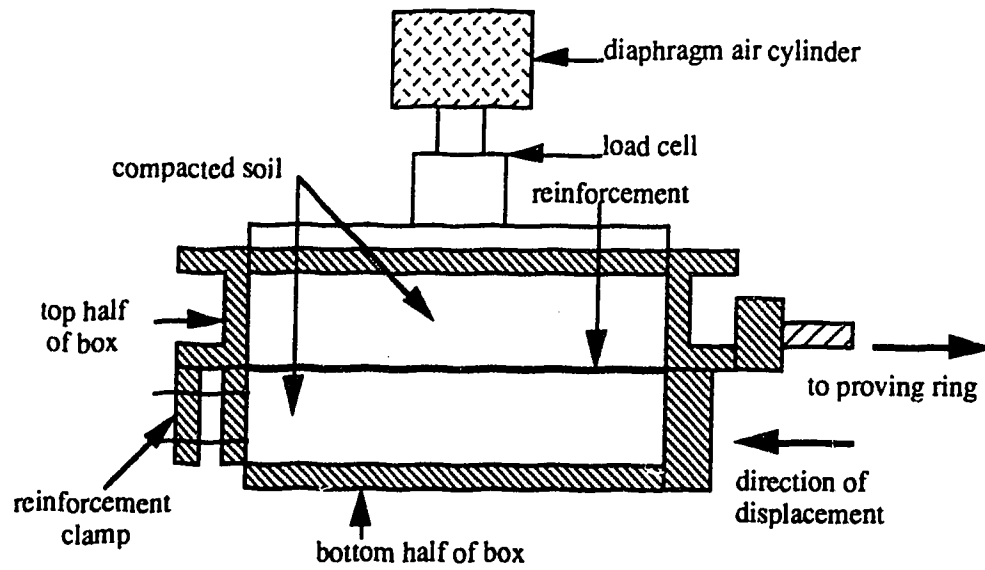


Figure 3.8 Direct Shear Box Apparatus (modified from Bobey, 1988)

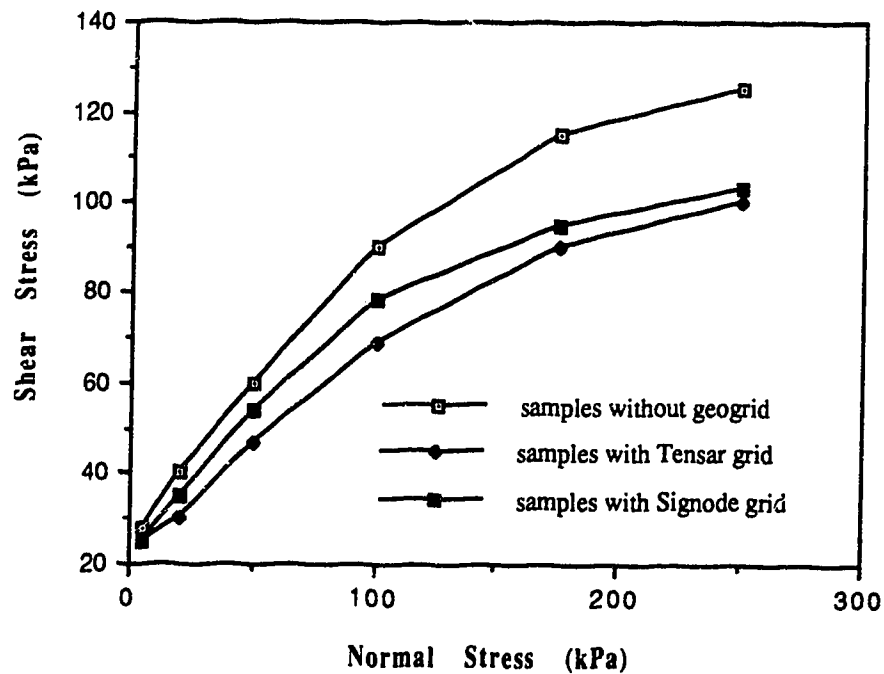


Figure 3.9 Strength Envelopes from Direct Shear Tests (modified from Bobey, 1988)

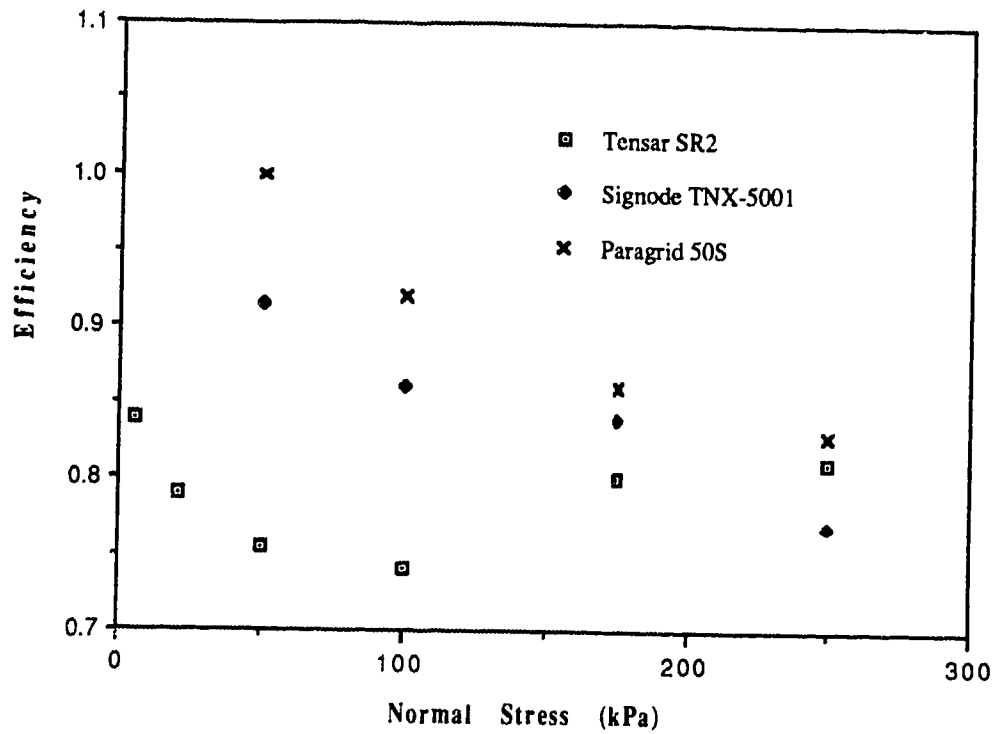


Figure 3.10 Efficiency of Interfacial Shear Resistance (modified from Bobey, 1988)

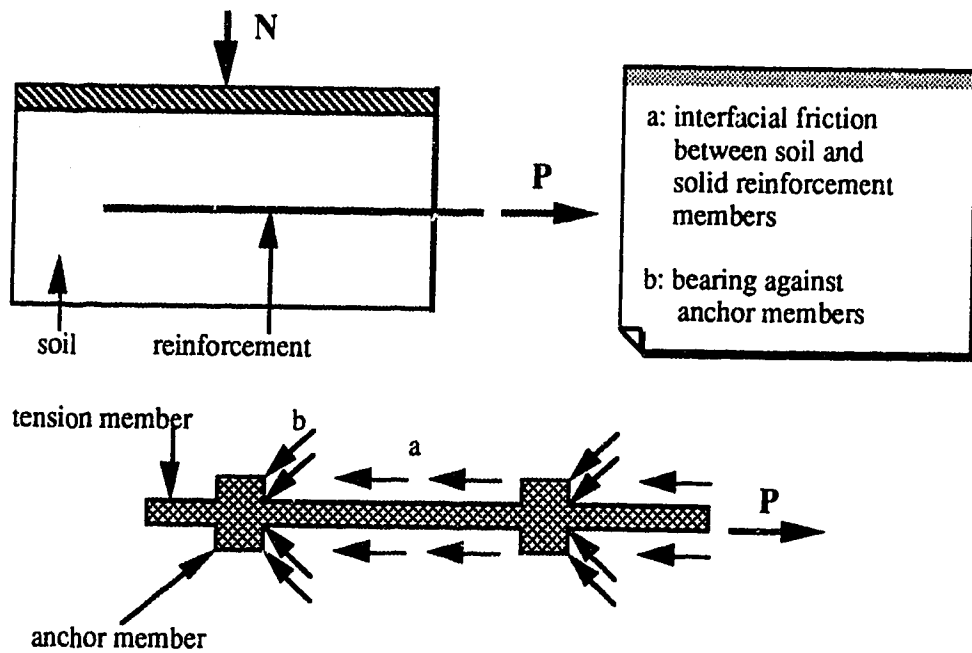


Figure 3.11 Typical Configuration and Basic Mechanisms of Pullout Tests

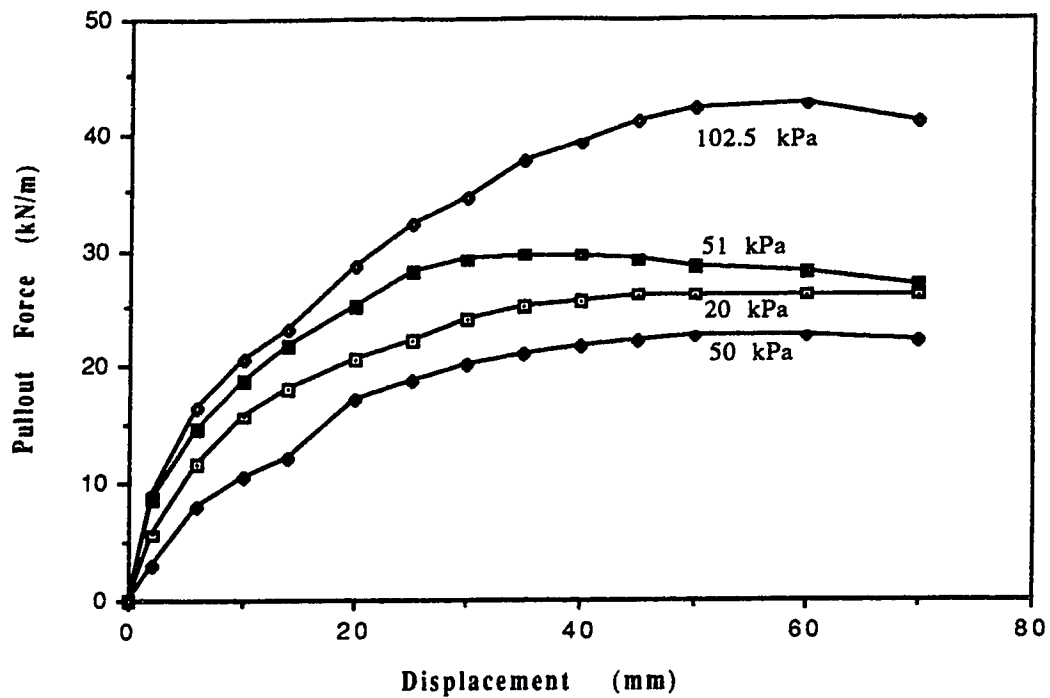


Figure 3.12 Pullout Curves of Tensar SR2 Grid (modified from Costalonga, 1988)

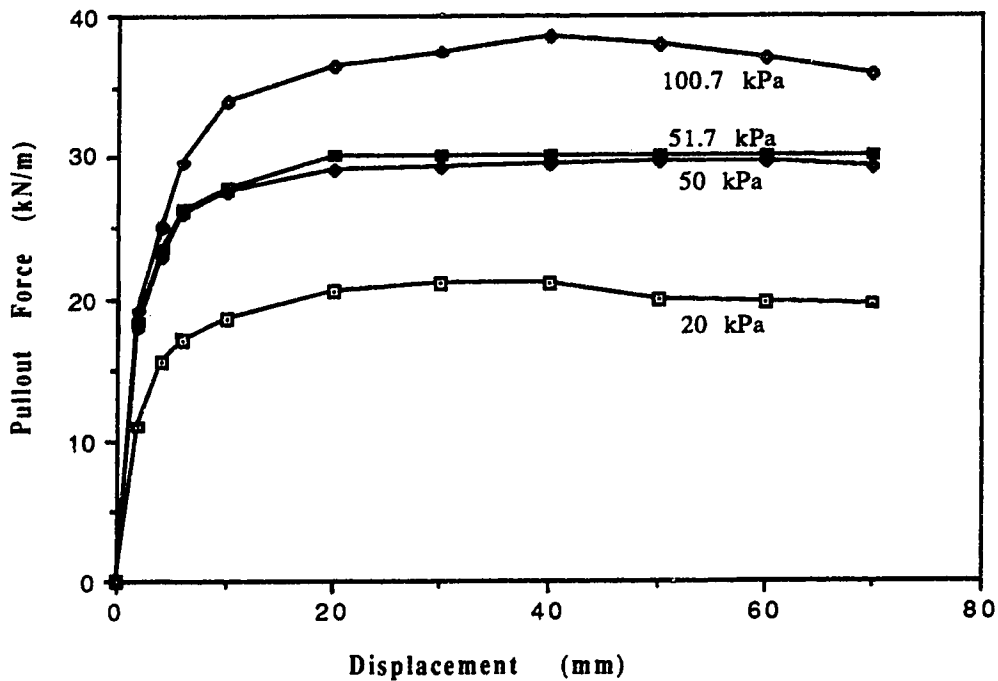


Figure 3.13 Pullout Curves of Signode TNX5001 Grid (modified from Costalonga, 1988)

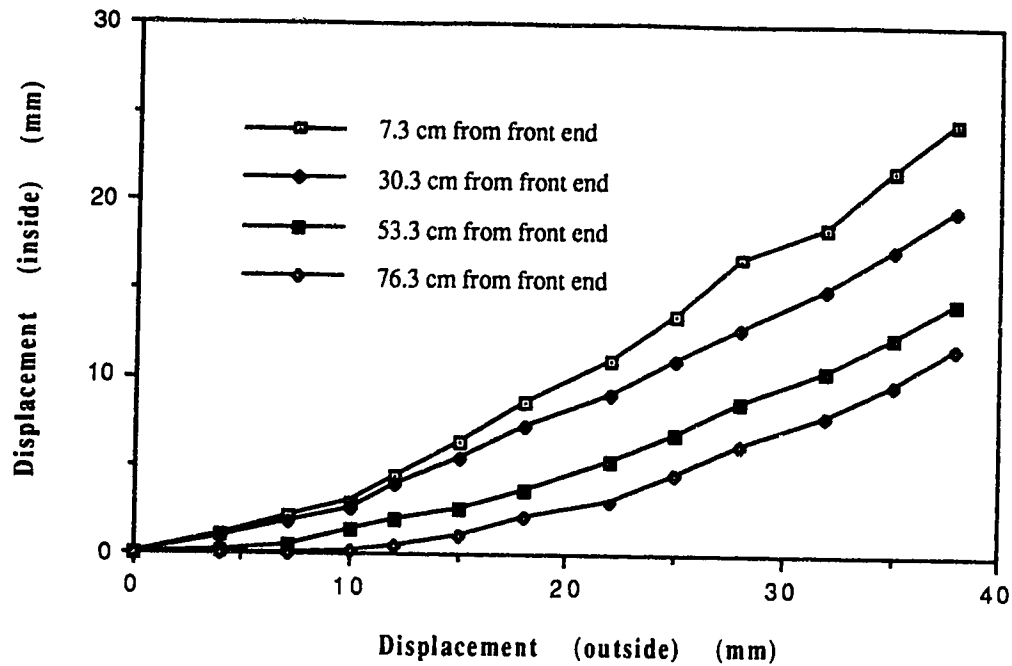


Figure 3.14. Progressive Displacements versus Pullout Displacements for Tensar SR2 Grid (modified from Costalonga, 1988)

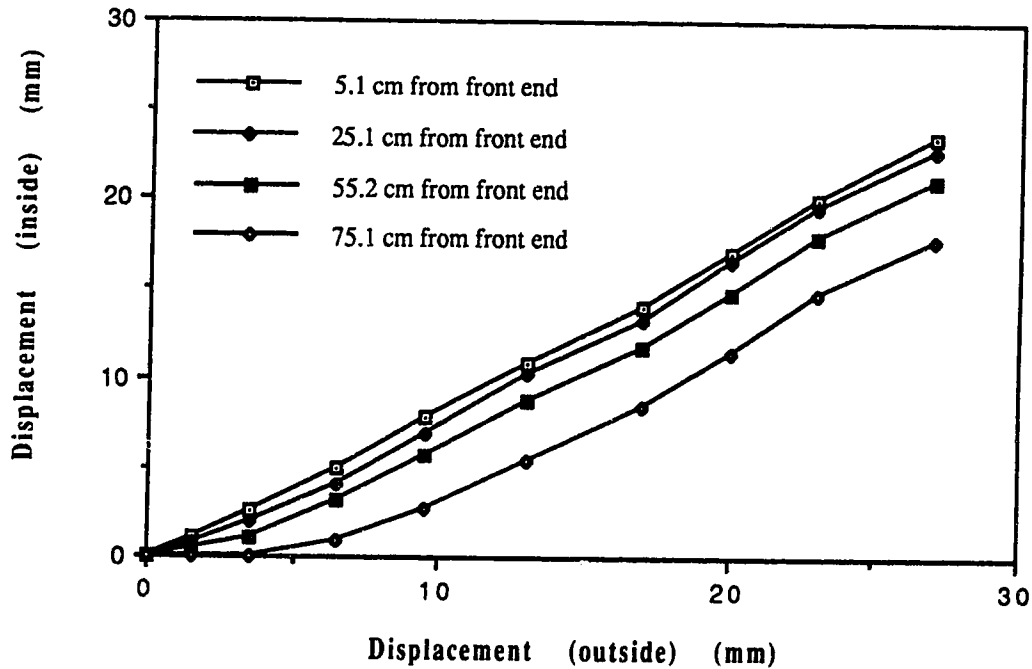


Figure 3.15 Progressive Displacements versus Pullout Displacements for Signode TNX5001 Grid (modified from Costalonga, 1988)

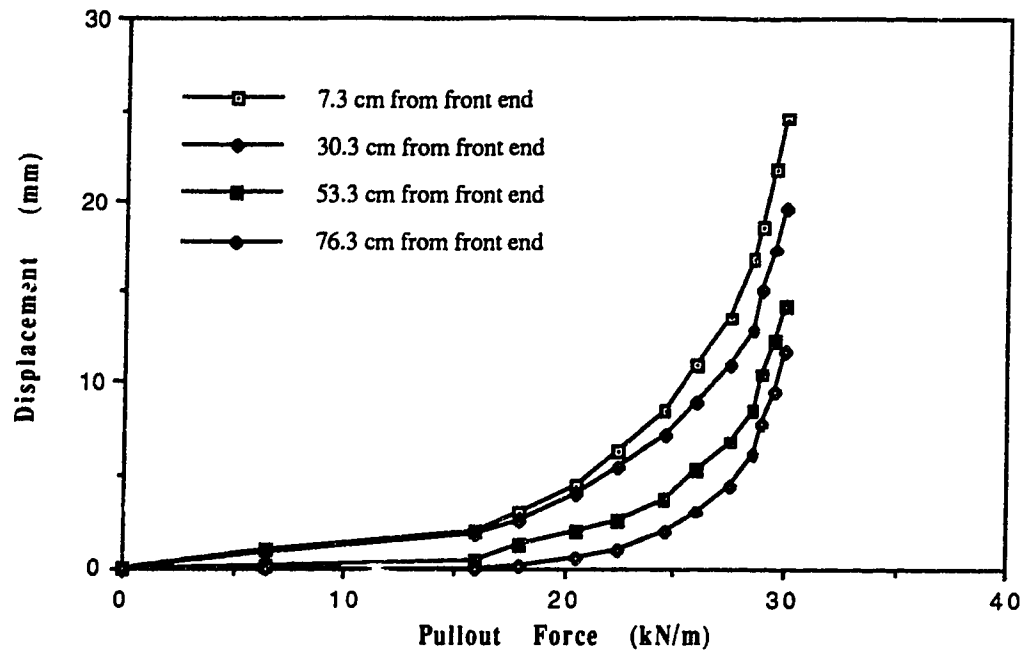


Figure 3.16 Progressive Displacements versus Pullout Forces for Tensar SR2 Grid (modified from Costalonga, 1988)

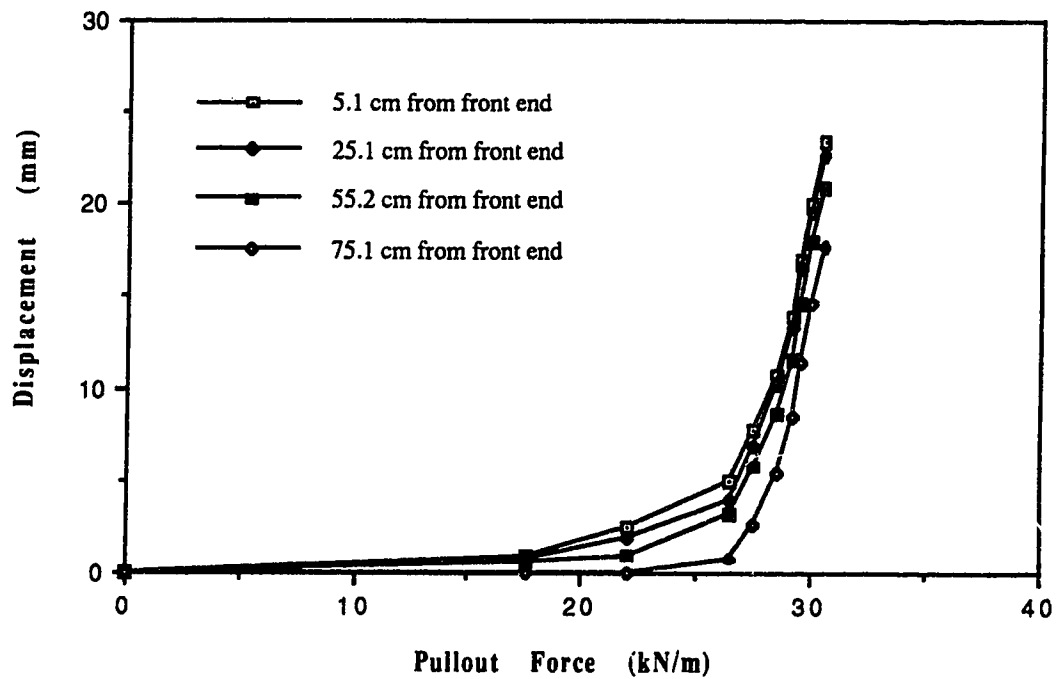


Figure 3.17 Progressive Displacements versus Pullout Forces for Signode TNX5001 Grid (modified from Costalonga, 1988)

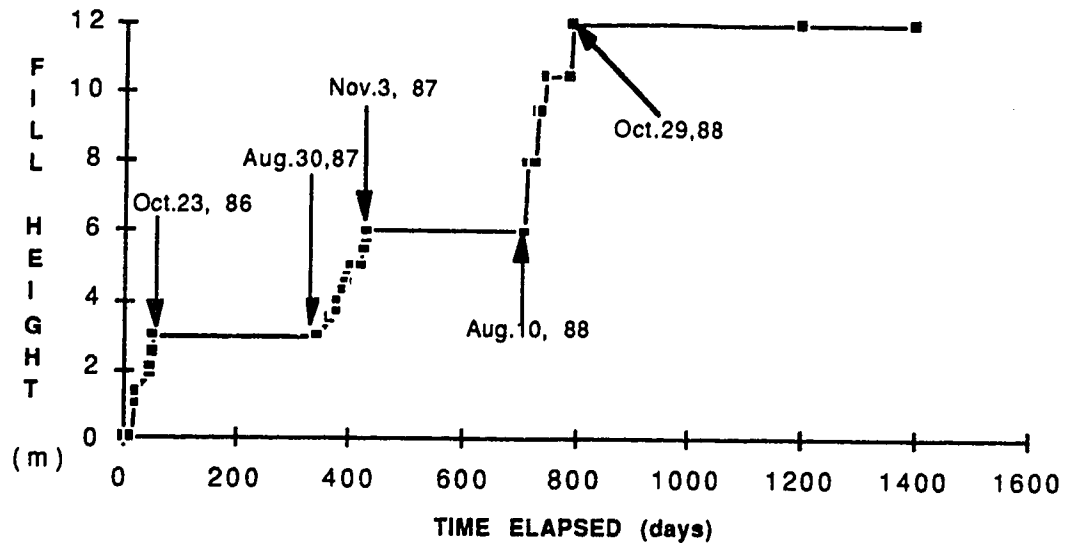


Figure 3.18 Construction Schedule of Devon Test Fill

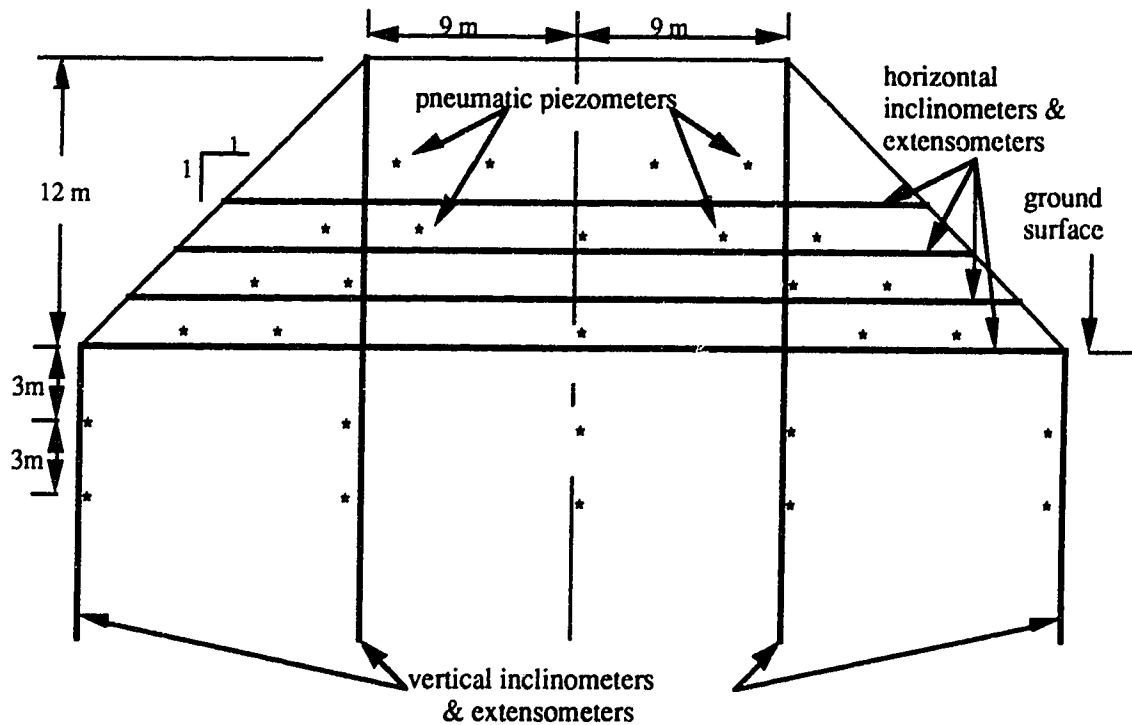


Figure 3.19 Layout of Soil Instrumentation in Devon Test Fill

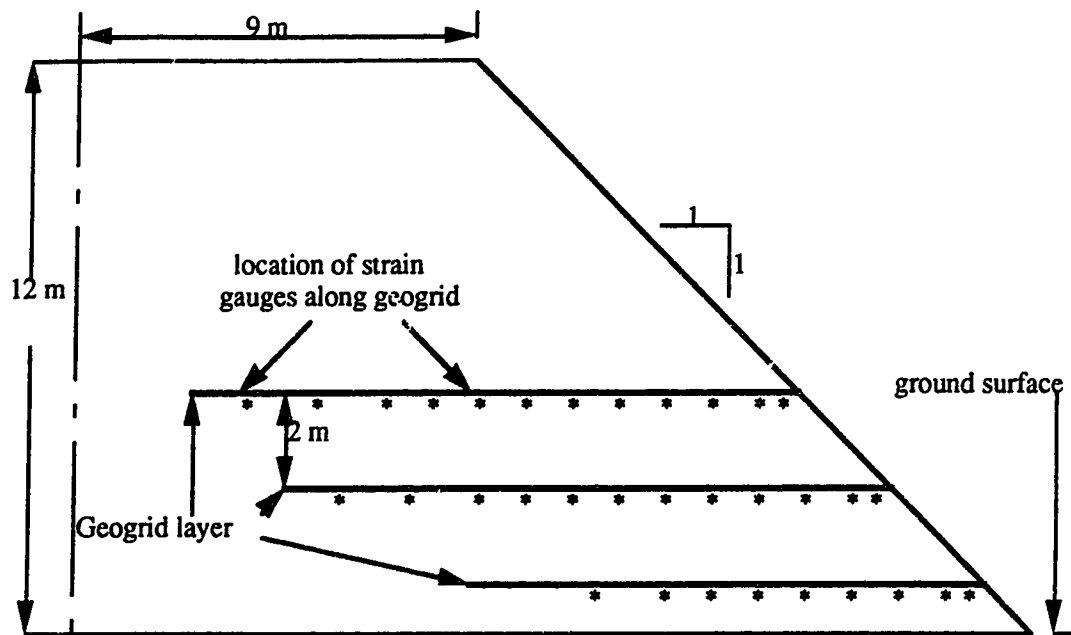


Figure 3.20 Layout of Geogrid Instrumentation in Devon Test Fill

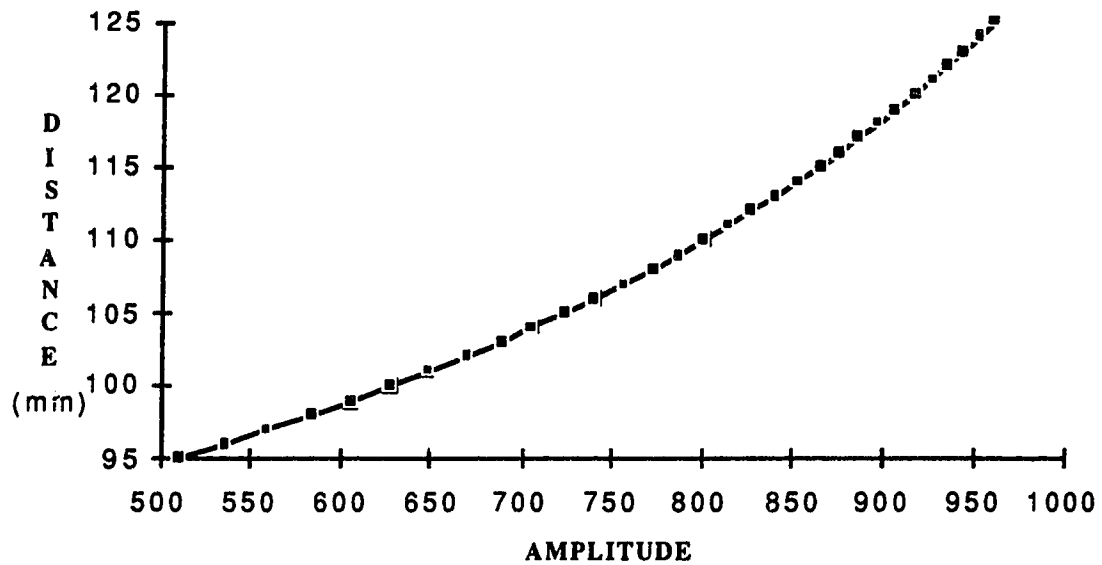


Figure 3.21 Calibration Curve of Inductance Coils (range 2)

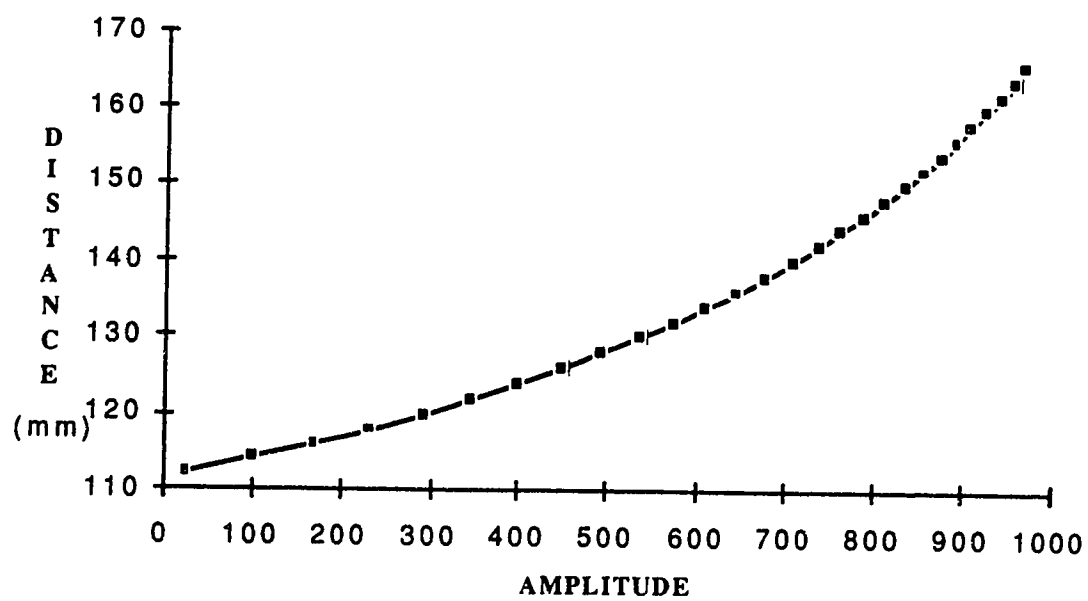


Figure 3.22 Calibration Curve of Inductance Coils (range 3)

Chapter 4. Interpretation of Field Measurements

4.1 Introduction

Performance of the Devon geogrid test fill was monitored using extensive field instrumentation. The instrumentation includes electrical wire resistance strain gauges (EWR), inductance coils, multipoint magnetic extensometers, telescoping inclinometers and pneumatic piezometers. In addition, surface survey measurements were also carried out. Field readings have been taken during and after construction of the test fill. The number of field readings obtained are summarized in Table 4.1. In this chapter, details of the interpretation of field measurements are presented, coupled with the analyses and justification of the interpretation. Performance of the geogrids and the soils in different test sections within the embankment is illustrated.

4.2 Strains in Longitudinal Members of Geogrids

Strains in the longitudinal members of geogrids were measured using electrical wire resistance strain gauges. Field readings were taken using a readout box. The reading taken immediately after laying out of a geogrid layer was adopted as the datum. In some locations, however, where the strain measured during the second field measurement was unreasonably large or small (negative), the second reading was taken as the datum. This adjustment was based on a review of the measurements of adjacent strain gauges, to eliminate the errors caused by localized construction activities.

In order to estimate apparent strains developed in geogrids due to variation in temperature, thermal expansion tests were conducted in laboratory. EWR strain gauges were bonded to pieces of geogrid materials, Tensar SR2, Signode TNX5001 and Paragrid 50S, in the same manner as they were bonded for use in the test fill. Strains were measured at different temperatures under stress-free condition, i.e., without confinement due to the soil and without load being applied to the geogrid. Thermal expansion coefficients of the geogrids were calculated to be 0.017, 0.027 and 0.011 percent strain per K for the Tensar, Signode and Paragrid materials respectively. The measured coefficient of thermal expansion for the Tensar SR2 geogrid was confirmed by the manufacturer. (The thermal expansion coefficient of the strain gauges is one order of magnitude lower than that of geogrids.)

During the field measurements, the temperature at each instrumentation location was monitored using a thermocouple. (Since no record of temperature measurement for the first set of field reading was found, the regional average temperature of the day, obtained from Environment Canada, was used as the initial value.) The temperature induced strains were then calculated as the product of the thermal expansion coefficients of the geogrids and the temperature differences. The temperature induced strains were subtracted from the measured total strains, resulting in strains developed in a geogrid due only to the loading applied by the test fill.

4.2.1 Tensar Bottom Layer

There are nine pairs of EWR strain gauges installed on the instrumented strip of the Tensar geogrid in the bottom primary reinforcement layer. They were installed at distances of 0.5, 1, 2, 3, 4, 5, 6, 7 and 8.5 m respectively from the slope surface. The pair of gauges at the 0.5 m location and one gauge at the 1 m location failed in September 1987. At the 2 and 3 m locations, one gauge in each pair failed in November 1988.

At locations where one gauge failed, bending of the geogrid could not be determined. From field measurements, however, it was found that bending occurred mainly during the summer of 1986, due to the construction activities. At the 3 m location, for example, during the first construction season (fill height up to 3 m), the strains measured in the top and bottom gauges were 0.343 and 0.445%, with a difference of 0.102% strain indicating bending deformation of the grid at the location. In contrast, the strain increments in the top and bottom gauges between November 1986 and November 1987 were 0.151 and 0.139%, indicating a nearly pure tensile deformation of the geogrid. Even during the first construction season, strain differences measured by the top and bottom gauges on the geogrid were less than 0.2% at most instrumented locations. Figure 4.1 shows the strains measured from the top and bottom gauges installed at the 5 m location. The strains measured by the top and bottom gauges varied consistently throughout the observation period. Therefore, failure of one gauge in a pair did not significantly affect the strain measurements at that location.

At locations where both strain gauges worked properly, average values were used to indicate the strains within the geogrids. At locations where one of the pair failed, summations of the average strains before failure and the strain increments, measured thereafter by the remaining gauge, were used to represent the strain. For instance, at the 2 m location where one gauge failed in November 1988, the total strain determined by averaging the measured values of the two gauges before failure was 0.608%; the strain increment measured by the working gauge which did not fail was 0.33% between September and November. Hence, the strain in November 1988 was to be 0.938% ($0.608\% + 0.33\%$). Since bending of geogrids occurred mainly during the first construction season, the reading from one strain gauge could reasonably indicate the deformation of the geogrid at each location subsequent to the construction activities in 1986. At the 0.5 m location, where both gauges failed in September 1987, strains after the failure were estimated based on the strains at the 1 m location and the ratio of the measured strains at the two locations prior to the failure. For example, the average ratio between strains at the 0.5 and 1 m locations before the failure was 0.6; the strain at the 1 m location was measured to be 0.564% in November 1988. Therefore, at the 0.5 m location, the strain of the geogrid in November 1988 was estimated to be 0.338% ($0.6 \times 0.564\%$). According to finite element analyses (Chalaturnyk, 1988) on a geogrid reinforced slope, the peak of the strain profile within a geogrid layer tends to move into the slope as the embankment height increases. The peak of the strain profile in September 1987 occurred at the 1 m location. Hence, it seemed unlikely that the geogrid at the 0.5 m location would develop a higher strain than occurred at the 1 m location. Therefore, it was reasonable to assume that the strains at the 0.5 m location was developed in the same ratio (relative to the 1 m location) as before the failure of the pair of strain gauges at the 0.5 m location.

The first set of field measurements, taken in September 23, 1986, were considered as the initial strains and were subtracted from the total strains measured thereafter. Adjustment was made to the strains at the 8.5 m location. The initial field reading indicated -0.023% of strain; a reading taken two days later gave -0.087%, showing that construction activities caused localized compression of the geogrid. To eliminate further negative strains, the

measurement of -0.087% was used as the initial value and subtracted from future measured total strains.

Figure 4.2 shows the strain profiles within the Tensar bottom geogrid layer before the adjustment to the field measurements; Figure 4.3 presents the adjusted strain profiles. To limit the number of figures but not to reduce the information presented, strain profiles are organized to represent the behavior of the geogrid during the construction and during the subsequent consolidation under different fill height in construction stages. The strain development within the geogrid, from the time of installation to two years after completion of construction, at typical locations is illustrated in Figure 4.4. The development of the strains can be directly related to the construction stages, as shown in Figure 3.18.

Strain profiles of the bottom layer of the Tensar geogrid are shown in Figure 4.3. At the end of the first construction season when the fill height was 3 m, the tensile strain of the geogrid increased from the slope surface and reached a maximum of about 0.5% at the 1 m location; it gradually decreased further into the fill. Immediately after the 1987 construction, when the fill height increased to 6 m, no significant change occurred in the strain profile. The location and the magnitude of the peak strain remained the same and the strains along the geogrid after the peak showed slight increases due to the fill construction. The strain profile, however, differed significantly when the fill reached 12 m at the end of the 1988 construction season: the peak of the strain profile moving to the 3 m location and increasing to a magnitude of 1.1%. The tensile strain within the geogrid dropped rapidly to 0.65% at the 4 m location and decreased gradually further into the fill. Strain profiles one and two years after completion of construction were almost identical to that at the end of construction (November 1988).

Figure 4.4 shows an entire view of the strain development, at the 2, 3, 5 and 7 m locations, from the installation until two years after completion of the fill. The tensile strain of the geogrid increased during the first construction season and remained nearly constant through the first winter; the strain dropped between 0.1 and 0.15% due to consolidation which occurred during the spring of 1987. During the second construction season and during the subsequent consolidation the strains developed in a similar manner to the first

year but were smaller in magnitude even though the increment of fill height was also 3 m. The strains then increased significantly during the 1988 construction season and remained virtually unchanged thereafter.

The decrease of strains during spring can be attributed to two possibilities. First, as the fill and foundation soils consolidated, a portion of the load might transfer from the geogrid to the fill soil due to increase in soil stiffness, resulting in a decrease in the tensile strains within the geogrid. The other possibility is related to thermal expansion of the geogrid. In the interpretation of field strain measurements, the apparent strains, product of the thermal expansion coefficient of the geogrid and the temperature variations, were subtracted from the measured total strains. The thermal expansion coefficient of the geogrid was measured in the laboratory in a stress-free condition. In other words, the geogrid was free to expand or contract when the temperature was varied. In the test fill, however, the geogrid was confined with the fill. The geogrid thus might not be able to expand or contract in the same manner as when it was stress-free in the laboratory. As a result, the apparent strain of the geogrid might be overestimated during summer when the temperatures in the test fill were higher than that in winter. Hence, this phenomenon might result in the decrease of strains during the spring.

4.2.2 Tensar Middle Layer

Eleven pairs of EWR strain gauges were installed in the middle primary reinforcement layer, at locations of 0.5, 1, 2, 3, 4, 5, 6, 7, 8, 9 and 10.5 m respectively from the slope surface, in the Tensar section. No strain gauge failed during or subsequent to the fill construction.

Strain profiles of the geogrid in the Tensar middle layer are illustrated in Figure 4.5. Immediately after the 1987 construction season, the tensile strain increased smoothly from the slope surface into the fill, reached the maximum of 0.71% at the 4 and 5 m locations and decreased gradually further into the fill. The strain profile at the end of the 1988 construction differed. Near the slope surface, the tensile strain did not change. At the 2 m location, for example, the strain increased from 0.31% in November 1987 to 0.48% in November 1988. However, at the 5 m location, the strain increased from 0.7 to

1.75%. The profile was characterized by high strain localization at the peak location 5 m from the slope surface. The strain profile in October 1990 was almost identical to that in November 1988 except at locations beneath the fill crest where strain increments of about 0.15% were developed due probably to differential consolidation settlement of the fill and the foundation soils.

The development of the tensile strain within the geogrid, at the 1, 3, 5, 7 and 10.5 m locations, during and subsequent to the construction seasons is shown in Figure 4.6. The strain increased during the 1987 construction season and decreased slightly during the winter shut-down; it increased again during the 1988 construction and remained nearly constant thereafter. It is interesting to note that the amount of strain reduction during the spring of 1988 increased as the distance from the slope surface decreased. In other words, the closer to the slope surface, where the temperature varied significantly, the larger fluctuation of the strain were observed. This phenomenon corresponds to the possibility of an overestimation of the apparent strains in thermal expansion correction on field measurements, as discussed in last section.

4.2.3 Tensar Top Layer

There are eleven pairs of EWR strain gauges, placed at locations 0.5, 1, 2, 3, 4, 5, 6, 7, 8, 9 and 10.5 m from the slope surface, in the top primary reinforcement layer of the Tensar geogrid. Three pairs of gauges at the 0.5, 1 and 3 m locations and one gauge at the 4 m location failed during the 1988 construction season. Since no significant bending of the geogrid was observed, tensile strains at the 4 m location were represented by the summation of the average strain before the failure and the strain increment of the remaining gauge.

At the 0.5 and 1 m location, strains after August 1988 were estimated from products of the measured strains at the 2 m location and the average ratio between the strain at each location and the strain at the 2 m location. Because the maximum strain before the failure of the gauges occurred at the 3 m location, the method of estimating strains at the two locations was reasonable, as discussed in an earlier section. The strains of the geogrid at the 3 m location, where the pair of gauges failed when the fill height was 10.5 m, could

be estimated in two ways: either taking average values of strains measured in two adjacent locations (2 and 4 m from the surface) by assuming that the maximum strain occurred at the 4 m location, or taking products of the strains at the 4 m location and the ratio between strains at the two locations before the failure by assuming that the peak of the strain profile remained at the 3 m location. The later seemed to be more reasonable according to the inductance coil measurements, which indicated that the maximum strain after September 1988 remained at the 3 m location.

Figure 4.7 shows profiles of the tensile strain in the top layer of the Tensar geogrid. The maximum strain of 0.24% occurred at the 1 m location after the 1987 construction. At the end of 1988 construction season, however, when the fill reached the final height of 12 m, the peak strain moved to the 3 m location and the maximum increased to 2.95%; beyond the 5 m location the strain decreased rapidly and dropped to 0.53% at the 8 m location. Comparing the strain profile of October 1990 with that of November 1988, only minor increments of 0.1 to 0.15% were observed at locations beneath the crest and further into the fill.

Diagrams indicating entire strain development at the 2, 4, 7 and 10 m locations are shown in Figure 4.8. The field measurements were consistent and showed the same tendency of seasonal fluctuation, as discussed before.

4.2.4 Signode Bottom Layer

Nine pairs of EWR strain gauges were installed, at locations 0.5, 1, 2, 3, 4, 5, 6, 7 and 8.5 m from the slope surface, on the instrumented strip of the bottom primary reinforcement layer of the Signode geogrid. At the locations 3, 5 and 8.5 m from the slope, one gauge in each pair failed during the 1986 construction, so strains at these locations were estimated based on measurements of the remaining gauges. The pairs of gauges at the 2, 3 and 4 m locations failed totally during the 1988 construction season. The peak strain before the failure was located 6 m from the slope. Thus, strains at the 2, 3 and 4 m locations were estimated from interpolation of strains at the 1 and 5 m locations based on the ratios of the strains before the failure in the summer of 1988. At the 7 m location, one gauge failed in October 1986. Even though the other gauge kept working throughout the monitoring period, the

measurements showed no change of the strain occurred as the fill was placed to the final 12 m height. Therefore, this pair of gauges was considered as having failed and strains at the location were estimated by taking averages of the strains at the 6 and 8.5 m locations.

Profiles of the strain distribution along the bottom layer of Signode geogrid are shown in Figure 4.9. At the end of the first construction season, the maximum tensile strain of 0.79% occurred in the geogrid at the 0.5 m location and strains at other locations were of magnitudes between 0.6 and 0.71%. The peak of the strain profile moved to the 6 m location after the second construction stage and increased to 0.84%. At the end of the final construction season, the strain increased from the slope surface into the fill and reached the maximum of 1.58% at the 6 m location; it then decreased further into the fill and dropped to 1.07% at the 8.5 m location. The strain profile in October 1990 is almost identical to that in November 1988, whereas the profile in June 1989 shows differences between 0.02 and 0.25% along the geogrid. The differences were most likely caused by the thermal expansion correction, as discussed in the previous section.

The development of tensile strains at locations along the Signode bottom layer of geogrid is illustrated in the strain-time diagrams, shown in Appendix A.

4.2.5 Signode Middle Layer

Twelve pairs of EWR strain gauges were installed to monitor the tensile strains developed in the middle primary reinforcement layer of the Signode geogrid. The gauges were placed at locations 0.5, 1, 2, 3, 4, 5, 6, 7, 8, 9, 10.5 and 12 m from the slope surface. At the 1 and 8 m locations, one in each pair of gauges failed at the end of the 1988 construction season.

Profiles of strain distribution along the geogrid are illustrated in Figure 4.10. Immediately after the 1987 construction season, the strain varied smoothly from zero at the slope surface to its maximum of 0.57% at the 5 m location and to 0.13% at the 12 m location. No localization of strain is observed in the profile. At the end of the 1988 construction, when another 6 m of fill was placed on the test embankment, the field measurements showed

significant changes in the strain distribution. The peak of the profile moved to the location 7 to 9 m from the slope surface and the magnitude was up to 1.99%. The profile shows a rapid increase from 0.59% at the 3 m location to 1.98% at the 7 m location and a decrease from 1.99% at the 9 m location to 0.58% at the 12 m location. This variation apparently indicates the movement and shearing development of the soil within the reinforced slope.

Measurements after November 1988 did not show any significant changes in the magnitude and shape of the strain profiles except at some locations close to the slope surface where fluctuation of strain occurred due to thermal correction. The full development of the tensile strain at locations along the geogrid layer can be observed in the strain-time diagrams shown in Appendix A.

4.2.6 Signode Top Layer

Twelve pairs of EWR strain gauges were installed, at locations 0.5, 1, 2, 3, 4, 5, 6, 7, 8, 9, 10.5 and 12 m from the slope surface, in the top primary reinforcement layer of geogrid in the Signode section. One gauge in the pair at the 1 m location failed at the end of the 1988 construction season and the strains were determined by the remaining gauge. The pair of gauges at the 0.5 m location failed at the beginning of the 1988 construction, so the strains at the location were estimated from the measurements at the 1 m location.

Figure 4.11 shows the profiles of strain distribution along the geogrid layer. The strains developed during the 1987 construction season were negligible since only one metre of the fill had been placed on the top of the layer. At the end of the 1988 construction, the strain rapidly increased from 0.6% at the 1 m location to 1.32% at the 5 m location; it then gradually increased until the peak of 1.68% at the 10.5 m location was reached; the strain after the peak dropped to 0.64% at the 12 m location. Besides the seasonal fluctuation of the strain, measurements taken after the completion of the test fill did not show significant changes in either the profile or the magnitude of the strain except at the locations near the slope surface where large increments of the tensile strain were observed. These increments were induced by the excessive shallow movement of the soil, caused most likely by

freezing-thawing cycles. The development of the strain can also be observed in the strain-time diagrams shown in Appendix A.

4.2.7 Paragrid Bottom Layer

Nine pairs of EWR strain gauges were installed in the bottom primary reinforcement layer of the Paragrid geogrid at locations 0.5, 1, 2, 3, 4, 5, 6, 7 and 8.5 m from the toe of the test embankment. All gauges worked well during the monitoring period.

Profiles of tensile strain of the geogrid are illustrated in Figure 4.12. At the end of the first construction season, the strain increased from the slope surface to a maximum of 0.73% at the 2 m location and then decreased gradually further into the fill. The profile of the tensile strain measured at the end of the second construction shows the same distribution as the profile in November 1986. A maximum increment of the strain of 0.17% was developed during the second construction season with an additional 3 m of fill placed. Different from geogrids in the other sections, there were no dramatic changes of the strain measured in the Paragrid geogrid, in either the distribution or the magnitude, during the third construction season. The peak strain increased from 0.87% in November 1987 to 1.19% in November 1988 and the maximum increment of 0.5% occurred at the 4 m location. Profiles of the strain measured one and two years after the final construction are almost identical to the profile at the end of the construction.

The development of the tensile strain at different stages of construction and consolidation is shown in the strain-time diagrams in Appendix A.

4.2.8 Paragrid Middle Layer

Twelve pairs of EWR strain gauges were installed, at locations 0.5, 1, 2, 3, 4, 5, 6, 7, 8, 9, 10.5 and 12 m from the slope surface, in the middle primary reinforcement layer of the Paragrid geogrid. No gauges failed after the 1987 construction season.

Figure 4.13 shows profiles of the strain distribution along the middle layer of the Paragrid geogrid at different stages of construction and consolidation. The strain developed during 1987 had magnitude less than 0.23%. At the end

of the 1988 construction season, the total strain at the 0.5 m location increased to 0.5% due possibly to shallow movement of the fill soil; beyond the 2 m location into the fill, the strain increased gradually and reached a maximum of 0.55% at the 9 m location. The strain of the geogrid at locations near the slope surface kept developing during the subsequent consolidation period as freezing-thawing affected the surface of the slope and weakening the soil near the surface; the strain increment of the geogrid at locations deep into the fill, on the other hand, was small during the period. The increment at the 9 m location was 0.06%.

4.2.9 Paragrid Top Layer

Twelve pairs of EWR strain gauges were installed in the top primary reinforcement layer of the Paragrid geogrid at locations 0.5, 1, 2, 3, 4, 5, 6, 7, 8, 9, 10.5 and 12 m from the slope surface. One gauge at the 0.5 m location and one at the 1 m location failed during the 1988 construction season. The strains after the 1988 construction at the two location were estimated using the measurements of the remaining gauges, as previously described. At the 12 m location, the measurement, taken on October 23, 1987 when only 0.5 m of fill soil was placed above the top layer, indicated compressive strains in the geogrid in the longitudinal direction. This compressive strain was apparently not the real behavior of the geogrid. Therefore, the measured strains were adjusted by taking the -0.25% as the initial measurement.

Profiles of the tensile strain distribution along the top layer of the Paragrid geogrid were illustrated in Figure 4.14. The strains developed during the 1987 construction season were less than 0.28% with a maximum at the 1 m location. At the end of the 1988 construction season, the peak strain moved to the 4 m location and jumped to 1.27%. In the profile, the strain increased rapidly from the slope surface to the 4 m location, dropping to 0.54% at the 6 m location and then gradually decreased. There was no significant change in the strain during the consolidation period from November 1988 to October 1990.

4.3 Strains Between Adjacent Transverse Members of Geogrids

Strains between adjacent transverse members of geogrids were measured using inductance coils. Ten inductance coils were installed along each instrumented primary reinforcement layer of the geogrids at locations 1, 2, 3, 4, 5, 6, 7, 8, 9 and 10.5 m from slope surface except in the bottom layer of Tensar geogrid, in which nine pairs of gauges were placed at locations 1, 2, 3, 4, 5, 6, 7.75 and 8.5 m from the slope surface. Field readings in terms of amplitudes were taken using a readout indicator then converted to distances between centers of pairs of sensors, using laboratory determined calibration curves. By subtracting the initial distances from the measured central distances, deformations and strains of the geogrids were calculated. In some instrumented locations where the second set of field readings were affected by the construction activities, the central distances from the second set of readings were used as the initial values. Dummy inductance coils were used to account for zero drift of the readout box. (For example, the amplitudes read in May 1989 were excessively large due to improper set up of the readout box. Therefore, that set of the field measurements were adjusted based on the variation in the amplitude from a set of dummy gauges.) No other specific corrections were applied to account for influences of temperature and moisture content of the soil.

4.3.1 Tensar Bottom Layer

The two sensors of each inductance coil were placed about 105 to 115 mm apart in the Tensar geogrid. All gauges installed in the bottom layer of the Tensar geogrid worked well throughout the monitoring period.

The first field reading was taken in September 1986, immediately after the bottom layer of geogrid was placed. Sensor spacing measured in the first set of readings was supposed to be the initial set. However, at most instrumented locations, the spacing measured in the second set of field readings, taken in October 1986, was even smaller. In other words, the geogrid appeared to be compressed in the longitudinal direction, instead of elongated. The sensor spacing measured in November 1986 again indicated compression. These fluctuations can be more clearly observed in the measurements during the

1989-1990 seasons when the fill construction was complete. As shown in Figure 4.15, at the 1, 5 and 8.5 m locations, the measured strains decreased from 0.56, 1.04 and 0.8% to 0.25, 0.78 and 0.5% respectively between July 1989 (1054 days) and January 1990 (1237 days). The strain fluctuation in the magnitude between 0.25% and 0.3% appeared to be independent of difference in locations where temperature variation differed significantly. This tendency of fluctuation with season was probably caused by the effect of air-temperature variation on the readout indicator, which induced electric current and converted the electromagnetic coupling into an amplitude by means of an inductance bridge, even though the sensor itself might not be sensitive to temperature variation, as claimed by the manufacturer.

To eliminate the compression of the geogrid along the slope direction, which was unlikely to occur, during the first construction season and to adjust the subsequent strains to average values, the sensor spacings measured in October 1986 were taken as the initial values (air temperature in October is close to the annual average) and the average increments of strains between October 1986 and January 1987 were adopted as the strains in November 1986. Because the maximum fluctuation of strains was less than 0.3%, errors due to this adjustment on the initial sensor spacing was estimated to be less than 0.2%.

Strain profiles from the inductance coil measurements are illustrated in Figure 4.15. Strains due to the fill soil in the first construction season were less than 0.2% and therefore, were of little significance. At the end of the 1987 construction season, the strains developed uniformly along the geogrid with a maximum of 0.73% occurring at the 1 m location. Immediately after the last construction season in 1988 when the fill height reached 12 m, the strains showed significant localization. The strain jumped from 0.67% at the 1 m location to a maximum of 3.08% at the 3 m location; it dropped to 1.1% at the 4 m location and then decreased gradually within the fill. During the two year consolidation subsequent to the completion of the fill, the shape of strain profiles remained unchanged except for some small strain increments well into the fill.

Figure 4.16 shows the strain development in the geogrid at the 1, 2, 3, 5 and 8.5 m locations. The correspondence of the strain development with

construction activities can be observed except during the first construction season in which the measured elongation of the geogrid was negligible due possibly to the influence of air temperature on the readout indicator, as discussed earlier. In the figure, the location of the peak strain shifted into the slope as the fill height increased, and the strains fluctuated with the seasons.

4.3.2 Tensar Middle Layer

Several problems occurred at instrumented locations along the middle layer of the Tensar geogrid. The inductance coil at the 2 m location stopped working during September 1988. Even before September 1988, measured strains at the 2 m location varied randomly between positive and negative values in a series of field readings. These variations suggested that the coil failed at the beginning of 1987 construction season. At the 6 m location, field readings were continuously taken, but the measured strains showed virtually no change occurred between September 1988, when the fill height was at 4.6 m, and October 1990. This might also indicate failure of the coil. Hence, strains at these two locations (2 and 6 m from the surface) were estimated by taking the average of the strains measured in the adjacent coils. At the 3 m location, field measurements showed that the geogrid had been compressed in the slope direction since the beginning of the 1988 construction season. This phenomenon of compression, which was contrary to both the theoretical analyses and the readings of the electrical wire resistance strain gauges, apparently indicated failure of the monitoring system, although the coil was still providing erroneous readings. At this location, strains after September 1988 were estimated from the measurements of the inductance coil at the 5 m location, where the measured strains were very consistent, and the average ratio of strains at the two locations before failure.

The spacing between centers of the two sensors at each location, measured in the first set of field readings on September 1, 1987, was taken as the initial value. However, the strains at the 7 and 9 m locations were 0.52 and 0.37% on September 29, 1987 when the fill height was 4.6 m. These two strains deviated from the trend of the strain profile. To eliminate systematic errors, possibly initiated by construction activities, strains at the two locations were adjusted based on the shape of the strain profile obtained from the EWR strain gauge

measurements for the same time and the same geogrid layer. Strains at the two locations were adjusted to 0.21 and 0.11% respectively; strains measured thereafter at the two locations were also adjusted accordingly.

Figure 4.17 illustrates the strain profiles of the middle primary reinforcing layer of the Tensar geogrid. At the end of the 1987 construction season, the strain increased from the slope surface into the fill and reached a peak of 0.49% at the 5 m location; it decreased gradually further into the fill and dropped to 0.11% at the 10.5 m location. After the 1988 construction season, the location of the maximum strain remained the same, but its magnitude increased to 1.02%. The shape of the profile did not change compared with the November 1987 profile, except at the 1 m location where a strain increment of 0.8% was measured. Since the strain measured by EWR gauges on the same geogrid only changed by 0.08% between these two measurements, the large strain increment at the 1 m location was localized and not representative of overall strain behavior. From November 1988 to October 1989, the strain profiles were almost identical, whereas the profile in October 1990 showed a uniform increase of 0.1 to 0.15% at all locations along the geogrid. This change of the strain was probably caused by the influence of air temperature, as discussed in last section.

The entire strain development in the geogrid, at locations 1, 5, 7 and 10.5 m from the slope surface, is shown in Figure 4.18. It is similar to other strain-time diagrams discussed before and the variation of the strain is closely related to construction activities. The fluctuation of strain development with the seasons, as mentioned in last section, was not obvious during the 1987-1988 season because the fluctuation might have been compensated by loading from the fill during the construction. On one hand, strains were developed in the geogrid due to the fill placement; on the other hand, field readings, from the readout indicator, tended to decrease as air temperature decreased. The strain fluctuation between 1988 and 1990, however, was very clear, as shown in Figure 4.18. The rapid increase of the strain at the 1 m location can also be observed in Figure 4.18. From September (fill height of 10.5 m) to November 1988 (fill height of 12 m), the strain at the 1 m location jumped from 0.22 to 0.81%, whereas strain increments at other locations, including the location of the peak strain, were less than 0.15%. Therefore, it is reasonable to conclude

that the measurement of 0.81% does not represent the overall behavior of the geogrid within the test fill.

4.3.3 Tensar Top Layer

Among the ten inductance coils installed in the top layer of the Tensar geogrid, the coil at the 1 m location failed in September 1988; other coils worked well during the construction and the operation of the test fill. At the 1 m location, strains after September 1988 were estimated based on the strains at 2 and 3 m locations and the shape of strain profiles obtained from the EWR strain gauges.

Strain profiles of the geogrid in the Tensar top layer are shown in Figure 4.19. The strain developed during the 1987 construction was of minor significance since only 1 m of fill was placed on the geogrid. At the end of the final construction season when the fill height was 12 m, the strain increased sharply from the surface into the fill and reached its peak value of 2.28% at the 3 m location; it decreased to 1.71% at the 6 m location and then dropped rapidly to 0.38% at the spot 8 m from the surface. The strain profile of October 1990 was almost identical to that of November 1988, excluding minor increments of 0.15 to 0.2% at some locations. Figure 4.20 illustrates the full development of the strain at locations 2, 3, 5, 7 and 10.5 m from the slope surface. The strain increased a small amount in 1987, jumped significantly during the 1988 construction season and remained nearly constant during the subsequent consolidation. The fluctuation of strain with the seasons is clearly shown in the strain-time diagrams.

4.3.4 Signode Bottom Layer

The pairs of inductance coil sensors attached to the Signode geogrid were placed about 100 mm apart. The coils at the 7 and 8 m locations in the bottom layer of the Signode geogrid failed at the beginning of the first construction stage. The coils at the locations 1, 2, 3 and 4 m from the slope failed during the final construction season. Before the failures, the peak strain had occurred at the 5 m location. Therefore, it appeared reasonable to estimate the strains at the four locations according to the measured strain at the 5 m location and the

ratios between strains at the 5 m location and the each other locations before the failure.

Adjustment was made on the field measurements at the 2 and 3 m locations. The second field reading, taken on October 20, 1986 when the fill height was 2.1 m, showed strains of 1.64 and 0.18% at the two locations. The former was excessively large and the later was much smaller than the values in the trend of the strain profile and the measurements of the EWR gauge at the same location. These errors were caused either by construction activities or mistakes made during the original field reading. Thus, the strains at the two locations were adjusted by interpolating the strains at the 1 and 4 m locations. Strains measured thereafter were adjusted accordingly.

Figure 4.21 illustrates the profiles of tensile strain distribution along the bottom Signode geogrid layer. At the end of the first construction stage, the strain increased smoothly from the slope surface into the fill, reached the maximum of 1.28% at the 4 m location and decreased gradually further into the fill. The profile at the end of the second construction stage remained the similar shape with increments of the strain between 0.4 and 0.6% at different locations. During the final construction season, the strains did not change significantly at locations close to the slope surface and locations more than 7 m from the slope. The peak strain, however, moved to the 5 m location and increased to 2.35%. The strain around the peak was localized, whereas the strain at the 10.5 m location was of negligible magnitude.

The strains subsequent to the completion of the fill remained unchanged except for minor seasonal fluctuations, as discussed in previous sections. This feature can also be observed in the strain-time diagrams, shown in Appendix A.

4.3.5 Signode Middle Layer

The inductance coil at the 10.5 m location in the Middle layer of the Signode geogrid failed during the 1988 construction season. The strain at the location was estimated based on the measured strain at the 9 m location and the average ratio of strains at the two locations before the failure of the coil.

The middle layer of the Signode geogrid was placed on the field in early August, 1987 and a set of initial field readings were taken on August 17. Adjustments were made to the field measurements at the 7 m location. From August 17 to September 18, when the fill height increased from 3 to 4.3 m, the measured strain increased 0.8%, whereas the increments at the 5, 6 and 8 m locations were 0.29, 0.03 and 0.12% respectively during the same period. This excessive increment of the strain, possibly induced by construction equipments, was not representative of the real deformation of the geogrid at the location when compared with the EWR gauge measurements and the measurements in the Tensar section. Therefore, the average increment of strains measured at the 5, 6 and 8 m locations was assumed to have developed at the 7 m location during this period. The strains from the subsequent field measurements were adjusted accordingly.

Profiles of the strain distribution along the middle layer of the Signode geogrid are shown in Figure 4.22. During the 1987 construction season, the developed tensile strain varied smoothly along the geogrid layer with the maximum of 0.92% at the 4 m location. After the 1988 season, peak strain of 1.88% at the 4 m location continued, but another peak strain of 2.08% developed at the 7 m location. The largest increment of the strain between November 1987 and November 1988 occurred at the 8 m location with a magnitude of 1.84%. This increment of the strain might indicate the development of a shear zone within the soil of the reinforced slope while the final 6 m fill was placed on the test embankment. The measurements taken one and two years later did not show any significant changes either in the shape or in the magnitude of the strain profiles.

4.3.6 Signode Top Layer

The inductance coil at the 1 m location in the top layer of the Signode geogrid failed during the 1988 construction season, so the strain was estimated according to the measurements at the 2 and 3 m locations. Figure 4.23 illustrates the strain distributions along the geogrid. The tensile strains developed during the 1987 construction season were rather uniformly distributed along the geogrid except at the 2 m location where the measured strain was about 0.7% larger than the average value at the other locations. After the 1988 season, the strains at most locations increased considerably,

especially at the 7 and 9 m locations where strain increments of 2.04 and 1.76% were measured. At the 2 m location, the strain increased from 1.09% in November 1987 to 2.41%. Besides the 2 m location, the 9 m location developed the maximum strain of 2.28% and the 7 m location had the largest strain increment during 1988. No significant changes in strain other than the seasonal fluctuation were measured subsequent to the 1988 construction season.

The strain measurements at the 2 m location were questionable. From the very beginning of monitoring, the developed strains were considerably higher than at adjacent locations. For example, on October 23 and November 20, 1987, when the fill height was 5.5 and 6 m, i.e., only 0.5 and 1 m of fill above the geogrid layer, the strains were 0.58 and 1.09%, whereas the average strains at the adjacent locations were 0.21 and 0.38%. After the 1988 season, the strain at this location increased 1.32%, but the strain at the 3 m location increased by only 0.69%. The excessive strain, appeared to be loading-related can be attributed to either weak spot within the fill soil at this location or unknown problems with the instrumentation such as damage to the materials protecting the gauge. The former was less likely since the EWR strain gauge measurements did not show the same behavior (Figure 4.11). Nevertheless, the strain at the 2 m location, even if it did indicate the real deformation of the geogrid and shallow movement within the fill soil, would not affect the analysis of reinforcement mechanism and the overall behavior of the reinforced embankment slope.

4.3.7 Paragrid Bottom Layer

Sensors of inductance coils installed in the Paragrid geogrid were spaced between 145 and 155 mm. Although all coils in the bottom primary reinforcing layer of the Paragrid geogrid kept providing data during the monitoring period, there were several problems with the field measurements. At the 4 m location, strains measured during and shortly after the first construction season were negative (compression of the geogrid in the longitudinal direction). These negative strains were likely caused by construction activities. They were adjusted to the average values of the strains measured at the 3 and 6 m locations. Strains at the location after the first construction season were adjusted accordingly. At the 5 m location, the

measurement in October 1986 indicated a strain of -3.92%; from November 1986 to February 1987, the strain increased from 1.74% to 4.06%; after February 1987, the strain fluctuated between 2.6 and 5% . This indicates that the coil at the 5 m location failed during the first construction season. Therefore, the strains at the 5 m location were estimated by taking the averages of strains at the 4 and 6 m locations. The same problem occurred at the 9 m location where the strain varied irregularly between 3.8 and 5.3% after October 1986. The averages of strains at the 8 and 10.5 m locations was used to estimate the strains at the 9 m location. At the 10.5 m location, the strain measured on October 20, 1986, when only 1.3 m of fill was placed above the geogrid, was 2.17%. It was adjusted according to the trend of strain distribution in the other geogrids. The measurements after October 1986 were adjusted accordingly at the location.

Profiles of tensile strain distribution, after the adjustment, along the bottom layer of the Paragrid geogrid are shown in Figure 4.24. A maximum strain of 1.27% was developed at the 3 m location during the first construction season. At the end of the second construction season, the distribution of the strain remained the same; the magnitude increased about 0.8 to 1.1% with the peak strain of 2.31% occurring at the 3 m location. During the final construction season, in which the top 6 m of the fill was placed, no significant change of the strain was measured at all instrumented locations except the 4 m location where the strain jumped from 2.02% to 3.56%. In the consolidation period after the final construction, the strain remained constant except for fluctuations possibly caused by air temperature variations, as discussed in previous sections. The variation of the strain, at typical locations in the bottom Paragrid geogrid layer, at different stages of construction and consolidation can also be seen in the strain-time diagrams in Appendix A.

4.3.8 Paragrid Middle Layer

Measured strain distributions along the middle layer of the Paragrid geogrid, at different stages of construction and consolidation, were plotted in Figure 4.25. At the 1 and 7 m locations, the strains developed to 1.31 and -0.35% at the end of the 1987 construction season, to 2.54 and 0.78% during 1988 and to 3.41 and 1.03% in October 1990. If the negative strains developed during the 1987 construction season are adjusted to the averages of strains at the 6 and 8

m locations, the strains at the 7 m location become 1.34%, 2.47% and 2.71% at the above three stages respectively. At other locations, however, as also shown in Appendix A, the strains remained nearly unchanged, excluding the fluctuations due to temperature, during the 1988 construction season and the subsequent two years of consolidation. The peak strain at the end of the 1987 construction was 1.95% at the 5 m location and the strain measured thereafter at the 5 m location varied between 1.67 and 2.37% .

4.3.9 Paragrid Top Layer

At the instrumented location 8 m from the slope surface in the top primary reinforcing layer of the Paragrid geogrid, the strain measured by the inductance coil varied randomly between -0.78 and 0.06% before the coil stopped working in November 1988. Irregular variation of the strain also occurred at the 7 m location. The inductance coils at the 7 and 8 m locations were considered being failed during the 1987 construction season and the strains at the two locations were estimated by interpolating strains at the 6 and 9 m locations. The coil at the 9 m location stopped providing data in September 1988 and the strains since then were estimated from the measurements at the 10.5 m location.

Figure 4.26 illustrates distributions of the strain in the top layer of the Paragrid geogrid. Strains developed during the 1987 construction season were less than 1.1%. At the end of the 1988 construction season, a maximum strain of 4.9% was developed at the 1 m location; the strain decreased with distance from the slope surface except at the 5 m location where the strain was greater than at the 4 m location. The increment of the strain developed due to consolidation between November 1988 and October 1990 varied between 0.14% and 1.35% with the maximum increment occurring at the 5 m location. The increments of the strain beyond the 6 m location were insignificant.

4.4 Horizontal Movement of Fill and Foundation Soils

Horizontal movements of the fill soil at four levels, 0, 2, 4 and 6 m above the ground surface, were monitored using magnetic probe extensometers. By travelling through the PVC central access tube at each instrumented level, the probe measured distances between the target magnets and the west end of the

access tube. The field measurements were then converted into distances between the target magnets and the center magnet, placed along the center long axis plane of the test embankment. The center magnet was assumed not to move during the construction of the test fill. This assumption was justified by the field measurements that the induced error would be of little significance comparing with the amount of measured displacement, as discussed later. By subtracting the initial distances between the target magnets and the center magnet from the measured distances, the horizontal displacements of the target magnets, relative to the center magnet, were determined. Moreover, by comparing horizontal displacements at adjacent magnets which were approximately 2 m apart, average horizontal strains of the soil were calculated. To be consistent with the designation of the strain in the geogrids, extensive strain within the fill soil was designated as positive.

Horizontal movements of the fill and the foundation soils along vertical lines beneath the toe and the crest of each test section were monitored by using a vertical digital biaxial inclinometer operated in casings installed during the construction of the test fill. Field readings were taken from a digital indicator and converted into horizontal deflection between two pairs of wheels 60.96 cm apart, in directions parallel and perpendicular to the long axis of the embankment. Measurements were taken from the bottom of a casing, placed 12 m below the ground surface in a stiff till (assumed fixed), to the top and accumulated deflections along the casing were calculated. Field readings were recorded twice with the pairs of wheels rotated 180°, to eliminate zero errors caused by either the sensor or the indicator. Horizontal displacements at different locations along the vertical alignment were obtained by subtracting the initial configuration of the casing from the measured accumulated deflections.

During the summer of 1988, some severe damage was caused by the construction activities. The vertical casing at the crest of all test sections and the horizontal casing at the 6 m level in both the south and north instrumentation zones were blocked when the fill height reached 8 m. The horizontal casing at the 4 m level in the north zone was also damaged and blocked.

4.4.1 0 m Level in Tensar Section

Profiles of the average horizontal strains of the soil at the ground level in the Tensar section are shown in Figure 4.27. During the first construction season, the fill soil moved into the slope with a maximum displacement of 7 mm; the magnitude of the strain was less than 0.1% at all locations. As consolidation occurred and more fill was placed in the 1987 construction, the soil at the 0 m level moved outwards. Within the slope, the soil was extended; at the locations near the toe, however, the soil was compressed due to the boundary effect at the toe. The magnitudes of the strain were less than 0.2% after the second construction season when the fill height was 6 m. The trend of the compression and extension zone development in the soil at the 0 m level became obvious after the third construction season in 1988 when the fill height reached 12 m, as shown in Figure 4.27. The average strain of the soil close to the toe was -0.45%; the strain gradually increased further into the fill and developed to its maximum of 0.65% in the soil at 14 to 18 m from the toe. The profiles of October 1989 and September 1990 show the same strain development pattern.

Figure 4.28 shows the strain-time diagrams of the soil at typical locations. In the first construction season, the strain of the soil was of small magnitude. After the 1987 construction season, the strain within the slope remained small, but the soil close to the toe steadily developed compressive strain. During the 1988 construction season, both compressive and extensive strains of the soil increased. These strains remained approximately constant throughout the subsequent consolidation.

When field readings were taken, the probe was pulled from the west side of the embankment to the east, i.e., from the Tensar section through the center magnet to the Paragrid section. Therefore, it is worthwhile to compare displacements between the center magnet and its adjacent magnets on both sides. Before the third construction season, the displacements between the two magnets in the Tensar section were positive (outwards movement) and less than 3 mm. The displacements on the other side, i.e., in the Paragrid section, were similar. Even after the third construction, the displacements on both sides were of the same magnitudes between 11 and 16 mm. Hence, the

assumption that the center magnet did not move was valid, at the 0 m level of the north part of the test fill.

4.4.2 2 m Level in Tensar Section

Fourteen sets of field measurements were taken at the 2 m level in the Tensar section, between October 1986 and September 1990. The distances between the target magnets and the center magnet measured in the first field reading in October 1986 were considered as the initial values. However, the results of the second field reading, taken when the fill height was 3 m, indicated 0.85% compression of the soil 4 to 6 m from the slope surface and 0.7% extension in the soil 8 to 10 m from the surface. This highly localized phenomenon appeared not to represent the overall behavior of the soil since only one metre of the fill was in place above this level. To eliminate systematic errors, possibly caused by construction activities, the displacements of magnets at the 6 and 8 m locations in December 1986 were adjusted to the average values of their adjacent magnets. Displacements at the two locations measured thereafter were adjusted accordingly.

Profiles of the horizontal strain of the soil at the 2 m level in the Tensar section are shown in Figure 4.29. During the first construction season, the soil moved into the slope and the magnitude of the strain was less than 0.2%. During the second construction season, the soil moved outwards. In the soil less than 4 m from the slope surface (under the crest of the embankment at the time), the soil displaced off the fill, comparing with the original position of magnets; in the area further into the fill, the soil displaced still to the slope, but the magnitude of displacement decreased. The maximum strain occurred in the area 4 to 6 m from the slope surface. At the end of the final construction season, the strain of the soil increased uniformly about 0.5 to 0.6% along the instrumented level except in the soil 10 to 12 m from the surface where the strain was up to 1.65%. Profiles of the strain measured one and two years later were almost identical. The features of the strain development can also be observed in the strain-time diagrams, shown in Figure 4.30.

Comparing the deformations of the soil between the center magnet and its adjacent magnets on the both sides of the test embankment, it was found that

the center magnet might have moved. Before the end of the 1987 construction, the deformations in the Tensar section were between -12 and -15 mm, whereas the deformations in the Paragrid section were between 3 and 8 mm; the average deformations between the two magnets after the 1988 construction were 0 and 23 mm for the Tensar and Paragrid section respectively. It was estimated that the center magnet might have moved 5 to 10 mm towards the Paragrid section. This amount of movement was small comparing with the maximum relative displacement of 132 mm measured in the Tensar section and 226 mm in the Paragrid section. Moreover, the deformation of the soil within the slope was of more significance than the absolute displacement when considering the soil-geogrid reinforcement mechanism. Therefore, the possible 5 to 10 mm movement of the center magnet did not affect the accuracy of the extensometer measurements.

4.4.3 4 m Level in Tensar Section

Five sets of field extensometer readings were taken at the 4 m level in the Tensar section before the access tube was blocked, during the 1988 construction season, at a location about 19 m from the west end of the tube. No reading was taken since then until October 1989, when an effort was made and another set of measurements were taken.

Strain profiles of the fill soil at the 4 m level in the Tensar section are shown in Figure 4.31. At the end of the 1987 construction season, the soil displaced outwards with a maximum movement of 27 mm near the slope surface; the maximum strain of 0.25% occurred in the soil 2 to 4 m from the surface. After nine months of consolidation, the strain of the soil increased slightly in all locations at this level. From the measurement taken one year after the fill completion, it was seen that the strain of the soil developed due to loading of the 6 m fill in the 1988 construction was large. In the soil 2 to 4 m from the slope surface and the soil 10 to 12 m from the surface, for example, the strain jumped from 0.3 and 0.35% in August 1988 to 3.0 and 2.1% in October 1989. The profile of strain in October 1989 was highly localized in the two locations.

4.4.4 6 m Level in Tensar Section

Two sets of extensometer readings were taken in the summer of 1988 before the access tube at the 6 m level was blocked by the construction. The first reading was taken in early June when the fill height was 6 m; the second reading was taken in the middle August when the fill height was 8 m. A maximum strain of 1.9% was measured in the soil 2 to 4 m from the slope surface. Since only one set of field measurements, excluding the initial reading, was taken during the construction season in which severe damages occurred, the reliability and accuracy of the measurements were questionable.

4.4.5 Vertical Alignment beneath Toe in Tensar Section

Figure 4.32 shows the accumulated deformations in the foundation soils, in the slope direction (designated as direction A, which will be used throughout this thesis), along the casing installed vertically beneath the toe of the slope in the Tensar section. At the end of the first construction season, the foundation soils beneath the toe moved outwards a small amount. During the second construction stage, the soils around the upper part of the casing moved outwards a smaller amount than occurred the previous year, whereas the lower part of the casing moved slightly inward to the slope. The former, decreasing outward movement, was perhaps caused by differential settlement of the foundation soils which made the casing tilt into the fill; the later might be explained as buckling of the casing as it was dragged down by settlement of the foundation soils. After the 1988 construction, the soils deformed slightly into the fill around the bottom of the casing; the outward movement then increased approximately linearly as the elevation increased and reached about 12 mm near the ground surface. Increments of 3 to 4 mm horizontal movement developed rather uniformly along the vertical alignment from November 1988 to October 1989 and the displacement profile maintained the same shape.

Profiles of the horizontal displacements in the direction parallel to the long axis of the test embankment (designated as direction B, which will be used throughout this thesis) are shown in Figure 4.33. In November 1986, the amount of horizontal movement was less than 2 mm. During the 1987

construction season, the horizontal displacement increased from the bottom to the top of the casing. It is interesting to note that the horizontal displacement profile measured in November 1987 remained the same through the subsequent measurements. In other words, the horizontal deflections in the direction B were not sensitive to placement of the fill. Moreover, the magnitude of the deflections were smaller than in the slope direction. This characteristic of displacement development provides valuable indication of the state of stress and strain within the test fill, as will be discussed later in this thesis.

Figure 4.34 shows the horizontal deflection development with time in the direction A. The development of horizontal displacement with the construction activities is obvious. The outward movement increased in the first construction season and dropped during the following consolidation; it increased again in the second and third construction season and remained approximately constant after the construction. The features of horizontal deflection development in the direction B were similar. The horizontal displacement varied with respect to the construction activities in the 1986 and 1987 seasons; the displacement, however, did not respond to the third construction season during which 6 m of fill was placed on the embankment.

4.4.6 Vertical Alignment beneath Crest in Tensar Section

Horizontal movements of the soils along the vertical line beneath the crest of the test embankment were also monitored using the inclinometer. The casing of the inclinometer was extended during the construction of the fill so as to allow for measurement of the horizontal displacements of the fill soil along this alignment. Due to the construction activities, soil movements during the construction season could not be properly indicated. For example, the configuration of the casing in the bottom 3 m of the fill at the end of the first construction stage can only be considered as the initial configuration from which the fill would deform under subsequent fill placement. Because the vertical inclinometer casing beneath the crest was blocked during the 1988 construction season, only the horizontal deflections before August 1988 could be measured.

Horizontal deflections of the fill and the foundation soils in the slope direction (A) and the direction normal to the slope (B) are illustrated in Figure 4.35 and Figure 4.36. Both figures show movements of less than 2 mm in the two directions after the first construction. After the 1987 construction season, the outward movement of the foundation in the A direction occurred in the top 3 to 4 m soils and increased with elevation until it reached a maximum displacement of 12 mm near the ground level (elevation 702 m) in August 1988. The horizontal displacement of the foundation soils in the direction B showed the same feature of increasing with elevation, but the magnitude was smaller than in the direction A.

4.4.7 0 m Level in Signode Section

Profiles of the horizontal strain of the soil at the ground level in the Signode section are illustrated in Figure 4.37. The strains developed during the first construction season were less than 0.1%. The soil moved into the fill at most locations with a maximum value of 6 mm during the period. During the second construction season, only minor changes less than 0.2% of strain occurred at locations along the elevation except for the soil near the slope surface where a strain of 0.3% developed. At the end of the final construction season, the strain in the fill had the same distribution as was found in the Tensar section. The soil near the toe was compressed as the fill was placed to 12 m height; the strain of the soil increased from the toe into the fill and reached a maximum of 0.65% at the 17 m location. No significant changes were observed from the strain profiles measured one and two years after the fill was completed. The development of the strains at representative locations along the instrumented elevation with respect to the construction and consolidation stages of the test fill can be seen in the strain-time diagrams shown in Appendix A.

Similar to the discussion in previous sections, to check the assumption that the center magnet did not move, it is worthwhile to compare the relative movement between the center magnet and its adjacent magnets on the east and the west side of the fill. After the final construction season, the magnet in the Signode section displaced between 4 and 7 mm outwards; the magnet in the unreinforced section moved about 8 mm outwards. This fact justified again

the validity of the assumption that the center magnet remained fixed in its original position within the fill.

4.4.8 2 m Level in Signode Section

Fifteen sets of horizontal extensometer field readings were taken at the 2 m level in the Signode section. The second field reading was taken at the end of the first construction season when 1 m of fill was placed above this level. The magnet at the 16 m location moved 12 mm inward in the fill. It meant that about 1% of extension strain developed within the fill between 14 and 16 m from the slope surface, while the average horizontal strains within the soil at other locations were less than 0.1%. This movement was most likely induced by construction equipment. Thus, a zero extension strain was assumed in the soil between 14 and 16 m from the slope surface and the movement of the magnet at the 16 m location was adjusted systematically.

Figure 4.38 shows the horizontal strain profiles of the soil at different stages of construction and consolidation. The strain within the soil developed during the 1986 construction season was of little significance since only 1 m of the fill was placed above this level. At the end of the 1987 construction, the strain varied smoothly along the level with a maximum average strain of 0.65% occurring in the soil 4 to 6 m from the slope surface. After the placement of the top 6 m of the fill during the 1988 construction season, the strain distribution changed significantly. The average horizontal strain increased sharply from 0.6% near the slope surface to 2.65% at the 3 m location. The strain remained nearly unchanged within the soil 2 to 8 m from the surface and dropped to 1.1% within the next 2 m. It then decreased gradually at further locations in the fill. The maximum strain increment of 2.2% occurred in the soil between 6 and 8 m from the surface. The horizontal strains developed due to consolidation after completion of the fill were small, as seen in Figure 4.38 and the strain-time diagrams shown in Appendix A.

The movement between the center magnet and its adjacent magnet in the Signode section varied between 7 and 15 mm after the 1988 construction season; the movement between the two magnets on the other side of center line (in the unreinforced section) was 10 to 13 mm. Therefore, it appeared that the center magnet did not displace significantly as the fill was placed.

4.4.9 4 m Level in Signode Section

Figure 4.39 illustrates profiles of the horizontal strain within the soil at the 4 m level in the Signode section. The strain developed during the 1987 construction season distributed smoothly with the maximum average strain of 0.3% occurring in the soil 2 to 4 m from the slope surface. During the 1988 construction season, the strain distribution changed considerably. In September when the fill height was 10.5 m, the maximum strain and the maximum strain increment occurred in the soil between 4 and 6 m from the surface. At the end of the 1988 construction season, a maximum strain of 2.5% remained in the soil between 4 and 6 m from the surface, but the maximum strain increment of 2.35% (from November 1987 to November 1988) occurred in the soil between 8 and 10 m from the surface. The strain and strain increment of the soil greater than 10 m from the slope surface decreased gradually to 1.45% at the location 14 m from the surface. The profile of the strain measured two years after the completion of the fill was identical to the profile in November 1988.

Again, the relative displacements between the center magnet and the adjacent magnets in both sides were compared. The movements were 21 mm in the Signode section and 15 mm in the unreinforced section at the end of the 1988 construction season. The possible movement of the center magnet was also of minor significance.

4.4.10 6 m Level in Signode Section

Three sets of extensometer field readings were taken at the 6 m level in the Signode section during the summer of 1988 before the access tube was blocked by construction activities. The first set of readings were taken before the construction as the initial measurements. The second set of readings, taken in August when the fill height was 8 m, showed some unexpected movements of the magnets. At the 0 and 6 m locations, the magnets moved 38 and 24 mm towards the slope; at the 2 and 4 m locations, however, the magnets moved 2 mm outwards and 46 mm inwards respectively. This set of measurements indicated an average horizontal compression strain of 3.5% developed in the soil between 4 and 6 m from the slope surface. This compression strain, which seemed not to be generated by the load of the 2 m of fill above the level, was

most likely caused by construction activities at the beginning of the construction season. By comparing this set of measurements with the measurements taken in early September, the maximum increment of the average horizontal strain, when the fill height increased from 8 to 9.5 m, was found to be 1.25% and it occurred in the soil between 6 and 8 m from the surface. Since no more field readings were available, it is impossible to make adjustment for the construction activities to produce strain profiles along the level.

4.4.11 Vertical Alignment beneath Toe in Signode Section

Fourteen sets of field readings were taken along the vertical casing installed beneath the toe of the slope in the Signode section between September 1986 and September 1990. Profiles of the horizontal deflection of the foundation soils along the casing in the direction A, at different stages of construction and consolidation of the test fill, are illustrated in Figure 4.40. During the first construction season, the foundation soils moved into the fill less than 2 mm. At the end of the second construction season, the soils below the -6 m level showed almost no displacement, whereas the deflections of the soils above this level increased with elevation and reached a maximum of 8.4 mm near the ground surface. After the final construction stage, the shape of the displacement profile remained the same as during the previous year, but the magnitude of the movement increased considerably. Above the -6 m level, the deflection of the foundation soils increased approximately linearly with elevation to its maximum of 30.3 mm near the surface. Increments of the horizontal deflection between 2 and 3 mm developed above the -6 m level during the consolidation period from November 1988 to September 1990.

Profiles of the horizontal deflection of the foundation soils in the B direction are shown in Figure 4.41. The deflection increased with elevation in all profiles, similar to the profiles in the A direction. The magnitudes of the deflection in the B direction, however, were much smaller than in the A direction. Moreover, the relationship between the development of the horizontal movement and placement of the fill was not as clear as in the A direction. Apparently, the horizontal movement in the direction normal to the slope (B) was of minor significance compared to the movement in the slope direction (A). The development of the horizontal displacement of the

foundation soils beneath the toe of the slope in both directions can also be seen in the displacement-time diagrams, shown in Appendix A.

4.4.12 Vertical Alignment beneath Crest in Signode Section

Ten sets of vertical inclinometer measurements were taken in the vertical casing beneath the crest of the slope in the Signode section before the casing was blocked by construction equipment in the summer of 1988. Figure 4.42 shows profiles of the horizontal deflection of the fill and foundation soils along the vertical alignment in the A direction. Profiles at different stages of construction show the same features of increasing outward movement with elevation except at the ground level where inward displacement of the casing of about 15 mm was detected throughout the monitoring period. This displacement indicated possible buckling of the casing at the ground surface. Therefore, the measurements at the ground level was omitted and the profiles of the horizontal movement was adjusted, as shown in Figure 4.43. In the foundation soils, the movement during the first construction season was little; the movement after the second construction increased gradually with elevation, with a maximum displacement of 7.3 mm occurring near the ground surface in August 1988. This amount of displacement was slightly smaller than the displacement beneath the toe at the same time. The horizontal movement of the fill soil increased nearly linearly with elevation in all profiles, but the rate of the increase in 1987 was much higher than in 1986. During the period between November 1987 and August 1988, average increments of displacement of 8 to 10 mm were measured in the bottom 3 m of the fill soil.

Profiles of the horizontal movement of the soils beneath the crest of the slope in the B direction are illustrated in Figure 4.44. The measurements showed that the displacement increased with elevation, but the magnitude of the movement in the foundation soils was less than 4 mm. These were smaller than the movement in the A direction, as discussed in previous sections.

4.4.13 0 m Level in Paragrid Section

Profiles of the average horizontal strain of the soil at the ground level in the Paragrid section are shown in Figure 4.45. The horizontal strain

developed sequentially, in a manner similar to the Tensar and Signode sections, as the fill was constructed. The strain developed during the first construction season was less than 0.15%. The increment of the strain due to fill placement in the second construction stage was about 0.05% at most instrumented locations at the ground level and the strain was distributed rather evenly. After the final construction season the strain distribution changed. Near the toe of the slope, the soil compressed about 0.1%; the strain increased with distance from the slope and reached a maximum of 0.6% at the location near the center of the test fill. There were no significant changes to the strain pattern during the two years of consolidation subsequent to the final fill placement. The development of the strain at the ground level is presented in the strain-time diagrams in Appendix A.

4.4.14 2 m Level in Paragrid Section

The first field reading of extensometers at the 2 m level in the Paragrid section was taken in October 1986. The second measurement, taken at the end of the first construction season when 1 m fill was placed above the level, indicated 0.15% compression in the soil between 12 and 14 m from the slope and 0.95% of extension in the soil 14 to 16 m from the slope. These unreasonable movements of the soil were likely due to the excessive outward displacement of the magnet at the 14 m location, perhaps caused by construction equipments. The strains in the soil at these locations at the end of the first construction season were, therefore, adjusted based on the trend of the strain profiles in the other sections and the strains measured thereafter at the locations were adjusted accordingly.

Profiles of the horizontal strain at the 2 m level are illustrated in Figure 4.46. The strain developed during the first construction season was smoothly distributed along the level with a maximum of 0.65% around the 5 m location. During the second construction, the maximum increment of the strain was 0.3% at the 7 m location and the peak strain remained at the 5 m location. After the final construction season, the peak strain moved to the 7 m location and increased to 2.05% with a high degree of localization at this location. Further into the fill, the strain decreased to about 0.7% near the center of the fill. The distribution and the magnitude of the strain during the following two year consolidation remained nearly unchanged.

4.4.15 4 m Level in Paragrid Section

The extensometer magnets and the access tube at the 4 m level in the Paragrid section were installed in September 1987. The second set of field readings taken in October showed that the magnet at the 12 m location moved 6 mm inwards while adjacent magnets moved outwards. This inward displacement, likely induced by localized activities, was adjusted to the average value of the displacements at the adjacent magnets and the measurements after the second set of field readings were adjusted accordingly.

The access tube at the 4 m level was blocked during the 1988 construction season in the middle of August when the fill height was 8 m. Figure 4.47 shows the strain profiles prior to August 1988. The strain developed during the 1987 construction was less than 0.2%. When another 2 m of fill was placed above the level, the strain jumped considerably near the slope surface, increasing about 0.2% at the middle locations and remained approximately the same near the center of the fill.

4.4.16 6 m Level in Paragrid Section

Two sets of field horizontal extensometer measurements were taken at the 6 m level in the Paragrid section before the access tube was blocked by construction equipments. The second set of field readings indicated that a maximum horizontal strain of 3.05% developed in the soil between 2 and 4 m from the slope surface when the fill height was 8 m. The consistency and the reliability of the measurements were not evaluated since no additional field readings were available.

4.4.17 Vertical Alignment beneath Toe in Paragrid Section

The vertical inclinometer operating casing installed beneath the toe of the Paragrid geogrid reinforced slope was blocked during the 1988 construction. The horizontal deflection profiles in the slope direction (A), prior to the late August 1988 when the fill height was 8 m, are illustrated in Figure 4.48. The horizontal deflections developed during the first construction season were negligible. The profile of the deflection at the end of the second construction and the profile in August 1988 show steady increases of the deflections from the bottom of the casing to the ground surface. Near the ground surface, the

rate of the increase was larger than at other locations along the casing. Figure 4.49 shows the horizontal deflection profiles of the soils in the B direction. Although the profiles indicate the same feature of increase with elevation, the magnitude of the deflection in the A direction was considerably larger than in the B direction after the second construction season.

4.4.18 Vertical Alignment beneath Crest in Paragrid Section

Nine sets of field readings were taken along the vertical inclinometer casing beneath the crest in the Paragrid section before the casing was blocked during the 1988 construction season. At the elevation 701.1 m, field measurements showed that the horizontal deflections after the beginning of the second construction season were considerably different from the deflection profiles at locations above and below this elevation. This discrepancy most likely indicated buckling of the casing around the elevation 701.1 m. To represent the overall behavior of the soil deformation, the horizontal deflection at this location was adjusted by taking the average value of the deflections at locations 0.6 m above and below the elevation. At the beginning of the 1987 construction season, a horizontal deflection value of 29.5 mm was measured between elevation 704.2 m and 704.8 m. This excessively large movement was likely induced by construction equipment operating near the casing. Therefore, the deflection between the two elevation levels was estimated based on the measurements in the other sections and the deflections measured thereafter were adjusted accordingly.

Profiles of the horizontal deflections of the soils, in the A direction are shown in Figure 4.50. The deflections of the foundation soils were less than 5 mm prior to August 1988. The deflection of the fill soil generally increased with elevation and increased as more fill was placed. Figure 4.51 illustrates the profiles of the deflection in the B direction. The profiles show that the casing buckled immediately above the ground level. Again, the magnitude of the deflection in the B direction was significantly smaller than in the A direction.

4.4.19 0 m Level in Unreinforced Section

The first set of horizontal extensometer readings at the ground level in the unreinforced section were taken in early September 1986, immediately after the installation of the casing. The magnet located 4 m from the slope surface, however, indicated 14 mm of inward movement, 8 mm larger than the movements at the 2 and 6 m locations, when the fill height was less than 1 m. This excessive movement, apparently caused by construction activities, was adjusted to the average value of the adjacent magnets and the future readings were adjusted accordingly.

Profiles of the average horizontal strains of the fill along the ground level are shown in Figure 4.52. During the first and the second construction seasons, the strain was of magnitudes less than 0.2% at all locations. After the third construction season, changes to the strain distribution occurred. Excluding the 7 m location where almost no deformation was measured throughout the monitoring period, the strain increased gradually from zero at the toe into the fill, reaching about 1% at the 13 m location and decreased further into the fill. Although some fluctuation of the strain were detected, the strain distribution along the ground level did not change significantly during the consolidation. The horizontal strain distributions of the soil at the ground level in the unreinforced slope were similar to the distributions in reinforced slopes, as discussed in previous sections.

4.4.20 2 m Level in Unreinforced Section

Magnets and the access tube were installed at the 2 m level of the unreinforced section in October 1986 and the first field reading was taken immediately after. The second reading, taken at the end of the 1986 construction when the fill height was 3 m, indicated 0.25% of horizontal compression strain in the soil between 12 and 14 m from the slope surface. This deformation was much larger than the deformations of the soil at adjacent locations and was likely induced by construction activities. Therefore, it was adjusted according to the measurements at the adjacent locations and the related strain distribution in other sections of the test fill. Strains measured thereafter were adjusted accordingly as well.

The profiles of the average horizontal strain, after the adjustment, are illustrated in Figure 4.53. The strains were small during the first and the second construction seasons at most locations other than the 7 m location where average strains of 0.8 to 0.9% were measured. At the end of the final construction season when the upper 6 m of fill was placed, the distribution of the strain in the soil changed significantly. The strain distribution was characterized by localizations at three locations: 0.9% strain at the 1 m location due mainly to shallow movement of the fill, a maximum of 1.6% and sharp variation at the 7 m location and another peak of 1.4% occurred at the 13 m location. During the consolidation period between November 1988 and September 1990, the strain distribution of the soil remained nearly unchanged, as shown in Figure 4.53 and the strain-time diagrams in Appendix A.

4.4.21 4 m Level in Unreinforced Section

Eight sets of horizontal extensometer measurements were taken at the 4 m level before the access tube was blocked, at 2 to 4 m from the slope surface, during the summer of 1989. Figure 4.54 shows the profiles of the average horizontal strain along the 4 m level. The strains developed during the 1987 construction season was of negligible magnitude. A maximum increment of the strain of 0.5% developed in the six month consolidation period subsequent to the 1987 construction. The strain increased rapidly during the 1988 construction season and reached a peak of 2.45% at the 3 m location at the end of the fill placement. The profile shows a sharp increase in the strain from zero at the slope surface to the peak and a drop from the peak to 1% at the 7 m location. Beyond the 7 m location, the strain increased slightly further into the fill. No significant changes appeared in the profile of the strain distribution six months after completion of the test fill. The maximum increment of the strain was 0.2% which occurred at the 3 m location during the period.

4.4.22 6 m Level in Unreinforced Section

Three sets of field extensometer readings were taken at the 6 m level in the unreinforced section. The first set of readings were taken as the initial measurements before the upper 6 m of fill was placed. The second set of

measurements indicated 2.5 and 1.5% of average horizontal strains in the soil at the 3 and 5 m location when the fill height was 8 m; the strains measured in September 1988, when the fill height was 9.5 m, were 5 and 2.5% at the two locations. The strains of the soil at other locations were relatively small in the two sets of field measurements.

4.4.23 Vertical Alignment beneath Toe in Unreinforced Section

Profiles of the horizontal deflections of the foundation soils, in the slope direction, along the casing vertically installed beneath the toe of the slope in the unreinforced section, are shown in Figure 4.55. The horizontal displacement developed during the first construction season was of negligible magnitudes. At the end of the second construction stage, the casing was bent towards the fill with displacement magnitudes less than 8 mm. The inward movement increased from the bottom of the casing to the -3 m level and then decreased as near the ground surface. After the final construction season, the displacement below the -6 m level remained constant; above this level, the outward displacement increased with elevation and reached 10 mm near the ground surface. The displacement of the soil above the -6 m level kept increasing with consolidation. The maximum increment was 10 mm which occurred near the ground surface. The profile of the deflection measured in September 1990 is almost identical to the profile in October 1989.

Profiles of horizontal deflections of the soils in the B direction are illustrated in Figure 4.56. The horizontal movements of the foundation soils in this direction showed the same features as in the A direction, but the magnitudes of the former were considerably smaller except at the ground surface where the measurements were possibly affected by disturbance near the casing. Below the -1 m level, the horizontal movements in the B direction were of negligible magnitude.

4.4.24 Vertical Alignment beneath Crest in Unreinforced Section

Nine sets of inclinometer measurements were taken along the vertical casing beneath the crest of the slope in the unreinforced section before the casing was blocked. The last set of field readings were taken in August 1988 when the fill height was 8 m. Figure 4.57 and 4.58 show the profiles of the

horizontal deflections in the direction A and B. The horizontal displacements of the foundation soils along the vertical alignment beneath the crest were negligible in both directions before August 1988. In the fill soil, the horizontal movement in the A direction increased with elevation, whereas the movement in the B direction scattered along the casing. Nevertheless, the magnitude of the movement in the B direction were significantly smaller than in the A direction.

4.5 Vertical Movements of Fill and Foundation Soils

Relative vertical movements of the fill soil within the test embankment at level 0, 2, 4 and 6 m above the ground surface were monitored using a horizontal inclinometer. The inclinometer was operated in horizontally installed casings. By travelling through a casing from one side of the embankment to the other, the probe detected vertical deflection of the casing at intervals of 61.0 cm. Field readings, taken from the digital indicator, were converted into deflections between each set of two measuring points. From comparison of measured configurations of the casing with its original configuration, obtained in the first field reading, accumulated vertical displacement at each point with respect to a reference point along the casing was calculated. To eliminate systematic errors, field measurements were taken consistently with the indicator connecting to the west end of the inclinometer probe. Therefore, the west end of the casing became the reference point. The locations of the reference points were established by surveying techniques throughout the field research.

Continuous field readings had been taken since the installation of the horizontal casings. Results of the field measurements before May 1988 showed remarkable consistency; later results were also consistent and repeatable. The two series of results, however, did not match each other at all levels. Configurations of the casings measured after May 1988 differed dramatically and unreasonably from configurations measured before. There is neither a theoretical basis nor practical reason for this abrupt change. Obviously, some technical problems occurred with the measuring system for unknown reasons. Calibration tests on the probe and the digital indicator were, therefore, conducted again in February 1990 and the calibration coefficient was found to be identical to that obtained before May 1988. Most likely, this

change was caused by a zero drift or other similar instrumentation problem. In order to maintain consistency, field measurements were adjusted by taking the configuration of each casing measured in May 1988 as another initial configuration for measurements taken thereafter. A summation of the relative vertical displacement before May 1988 and an increment of the displacement from May 1988 to the time when field readings were taken became the total vertical movement of the soil at the instrumented point relative to the reference point. For example, at a point, the displacement measured in November 1987 was A, referred to the west end of the casing; the vertical deflections were B in May 1988 and C in November 1988. Therefore, the total relative vertical displacement of the point in November 1988 was calculated as $(A+C-B)$. The results after the adjustment were consistent, reasonable and meaningful. However, soil deformations in the period from November 1987 to May 1988 were missed in the adjustment, because of the problems which occurred with the measuring system. Nevertheless, since no construction was carried out and soils on the surface was frozen during this period, errors of soil deformation in the period would not be significant.

The horizontal inclinometer measured vertical deflections of the casings relative to a certain datum point. Where the settlement within the test fill was concerned, however, the absolute movement of the datum point was required. The sums of the relative vertical displacements along the casing and the absolute movement of the soil at the datum point provide the settlement profile at the instrumentation level. There were two approaches to monitor the absolute movements of the casings in the test fill. Elevation survey measured the vertical movements of each ends of a casing; vertical extensometers detected vertical movements between target magnets. The vertical movements of the casing at the locations beneath the crest were obtained by interpolating the displacements of the magnets located above and below the horizontal casing. Comparatively, measurements from the vertical extensometer were more reliable and more accurate than the elevation survey, because more potential errors existed in the survey.

There were four specific points, both ends of each horizontal casing and the locations beneath the crest of the east and west sections, at which absolute vertical displacements could be obtained. Hence, four settlement profiles of

the soil along the instrumentation level would be available after each set of measurements. These profiles were supposed to represent the same picture of soil deformations along the same horizontal casing, but, as a matter of fact, they did not. Profiles of settlement based on different measurements of absolute vertical movements showed the same shape but significantly different magnitude. Nevertheless, in most cases, there were usually two or three profiles, for each horizontal casing and each set of measurements, which matched to each other reasonably well. Moreover, from evaluation of settlement profiles at different sections and levels, it was found that the profiles obtained based on the results of the vertical extensometer measurements on the west side of the embankment, i.e., in the Tensar section and the unreinforced section, were usually consistent and compatible with one or two profiles based on independent other measurements, i.e., vertical extensometer measurements on the east side or elevation survey measurements. Therefore, it appeared appropriate to use the absolute vertical displacements measured beneath the crest on the west side of the test fill for settlement calculation. The absolute vertical displacement were checked and adjusted by other related field measurements.

Since the vertical extensometer tubes beneath the crest of all test sections were blocked during the 1988 construction season, the absolute vertical movements of the casings at different levels after incident could only be obtained from the elevation survey. Unfortunately, no survey records during the 1988 construction season were available in the field documents. Therefore, the settlement after completion of the fill can only be evaluated from the profiles based on the elevation survey at the west end of each casing (the bench mark for elevation survey is located on the west side of the test fill.) in May 1989 and October 1990 when the survey was carefully carried out.

Vertical movements of the fill and foundation soils along vertical alignments beneath the toe and the crest of each test section were monitored using extensometers. The extensometer measures distances between target magnets and datum magnets at the bottom of access tubes. The datum magnets were installed at locations 12 m below the original ground surface in stiff till, to ensure that they would not be displaced by the test fill. Subtracting the

original distances, obtained during the first field reading, from the measured distances, the vertical displacements of target magnets were determined.

4.5.1 0 m Level in Tensar Section

Fifteen sets of field measurements were taken along the horizontal inclinometer casing at the 0 m level of the Tensar section between September 1986 and September 1990. Before November 1988, the absolute vertical displacements at the location beneath the crest were determined by interpolating the displacements, obtained from the vertical extensometer measurements, at the locations 0.5 m above and 0.5 m below the ground surface; after November 1988, the absolute vertical displacements at the west end of the casing were determined from ground elevation survey. The deflections of the casing and the absolute vertical displacements at the specific points provided a view of the settlement of the test fill at the ground level, i.e., a view of the deformations of the foundation soils.

Settlement profiles at the ground level in the Tensar section are shown in Figure 4.59. During the first construction season, a maximum settlement of 21 mm occurred at the center of the fill. Uniformly distributed settlements of 5 to 8 mm developed during the consolidation subsequent to the first construction. At the end of the second construction season, the settlement at the ground level increased gradually from 20 mm at the toe to 68 mm at the center of the fill. It then had increments between 15 and 25 mm due to consolidation and the placement of another 2 m of the fill. During the final construction season and for a period of six month of consolidation, the settlement distribution changed significantly. Near the toe (The large vertical movement at the toe was likely caused by the construction of a drainage ditch at the toe near the instrumented zone in the early summer of 1989.), the amount of settlement was 56.4 mm. The increment was only 20 mm when comparing to the previous year. The total settlement increased rapidly from the toe into the fill and reached the maximum of 221 mm at the center. The amount of the consolidation settlement during the period from May 1989 to September 1990 varied between 3 mm near the toe and 12 mm at the center.

From Figure 4.59, it is seen that the measurements of the horizontal inclinometer are consistent. The settlement at the ground level varied in a

uniform manner: nearly linearly increasing from the toe to the center. No significant localization of settlement is observed.

The development of the settlement at typical locations along the casing at the ground level is presented in Figure 4.60. The vertical displacements increased following the construction and subsequent consolidation periods. The displacements due to placement of the fill varied at different locations: near the center, there were larger increments of displacement than at locations near the slope surface. This feature can be clearly observed during the 1988-1989 seasons. For example, within 276 days (day 718 to day 994), the settlement at the 1 m location increased from 36.6 to 56.4 mm, whereas the settlement at the center increased from 93 to 221 mm. At different locations, the displacement was developed in different rates, as shown by the slopes of the settlement-time diagrams in Figure 4.60. Comparatively, the differences in the settlement due to consolidation were small. The settlement-time diagrams during consolidation periods are nearly parallel.

4.5.2 2 m Level in Tensar Section

Settlement profiles of the soil at the 2 m level, indicating the overall movements of the foundation soils and the fill soil below the 2 m level, in the Tensar section are shown in Figure 4.61. The settlement due to the placement of the fill during the first construction season were rather uniformly distributed and varied between 12 and 31 mm along the instrumentation level. An increment of about 13 mm developed during the subsequent consolidation period. After the second construction season, the total settlement at the level increased gradually from 77 mm at the slope surface to 109 mm near the center of the fill. The increments of vertical displacement due to the consolidation and the placement of 2 m of the fill also increased slightly from the surface to the center where an increment of 52 mm was measured. The measurements taken in May 1989 showed considerable increases in the settlement. The total settlement varied between 167 mm near the slope surface and 310 mm near the center. The settlement increased approximately linearly from the surface to the center of the fill without significant indications of localization. During the consolidation period from May 1989 to September 1990, the increments of the settlement were measured between 13 mm around the slope surface and 36 mm near the center. The development of the settlement at different stages of

construction and consolidation and the settlement at different locations along the instrumented level at 2 m can also be clearly seen in the settlement-time diagrams shown in Figure 4.62.

4.5.3 4 m Level in Tensar Section

The settlement profiles, indicating the overall movements of the fill and the foundation soils below the 4 m level, are shown in Figure 4.63. After the 1987 construction season, the measured settlement varied between 51 mm at the slope surface and 83 mm at the center of the fill. Rather uniform increments of vertical displacement between 50 and 62 mm developed from May to August 1988 when the fill height was 8 m. The profile of settlement in May 1989 showed large differences in both shape and magnitude when compared to the profile of August 1988. The amounts of the total vertical displacement increased to 166 mm near the slope surface and 304 mm at the center of the embankment with an obvious localization at the location between 3 and 4 m from the surface. The amount of the settlement developed during the consolidation period between May 1989 and September 1990 varied between 30 and 40 mm at most locations along the instrumented level.

The development of settlement at the 4 m level throughout the whole monitoring period is illustrated in Figure 4.64. The same features of the vertical displacement variation, as discussed in the previous sections, can also be seen in the settlement-time diagrams.

4.5.4 6 m Level in Tensar Section

Three sets of field inclinometer readings were taken at the 6 m level in the Tensar section during the 1988 construction season. The first reading was taken in May 1988, before the fill construction was resumed, as the initial measurement. Since neither vertical extensometer nor elevation survey results were available, only vertical deflection profiles could be obtained from the horizontal inclinometer measurements. The vertical deflections were calculated relative to the center of the fill. In other words, the displacements were relative to the center of the fill (upward relative movement is positive).

The deflection profiles of the soil at the 6 m level in the Tensar section are illustrated in Figure 4.65. The profile in August 1988, when the fill height was

8 m, gave a clear view of the soil movements. The downward movements of the soil decreased from the center to the crest; it increased rapidly with a magnitude of 15 mm from the 7.5 m location to the 5 m location and then increased slightly to the slope surface. The profile in November 1988 showed the same features of the deflection variation, but it also showed considerable localization of settlement. At two locations 2.5 and 5 m from the surface, measurements indicated large downward movements. The field records of the measurements at the two locations appeared to be reasonable and no errors were found. Since no field measurements were taken thereafter due the blockage of the casing, the consistency of the field readings could not be checked. Nevertheless, the localization of the vertical movement can be considered as an indication of the development of shear zones within the reinforced soil.

4.5.5 Vertical Alignment beneath Crest in Tensar Section

Vertical movements of the fill and foundation soils along the vertical alignment beneath the crest of the test embankment were monitored using extensometers. Magnets were installed in the foundation soils, through a borehole, and in the fill soil at locations 6, 2.5 and 0.5 m below the ground surface and 0.5, 1.5, 2.5, 3.5, 4.5 and 5.5 m above the surface. The access tube was blocked during the 1988 construction and no field reading was taken after August 1988. Because the magnets in the fill soil were added when the fill was placed, the measured settlements indicated the displacement accumulated since the time of magnet installation. For example, the measured settlement at the -0.5 m level represented the movement of the point since early September of 1986, whereas the settlement at the 1.5 m level indicated the displacement of the point since early October, 1986.

Figure 4.66 shows the profiles of the settlement along the vertical alignment. Measured settlement at the -6 m location were considerably larger than at the -2.5 m location. This phenomenon indicated extension deformation of the foundation soils between the two locations. This extension seemed impossible. As mentioned in last chapter, the soils between the two magnets are silty clay; the soils 6 m below the ground are stiff sandy clay and very dense sand. This measured displacement was apparently caused by buckling of the access tube. Therefore, the settlement at the -6 m location was

adjusted based on the settlement measurements at the -6.5 m location beneath the toe of the slope in the Tensar section.

The adjusted profiles of settlement are illustrated in Figure 4.67. The settlement developed following construction and consolidation. As shown in Figure 4.67 and 4.68, the settlement increased during the first construction season and kept developing, but with a smaller magnitude, during subsequent consolidation; this process repeated during the second construction and the following consolidation period at a larger rate than during the previous year. In each profile, below the -2.5 m level, the vertical displacement was small; above the level, the displacement increased approximately linearly to the ground surface and in the fill soil as the elevation increased. However, because the measured settlement indicated the displacement accumulated since the magnet installation, the real compression of the fill soil for each fill placement or consolidation period was larger than the compression of the upper foundation soils.

4.5.6 Vertical Alignment beneath Toe in Tensar Section

The development of the settlement at the locations 6.5, 3.5 and 0.5 m below the ground surface along the vertical alignment beneath the toe of the slope in the Tensar section is illustrated in Figure 4.69. No settlement was detected during the 1986-1987 seasons. A maximum of 3 mm vertical displacement was developed in the foundation soils beneath the toe during the 1987-1988 seasons. At the end of the 1988 construction, the maximum settlement increased to 6 mm.

4.5.7 0 m Level in Signode Section

As discussed in previous sections, the settlement profiles were obtained by combining the relative vertical deflections with the absolute vertical displacements which were determined from the vertical extensometer measurements (before August 1988) beneath the crest of the west slope of the fill and the ground elevation survey measurements (after August 1988) at the west ends of the casings. The settlement profiles on the east side of the test fill (Paragrid and Signode sections) were obtained from the relative deflections and the absolute vertical displacements at the center point of each casing

which were calculated based on the measurements on the west side of the fill (Tensar and unreinforced sections).

Settlement profiles at the ground level in the Signode section are illustrated in Figure 4.70. A rather uniform settlement about 10 mm was developed during the first construction season and another 3 mm in the subsequent five months of consolidation. At the end of the second construction season, the settlement increased gradually from the toe into the fill and reached a maximum of 45 mm at the location 10 m from the toe. Beyond the 10 m location, the settlement decreased slightly. The settlement due to the consolidation and the placement of another 2 m of the fill varied between 11 mm near the toe and 19 mm at the center of the fill. In the spring of 1989, six months after the completion of the fill, the settlement near the toe remained almost the same, whereas the settlement into the fill changed dramatically. The settlement increased linearly from 13 mm at the toe to 129 mm beneath the crest and remained approximately the same beyond the crest further into the fill. The maximum increment of the vertical displacement of about 85 mm, induced by the placement of the top 4 m of the fill and the consolidation during the following six months, occurred near the center of the fill. The settlement developed during the consolidation period between June 1989 and September 1990 varied between 6 mm near the toe and 13 mm near the center.

The settlement at the ground level varied mainly with locations along the casing. No significant localization was observed in the profiles. The development of the settlement at representative locations can be seen in settlement-time diagrams shown in Appendix A.

4.5.8 2 m Level in Signode Section

The profiles of the settlement at the 2 m level in the Signode section, indicating the overall deformation of the foundation soils and the bottom 2 m of the fill soil since October 1986, are shown in Figure 4.71. The total settlement developed during the first construction and the subsequent consolidation period was distributed randomly along the level and was less than 23 mm. At the end of the second construction season when another 3 m of the fill was placed, the increments of the vertical movement of about 35 mm

were developed at most locations along the instrumented level. The increments of settlement between May and August 1988, when the fill height was 8 m, varied between 12 mm near the surface and 19 mm at the center. The profile of settlement measured in June 1989 had a similar shape as the profile in August 1988, but the magnitudes at most locations changed considerably. The total settlement increased from 25 mm near the surface of the slope to 167 mm at the location beneath the crest. In the soil beyond the 10 m location, the total settlement fluctuated a range of 30 mm. This profile also showed localization of the vertical deformation at the 5 and 7 m locations from the slope surface. The settlement developed during the consolidation period between June 1989 and September 1990 increased gradually from 22 mm near the surface to 36 mm at the center of the fill.

The settlement-time diagrams, shown in Appendix A, provide a view of the entire development of the settlement related to loading and consolidation of the fill at typical locations.

4.5.9 4 m Level in Signode Section

Settlement profiles at the 4 m level in the Signode section are illustrated in Figure 4.72. The total settlement developed during the 1987 construction season varied smoothly between 40 and 60 mm. A uniformly distributed increment of the vertical displacement of about 35 mm was measured in the subsequent consolidation period. In June 1989, the measured total vertical displacement increased from 120 mm at the slope surface to 245 mm beneath the crest, decreased slightly in the next 3 m of the soil and then remained constant further into the fill. The maximum increment of 148 mm from August 1988 to June 1989 appeared in the soil beneath the crest. Increments of settlement during the consolidation period from June 1989 to September 1990 varied between 12 and 40 mm at locations along the 4 m level.

4.5.10 6 m Level in Signode Section

Two sets of horizontal inclinometer measurements were taken at the 6 m level in the Signode section before the casing was blocked during the 1988 construction season. The first set of readings was taken as the initial measurements before the construction; the second was taken in late August

when the fill height was 8 m. Figure 4.73 shows the measured deflection profile of the soil at the 6 m level. The value of the deflection in the profile represents the vertical displacement at each point relative to the center point, as discussed in the Tensar section. Within the 6 m from the center of the fill, the vertical displacement remained constant; further towards the slope surface, the downward movement of the soil decreased and reached the minimum beneath the crest. Beyond the crest to the slope surface, the downward movement of the soil increased 28 mm sharply in 2.5 m of the soil. It then decreased gradually from the 3.5 m location to the slope surface. The features of the deflection profile are similar to the profiles described for the Tensar section. In spite of the fact that the set of measurements was taken during the construction season, the sharp increase in the downward displacement might indicate the development of shear zones within the fill.

4.5.11 Vertical Alignment beneath Crest in Signode Section

Vertical movements of the soil beneath the crest of the slope in the Signode section were monitored by measuring the displacements of the magnets placed at locations 6, 3 and 1 m below the ground surface and 0.5, 1.5, 2.5, 3.5, 5 and 5.5 m above the ground surface. Because the access tube was blocked during the 1988 construction season, only the movements before August 1988 are reported.

Settlement profiles along the vertical alignment beneath the crest of the Signode section are illustrated in Figure 4.74. As mentioned in the Tensar section, the measured settlement at the -6 m level were unrealistically large, for some unknown reasons. The settlement at the -6 m level was adjusted in the same way as discussed in the section on the Tensar reinforced slope. From the settlement profiles, it is seen that the settlement increased with elevation; the rate of the variation (with elevation) increased as more soil was placed on the test fill. The foundation soils near the ground surface displaced much more than the soil lying underneath. In spite of the linearity between the settlement and elevation above the -1 m level, the actual compression of the upper fill was larger than the lower fill soil and of foundation soils, as discussed in the Tensar section.

4.5.12 Vertical Alignment beneath Toe in Signode Section

The development of the settlement of the foundation soils at locations 1, 3.5, 6 and 9 m beneath the toe of the slope in the Signode section is shown in Figure 4.75. The settlements developed during the first and second construction and consolidation periods were of small magnitudes. A maximum settlement of 10 mm was measured at the -1 m level at the end of the final construction stage.

4.5.13 0 m Level in Paragrid Section

Figure 4.76 illustrates the settlement profiles at the ground level in the Paragrid section. The vertical deformation of the foundation soils was developed closely following the construction sequences of the test embankment. During the first construction season, a maximum settlement of 32 mm was developed near the center of the fill. It decreased gradually as the distance from the slope surface decreased. In the following six month consolidation period, increments of about 10 mm were measured along the ground level. At the end of the second construction season, the total settlement increased from 12 mm close to the slope surface to 83 mm near the center. The amount of the vertical deformation due to the subsequent consolidation and the placement of another 2 m of fill varied between 4 mm at the surface and 25 mm at the center. In May 1989, seven months after the completion of the fill construction, the maximum settlement increased to 230 mm near the center of the fill; the settlement decreased gradually to 30 mm as one approached the slope surface. The settlement developed during the consolidation period from May 1989 to September 1990 was about 10 mm.

The overall vertical deformation of the foundation soils varied proportional to the height of the fill soil above the instrumented locations at the ground level. Besides the pore pressure dissipation, no other factors, such as over-stressed zones, appeared to be related to the development of the settlement at the ground level. The characteristics of the settlement development can also be seen in the settlement-time diagram in Appendix A.

4.5.14 2 m Level in Paragrid Section

Profiles of the settlement at the 2 m level in the Paragrid section are shown in Figure 4.77. These profiles represent the distribution of the settlement along the 2 m level as well as the variation of the settlement as the fill was sequentially constructed. The settlement during the first construction season varied between 15 and 35 mm. The increments of the vertical deformation due to the subsequent six month consolidation were about 12 mm. At the end of the second construction season when the fill height was 6 m, the settlement profile was smooth varying from 58 mm near the slope surface to 119 mm close to the center of the fill. The average increment of the vertical deformation due to the consolidation and the placement of the 2 m fill soil at the beginning of the 1988 construction was 50 mm. In June 1989, the measured settlement distribution changed significantly. Near the slope surface, the vertical displacement only increased 33 mm since August 1988; beyond the crest, the displacement increased about 130 to 145 mm. Moreover, some localizations of the displacement, around the 4 m location, for example, can be observed in the profile. The settlement developed due to the consolidation from June 1989 to September 1990 varied between 28 mm near the slope surface and 36 mm at the center of the fill.

Features of the entire development of the vertical deformation of the soils below the 2 m level are seen in the settlement-time diagrams in Appendix A.

4.5.15 4 m Level in Paragrid Section

Figure 4.78 shows the profiles of the settlement at the 4 m level in the Paragrid section. The settlement developed during the 1987 construction distributed uniformly along the instrumentation level with an average magnitude about 75 mm. The increment of the vertical displacement due to the consolidation and the placement of the 2 m fill in the period between November 1987 and August 1988 increased slightly from 50 mm near the slope surface to 61 mm at the center of the fill. In May 1989, the total settlement varied from 210 mm near the slope surface to about 290 mm beneath the crest and then remained constant further into the fill. Although the settlement profile appeared to be smooth, certain localization of the vertical displacement

around the 4 m location can be observed. The settlement due to consolidation from May 1989 to September, 1990 varied between 20 mm near the surface and 47 mm at the center of the test embankment.

4.5.16 6 m Level in Paragrid Section

Three sets of horizontal inclinometer field readings were taken before the casing was blocked in November 1988. The obtained vertical deflection profiles at the 6 m level are shown in Figure 4.79. The deflections in the profiles was the displacements relative to the center of the fill. The deflections measured in August 1988 distributed as expected: the soil close to the center settled more than the soil close to the slope surface. The profile of the displacements measured at the end of the 1988 construction, however, show significant localizations. Large differential movements of the soil occurred at the 7 m and 4 m locations, indicating possible development of overstressed zones at the locations.

4.5.17 Vertical Alignment beneath Crest in Paragrid Section

Eleven sets of vertical extensometer field readings were taken along the access tube beneath the crest of the Paragrid geogrid reinforced slope before the tube was blocked in the 1988 construction season. In most of the field readings, the measurements indicated that the magnets installed in the foundation soils displaced upwards as the fill soil was placed. These displacements, which were obviously not the real behavior of the foundation soils, could be related to two possibilities. One was that the magnets in the foundation soils along the access tube were not properly fixed at the instrumented locations. In other words, those magnets were shifting and providing erroneous data. The other possibility was that the datum point at the bottom of the tube had moved. By comparing with the measurements in the Tensar section which has the same geological profile of the foundation soils, as discussed in the last chapter, it was found that the vertical displacements in the Paragrid section were consistently smaller at all instrumented locations. It seemed more likely that the datum point had moved for some unknown reasons. Therefore, the measurements of the vertical extensometers in the Paragrid section were adjusted by the amount of estimated movements of the datum point by assuming that the magnet at the -3

m location in the Paragrid section displaced in the same amount as the magnet at the same location in the Tensar section.

After the adjustment, the same problem occurred that the magnet at the -6 m location settled more than at the -3 m location, as mentioned in previous sections. Hence, the measurements were adjusted again in the same way as discussed in the Tensar and Signode sections. Settlement profiles after the adjustment are shown in Figure 4.80. The settlement was developed as the fill was constructed. It increased as the elevation increased. The rate of the increase in the fill soil was larger than in the foundation soils. The characteristics of the vertical displacement of the soils beneath the crest in the Paragrid section are similar to the soils in other sections, as discussed before.

4.5.18 Vertical Alignment beneath Toe in Paragrid Section

The development of the settlement of the foundation soils beneath the toe of the Paragrid reinforced slope is illustrated in Figure 4.81. At the -1.5 m location, the vertical displacement was developed clearly corresponding to the construction and consolidation stages of the test fill. The settlement-time diagram at the -1.5 m location is comparable to the diagrams of the fill soil, as discussed in previous sections. At locations below the -3.5 m level, the correspondence was not as obvious and the magnitude of the settlement was considerably smaller than at the -1.5 m location.

4.5.19 0 m Level in Unreinforced Section

Figure 4.82 illustrates the settlement profiles at the ground level in the unreinforced section. The vertical deformation due to the placement of the bottom 3 m of the fill during the first construction season was less than 9 mm. Increments of the settlement up to 9 mm were developed during the following six month period of consolidation. At the end of the second construction stage, the total settlement increased from the toe to the 9 m location and remained at about 23 mm further into the fill. The increments of the vertical movement developed in the following consolidation period and the placement of two more meters of the fill in 1988 construction season varied between 10 mm near the toe and 20 mm at the center of the fill. In June 1989, six months after the

completion of the 12 m fill, the settlement profile changed significantly. The vertical deformation of the foundation soils increased sharply from zero at the toe to 120 mm at the 11 m location. Beyond the 11 m location, only minor fluctuation occurred with a range of 15 mm.

It is seen from the profiles that the distribution and the variation of the vertical deformation of the foundation soils were rather uniform. No significant localization was indicated. The development of the settlement closely followed the construction and consolidation stages, as also shown in settlement-time diagrams in Appendix A., indicating the consistency and repeatability of the field measurements.

4.5.20 2 m Level in Unreinforced Section

Profiles of the settlement at the 2 m level in the unreinforced section are shown in Figure 4.83. The overall vertical movement of the foundation soils and the fill soil below the level since the installation of the casing are represented in the profiles with respect to different stages of construction and consolidation. The settlement developed during the first construction season fluctuated between -4 and 19.6 mm. Increments of the vertical deformation in the soils due to the six month of consolidation were about 5 to 10 mm uniformly distributed along the casing. The maximum total settlement of 56 mm occurred at the 8 m location at the end of the second construction season; the settlement decreased gradually at locations approaching the slope surface and the center of the fill. Increments of the settlement, from November 1987 to August 1988 when the fill height was 8 m, varied between 19 and 32 mm with the largest increment appeared around the 8 m location. After the third construction season and the following six months of consolidation, the total settlement near the surface only changed from 60 to 78 mm, whereas the settlement at the center of the fill increased from 47 to 150 mm. The soils close to the center of the fill developed a large amount of settlement due to the placement of the upper 6 m of the fill. The increment of the deformation due to consolidation from June 1989 to September 1990 increased gradually from 26 mm near the surface to 36 mm at the center of the fill.

The settlement profile after the third construction stage is characterized by localization. Around the 8 m location, the settlement changed dramatically.

For example, between August 1988 and June 1989, the increment of the settlement increased from 11 mm at the 2 m locations to 37 mm at the 7 m location; within the next 2 m of the soil beyond the 7 m location, however, the increment jumped from 37 mm to 75 mm. Beyond the 9 m location, the rate of the increase was much smaller. This localization of the vertical displacement would provide an indication of a shear zone development within the unreinforced slope.

4.5.21 4 m Level in Unreinforced Section

Figure 4.84 illustrates settlement profiles at the 4 m level in the unreinforced section. The settlement, developed during the 1987 construction season when 2 m of fill was placed above the level, distributed smoothly along the casing, varying between 43 and 63 mm. An average increment of about 35 mm was developed from November 1987 to August 1988 when the fill height was 8 m. In June 1989, six months after the completion of the 12 m fill, a large amount of the settlement increased in the soil around the central part of the fill. The total settlement gradually increased from 128 mm near the surface to 207 mm beneath the crest and to 215 mm at the center. The maximum total settlement of 237 mm occurred at the 12 m location; the largest rate of the increment variation appeared at the 5 m location where the increment of the vertical displacement (from August 1988 to June 1989) varied from 26 to 90 mm within 2 m of soil. In the period from June 1989 to September 1990, the increment of the settlement due to consolidation increased from 25 mm at the 2 m location to 35 mm near the center of the fill. The excessive displacement of the soil within 1 m from the surface represented the shallow movement of the fill soil weakened by freeze-thaw cycles.

4.5.22 6 m Level in Unreinforced Section

Only two sets of horizontal inclinometer readings were taken at the 6 m level in the unreinforced section before the operating casing was blocked during the 1988 construction season. The profile of the vertical deflections, obtained from the field measurements taken in August 1988 when the fill height was 8 m, is shown in Figure 4.85. The profile indicates relative vertical displacement at different points along the casing with respect to the center of the fill. The smallest settlement occurred at the 9 m location; at the 5 and 7 m

locations, excessive downward displacements were measured. The feature of the deflection profile is similar to the profiles in reinforced sections, but the locations of the displacement localization are different.

4.5.23 Vertical Alignment beneath Crest in Unreinforced Section

Magnets were installed at locations 9, 6, 3 and 0.5 m below the ground surface and 1, 2, 3, 4, 5 and 6 m above the ground surface along the vertical alignment beneath the crest of the slope in the unreinforced section. Vertical movements of the soils at these locations, before August 1988, were measured. Same as in other sections of the test fill, the vertical displacement at the -6 m level was excessively large for some unknown reasons. It was adjusted in the same way as in other sections. Profiles of the settlement, after the adjustment, are shown in Figure 4.86. There was almost no movement detected 9 m below the ground surface. From the -9 m level approaching the ground surface, the vertical displacement increased gradually. Above the ground level, the displacement of the fill soil increased nearly linearly with elevation.

4.5.24 Vertical Alignment beneath Toe in Unreinforced Section

The development of the vertical displacement of the foundation soils 0.5, 2.5 and 6 m below the toe in the unreinforced section is illustrated in Figure 4.87. The measured settlement scatters with time in the diagrams and no clear relationship is found between the development of the displacement and construction activities. Nevertheless, the amount of the settlement in the foundation soils beneath the toe is of minor significance for engineering purposes.

4.6 Pore Pressure

Pore pressure within the fill and the foundation soils were monitored using pneumatic piezometers. Two piezometers were installed at each instrumented level, 3 and 6 m below the ground surface and 1, 3, 5 and 8 m above the surface, in each test section. Most of the piezometers at the 8 m level were damaged during the 1988 construction season; pore pressures measured by the remaining piezometers at the 8 m level fluctuated with time and were less than 10 kPa in all sections. Seven piezometers were placed in the fill and the

foundation soils in the center plane of the test fill. Pore pressures were detected using a readout indicator with a resolution of 1.0 kPa. A low flow rate was maintained throughout the monitoring period to limit the error due to head loss in the leading tubes. The field measurements were plotted in terms of pore pressure development versus time.

4.6.1 Fill Soil in Tensar Section

The development of pore pressures within the fill soil at different locations in the Tensar section is illustrated in Figure 4.88, 4.89 and 4.90. The correspondence of the pore pressure development with respect to the construction activities can be clearly observed in all diagrams. Pore pressures in the fill soil built up during the construction seasons and dissipated in the subsequent consolidation periods. The rate of the dissipation was smaller in the second consolidation periods than during the first period, possibly due to changes of the soil structure during the consolidation. The closer to the center of the embankment, the higher the pore pressure built up during the construction. But the pore pressures at different locations tended to equilibrate as the pore water migrated within the fill soil during the consolidation periods. The induced pore pressure at each individual location, however, depended predominantly upon the degree of saturation of the fill soil at the location. The ratio between the induced pore pressure and the total vertical stress varied significantly from one location to others. Generally, the ratio was larger in the soil placed during the 1987 construction season than in the soil placed during the 1986 season because the former has a higher degree of saturation. No pore pressure measurements were obtained within the upper 6 m fill soil.

The ratio between the induced pore pressure and the total vertical stress changed considerably at different locations within the fill soil due to the variation in the degree of saturation. However, the differences of the ratio tended to decrease after the first consolidation period. In other words, the soil improved in homogeneity during the consolidation phase. For example, at two locations 4 and 8 m from the slope surface at the 1 m level, the ratio changed from 0.1 and 0.61 at the end of the 1986 construction to 0.19 and 0.28 at the end of the 1988 construction; at the two locations at the 3 m level, as shown in Figure 4.6.2, the ratio changed from 0.57 and 0.15 to 0.3 and 0.22 respectively

after the 1987-1988 consolidation period. This feature made it possible to obtain a general view of the pore pressure response in different zones of the test fill from field piezometer measurements. This general view of pore pressure is important for the stability analysis of the test reinforced slopes.

4.6.2 Foundation Soils in Tensar Section

The measured pore pressure response of the foundation soils in the Tensar section is shown in Figure 4.91. The variation of the pore pressure in the foundation soils did respond to construction activities, but it was complicated by other factors such as groundwater table fluctuation. Nevertheless, the magnitude of the induced pore pressure in the foundation soils was of little significance for the purposes of this research.

4.6.3 Signode Section

The development of pore pressures within the fill soil in the Signode section is shown in Figure 4.92. The pore pressure variation with respect to construction stages can be observed in the measurements at all locations. Pore pressures increased during the construction seasons and dissipated in consolidations; the rate of dissipation tended to decrease as the construction-consolidation circle repeated. At the same levels, higher pore pressures were built up at the locations closer to the center; the pore pressures at different locations, however, tended to equilibrate during consolidation periods. The characteristics of the pore pressure response are identical to that discussed in the Tensar section, although the magnitude of induced pore pressure varied considerably due to the differences in degree of saturation of the soil placed in the test fill.

Pore pressures developed in the foundation soils in the Signode section are shown in Figure 4.93. The correspondence of the pore pressure development with construction activities is indicated in the diagrams. The magnitudes of the pore pressures are within the same range as in the foundation soils of the Tensar section.

4.6.4 Paragrid Section

Figure 4.94 and 4.95 show the development of pore pressures in the fill soil of the Paragrid section. The pore pressure response of the foundation soils is illustrated in Figure 4.96. The characteristics of the pore pressure variation with construction and consolidation of the test fill are same as in the Tensar and Signode sections.

4.6.5 Unreinforced Section

Pore pressure response of the fill soil in the unreinforced section is shown in Figure 4.97, and 4.98. The variation of pore pressures with respect to construction and consolidation stages in the reinforced slope was nearly identical to the variation in reinforced slopes. The magnitude of pore pressure developed at each location, however, depends predominantly upon the degree of saturation of the soil at the location. The figures show the development and dissipation of pore pressures during construction and consolidation periods and the equilibration of pore pressures at different locations due to pore water migration within the slope.

Figure 4.99 illustrates the pore pressure response of the foundation soils in the unreinforced section. No significant changes of pore pressure were measured after the third construction season in 1988.

Instrumentation		Paragrid	Signode	Tensar	Unreinforced
EWR Gauge	B	34	36	38	
	M	23	25	23	
	T	17	19	20	
Inductance Coil	B	18	20	18	
	M	11	15	14	
	T	11	13	12	
Horizontal Extensometer	0 m	15	17	15	17
	2 m	14	15	14	15
	4 m	6	12	6	12
	6 m	2	3	2	3
Horizontal Inclinator	0 m	15	14	15	14
	2 m	13	13	13	13
	4 m	10	10	10	10
	6 m	3	2	3	2
Vertical Extensometer	crest	11	10	11	10
	toe	14	15	14	15
Vertical Inclinator	crest	9	10	9	9
	toe	9	14	14	14
Piezometer		55 piezometers in four sections of Test Fill Maximum 21 field readings taken			

B--bottom layer of geogrid
 M--middle layer of geogrid
 T--top layer of geogrid

Table 4.1 Summary of Field Measurement

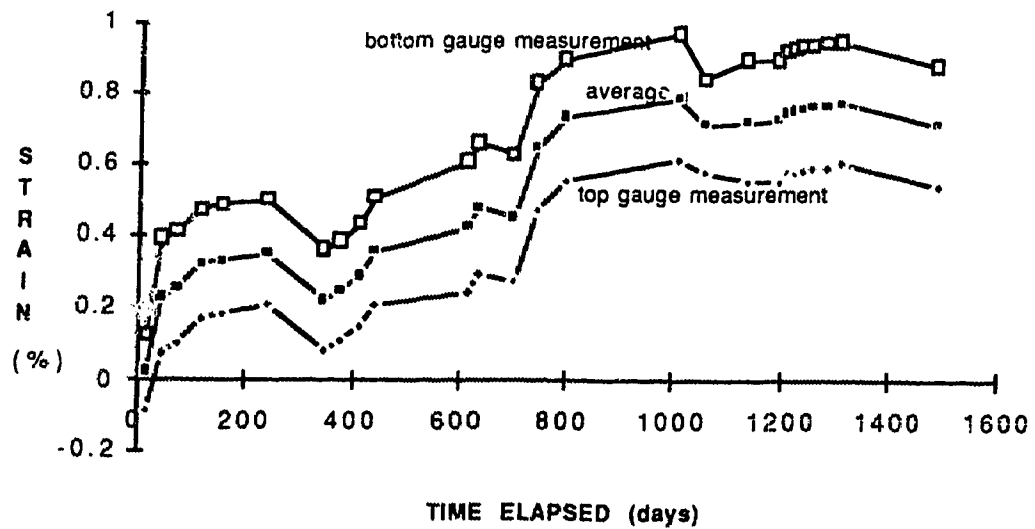


Figure 4.1 EWR Gauge Measurement in 5 m location in Tensar bottom Layer

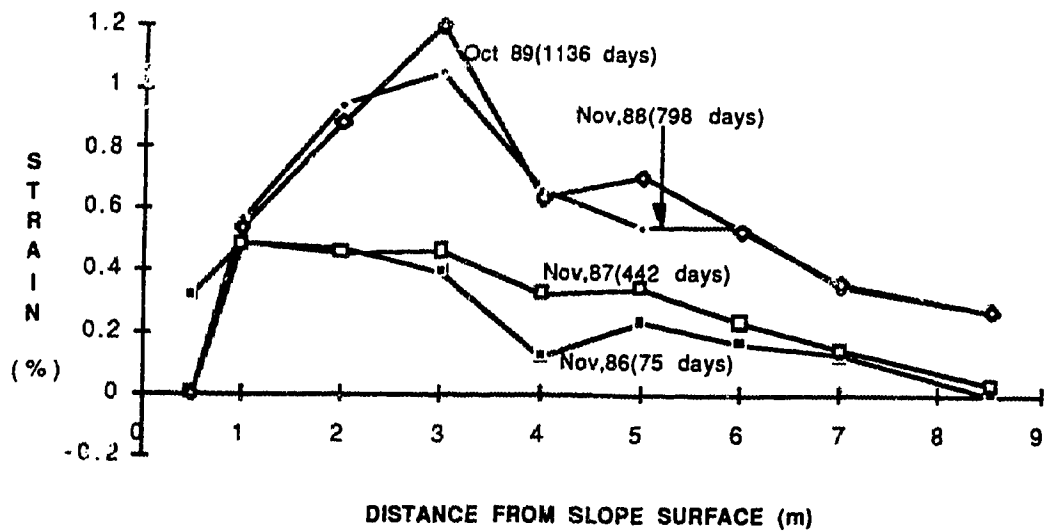


Figure 4.2 Strain (EWR) in Tensar Bottom Layer (before adjustment)

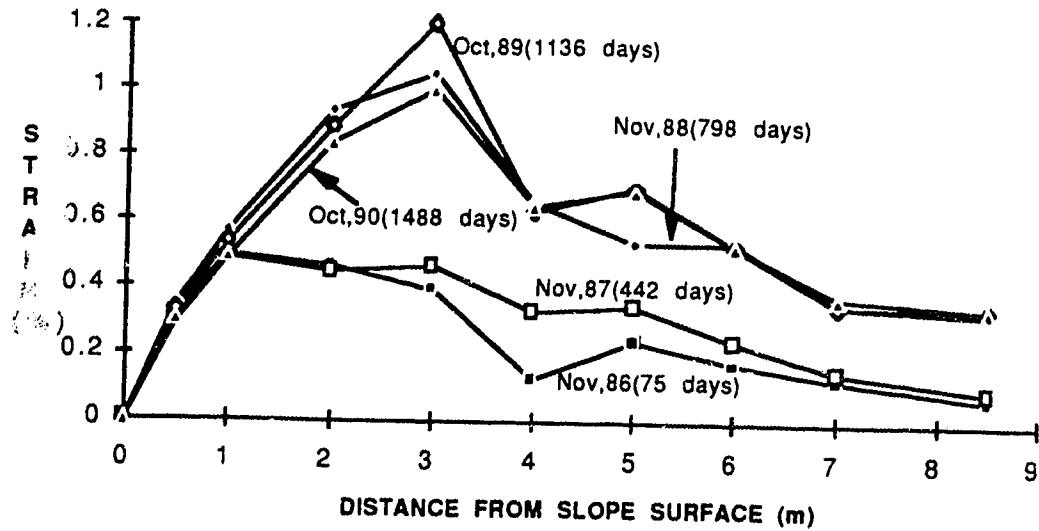


Figure 4.3 Strain Distribution (EWR) in Tensar Bottom Layer

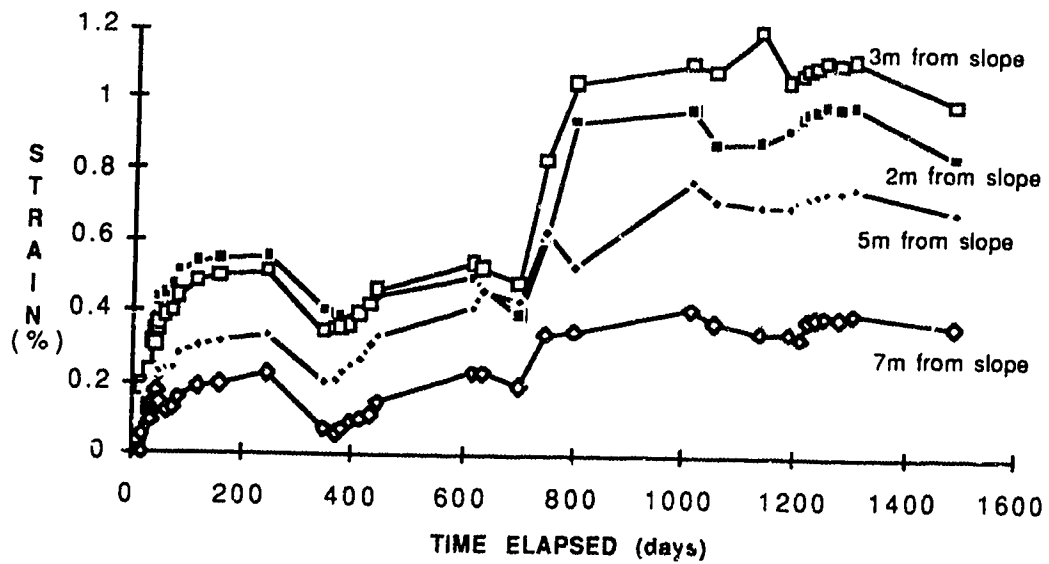


Figure 4.4 Strain (EWR) Development in Tensar Bottom Layer

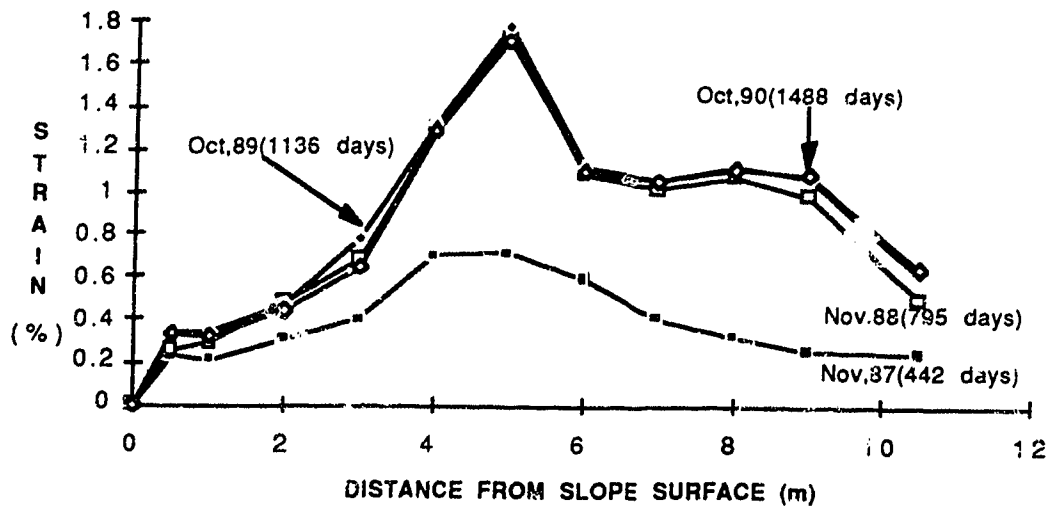


Figure 4.5 Strain Distribution (EVR) in Tensar Middle Layer

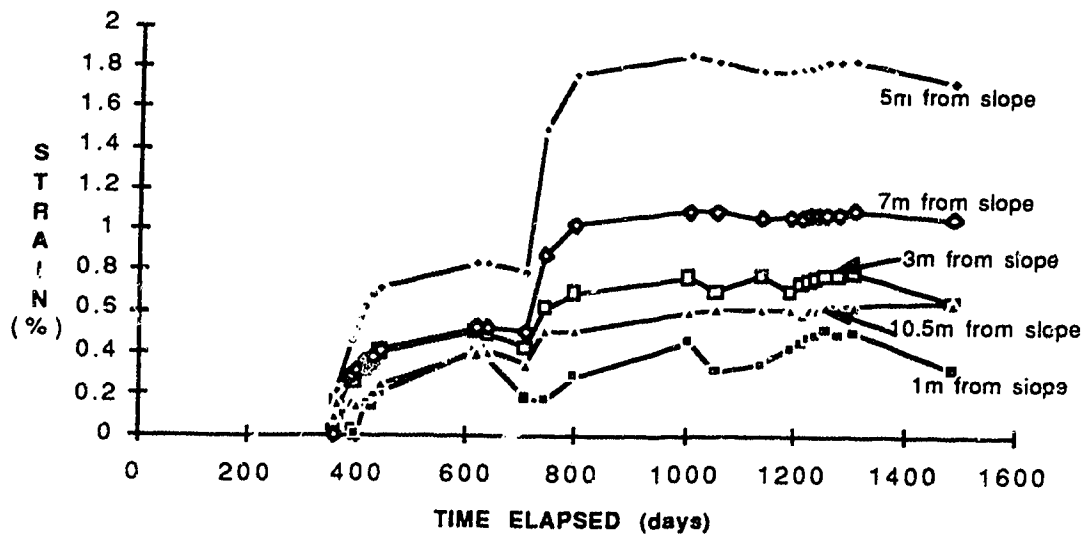


Figure 4.6 Strain Development (EWR) in Tensar Middle Layer

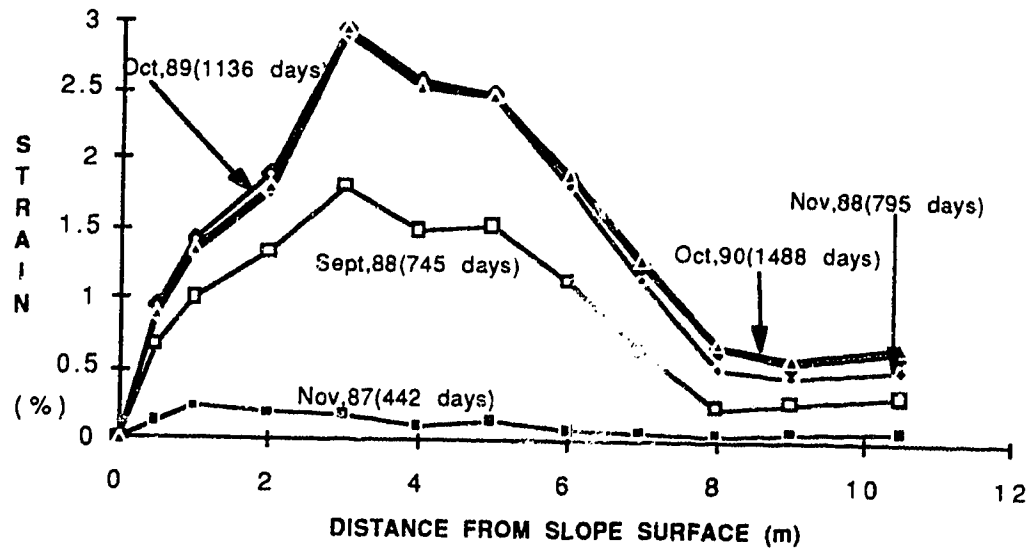


Figure 4.7 Strain Distribution (EWR) in Tensar Top Layer

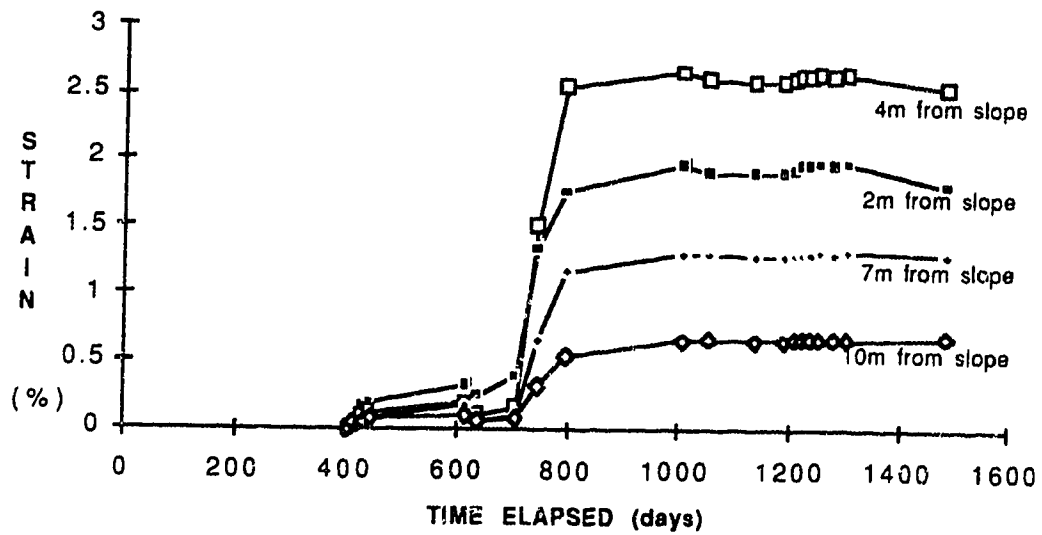


Figure 4.8 Strain Development (EWR) in Tensar Top Layer

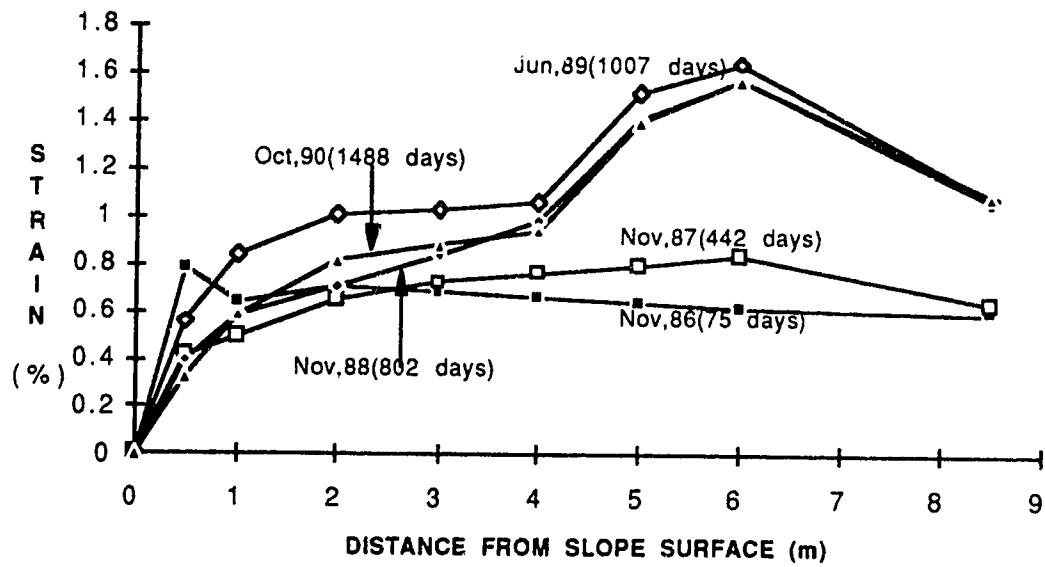


Figure 4.9 Strain Distribution (EWR) in Signode Bottom Layer

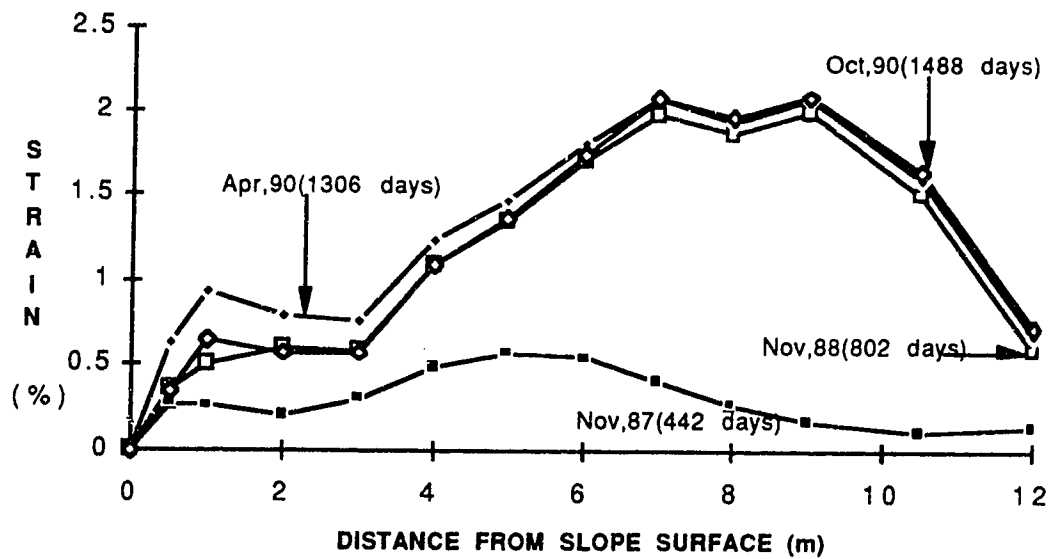


Figure 4.10 Strain Distribution (EWR) in Signode Middle Layer

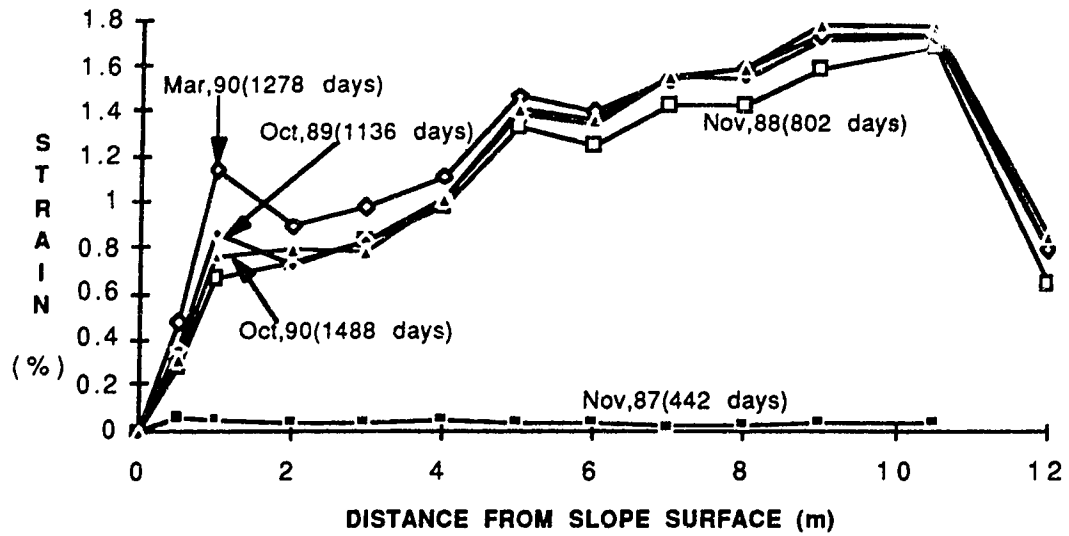


Figure 4.11 Strain Distribution (EWR) in Signode Top Layer

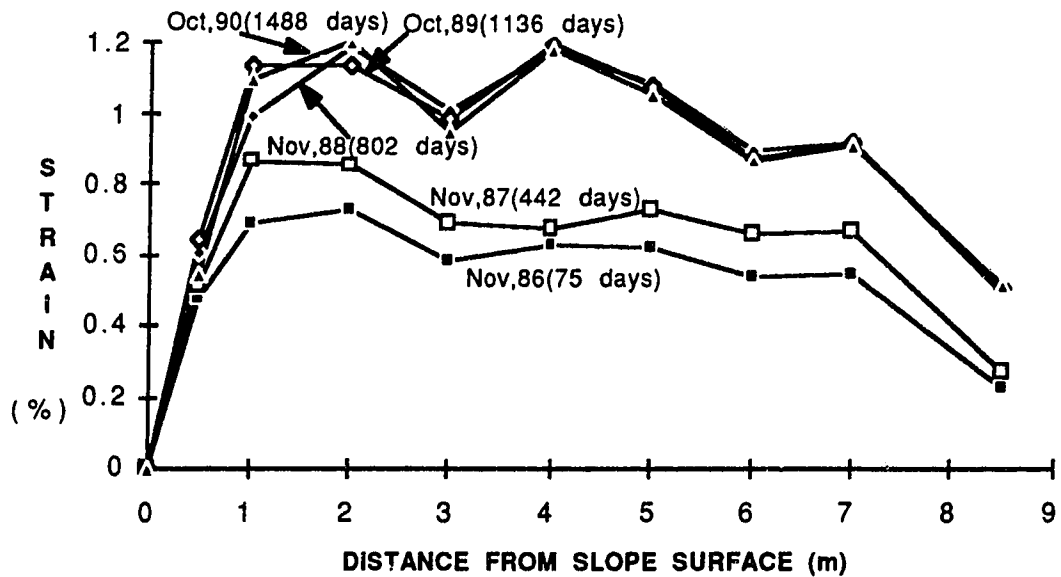


Figure 4.12 Strain Distribution (EWR) in Paragrid Bottom Layer

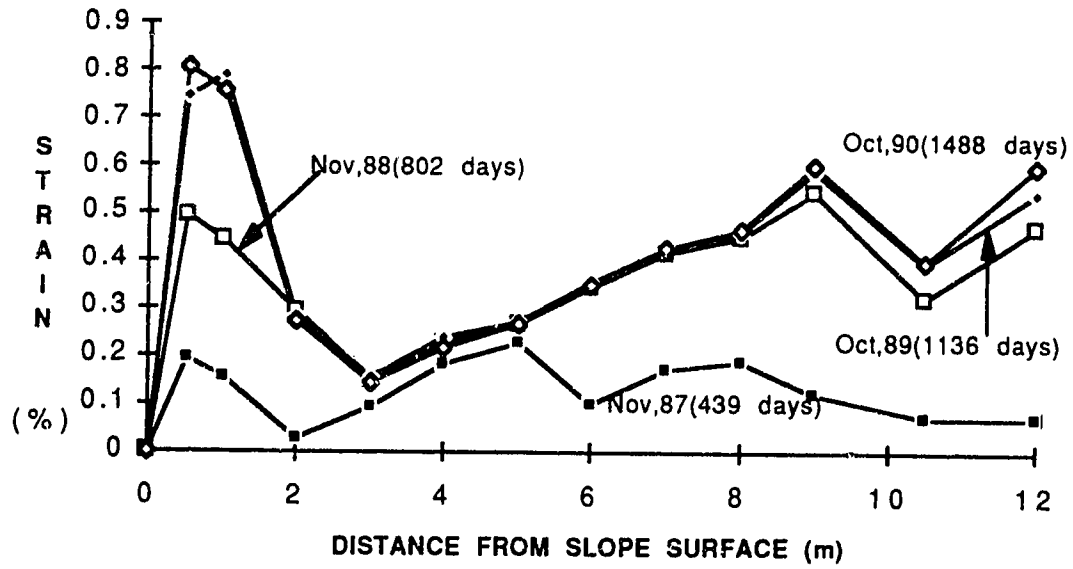


Figure 4.13 Strain Distribution (EWR) in Paragrid Middle Layer

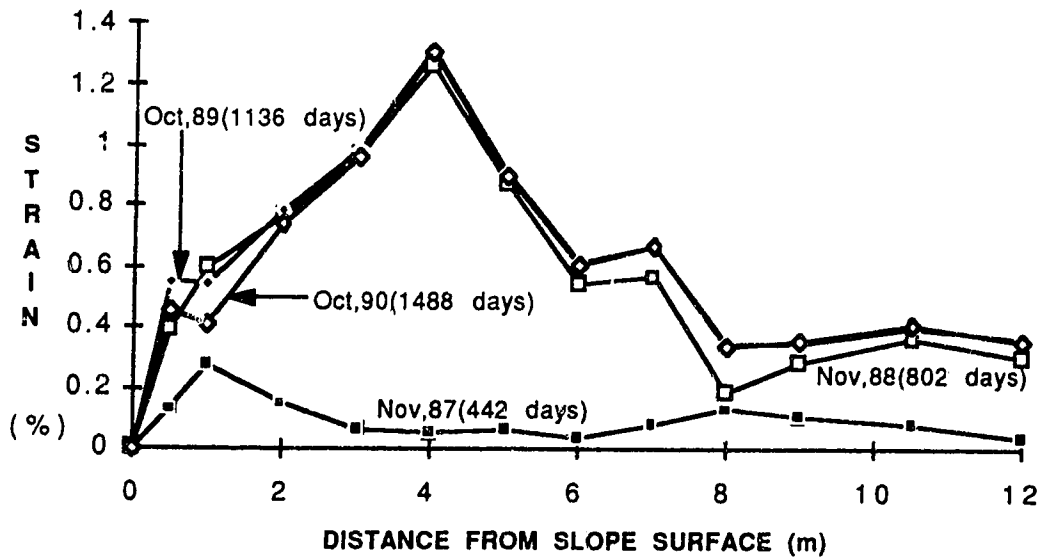


Figure 4.14 Strain Distribution (EWR) in Paragrid Top Layer

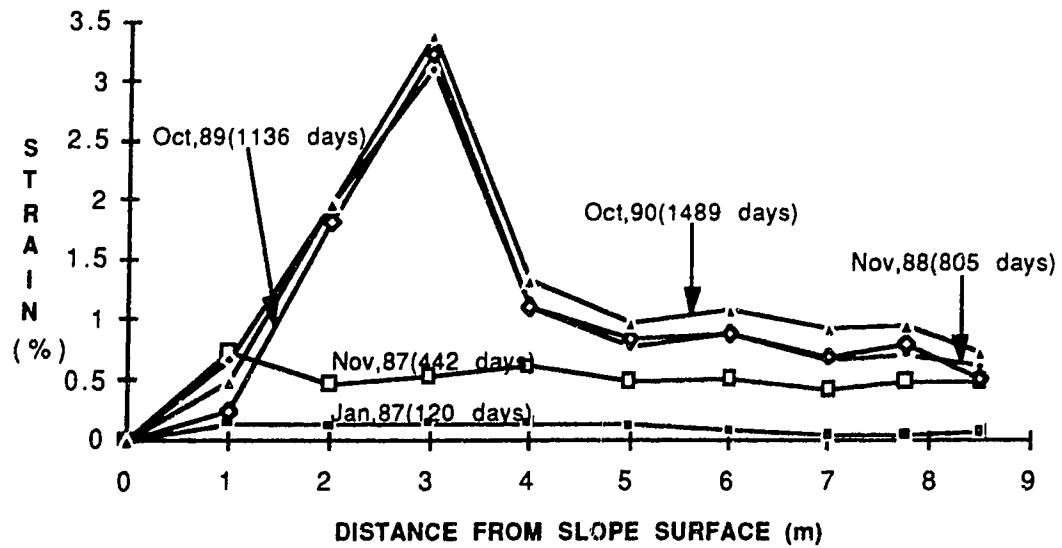


Figure 4.15 Strain Distribution (coil) in Tensar Bottom Layer

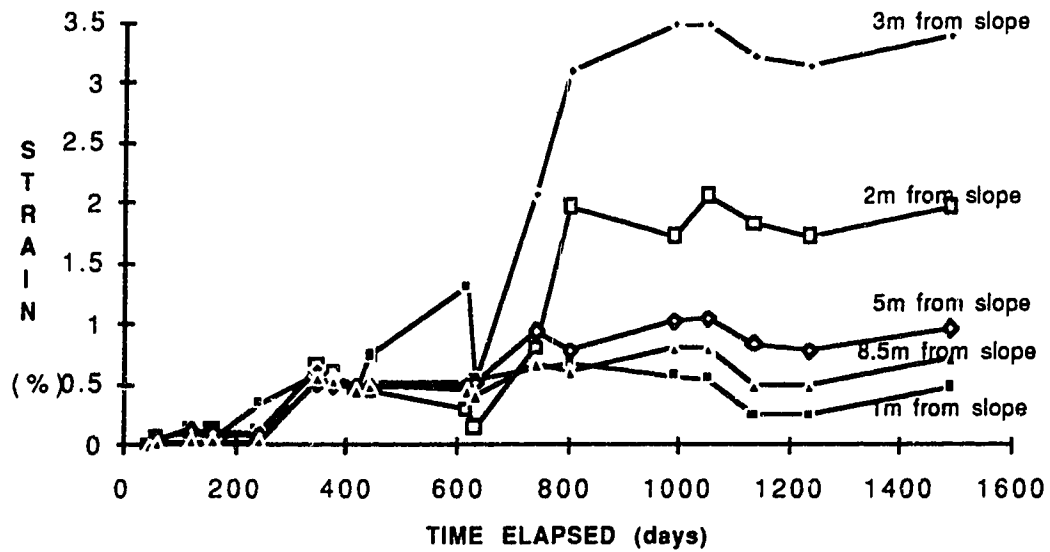


Figure 4.16 Strain Development (coil) in Tensar Bottom Layer

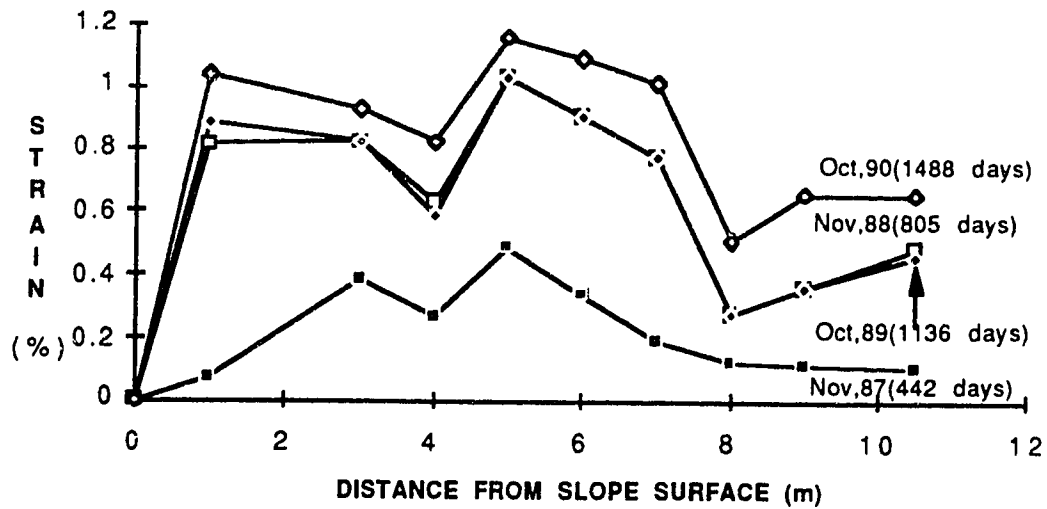


Figure 4.17 Strain Distribution (coil) in Tensar Middle Layer

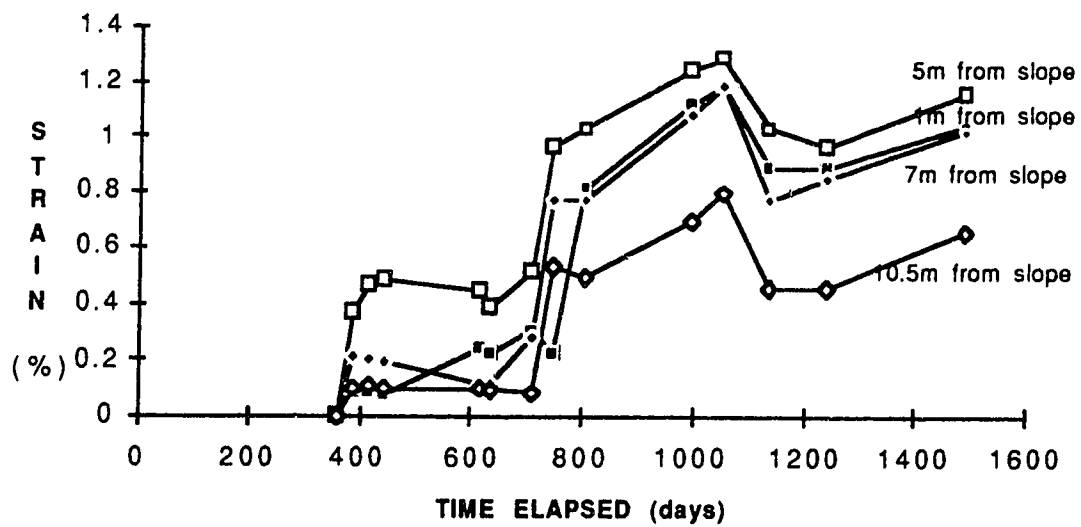


Figure 4.18 Strain Development (coil) in Tensar Middle Layer

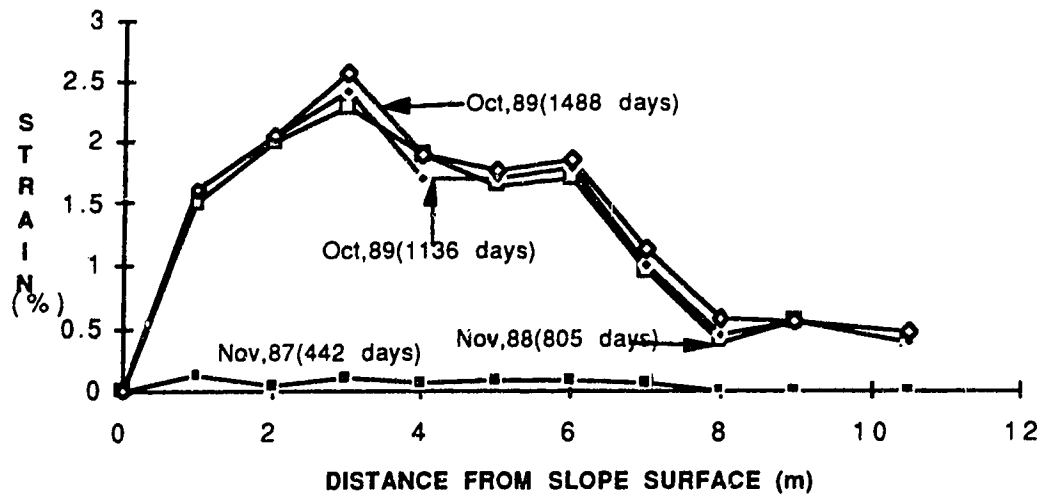


Figure 4.19 Strain Distribution (coil) in Tensar Top Layer

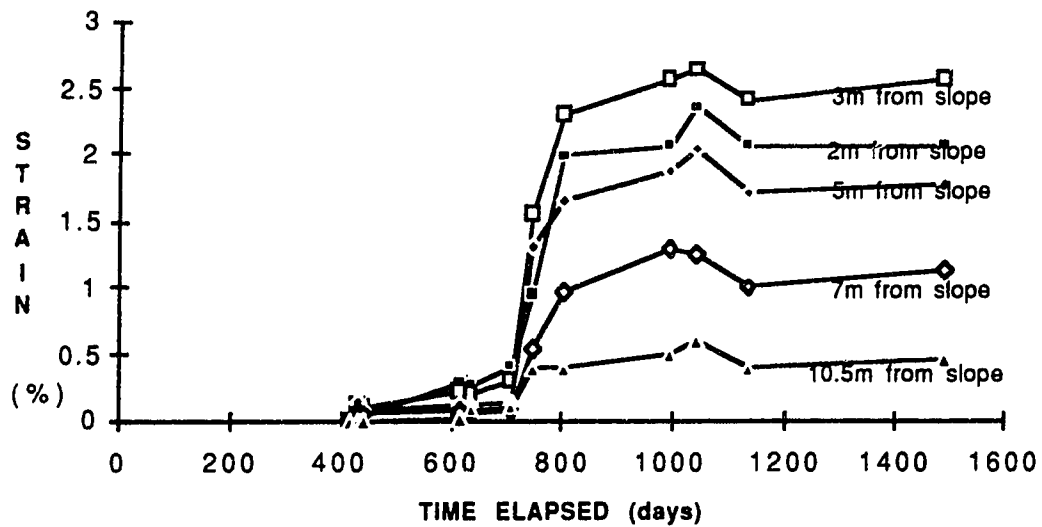


Figure 4.20 Strain Development (coil) in Tensar Top Layer

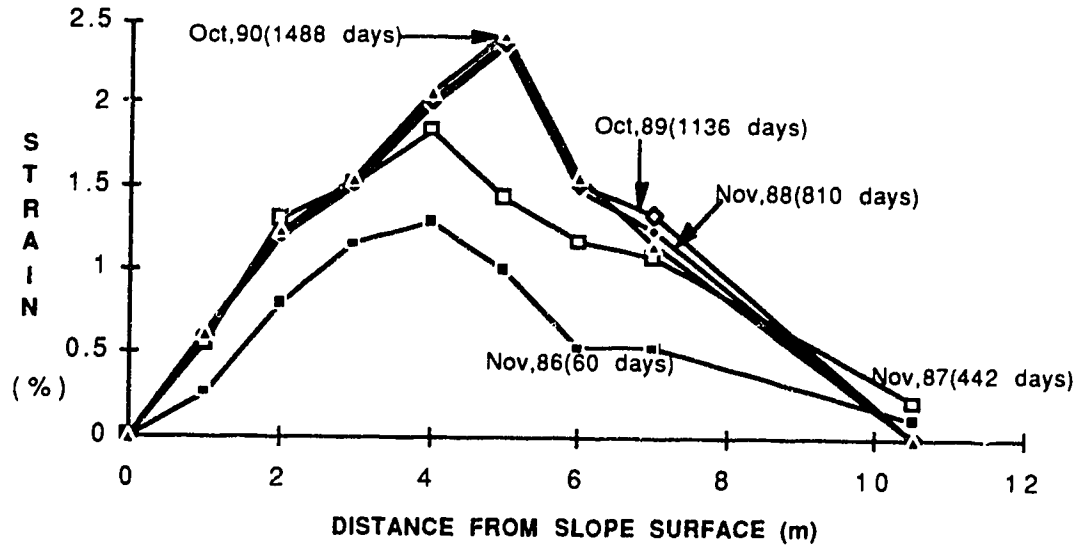


Figure 4.21 Strain Distribution (coil) in Signode Bottom Layer

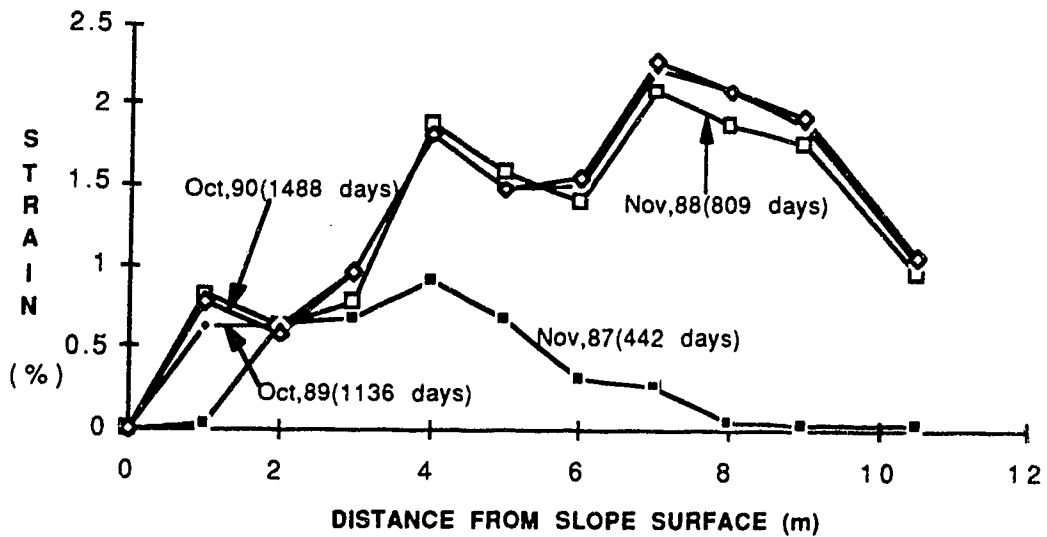


Figure 4.22 Strain Distribution (coil) in Signode Middle Layer

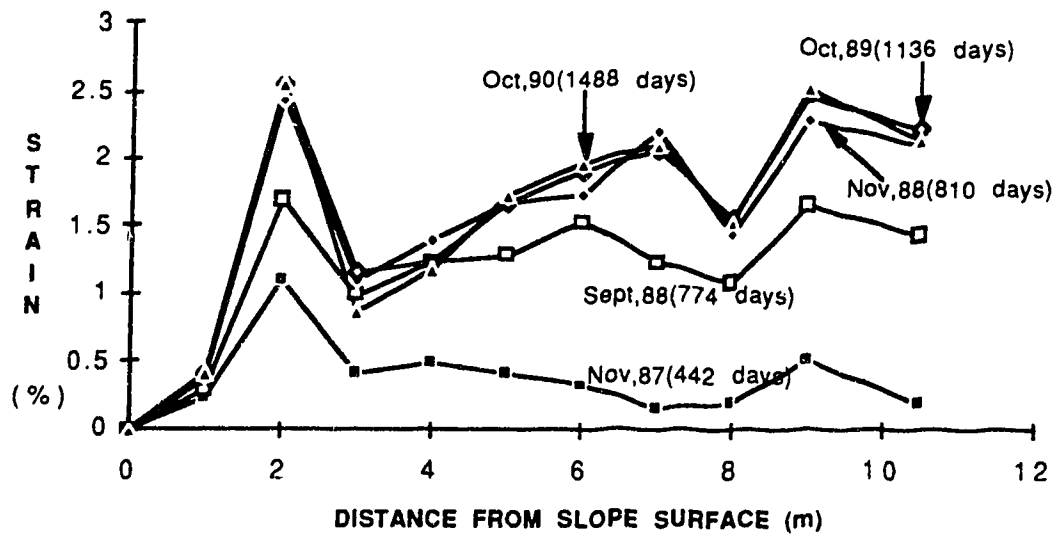


Figure 4.23 Strain Distribution (coil) in Signode Top Layer

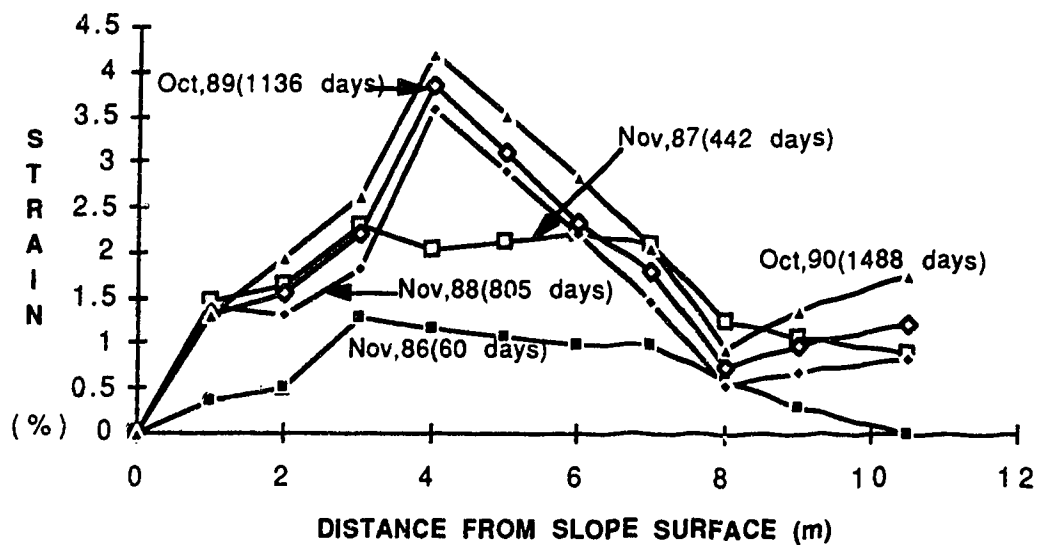


Figure 4.24 Strain Distribution (coil) in Paragrid Bottom Layer

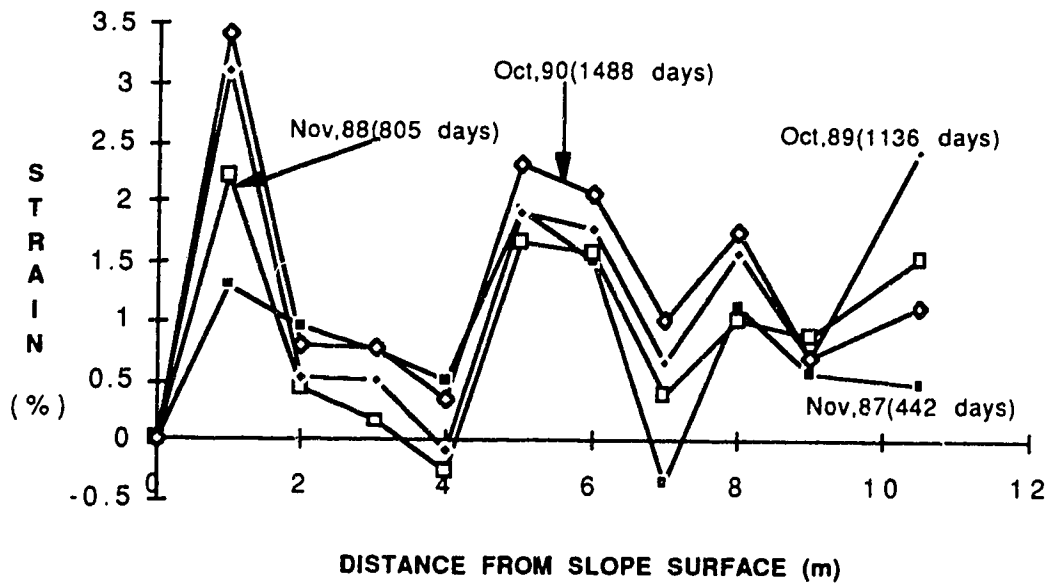


Figure 4.25 Strain Distribution (coil) in Paragrid Middle Layer

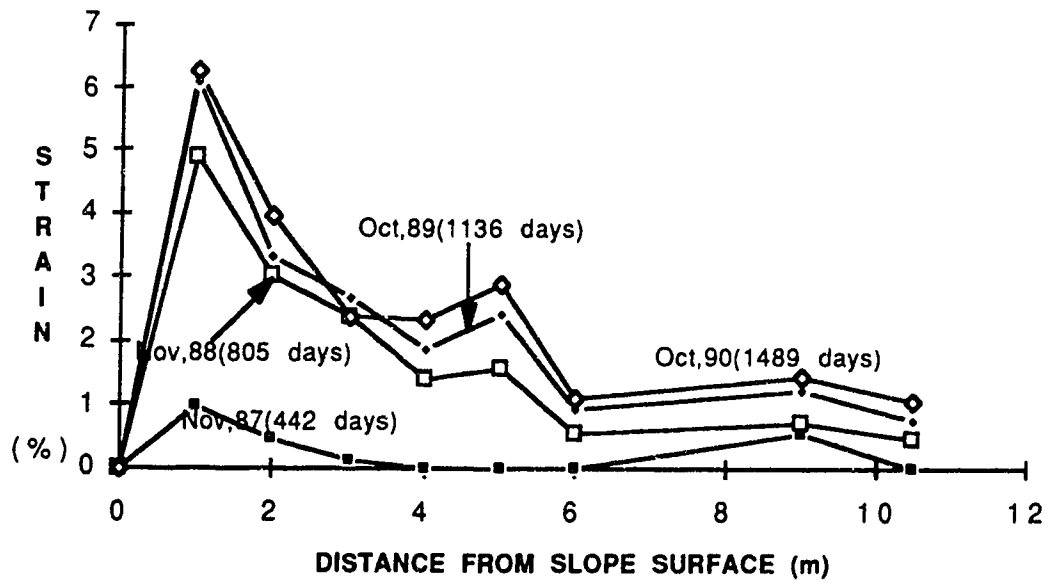


Figure 4.26 Strain Distribution (coil) in Paragrid Top Layer

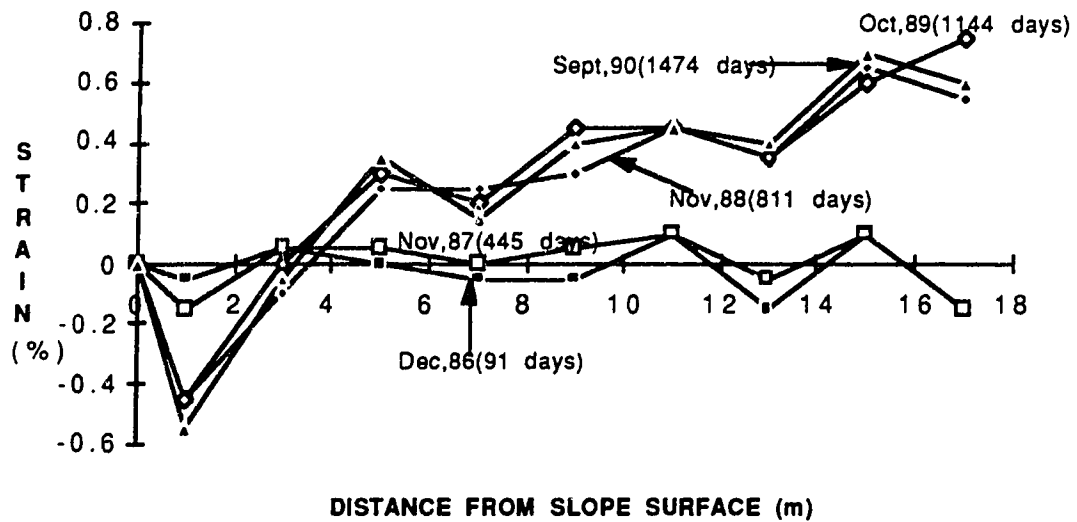


Figure 4.27 Distribution of Horizontal Strain of Soil at 0 m Level in Tensar Section

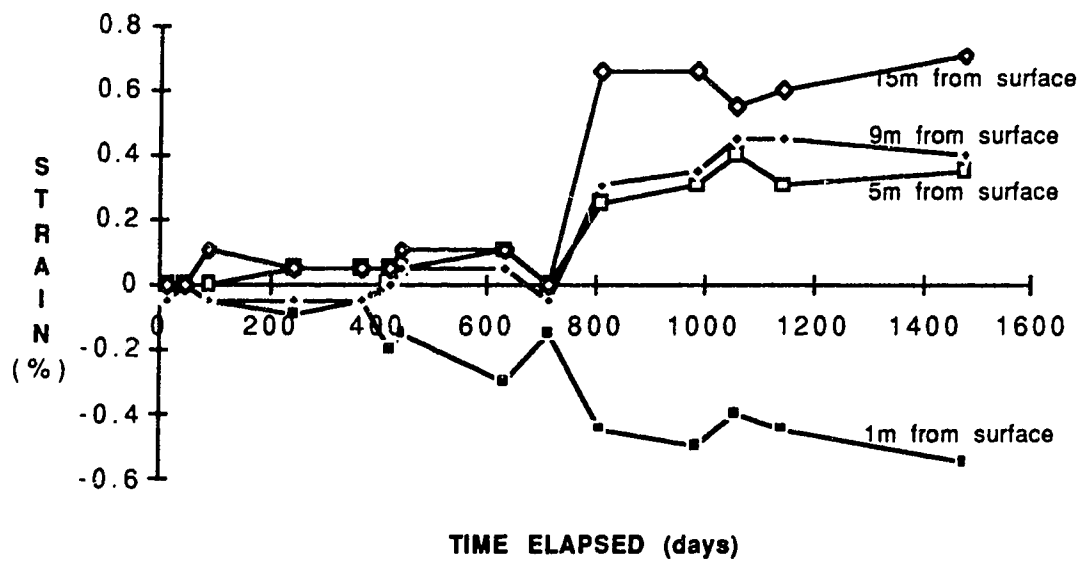


Figure 4.28 Development of Horizontal Strain of Soil at 0 m Level in Tensar Section

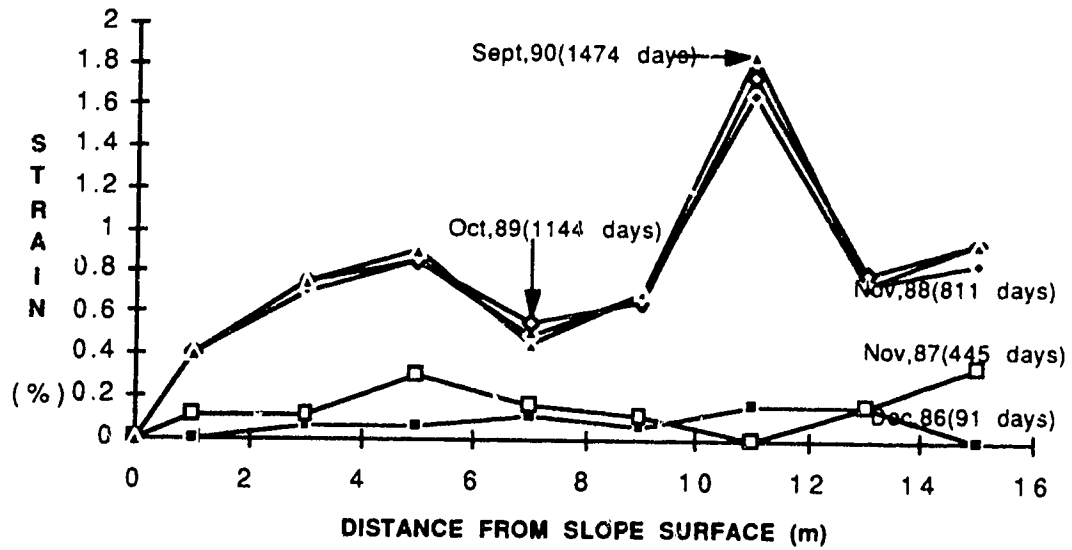


Figure 4.29 Distribution of Horizontal Strain of Soil at 2 m Level in Tensar Section

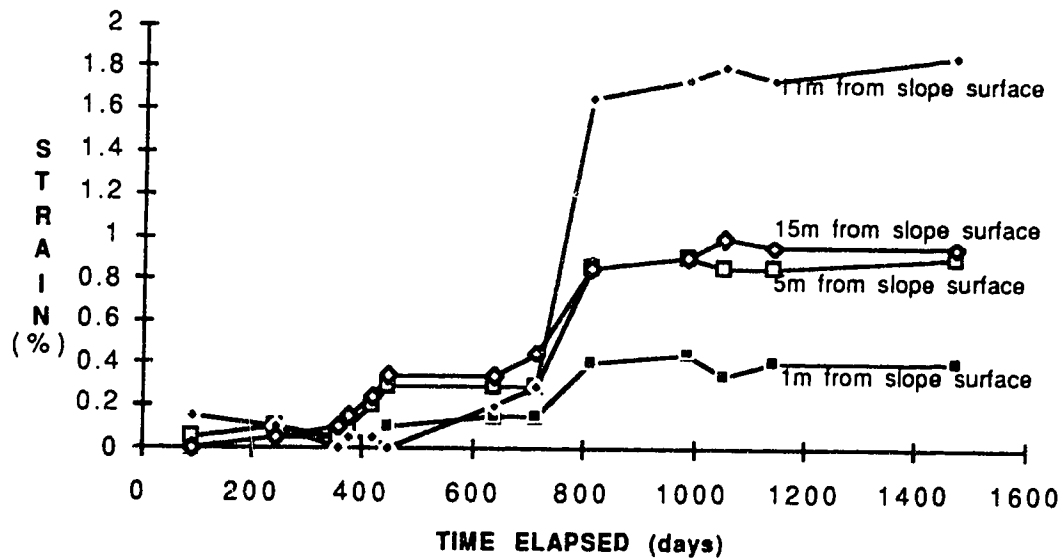


Figure 4.30 Development of Horizontal Strain of Soil at 2 m Level in Tensar Section

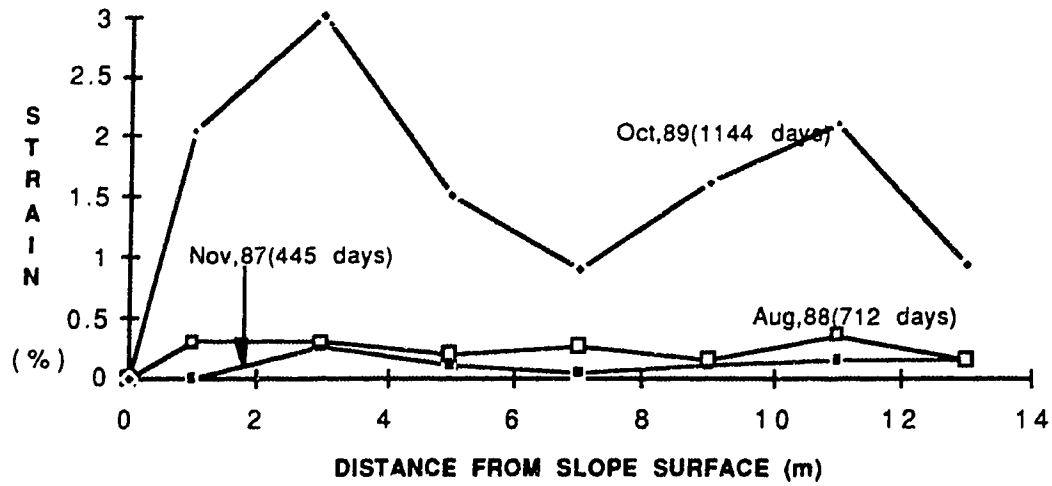


Figure 4.31 Distribution of Horizontal Strain of Soil at 4 m Level in Tensar Section

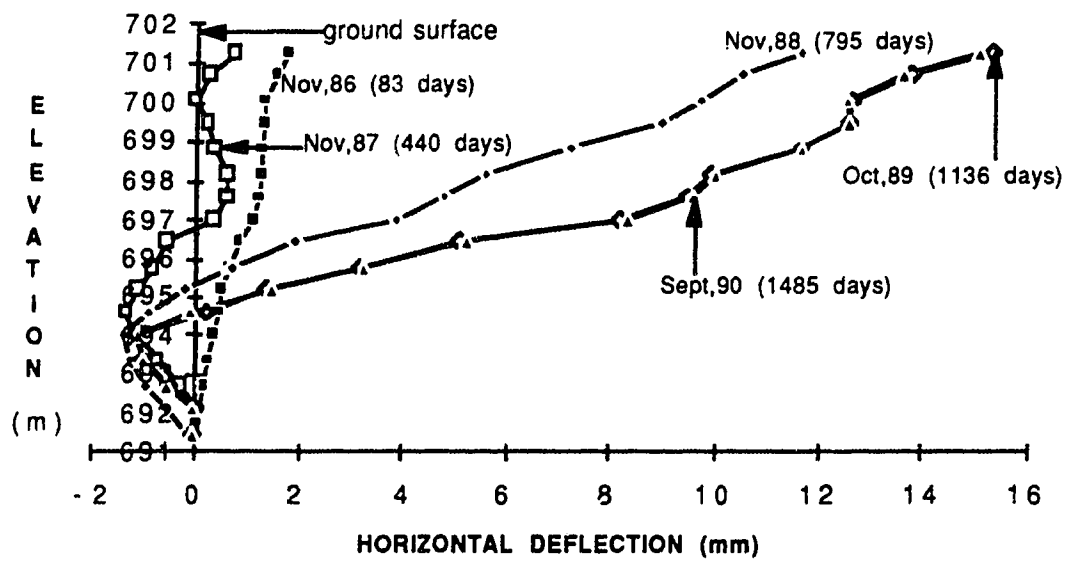


Figure 4.32 Horizontal Deflection (A) of Soils beneath Toe of Slope in Tensar Section

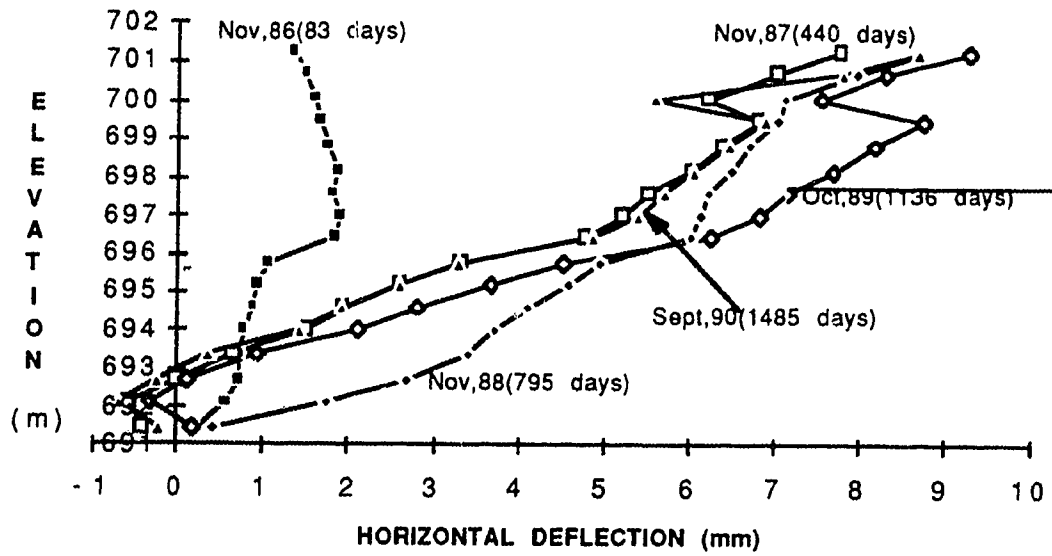


Figure 4.33 Horizontal Deflection (B) of Soils beneath Toe of Slope in Tensar Section

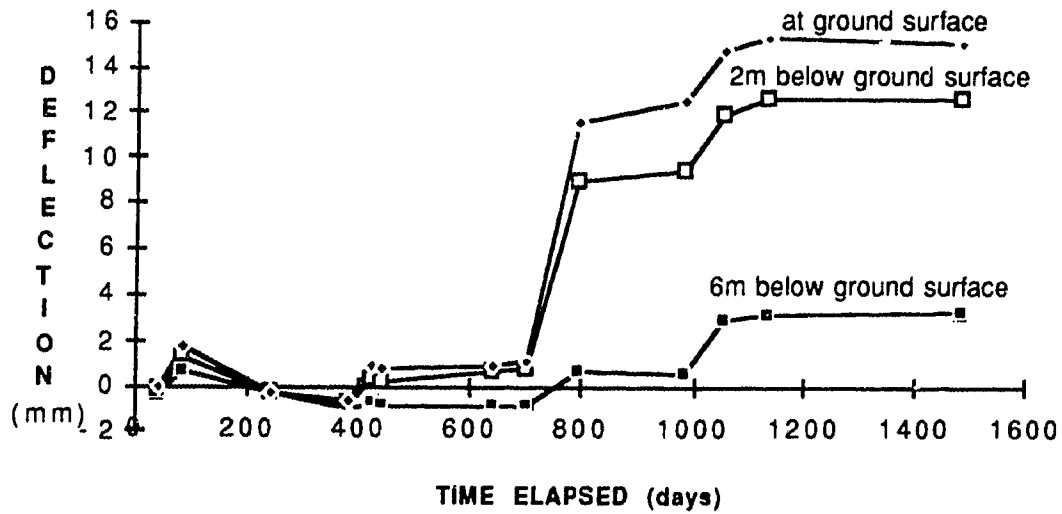


Figure 4.34 Development of Horizontal Deflection (A) of Soils beneath Toe of Slope in Tensar Section

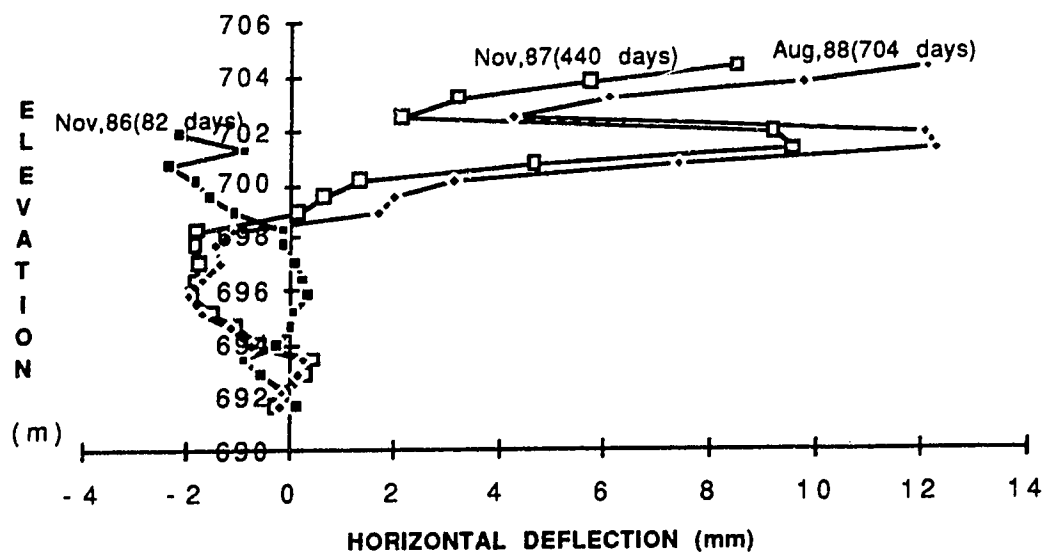


Figure 4.35 Horizontal Deflection (A) of Soils beneath Crest of Slope in Tensar Section

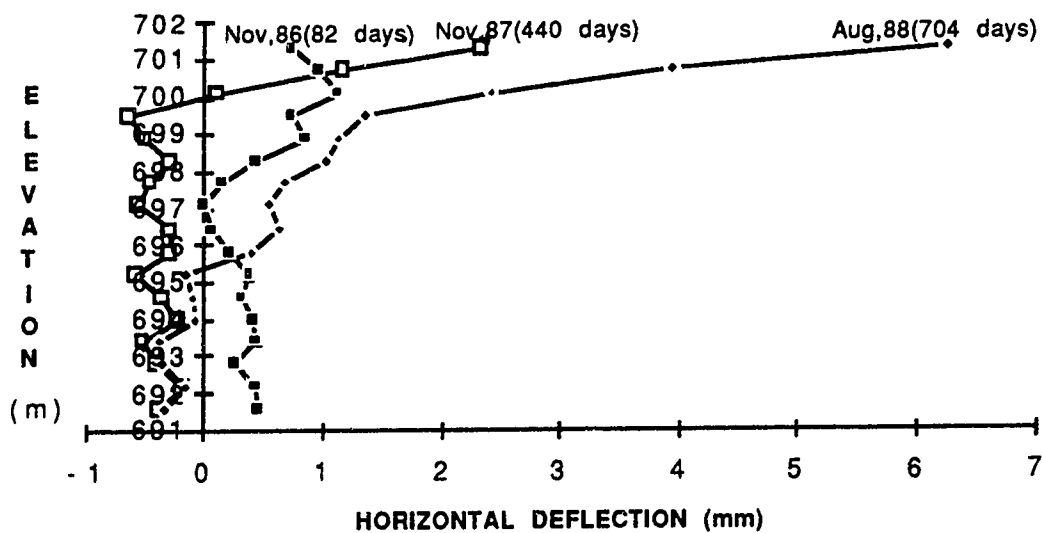


Figure 4.36 Horizontal Deflection (B) of Soil beneath Crest of Slope in Tensar Section

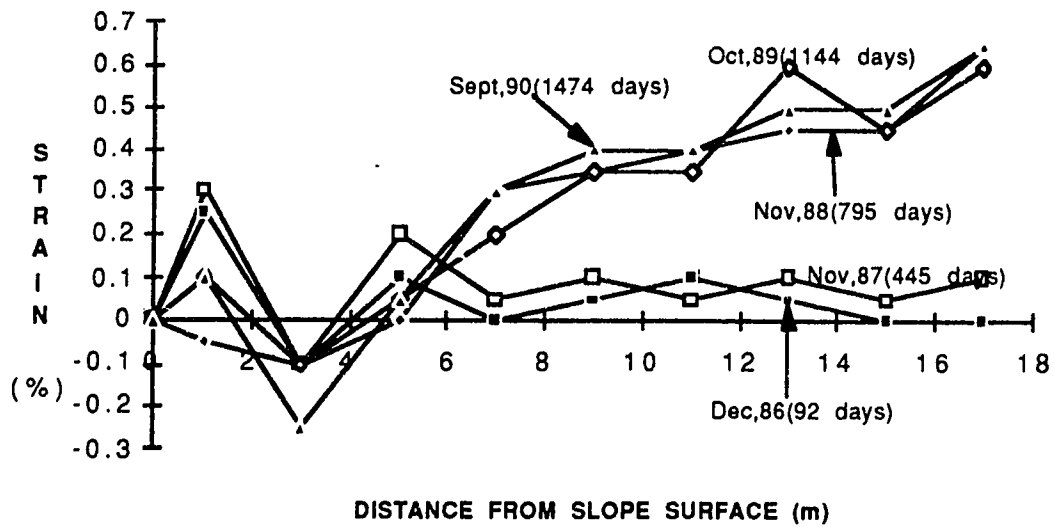


Figure 4.37 Distribution of Horizontal Strain of Soil at 0 m Level in Signode Section

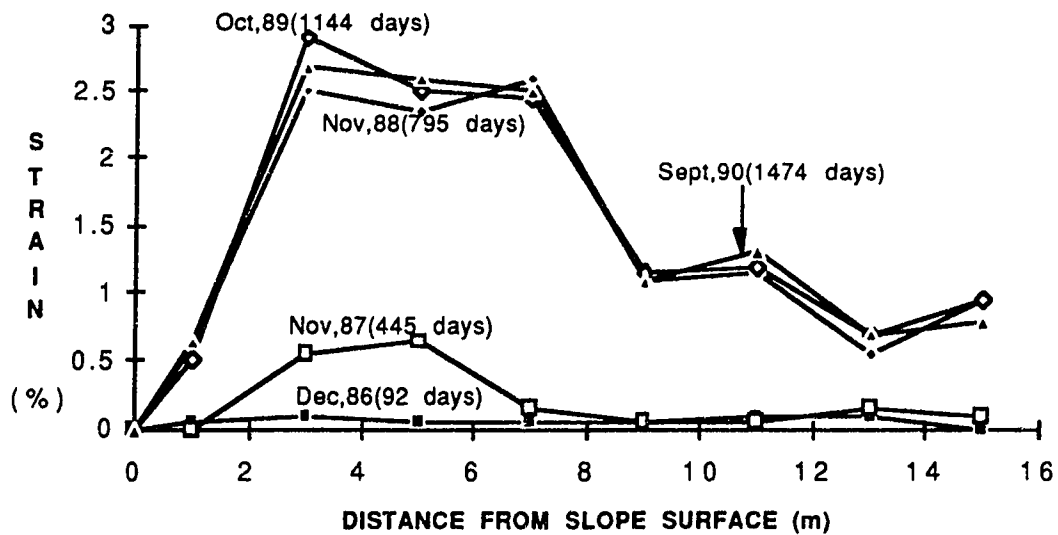


Figure 4.38 Distribution of Horizontal Strain of soil at 2 m Level in Signode Section

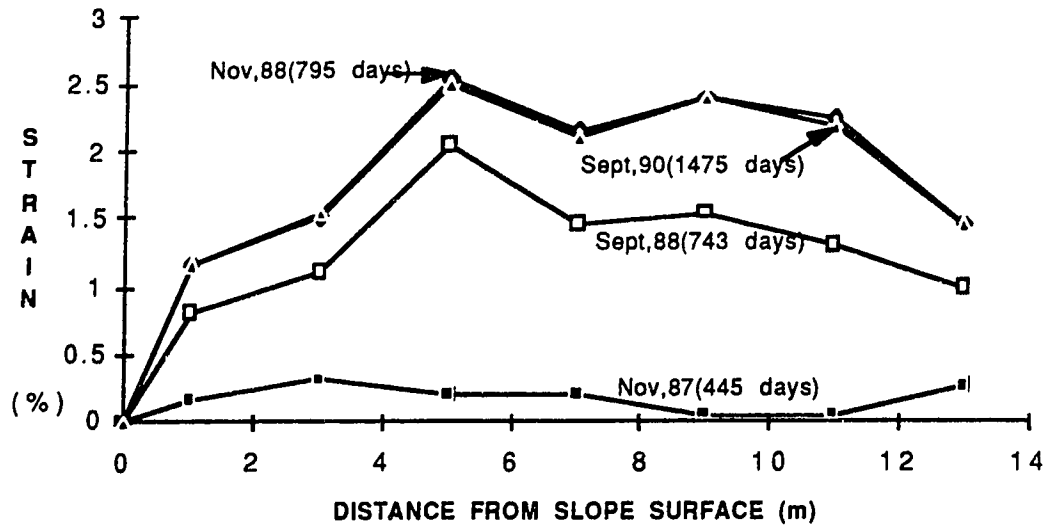


Figure 4.39 Distribution of Horizontal Strain of soil at 4 m Level in Signode Section

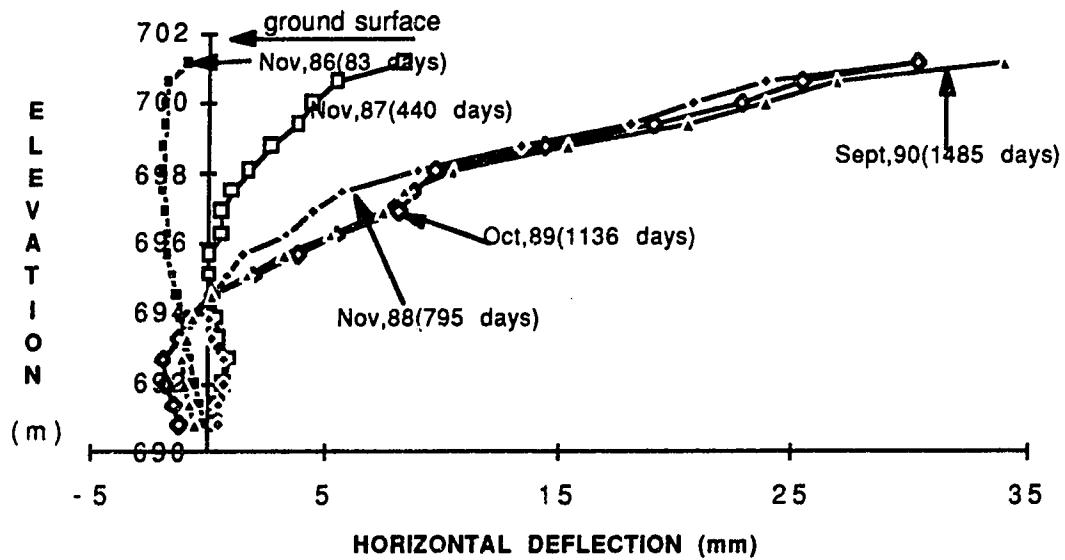


Figure 4.40 Horizontal Deflection (A) of Soils beneath Toe of Slope in Signode Section

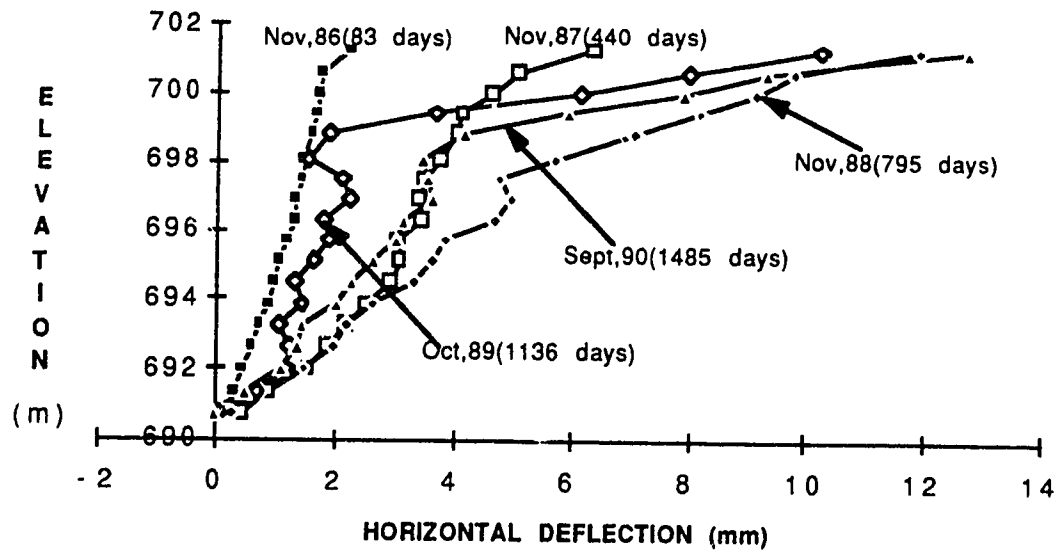


Figure 4.41 Horizontal Deflection (B) of Soils beneath Toe of Slope in Signode Section

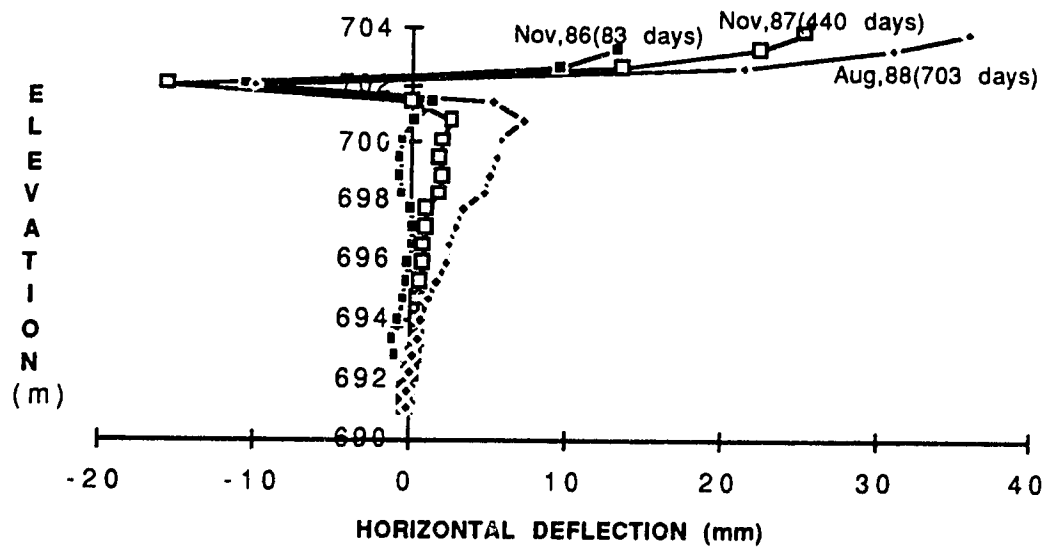


Figure 4.42 Horizontal Deflection (A) of Soils beneath Crest of Slope in Signode Section (before adjustment)

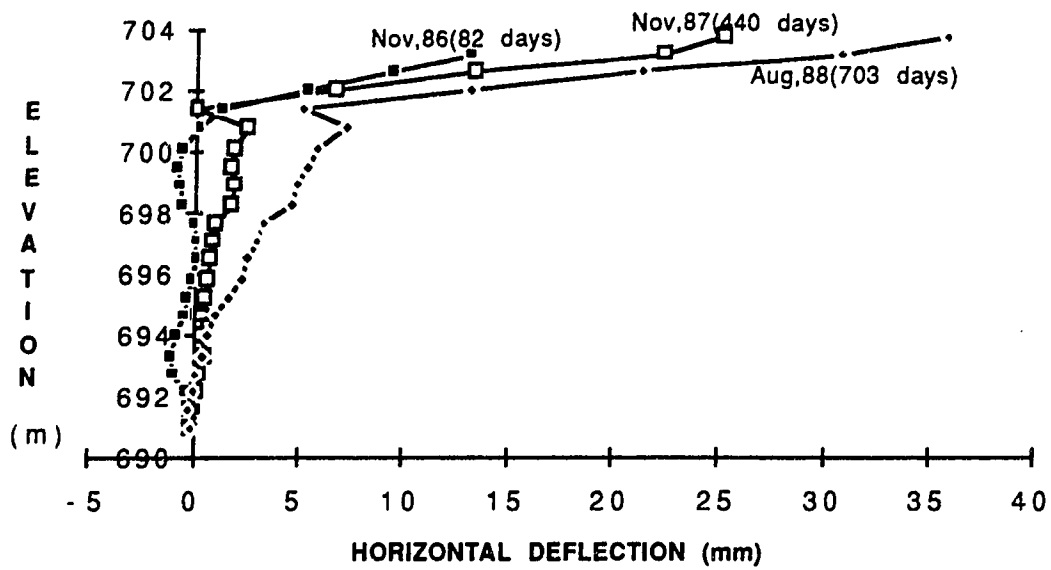


Figure 4.43 Horizontal Deflection (A) of Soils beneath Crest of Slope in Signode Section

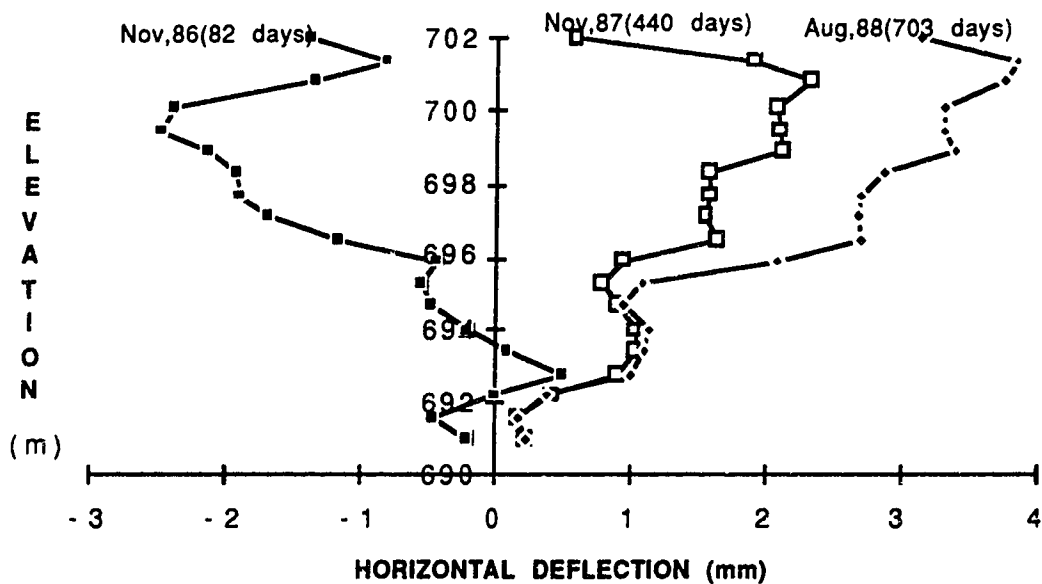


Figure 4.44 Horizontal Deflection (B) of Soils beneath Crest of Slope in Signode Section

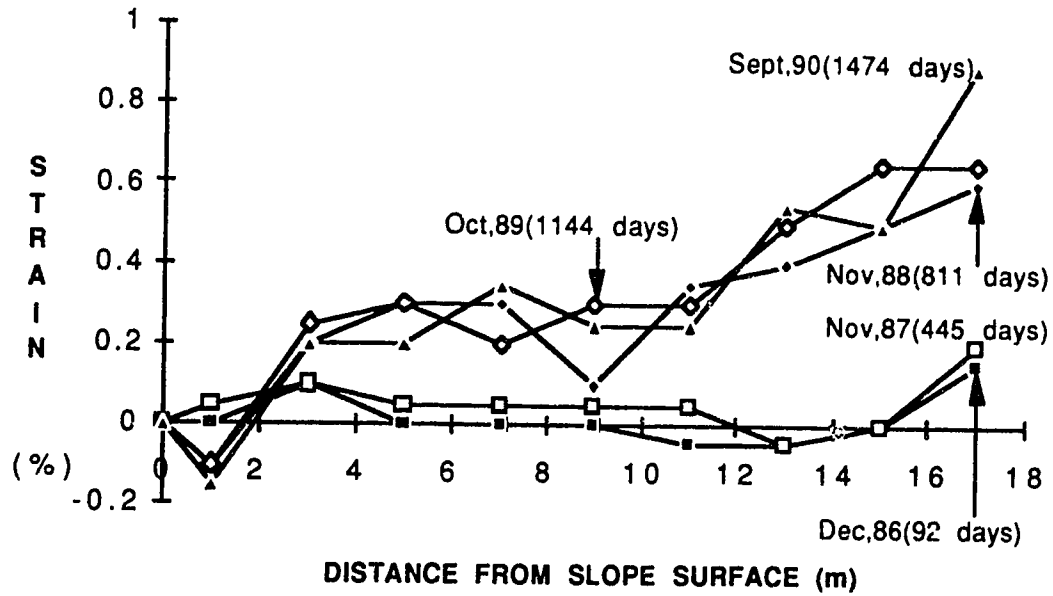


Figure 4.45 Distribution of Horizontal Strain of soil at 0 m Level in Paragrid Section

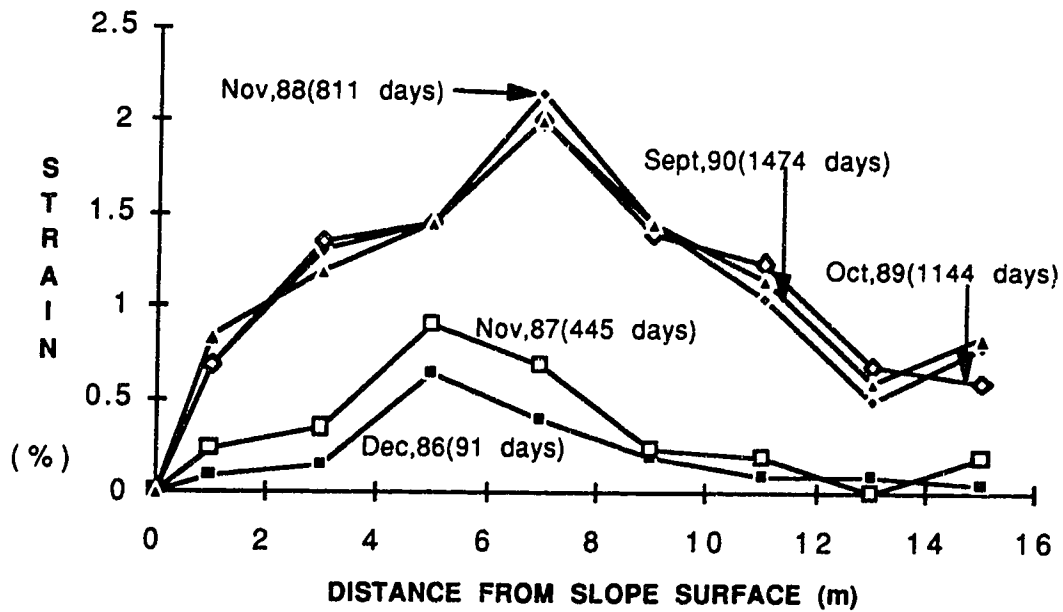


Figure 4.46 Distribution of Horizontal Strain of Soil at 2 m Level in Paragrid Section

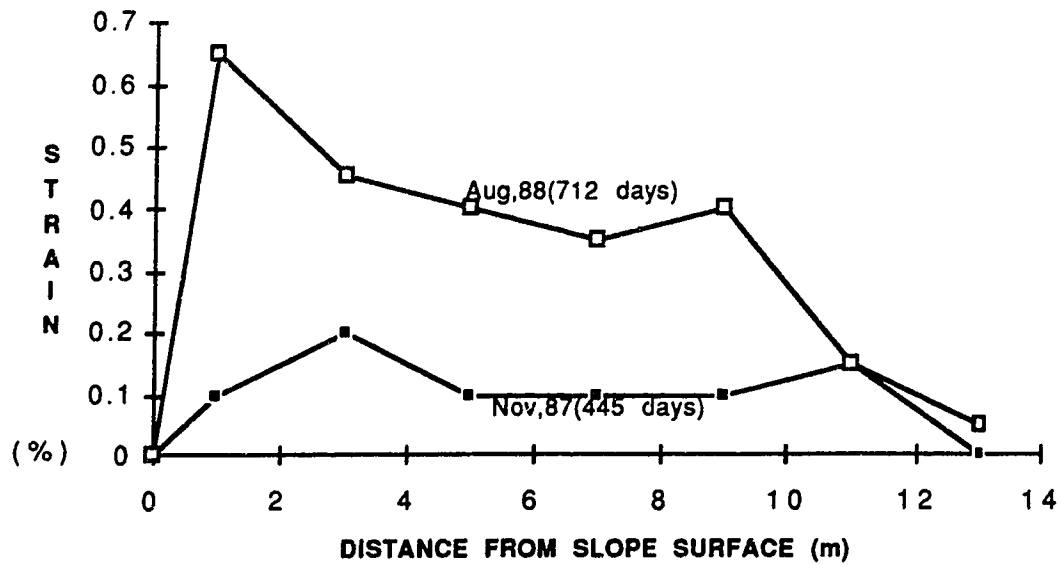


Figure 4.47 Distribution of Horizontal Strain of Soil at 4 m Level in Paragrid Section

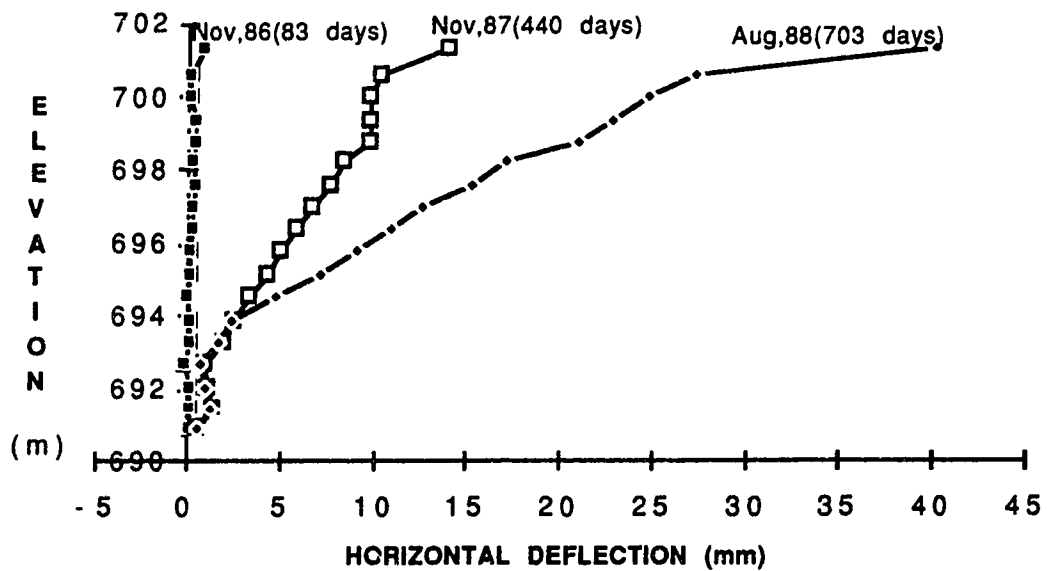


Figure 4.48 Horizontal Deflection (A) of Soils beneath Toe of Slope in Paragrid Section

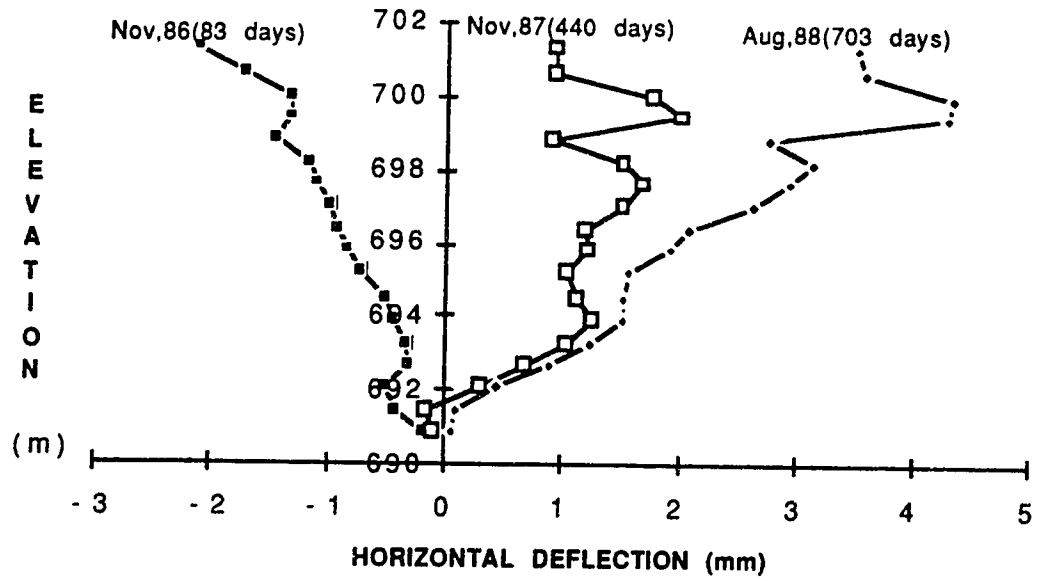


Figure 4.49 Horizontal Deflection (B) of Soils beneath Toe of Slope in Paragrid Section

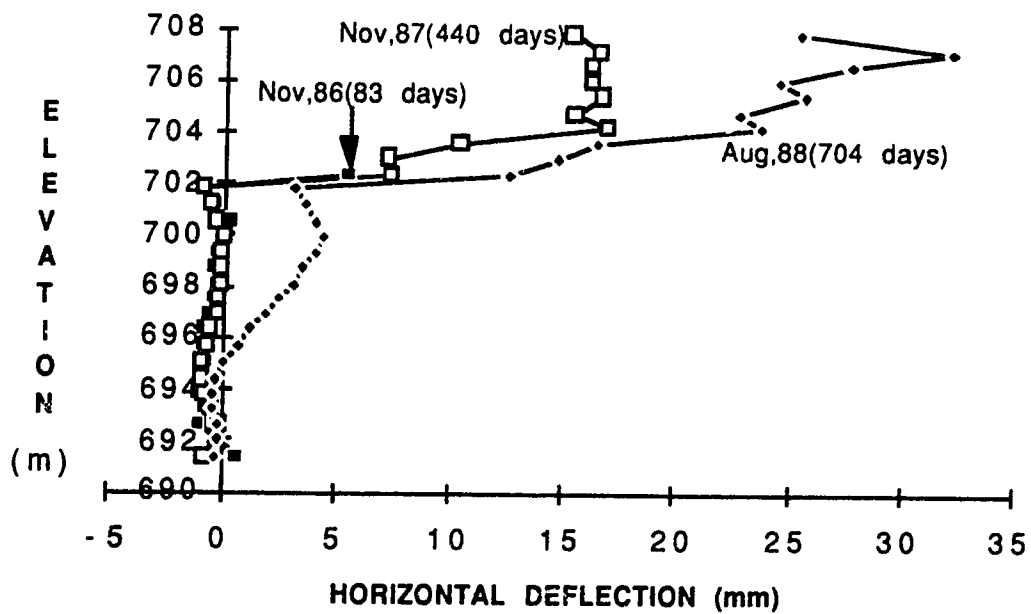


Figure 4.50 Horizontal Deflection (A) of Soils beneath Crest of Slope in Paragrid Section

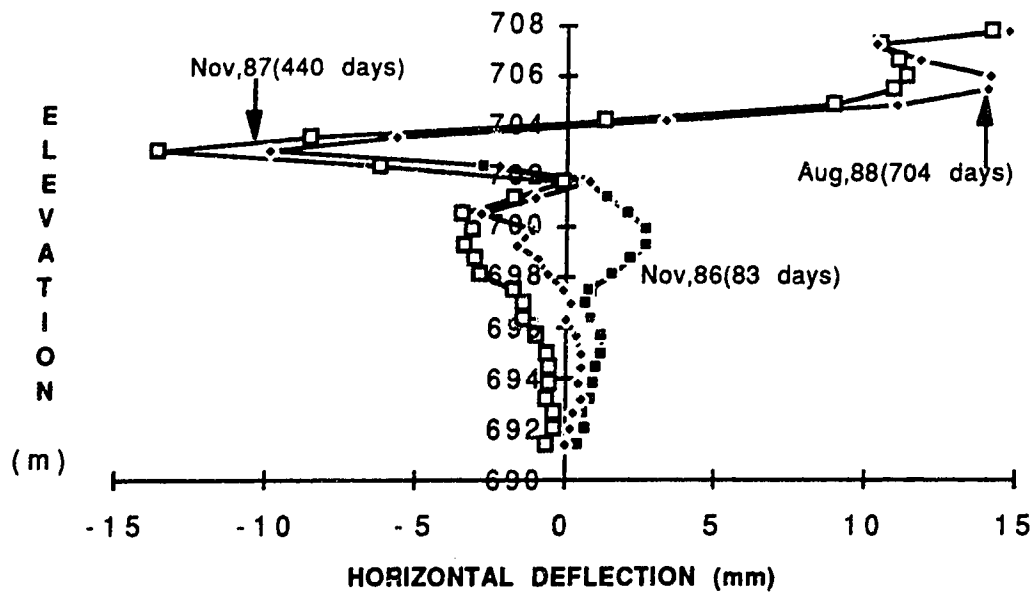


Figure 4.51 Horizontal Deflection (B) of Soils beneath Crest of Slope in Paragrid Section

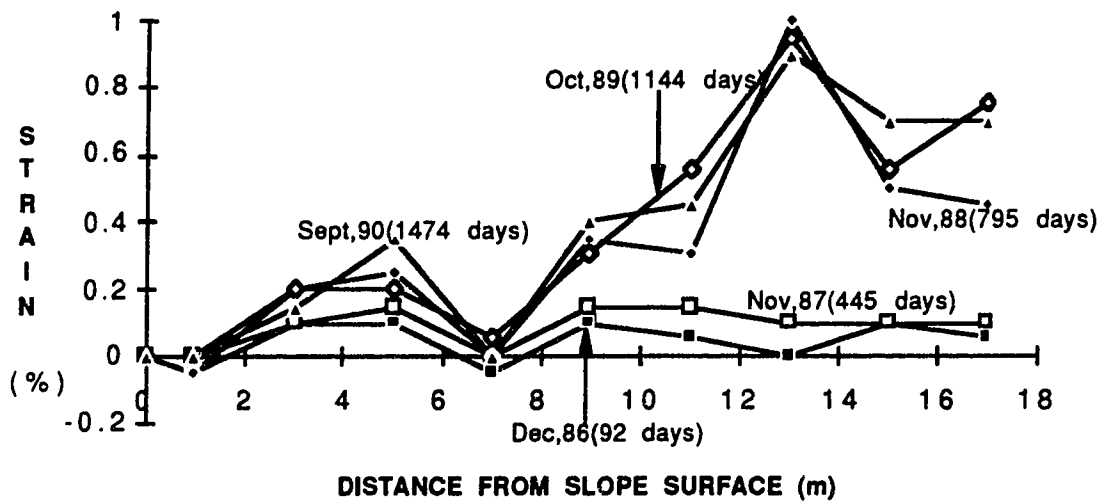


Figure 4.52 Distribution of Horizontal Strain of soil at 0 m Level in Unreinforced Section

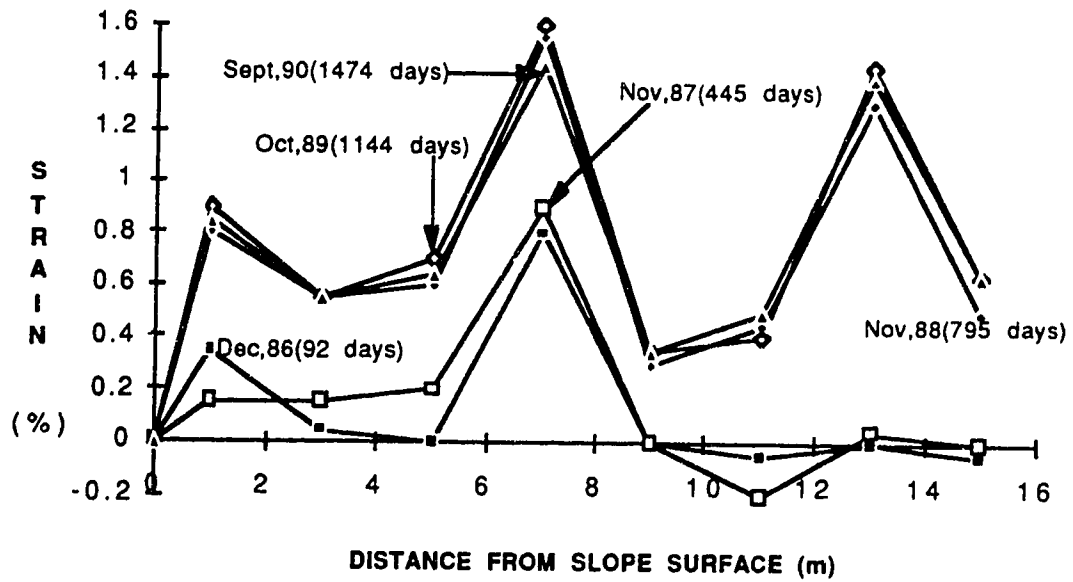


Figure 4.53 Distribution of Horizontal Strain of soil at 2 m Level in Unreinforced Section

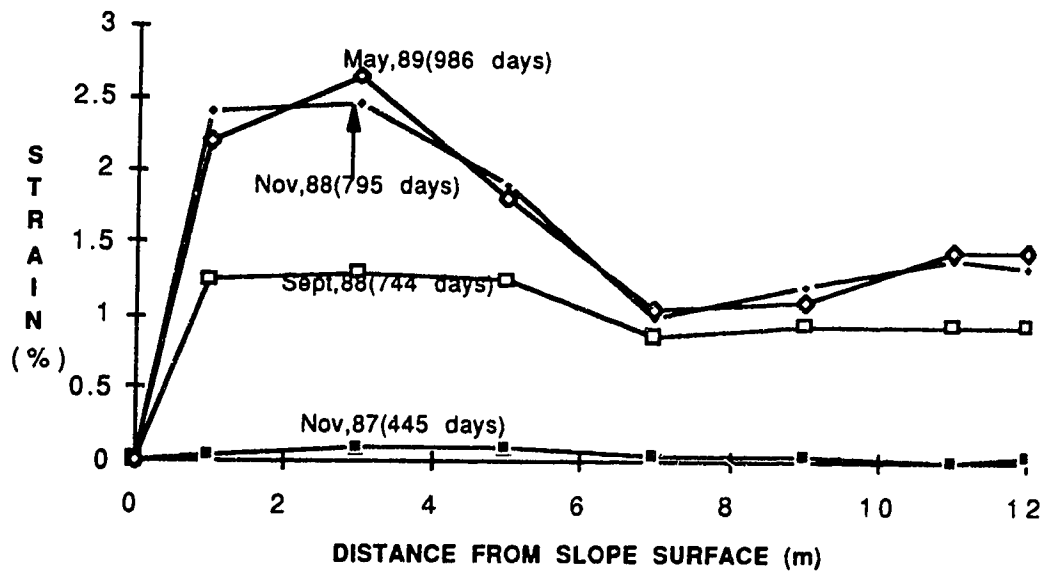


Figure 4.54 Distribution of Horizontal Strain of soil at 4 m Level in Unreinforced Section

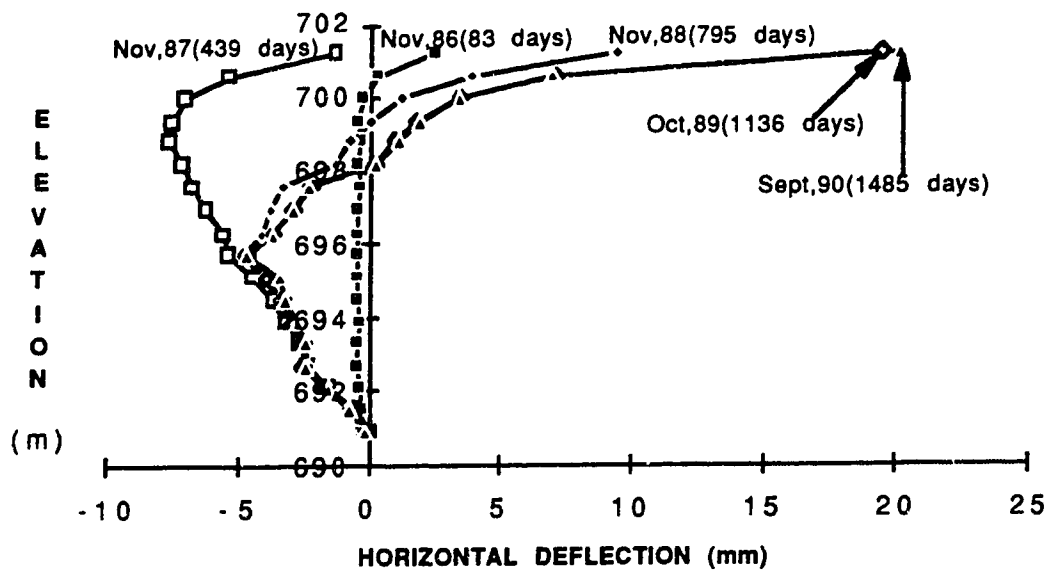


Figure 4.55 Horizontal Deflection (A) of Soils beneath Toe of Slope in Unreinforced Section

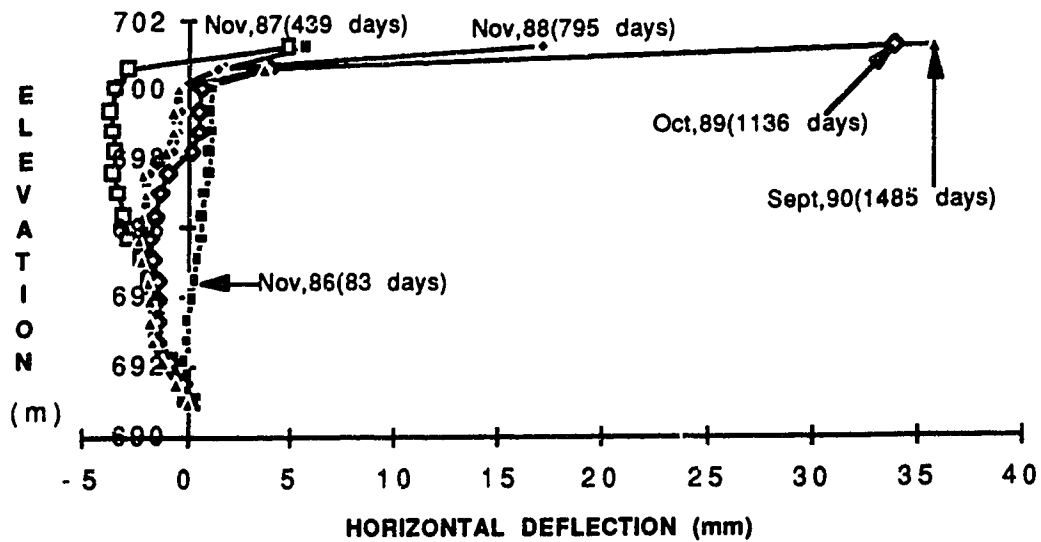


Figure 4.56 Horizontal Deflection (B) of Soils beneath Toe of Slope in Unreinforced Section

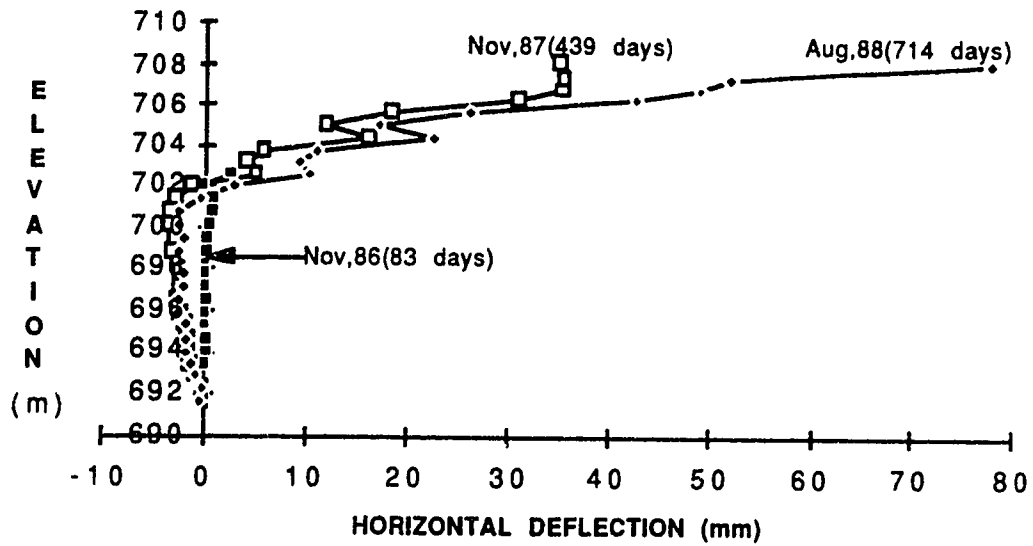


Figure 4.57 Horizontal Deflection (A) of Soils beneath Crest of Slope in Unreinforced Section

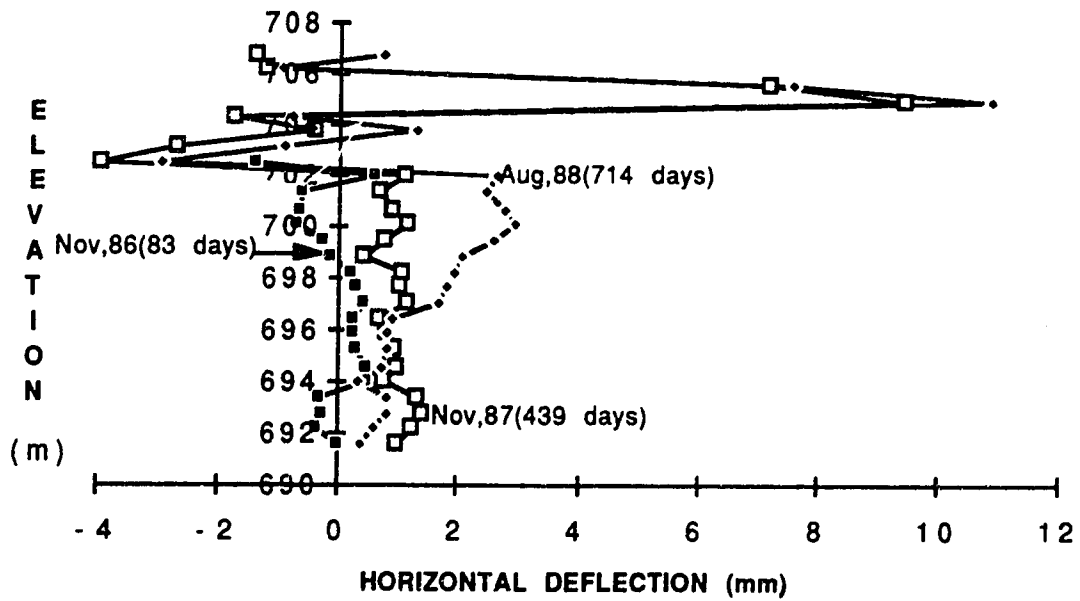


Figure 4.58 Horizontal Deflection (B) of Soils beneath Crest of Slope in Unreinforced Section

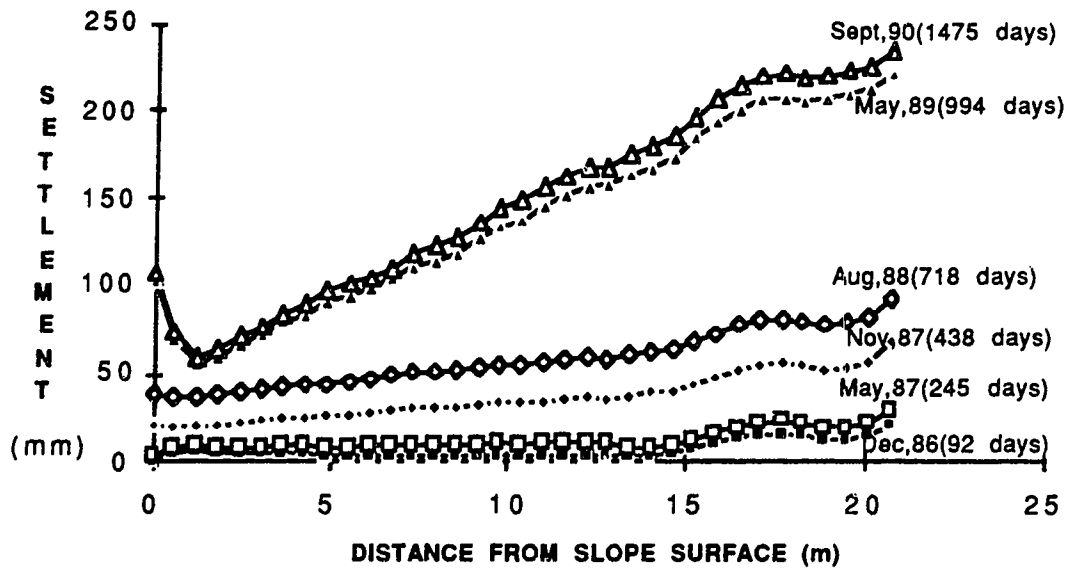


Figure 4.59 Settlement at Ground Level in Tensar Section

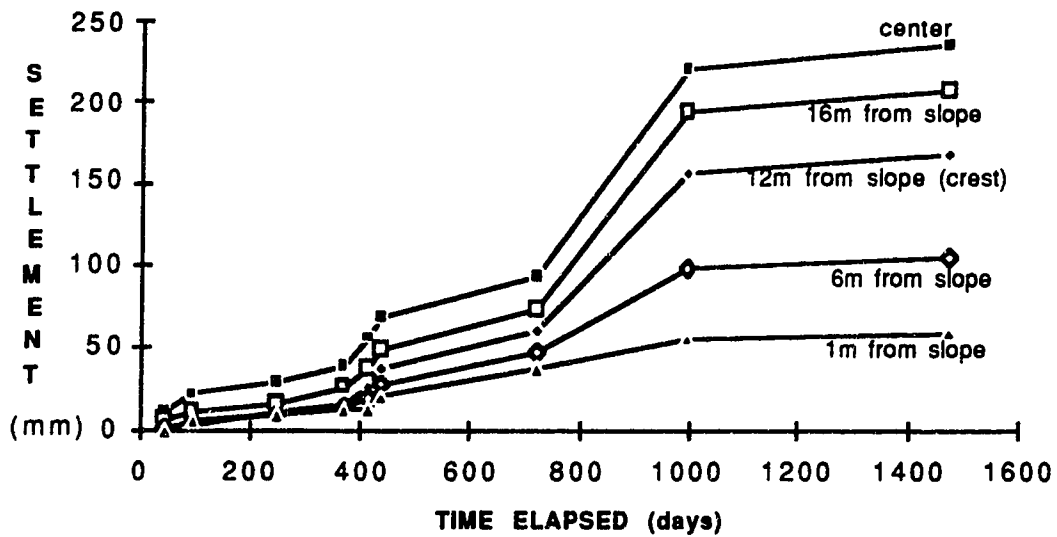


Figure 4.60 Development of Settlement at Ground Level in Tensar Section

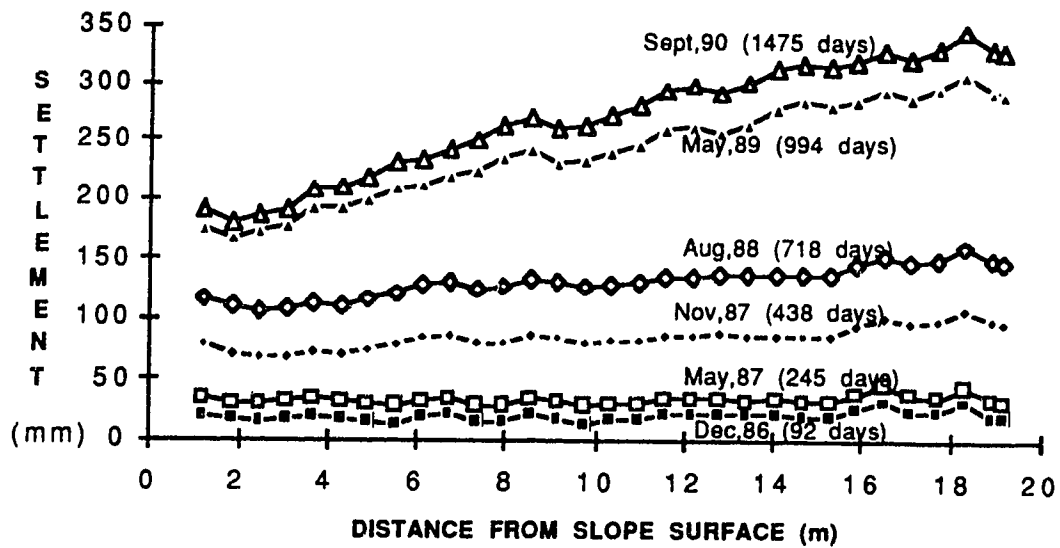


Figure 4.61 Settlement at 2 m Level in Tensar Section

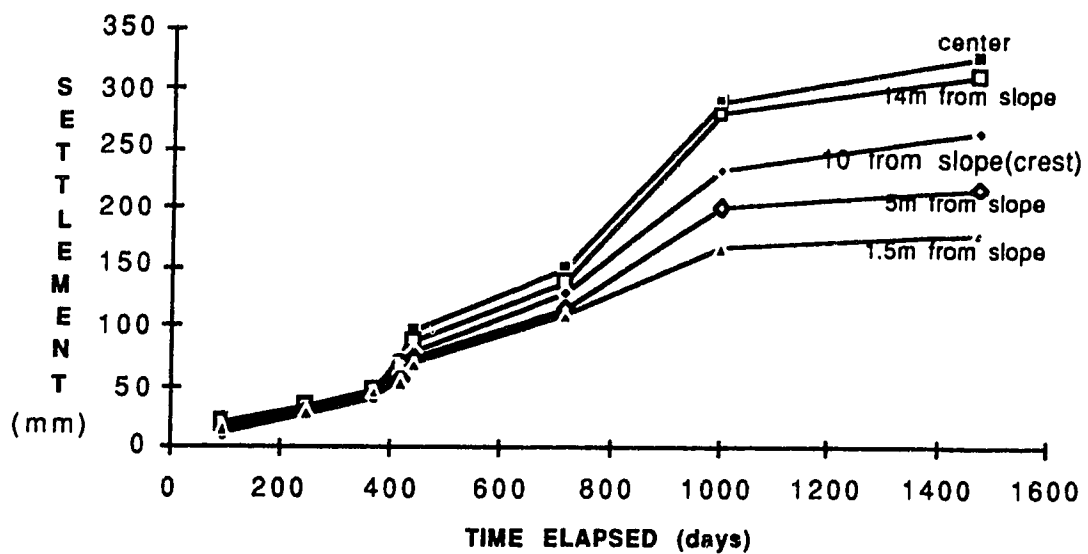


Figure 4.62 Development of Settlement at 2 m Level in Tensar Section

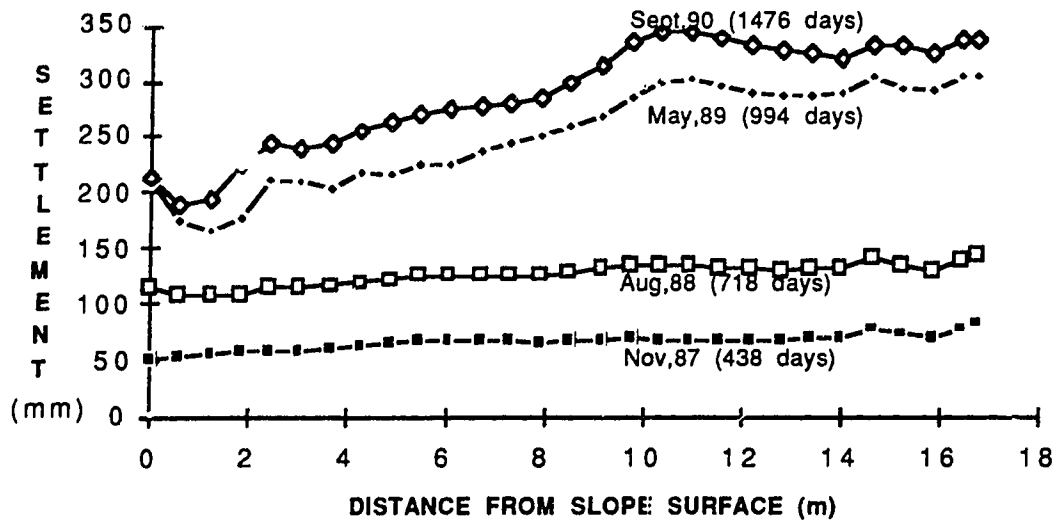


Figure 4.63 Settlement at 4 m Level in Tensar Section

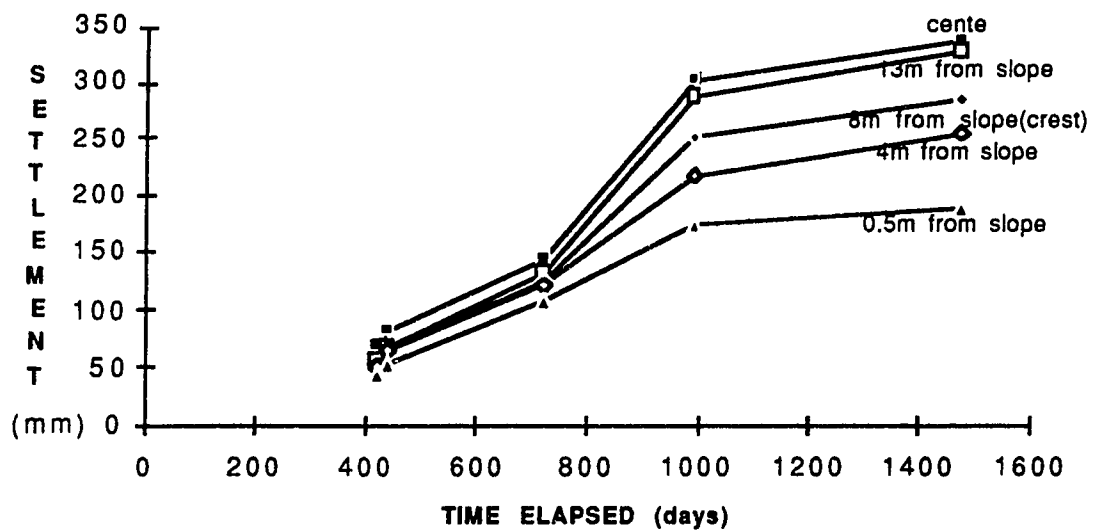


Figure 4.64 Development of Settlement at 4 m Level in Tensar Section

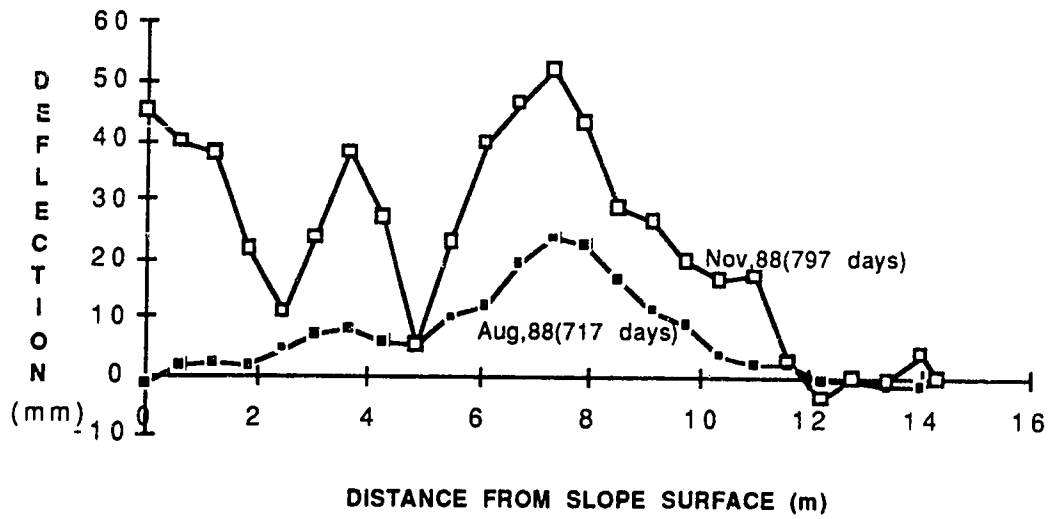


Figure 4.65 Vertical Deflection at 6 m Level in Tensar Section

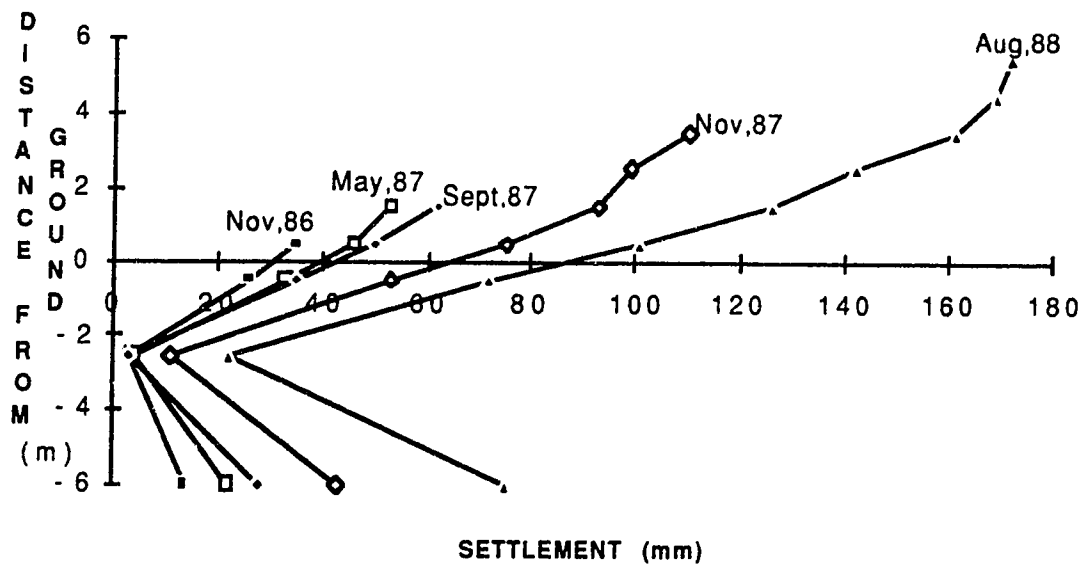


Figure 4.66 Settlement beneath Crest of Slope in Tensar Section (before adjustment)

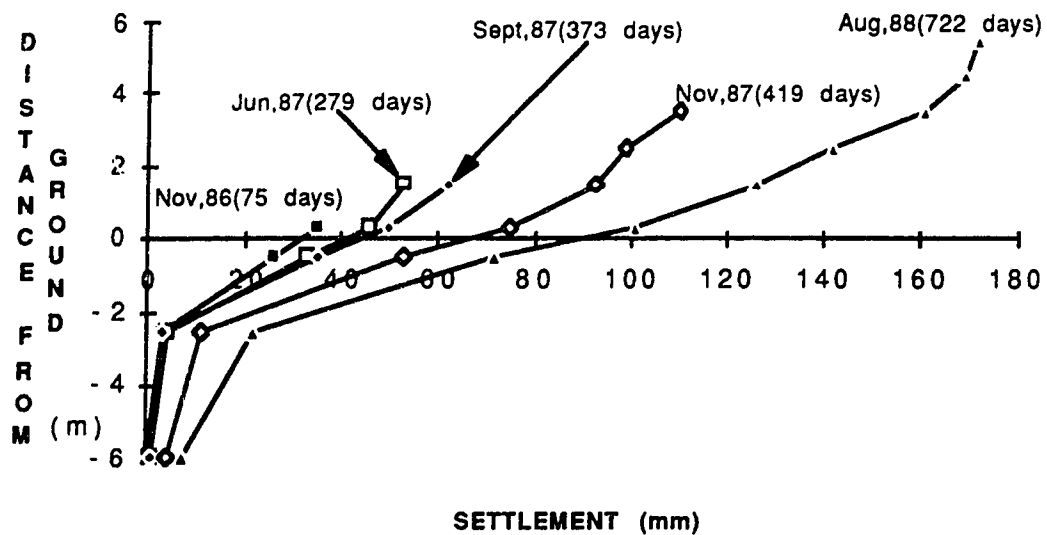


Figure 4.67 Settlement beneath Crest of Slope in Tensar Section (after adjustment)

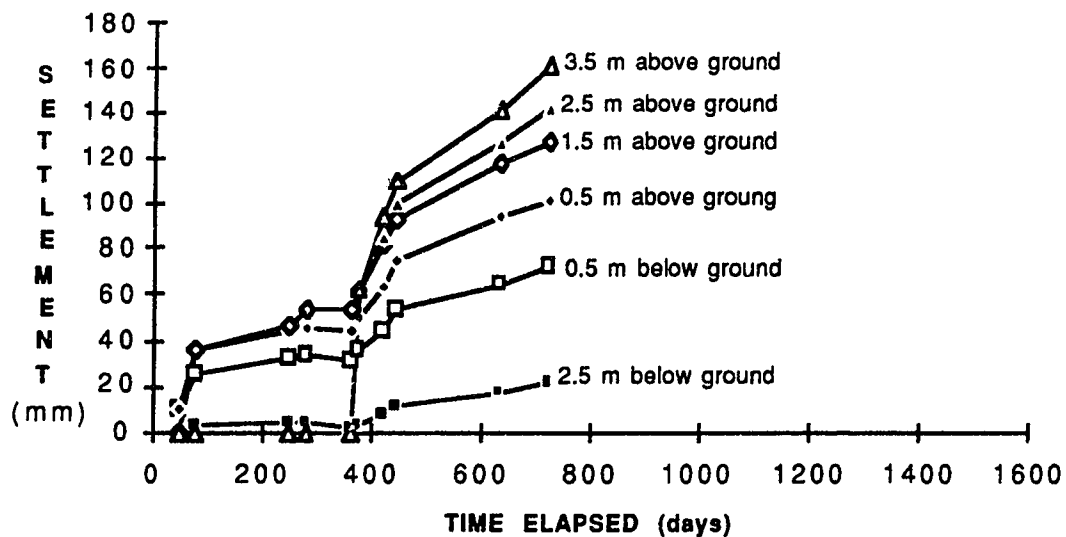


Figure 4.68 Development of Settlement beneath Crest of Slope in Tensar Section

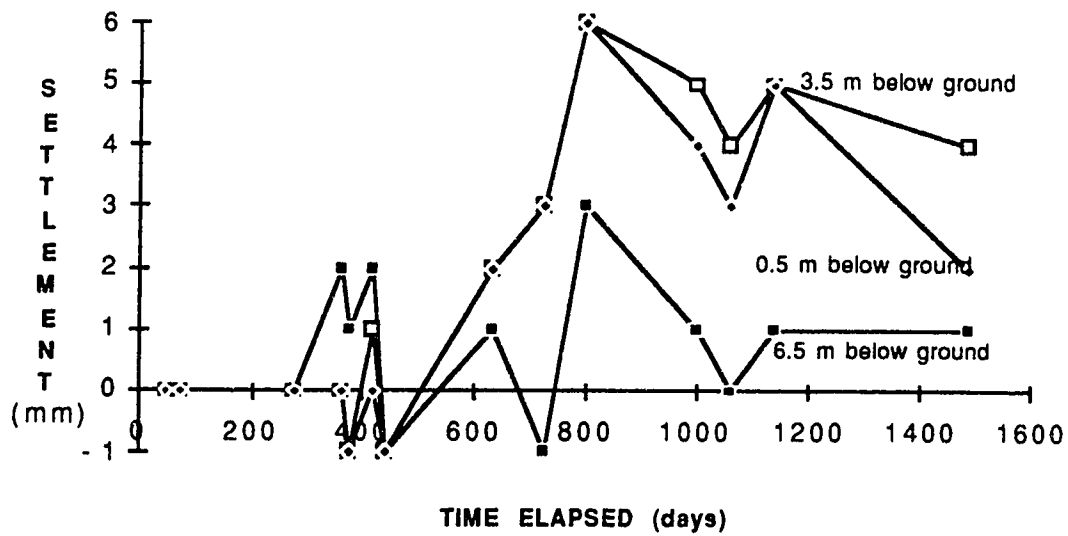


Figure 4.69 Development of Settlement beneath Toe of Slope in Tensar Section

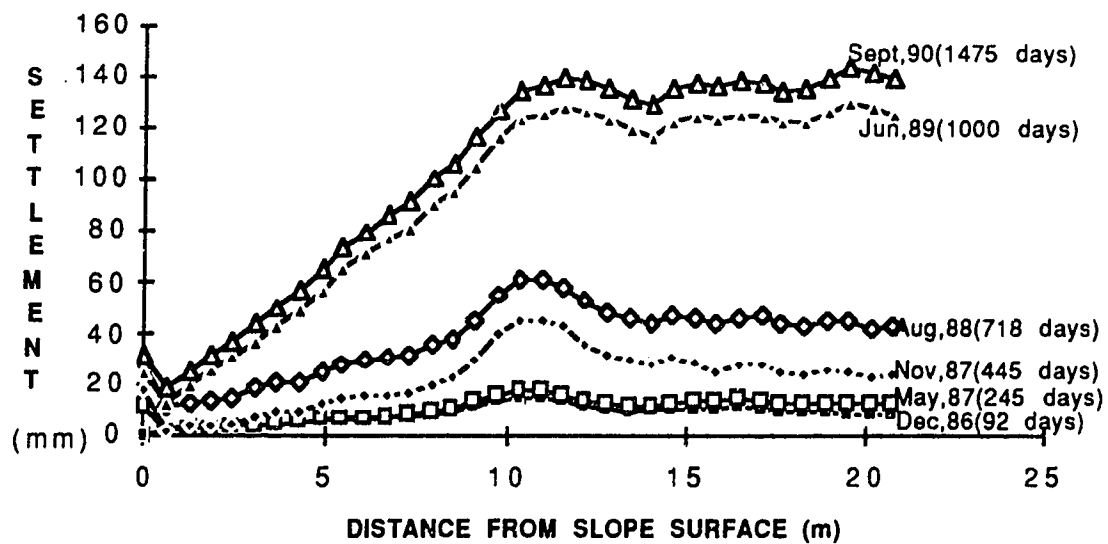


Figure 4.70 Settlement at Ground Level in Signode Section

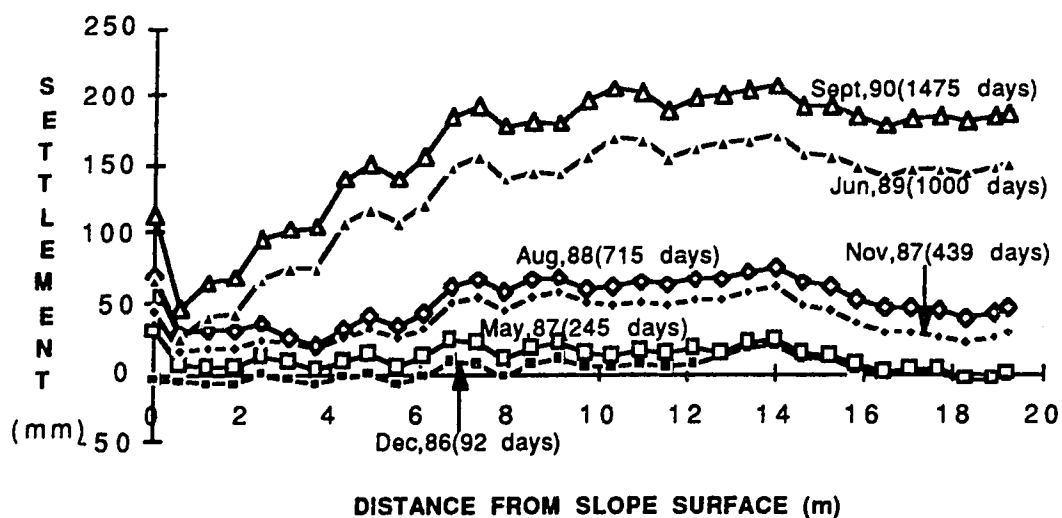


Figure 4.71 Settlement at 2 m Level in Signode Section

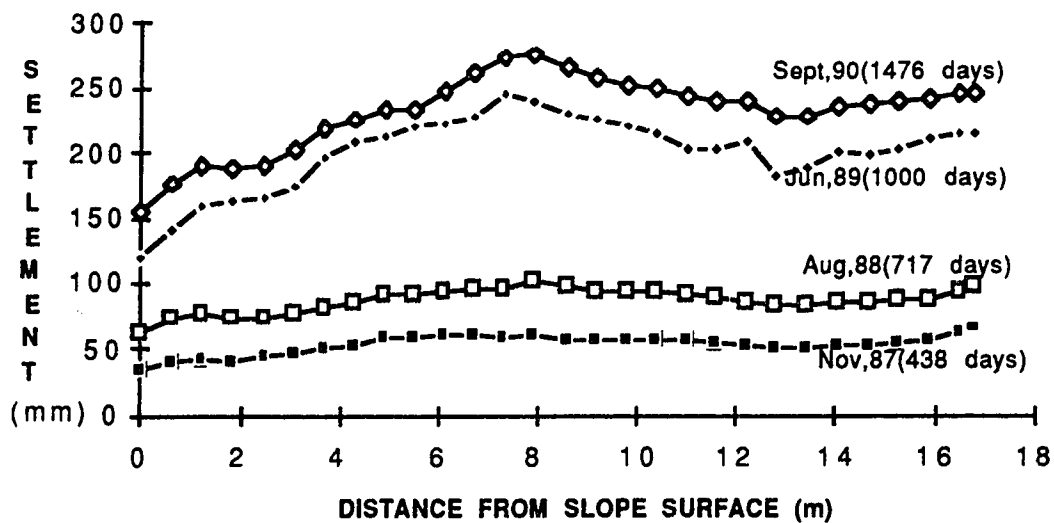


Figure 4.72 Settlement at 4 m Level in Signode Section

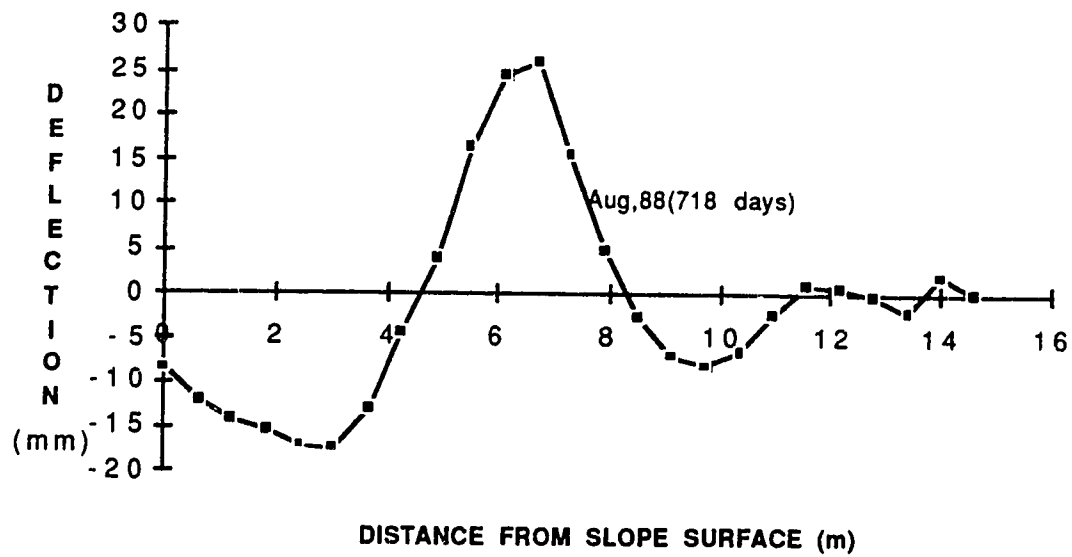


Figure 4.73 Vertical Deflection at 6 m Level in Signode Section

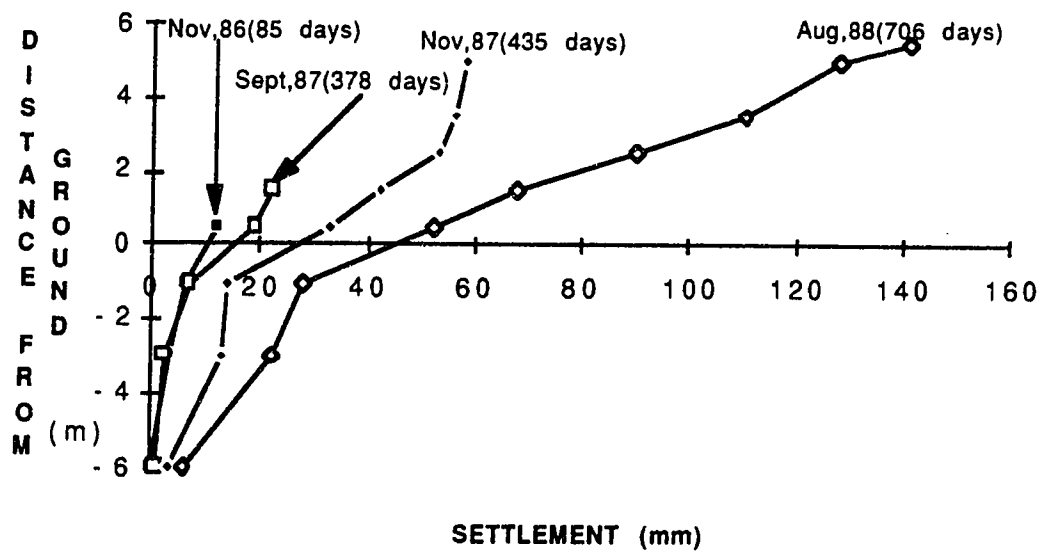


Figure 4.74 Settlement beneath Crest of Slope in Signode Section

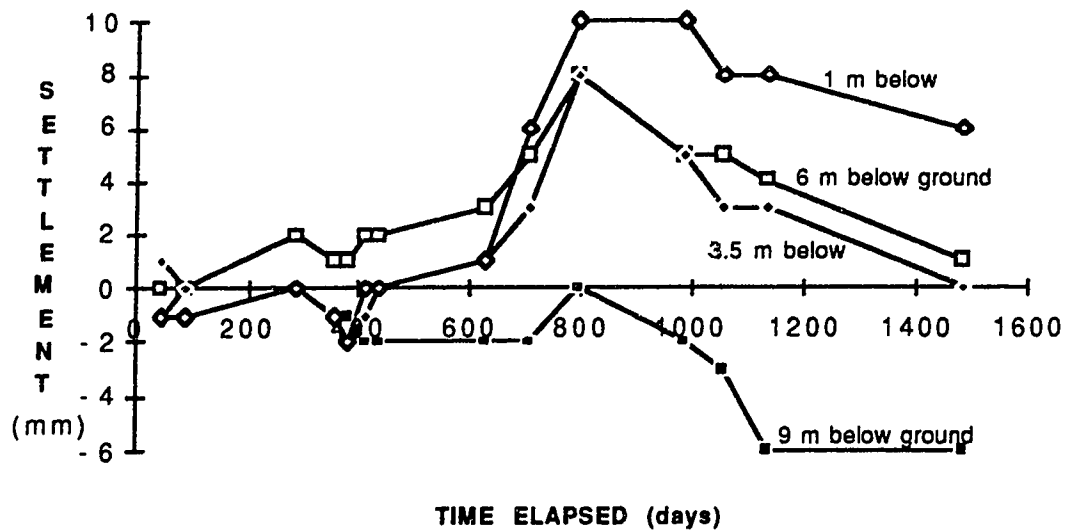


Figure 4.75 Development of Settlement beneath Toe of Slope in Signode Section

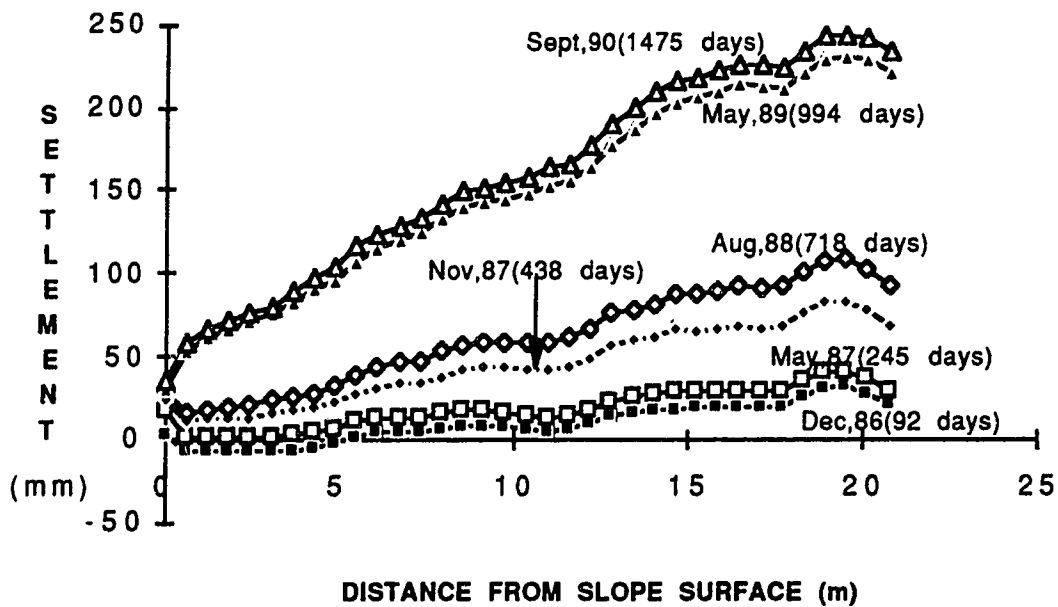


Figure 4.76 Settlement at Ground Level in Paragrid Section

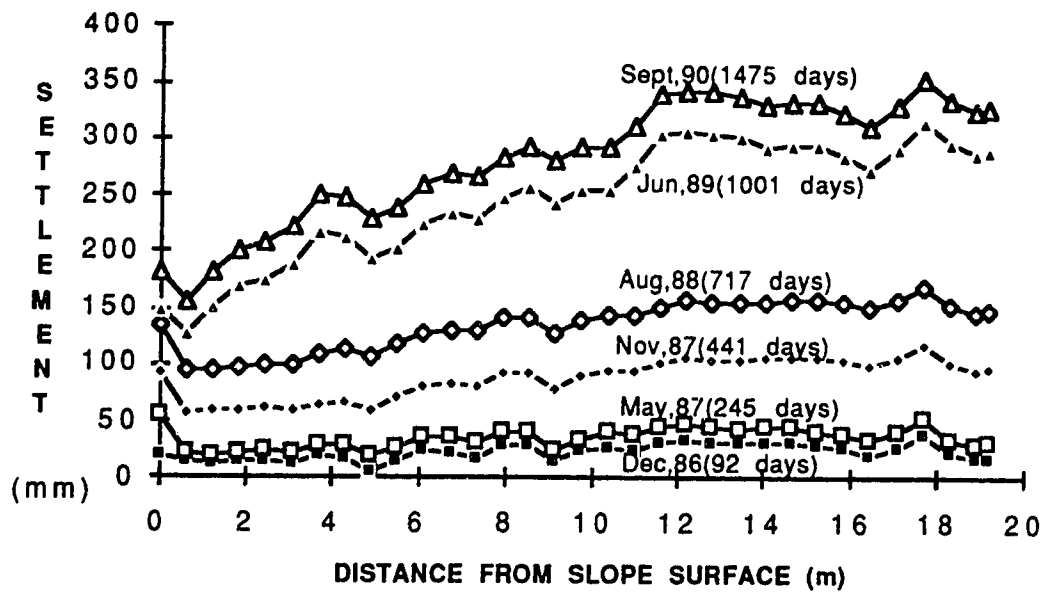


Figure 4.77 Settlement at 2 m Level in Paragrid Section

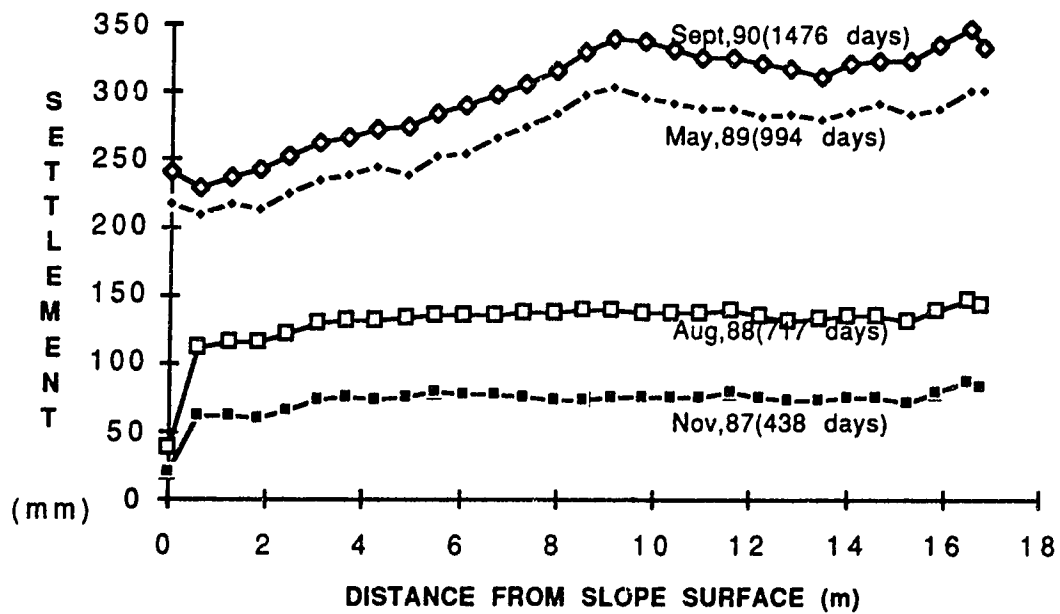


Figure 4.78 Settlement at 4 m Level in Paragrid Section

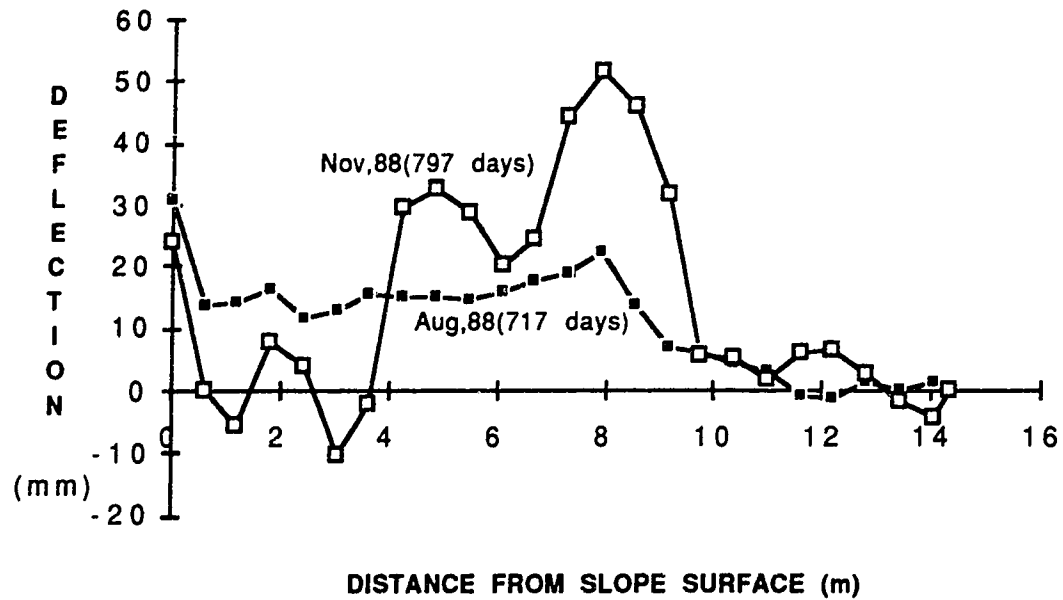


Figure 4.79 Vertical Deflection at 6 m Level in Paragrid Section

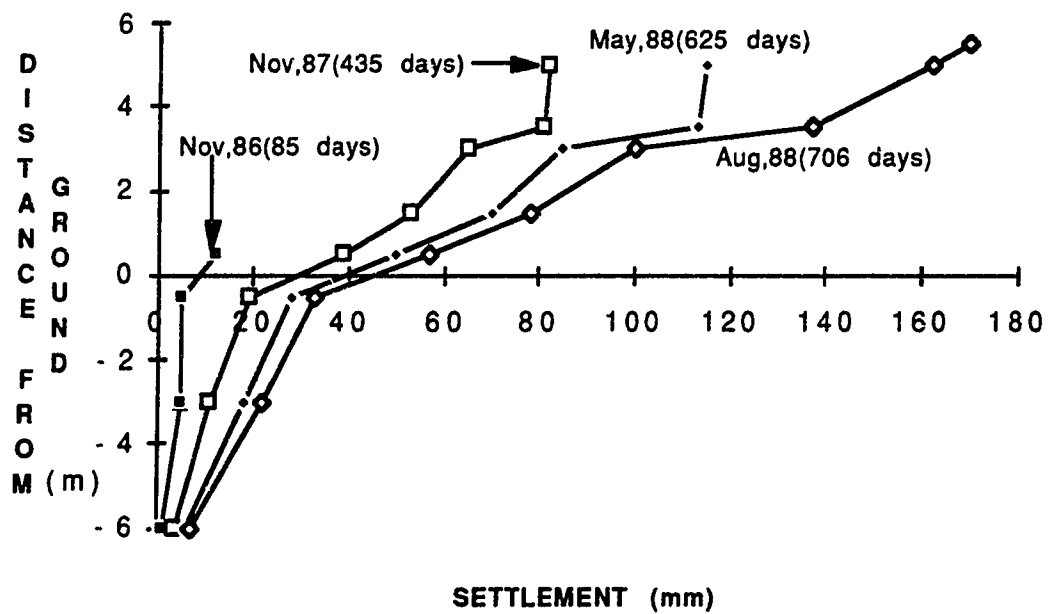


Figure 4.80 Settlement beneath Crest of Slope in Paragrid Section

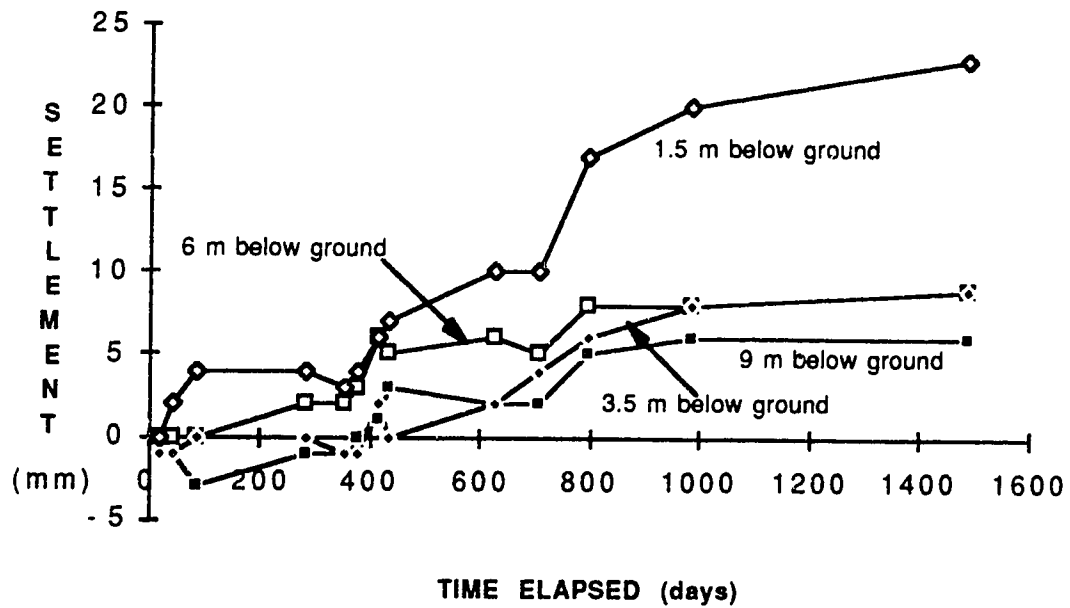


Figure 4.81 Development of Settlement beneath Toe of Slope in Paragrid Section

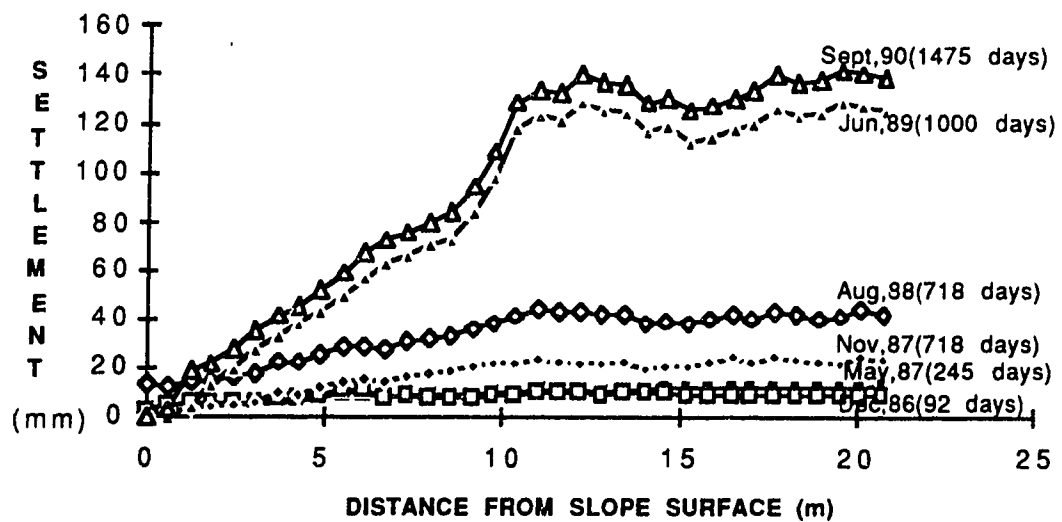


Figure 4.82 Settlement at Ground Level in Unreinforced Section

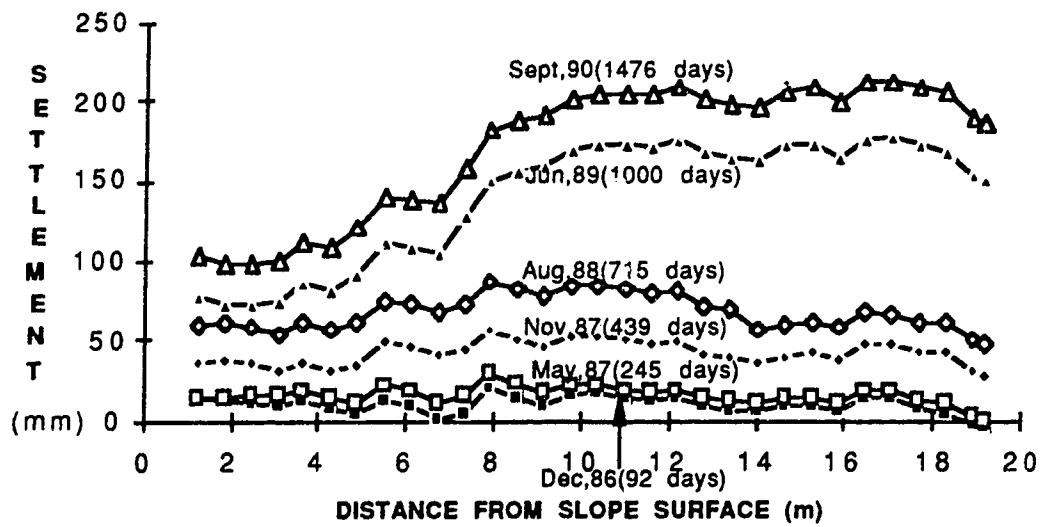


Figure 4.83 Settlement at 2 m Level in Unreinforced Section

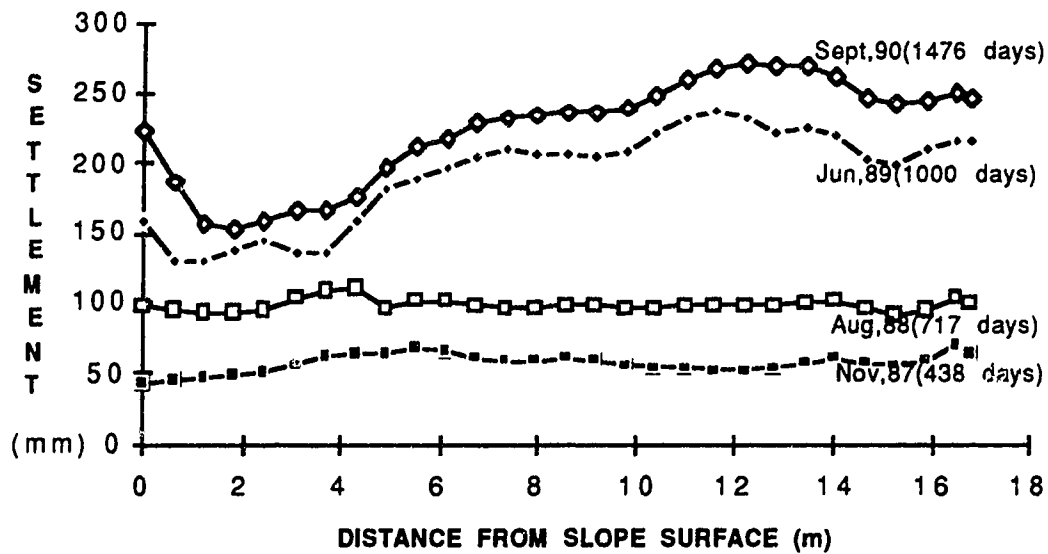


Figure 4.84 Settlement at 4 m Level in Unreinforced Section

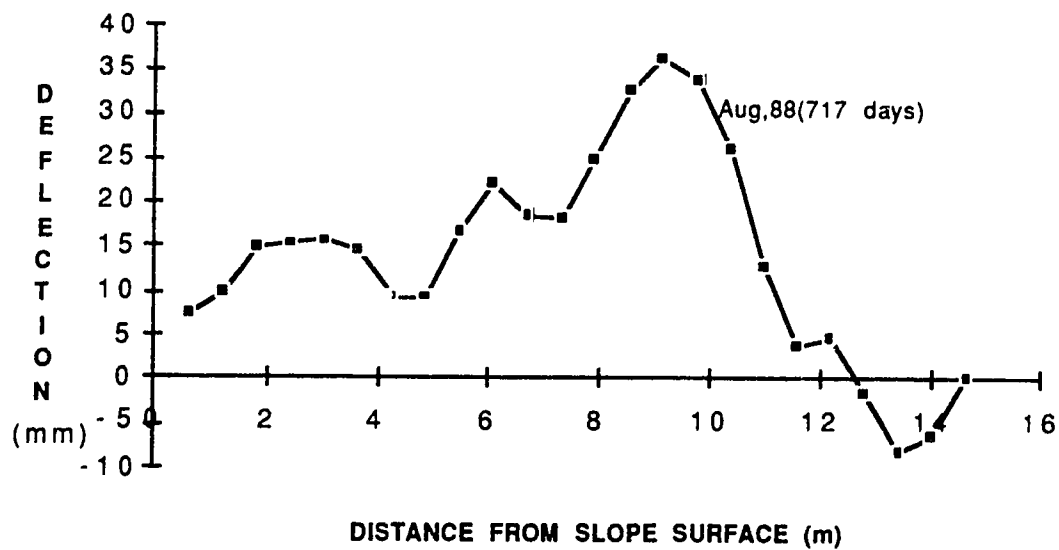


Figure 4.85 Vertical Deflection at 6 m Level in Unreinforced Section

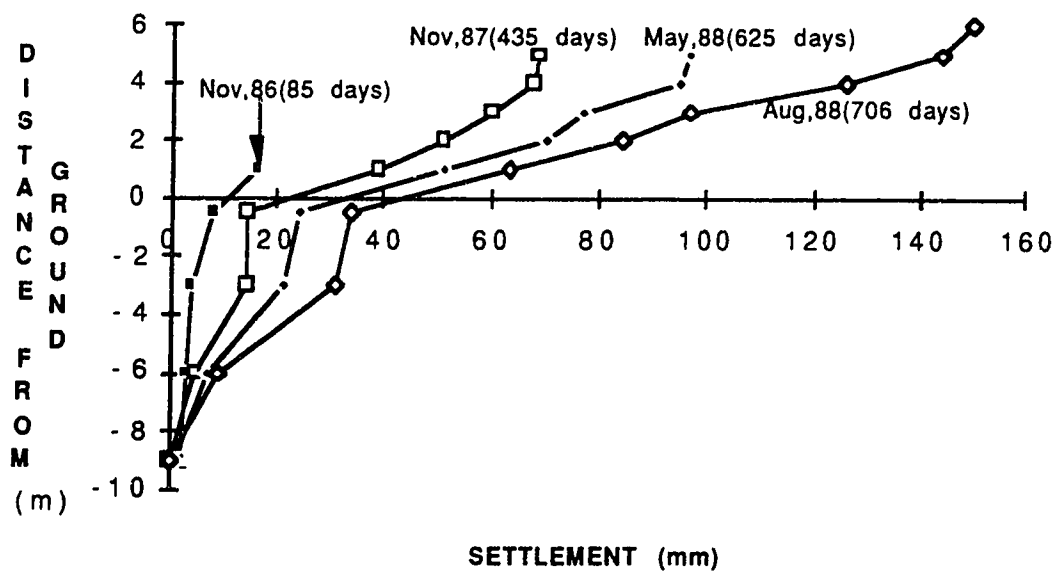


Figure 4.86 Settlement beneath Crest of Slope in Unreinforced Section

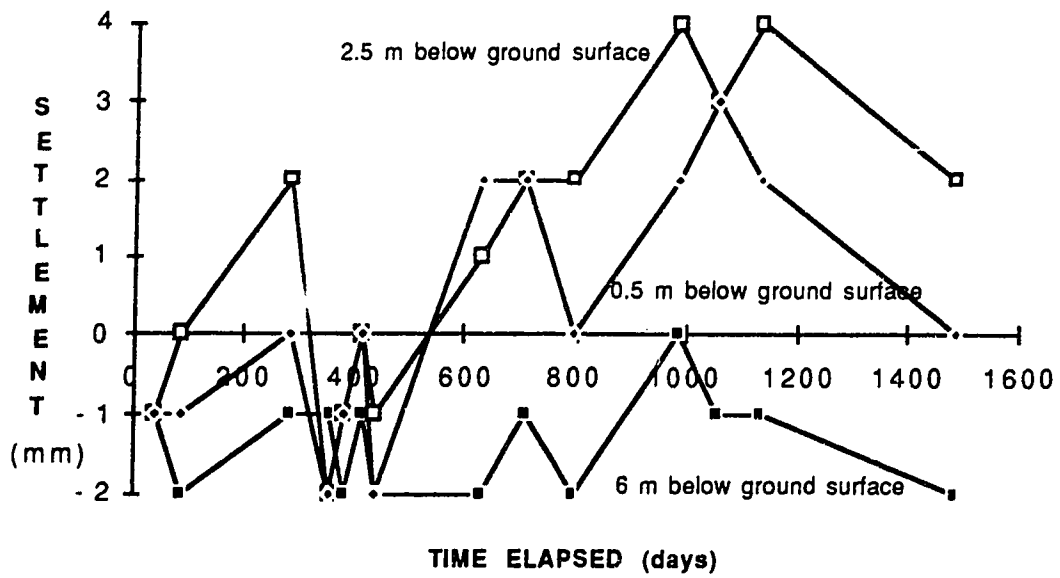


Figure 4.87 Development of Settlement beneath Toe of Slope in Unreinforced Section

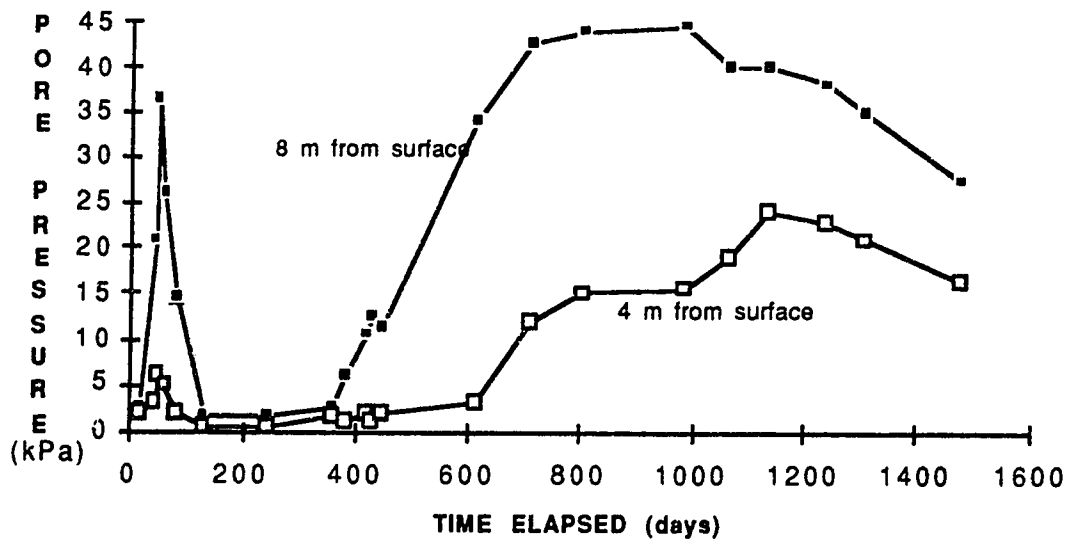


Figure 4.88 Development of Pore Pressure at 1 m Level in Tensar Section

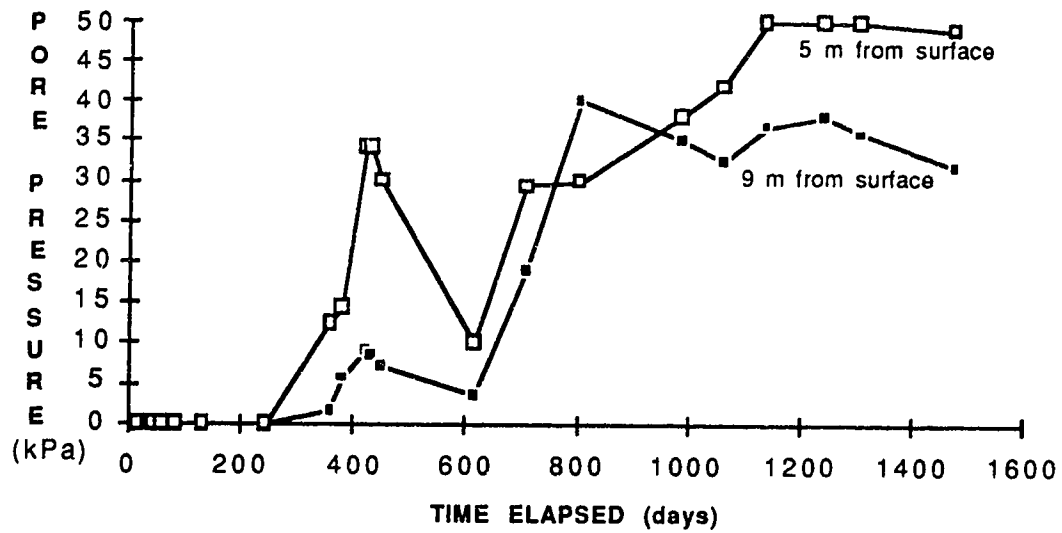


Figure 4.89 Development of Pore Pressure at 3 m Level in Tensar Section

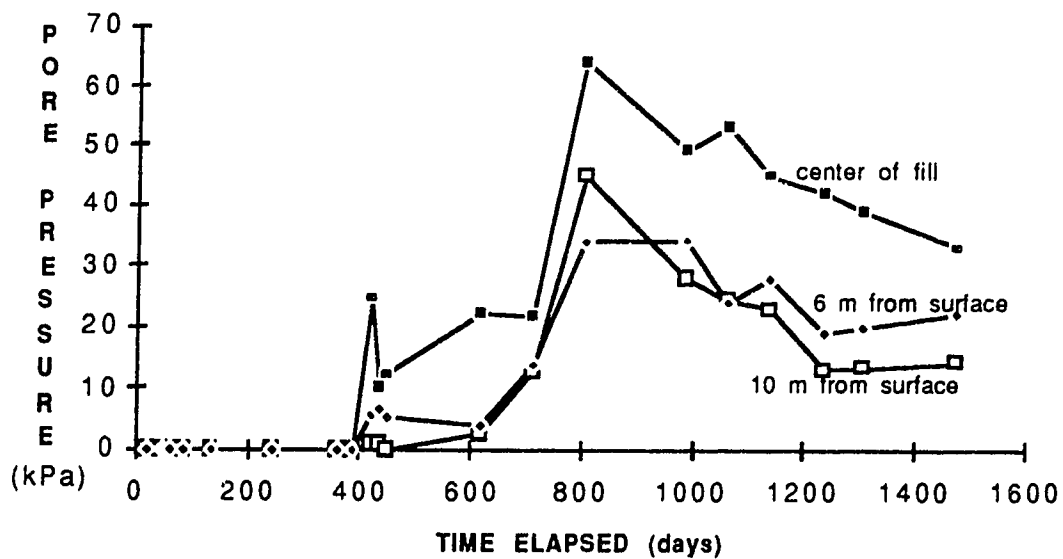


Figure 4.90 Development of Pore Pressure at 5 m Level in Tensar Section

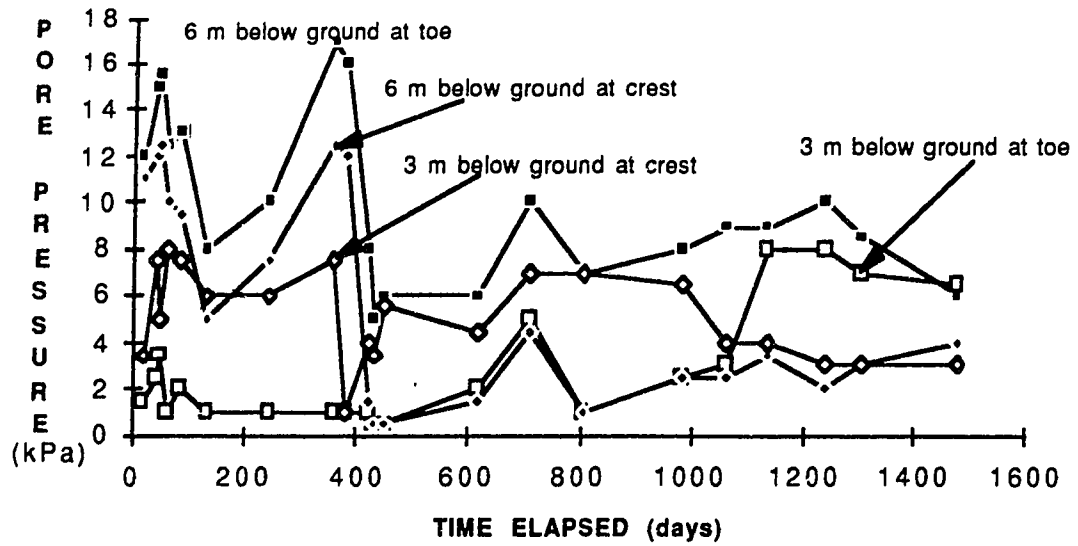


Figure 4.91 Development of Pore Pressure in Foundation Soils in Tensar Section

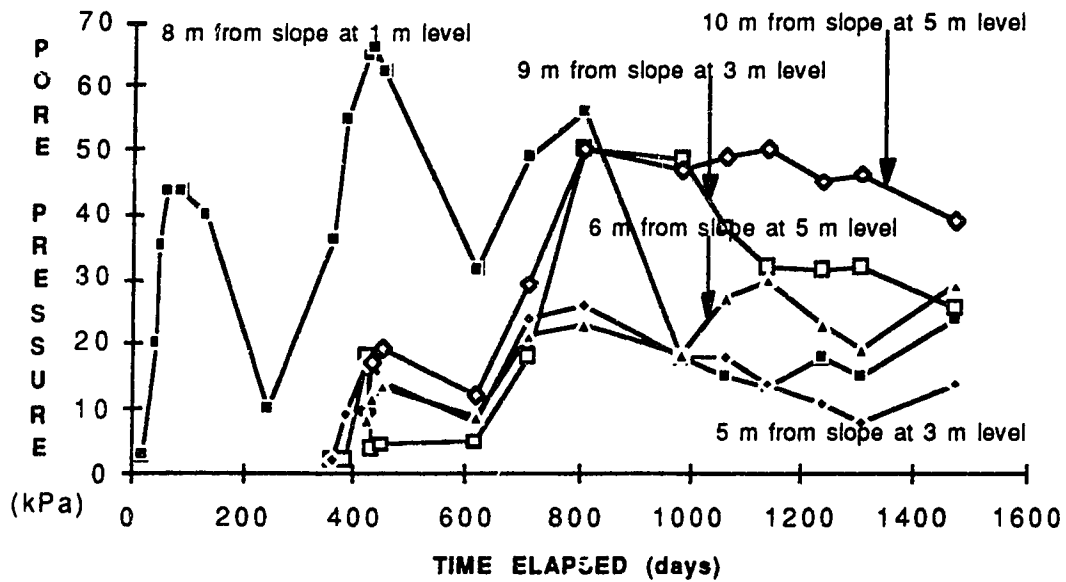


Figure 4.92 Development of Pore Pressure in Fill Soil in Signode Section

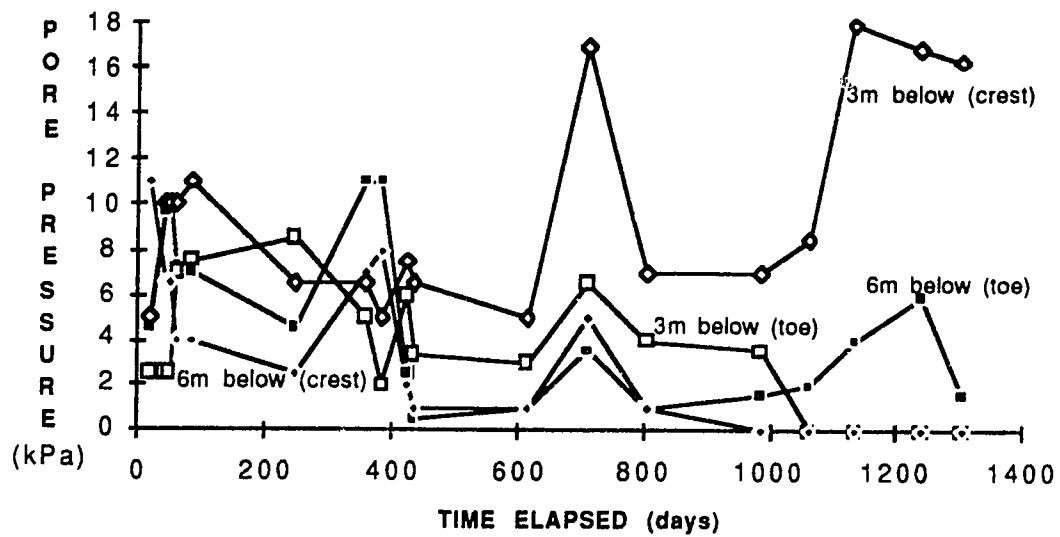


Figure 4.93 Development of Pore Pressure in Foundation Soils in Signode Section

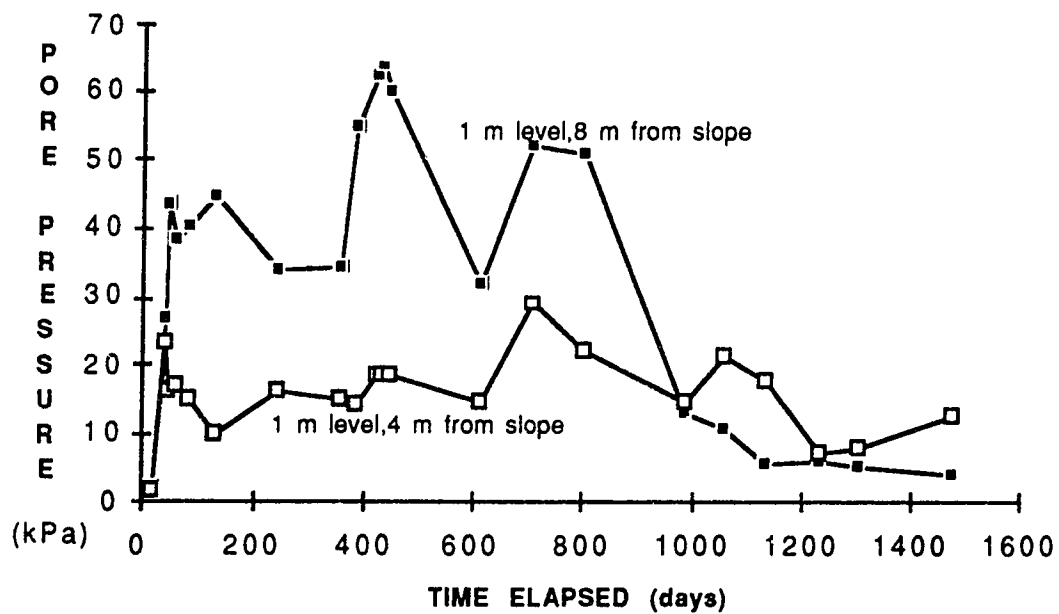


Figure 4.94 Development of Pore Pressure in Fill Soil in Paragrid Section

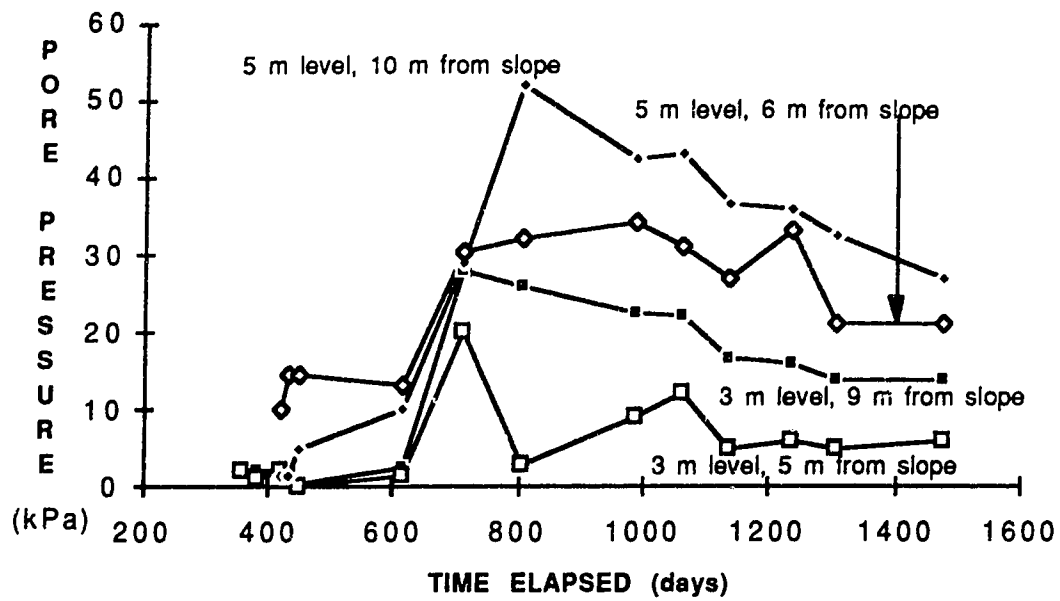


Figure 4.95 Development of Pore Pressure in Fill Soil in Paragrid Section

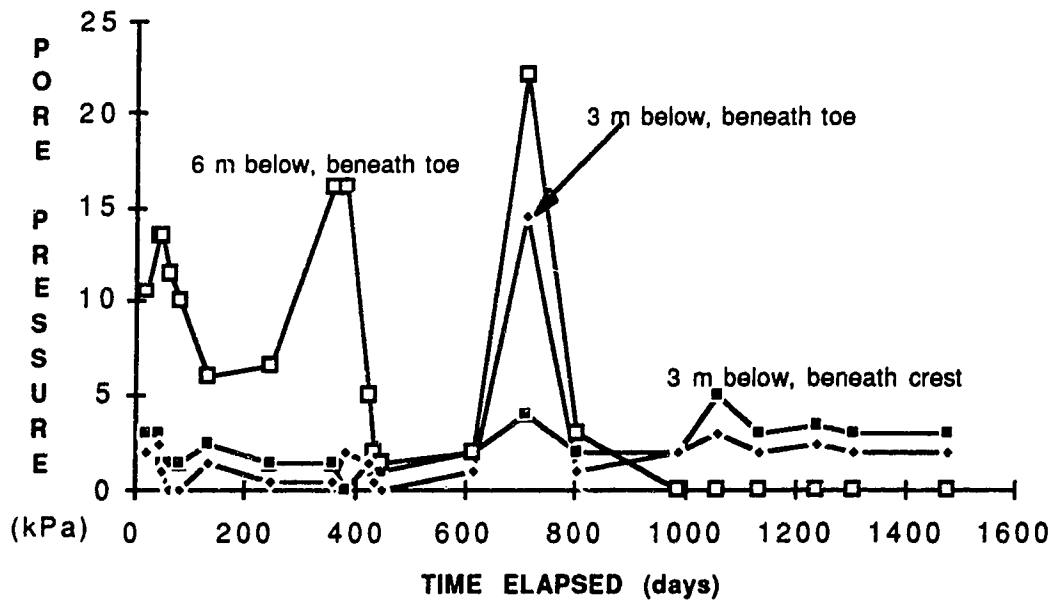


Figure 4.96 Development of Pore Pressure in Foundation Soils in Paragrid Section

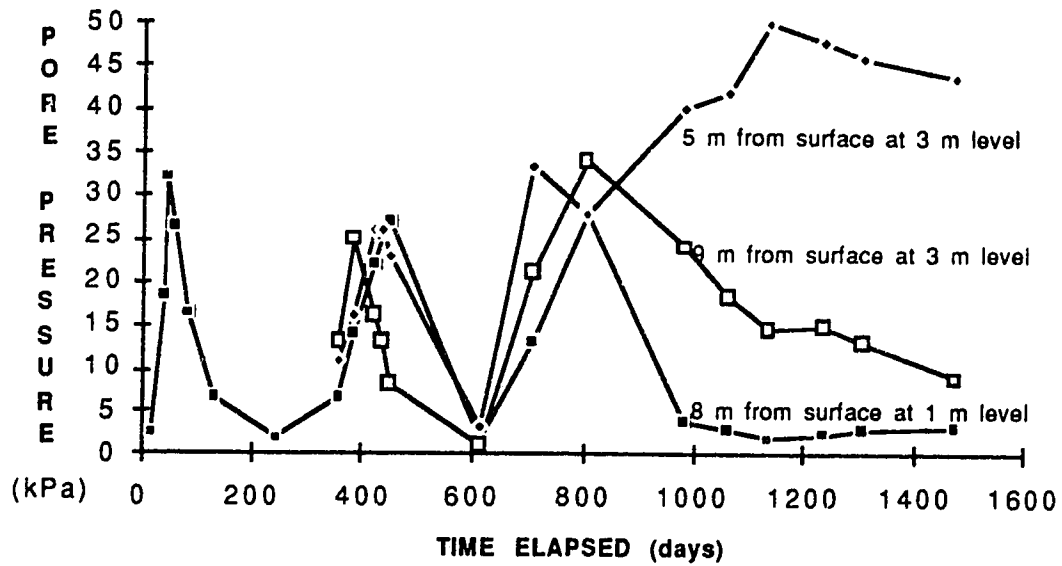


Figure 4.97 Development of Pore Pressure in Fill Soil in Unreinforced Section

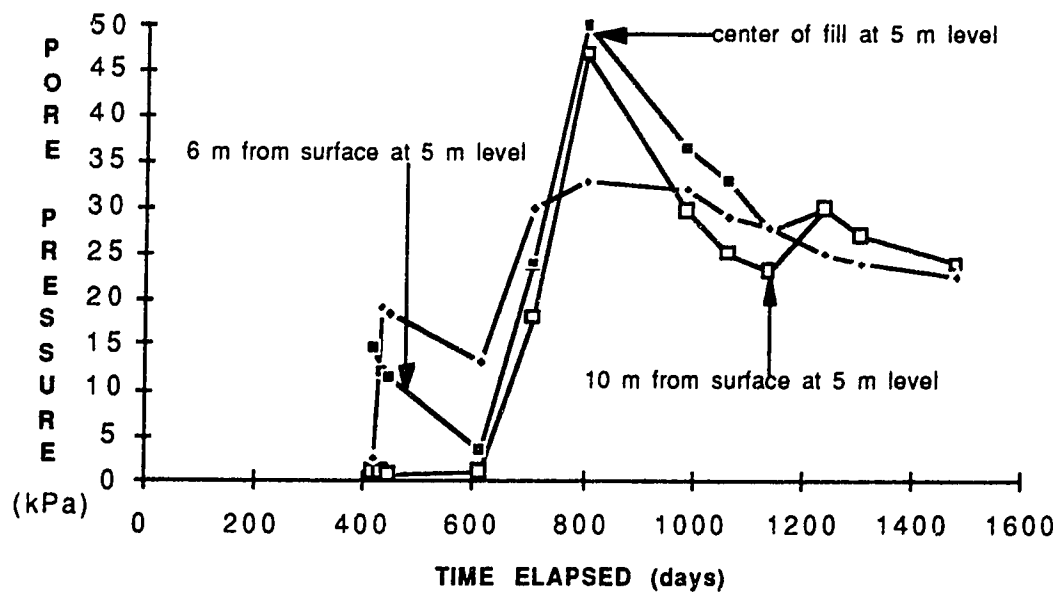


Figure 4.98 Development of Pore Pressure in Fill Soil in Unreinforced Section

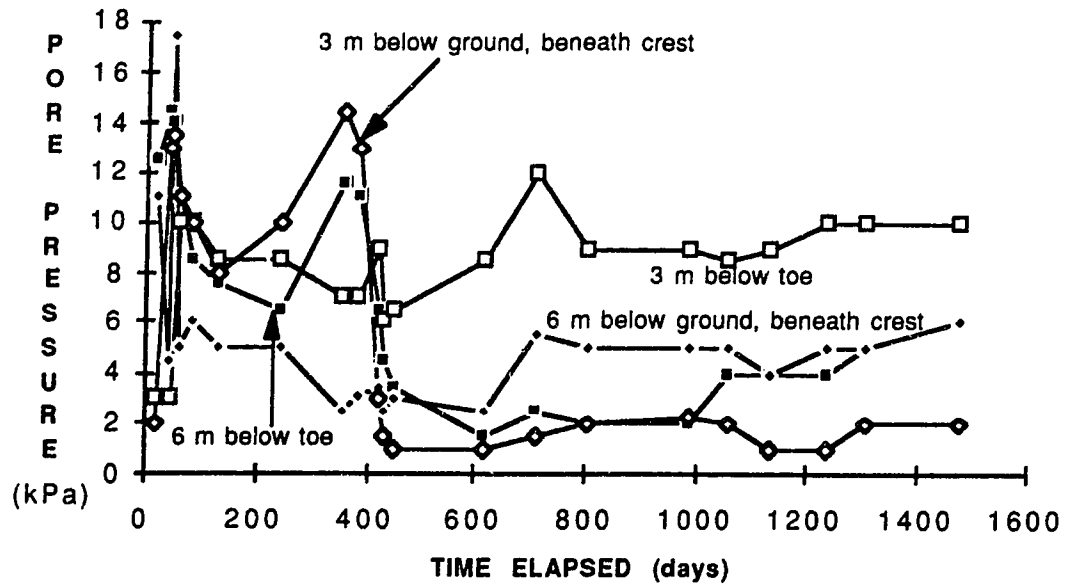


Figure 4.99 Development of Pore Pressure in Foundation Soils in Unreinforced Section

Chapter 5. Summary of Field Measurements

5.1 Introduction

The performance of the Devon geogrid-reinforced test embankment was discussed in Chapter 4. Detailed interpretation and adjustment of the field data were presented and justified in that chapter. For non-functioning instruments and missing data in the geogrid layers, the strains of the geogrids were estimated based on the measurements at adjacent locations. Most of the adjustments were made to the measurements of the inductance coils; only a few minor adjustments were made to the measurements of the electrical wire resistant (EWR) strain gauges. The analyses of the reinforced slope were mainly based on the EWR gauge measurements for two reasons. First, the EWR gauge measurements were found to be more consistent, reliable and accurate for this test fill. Second, the tensile strains in the tension members of the geogrids can be directly related to the tensile loads in the geogrids according to laboratory wide strip tensile tests of the geogrids. The measurements of the inductance coils were only used to assist the interpretation of the EWR gauge data. Therefore, the adjustments in the previous chapter will not significantly affect observations and conclusions presented in following chapters.

In this chapter, the field measurements from the test fill are summarized in terms of the geogrid strains, vertical and horizontal soil movements and pore pressure response within the embankment soils. Results from the different test sections are compared. Analyses of the data and the response of the test fill will be presented in the following chapters.

5.2 Strains in Geogrids

Strains in the geogrids in the test fill were monitored using electrical wire resistance (EWR) strain gauges and inductance coils. EWR gauges measured the strains in longitudinal (tension) members (or ribs) of the geogrids; inductance coils measured strains between adjacent transverse members (anchor members or bars). In spite of some errors induced by thermal expansion correction, as discussed earlier, the EWR gauges measured strains are more accurate and meaningful, especially when tensile forces in the

reinforcement are concerned. The inductance coil measurements were mainly used to check the strain distributions and to provide valuable estimates at instrumented locations where the EWR gauges failed or had other problems.

5.2.1 Strains in Tensar Geogrid

Excluding the 2 and 3 m locations in the bottom layer, the distributions of the tensile strain measured by EWR gauges and inductance coils were nearly identical to each other in the Tensar geogrid. Profiles of the strains in the three primary reinforcing layers at the end of the final construction season are shown in Figures 5.1 and 5.2, as measured by EWR gauges and inductance coils respectively. The magnitudes of the strains from the EWR gauges were slightly larger than the strains from inductance coils at most locations.

The tensile strains in the geogrid developed as the fill was sequentially constructed. The development was, however, not directly proportional to the fill height. The peak strains in the bottom, middle and top layer were 0.49, 0.71 and 0.18% at the end of the 1987 construction season while the peak strains at the end of the 1988 construction were 1.05, 1.75 and 2.9% in the same three layers. The bottom layer had the smallest increment of strain and the top layer had the largest increment as the fill increased from 6 to 12 m. Moreover, due to the increase of the fill height, the peak strains in the bottom and top layers translated from the 1 m location to the 3 m location as measured from the slope surface.

5.2.2 Strains in Signode Geogrid

Figures 5.3 and 5.4 show the profiles of the tensile strains, measured by EWR and inductance coils at the end of the 1988 construction season, in the three primary reinforcing layers of the Signode geogrid. As shown in the figures, the strain distributions obtained from the two types of measurements were similar to each other, whereas the magnitudes of the strains from inductance coils were larger at most locations. The differences could be caused not only by different deformation mechanisms which were influenced by both the geometrical and mechanical properties of the geogrids, but also by problems in the measuring systems such as thermal correction and read-out box sensitivity.

Similar to the discussion on the Tensar geogrid, the tensile strains in the Signode geogrid did not develop proportional to the placement of the fill. The peak strains at the end of the 1987 construction season were 0.84, 0.57 and 0.06% in the bottom, middle and top layers; then they increased respectively to 1.58, 1.98 and 1.68% immediately after the final construction stage. As the fill height increased from 6 to 12 m, the strains in the top layer increased the largest amount and the bottom layer the smallest amount. However, the total strains in the three reinforcing layers were of similar magnitudes when the test fill was completed in November 1988.

5.2.3 Strains in Paragrid Geogrid

As mentioned in Chapter 3, some of the high strength fibers in the tension members of the Paragrid geogrid were weakened or damaged at the intersections of the geogrid. This damage was most likely caused by over heating during manufacturing of the geogrid. As a result, the tensile strains measured using the EWR gauges differed significantly from the strains measured using the inductance coils. Also, there were several problems with the coil measurements as discussed in the last chapter.

Figures 5.5 and 5.6 show the profiles of the strains measured at the end of the final construction season using the two types of measurements. The measured strains in the longitudinal members (0.87, 0.23 and 0.28% peak strains in the bottom, middle and top layers at the end of the 1987 construction season and 1.19, 0.55 and 1.27% at the end of the 1988 season) were considerably smaller than the strains in the other two geogrids (Tensar and Signode), because the tension members were weakened by the defective welds and thus less load was carried by the tension members. On the other hand, the strains between adjacent transverse members (2.77, 1.95 and 0.47% in the three layers at the end of the 1987 construction season and 3.56, 1.67 and 4.89% at the end of the 1988 construction season) were larger than the other geogrids. Nevertheless, the strain profiles from the two types of measurements do indicate that the middle layer of the Paragrid geogrid had the smallest strain and the bottom and top layers had strains of similar magnitudes.

Due to some unknown problems with the inductance coil measurements in the Paragrid layers and due to the seasonal fluctuations, it was difficult to evaluate the creep behavior of the geogrid. However, the inductance coil measurements did show some time-dependent strains occurred in the Paragrid material. Comparing the strains measured in November 1988, October 1989 and October 1990 (the air temperatures during the three sets of the field readings were presumably similar to each other), it was found that the strains increased at most instrumented locations as time passed. The magnitudes of the increases varied considerably from one location to the others.

5.2.4 Comparison of Strains in geogrids

There are some common features in the strain profiles of the three different geogrids. The tensile strain increases from zero at the slope surface to the maximum at a certain depth in the fill and then decreased as the distance increases. As the placement of the fill soil continued, the locations of the peak strains moved inwards further away from the slope surface. The strain increments in the geogrid developed during the second construction season were smaller than during the first season. During the final construction season, the tensile strains in all three layers increased at a rate considerably higher than in the previous two construction seasons. No obvious creep strains were observed in the Tensar and Signode geogrids except at a few locations close to the slope surface where excessive shallow soil movements developed during the consolidation of the fill subsequent to its completion. In the Paragrid geogrid, the inductance coil measurements indicated some time dependent strains, which likely occurred at the damaged joints in the grid.

The magnitude and the location of the peak strains varied in the different layers and the different geogrids. A comparison of the magnitude (from EWR gauge measurements) and the location of the peak strains in the primary reinforcing geogrids, at the end of the final construction season, is presented in Table 5.1.

5.3 Horizontal Movements of Soils

Horizontal movements of the soils in the test fill were monitored using horizontal extensometers and a vertical inclinometer. The vertical inclinometer measured the horizontal deflections of the soils referred to a datum point 12 m below the original ground surface. The horizontal extensometers provided average horizontal strains of the fill at 0, 2, 4 and 6 m levels, by assuming that the magnet placed at the center point of each instrumented level did not move. By comparing the total displacements of each side of the test embankment, it was found that the assumption was reasonable with induced errors of less than 10 mm in the total horizontal displacement.

5.3.1 Movements of Fill Soils

Horizontal movements of the fill were closely related to the construction activities of the test fill. During the first construction season, the horizontal movements of the fill were small. The soil at many instrumented locations moved towards the center of the fill due to the settlement which occurred in the foundation soils. As more fill was placed during the second and third construction seasons, the fill began to deform outwards and localized zones of the horizontal displacement developed. At the ground level, profiles of the horizontal strain distribution in the different sections showed similar features. Near the toe of the slopes, the soil was compressed in the slope direction and negative strains were measured. As the distance from the slope surface increased, the horizontal strain increased. The strains at the ground surface level in all test sections were less than 1%. At the 2, 4 and 6 m levels, the magnitudes and the distributions of the horizontal strains varied considerably from one test section to another. Typical profiles of the soil strain distribution in the four test sections, at the end of the final construction season in November 1988 when the fill reached the 12 m designed height, are shown in Figures 5.7 to 5.10. No significant creep strains in the soil were measured in any section.

In the Tensar section, the total soil strain at the 2 and 4 m levels was distributed rather evenly with the maximum less than 0.4% before the last

construction season. After the top 6 m of the fill was placed, the horizontal soil strain at the 2 m level was highly localized at the 11 m location with a peak strain of 1.7%; two peak strains of 2.9 and 2.1% were measured at the 3 and 11 m locations at the 4 m instrumented level. At the 6 m level, a maximum strain of 1.9% was measured in August 1988 when 8 m of fill was placed. This strain was much larger than the comparable peak strain at the 4 m level. As shown in Figure 5.7, the peak horizontal strain increased from the ground level to the 2 m level and further to the 4 m level, whereas the strain at the 6 m level was larger than the three levels below according to the one set of field measurements taken before the access tube was blocked by the construction activities.

In the Signode section, the peak strains at the 2 and 4 m levels were 0.65 and 0.3% at the end of the second construction season. After the final construction stage, the peak strains jumped to 2.65 and 2.5% for the soil at the 2 and 4 m levels. At the 6 m level, the maximum increment of the horizontal strain was 1.25% at the 7 m location when the fill height increased from 8 to 9.5 m. This increment was considerably larger than the maximum increment at the 2 m level (0.65%) and the 4 m level (0.6%) during the same period. From Figure 5.8, it is seen that the peak soil strains at the 2 and 4 m levels were of similar magnitudes which were larger than the strains at the ground level. Beyond the peak strain location, the strains at the 4 m level were higher than the 2 m level. The horizontal strains at the 6 m level appeared to be considerably larger than at the other instrumented levels.

In the Paragrid section, the maximum horizontal strains at the end of the 1987 construction season were 0.9 and 0.2% for the soil at the 2 and 4 m levels. After the 1988 construction during which the top 6 m of the fill was placed, the peak strain at the 2 m level increased to 2.05% at the 7 m location. The access tube at the 4 m level were blocked during the 1988 construction season when the fill height was over 8 m. Examining the strain increment during the period when the fill height increased from 6 to 8 m, it was found that the maximum increment at the 4 m level (0.3%) was larger than the maximum increment at the 2 m level (0.2%). The maximum strain developed during the same period at the 6 m level was measured to be 3.05% at the 3 m location.

In the unreinforced section, a peak strain of 0.9% was measured, at the end of the second construction season, 7 m from the slope face at the 2 m level. At the 4 m level, the strain due to the second construction stage was negligible, but a maximum strain increment of 0.5% developed at the 1 m location during the consolidation after the second construction season. After the final construction season, a maximum strain of 1.6% at the 7 m location and the maximum increment of 1.4% at the 13 m location were measured at the 2 m level; the highly localized peak strain of 2.45% occurred at the 3 m location of the 4 m level. At the 6 m level, large horizontal strains of 2.5 and 1.5% were measured at the 3 and 5 m locations when the fill height was 8 m; the strains increased to 5 and 2.5% respectively at the two locations when the fill height increased to 9.5 m. As shown in Figure 5.10, the peak strain at the 4 m level was larger than the strains at the 0 and 2 m levels. The strains in the soil above the top reinforcing layer were considerably larger than in the soil below this layer.

From the above discussion, a common feature of the horizontal strain in the soil was found. Within the reinforced soil, the horizontal soil strains at the upper levels were larger than the strains at lower levels, similar to the observations for the unreinforced slope. The differences between the strains at the upper and lower levels depended upon the properties of the geogrids. Although the measurements at the 6 m level were questionable since the magnets might have been disturbed by the heavy construction equipment and the reliability and consistency of the measurements were not evaluated because of the limited number of field readings, the strain distribution at the 6 m level did provide some valuable information. Examining the strain increment during the period when the fill height increased from 8 to 9.5 m, it was found that the maximum increment in the Signode section (1.25%) was significantly smaller than in the unreinforced section (2.5%). The magnitude and the location of the maximum horizontal strains in different levels and test sections at the end of the final construction season are summarized in Table 5.2.

5.3.2 Deformations of Foundation Soils

Examining the horizontal deformation of the foundation soils in different test sections, several common features were observed. During the first and

second construction seasons, the horizontal deformation due to differential settlement of the foundation soils was an important part of the total movement. At many locations, the soils moved towards the center of the fill. As more fill was placed during the final construction season, the overall movements were outwards. The amount of outward movement of the foundation soils increased close to the original ground surface. The maximum horizontal deflections of the soils beneath the toe of the slopes varied from 12 to 30 mm in the different test sections except in the Paragrid section where a maximum of 42 mm was measured in the last field reading when the fill height was 8 m. The horizontal deflections of the foundation soils beneath the crest were slightly smaller than the soils beneath the toe. The maximum deflections in different sections varied between 5 and 10 mm before the casings became blocked in August 1988.

The horizontal deflections of the foundation soils, in the long axis direction of the test embankment, had similar features to the deflections in the slope direction. Their maximum values varied between 5 and 12 mm and were considerably smaller than the deflections in the slope direction.

5.4 Vertical Movements of Soils

Vertical movements of the soils in the test fill are illustrated in settlement profiles at different instrumented levels. Each profile represents the overall vertical deformation of the soils below the instrumented level after the installation of the horizontal inclinometer casing at the particular level. The vertical deformations of the soils developed following the construction and consolidation sequences of the test fill. The deformation increased rapidly during the construction seasons and continued during the consolidation. Reinforcement layers appeared to have no significant effects on the total amount of the settlement. The distribution of the settlement at the ground surface were smooth and nearly identical for each of the four sections. The distributions of the vertical displacement at the upper instrumented levels, however, varied from one section to the others. Figures 5.11 to 5.14 show the typical profiles of the vertical displacements, measured six months after the completion of the fill. The total vertical displacement might have been influenced by errors in ground elevation survey which were used to determine the displacements. The distributions of the displacement are

reliable and provide a great deal of insight into how the fill was deforming in the vertical direction.

In the Tensar section, the settlement varied smoothly along all instrumented levels. Excluding the downward movement of the soil near the slope surface, the settlement increased gradually with distance from the slope surface. From Figure 5.11, only one obvious localization of the vertical displacement was observed at the 3 m location on the 4 m level where the measured settlement was 25 mm larger than the expected value from the variation along the level. At the 2 m level, a possible localization was found near the 8 m location with a settlement 15 mm larger than the surrounding values. At the 6 m level, excessive vertical displacements were measured at the 2.5 m location (35 mm larger than normal value) and at the 5 m location (50 mm larger). All the localizations appeared to be induced by placing of the fill above each location.

In the Signode section, as shown in Figure 5.12, excessive vertical displacements of 25 to 30 mm larger than the normal values were measured at the 5 and 7 m locations of the 2 m level. No obvious localization of the settlement was observed at the 4 m level. The only possible location of a shear-zone development would be around 7.5 m from the slope surface. The sharp change at the 14 m location does not have significant meaning because it disappeared in the profile measured in September 1990. At the 6 m level, a localization zone with a maximum 40 mm larger than the normal was detected near the 4 m location when the fill height was 8 m.

In the Paragrid section (Figure 5.13), two localized vertical displacement zones were detected at the 4 m location (40 mm larger than normal value) and the 8 m location (20 mm larger) at the 2 m level. The large variation around the 17 m location seemed to be related to construction activities during the 1986 summer. Another excessive movement (about 15 mm larger) was measured at the 4 m location of the 4 m level. At the 6 m level, two localizations were found at the 6 m location (40 mm larger) and the 3 m location (45 mm larger). All the localizations appeared to be induced by placing of the upper fill.

In the unreinforced section (Figure 5.14), an excessive vertical displacement zone (20 mm larger than normal value) was detected around the 6 m location on the 2 m level. Another localized displacement of about 15 mm larger than normal value occurred at the 3 m location on the 4 m level. Around the 12 m location on the 4 m level, the soil settlement was about 30 mm larger than at adjacent locations, but the profile was smooth. At the 6 m level, two obvious localized zones of the vertical displacement were detected at the 7 m location (25 mm larger) and the 5 m location (20 mm larger), according to the measurements taken in August 1988 when the fill height was 8 m.

Locations of possible localized vertical displacements in the test fill at the end of the final construction stage are summarized in Table 5.3. Estimated amounts of the excessive displacements are included in the table as well.

5.5 Pore Pressure

Even though the pore pressures in the test fill depended predominantly upon the degree of saturation at the different locations, some common features of the pore pressure development were observed. As discussed in the last chapter, the pore pressures in the fill soil increased with fill placement during the construction seasons and dissipated during the subsequent consolidation periods. The rate of the dissipation decreased as the construction-consolidation phases were repeated. At a given instrumented level, the pressure increased highest at the center of the fill. The pore pressures at different locations on a given level equilibrated during the consolidation phase as the pore fluid drained toward the fill boundaries.

Figures 5.15 to 5.17 summarize the pore pressure measurements in the fill at the end of the second and the final construction seasons and one year after the fill completion. The pore pressure ratio r_u is also indicated in the figures. The pore pressure ratio in the fill soil at the end of the second construction stage in 1987 varied over a range 0.01 to 0.95, indicating the extremely non-homogeneous water content and the degree of saturation conditions in the fill. At the end of the 1988 construction season, the variation of the pore pressure ratio narrowed to the range 0.14 to 0.43, as shown in Figure 5.16. The soil in each test section could be divided into three zones: the bottom 3 m of the soil with an average pore pressure ratio 0.25 (standard deviation 0.05), the 3 to 6 m

levels with an average pore pressure ratio 0.33 (standard deviation 0.04) and the top 6 m of the fill. There were no reliable pore pressure measurements available from the top 6 m of the fill. According to field records, the water content of the upper 6 m of the fill was considerably higher than the lower 6 m of fill. Therefore, the pore pressure ratio in the upper soil would presumably be larger than in the lower 6 m of the fill soil. The pore pressure ratio in the fill soil decreased at most locations during the year of consolidation following fill completion, as shown in Figure 5.17.

The pore pressures measured in the foundation soils of the test fill did show correspondence with the cycles of construction-consolidation. The magnitudes of the pore pressures in the foundation soils were so small that they had little significance to this research.

Geogrid Layers	Tensar			Signode			Paragrid		
	B	M	T	B	M	T	B	M	T
Location of Peak Strain (meters from slope surface)	3	5	3-5	6	7-9	10	4	9	4
Magnitude of Peak Strain (%)	1.05	1.75	2.90	1.58	1.98	1.68	1.19	0.55	1.27

B-- bottom layer; M-- middle layer; T-- top layer

Table 5.1 Summary of Peak Strains in Geogrids

Instrumented Level		Location of Peak Strain (meters from slope)	Magnitude of Peak Strain (%)
Tensar Section	0 m level	15	0.65
	2 m level	11	1.65
	4 m level	3 (11)	3.0 (2.1)
	6 m level	3 #	---
Signode Section	0 m level	17	0.65
	2 m level	3-7	2.6
	4 m level	5 (9)*	2.5 (2.4)*
	6 m level	7 #	---
Paragrid Section	0 m level	17	0.6
	2 m level	7	2.15
	4 m level	---	---
	6 m level	3 #	---
Unreinforced Section	0 m level	13	1.0
	2 m level	7 (13)*	1.6 (1.3)*
	4 m level	3	2.45
	6 m level	3 (5) #	---

(): second peak location & strain; ()*: maximum increment location & strain

#: possible location of peak strain, during the 1988 construction season

Table 5.2 Summary of Peak Horizontal Strains in Fill Soil

Instrumented Level	Location of Possible Displacement Localization (meters from slope surface)			
	Tensar	Signode	Paragrid	Unreinforced
2 m level	8 (15)	5(25), 7(30)	4(40), 8(20)	6 (20)
4 m level	3 (25)	7.5	4 (15)	3 (15)
6 m level	2.5(35), 5(50)	4 (40)*	3(45), 6(40)	5(20), 7(25)*

(): estimated excessive vertical displacement in mm

*: from measurement taken in August 1988

Table 5.3 Summary of Localized Vertical Displacements in Fill Soil

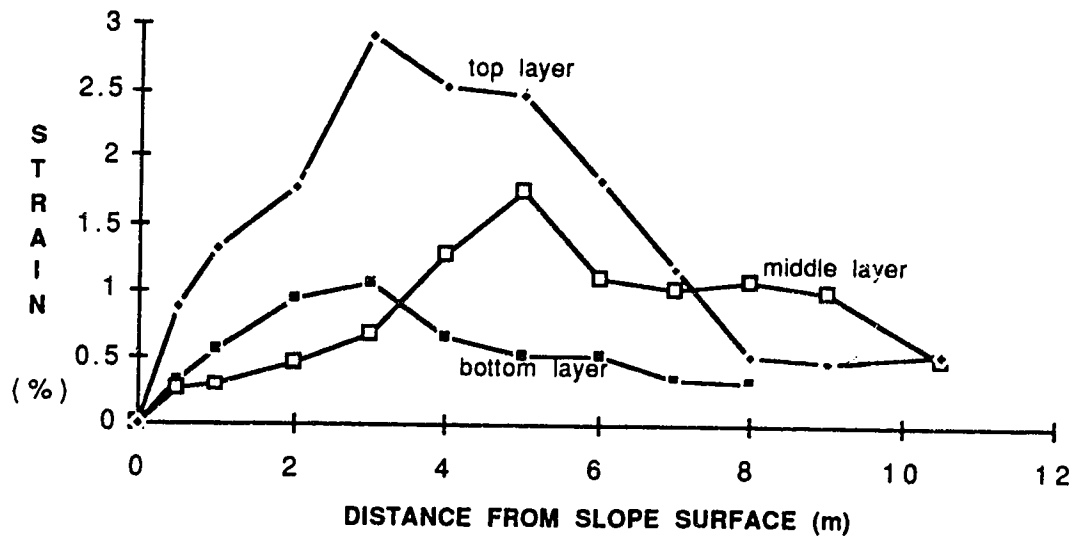


Figure 5.1 Strain Distribution (EWR) in Tensar Geogrid

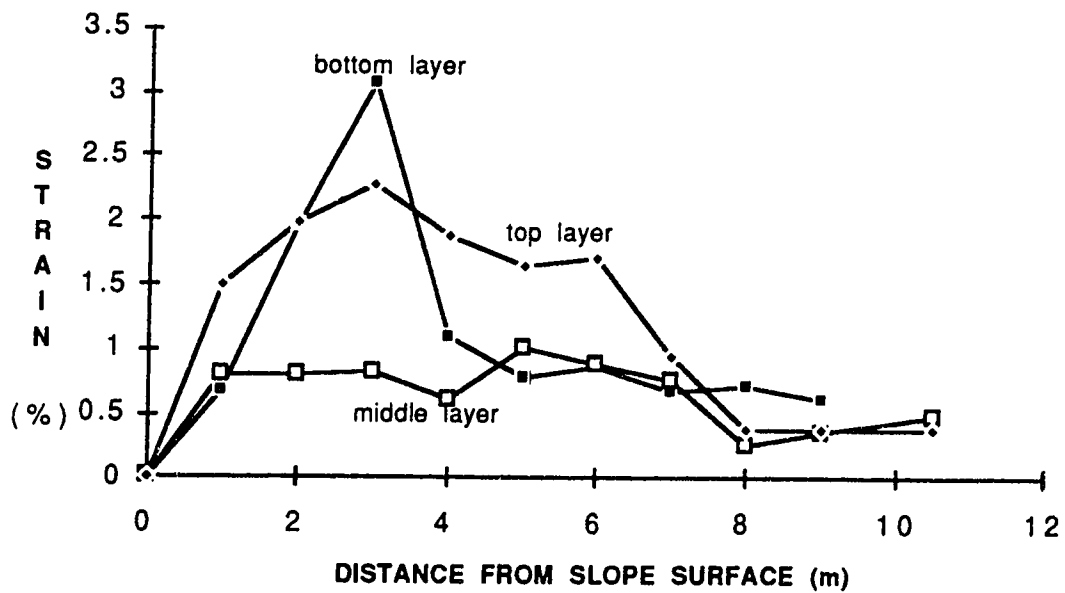


Figure 5.2 Strain Distribution (coil) in Tensar Geogrid

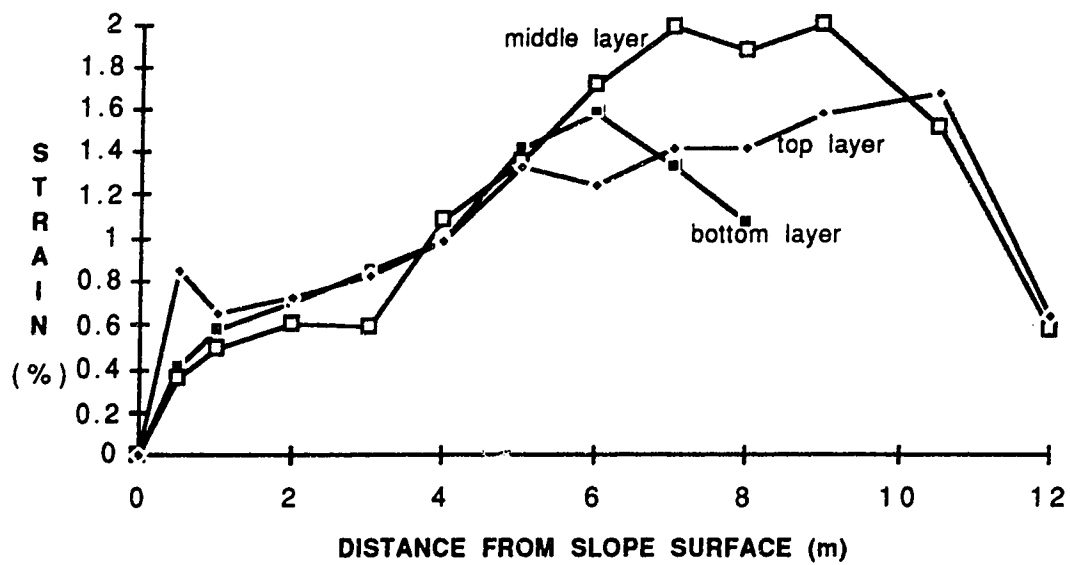


Figure 5.3 Strain Distribution (EWR) in Signode Geogrid

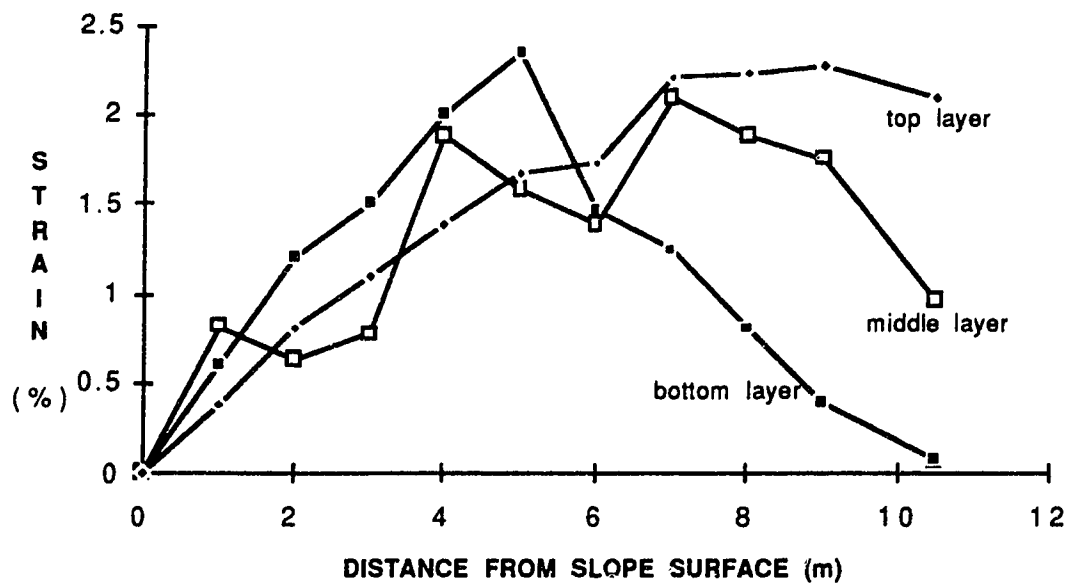


Figure 5.4 Strain Distribution (coil) in Signode Geogrid

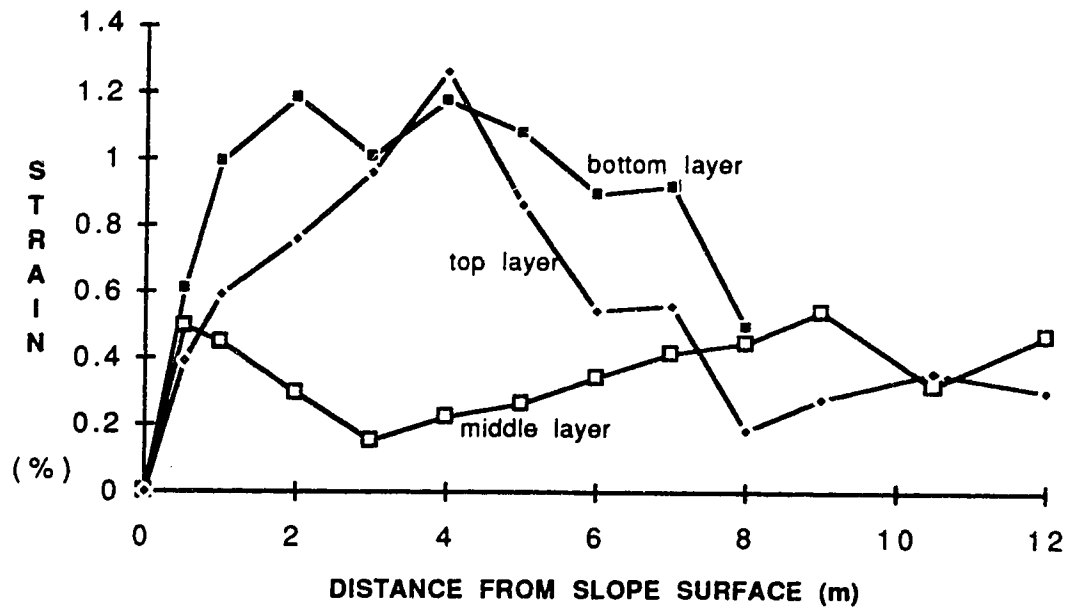


Figure 5.5 Strain Distribution (EWR) in Paragrid Geogrid

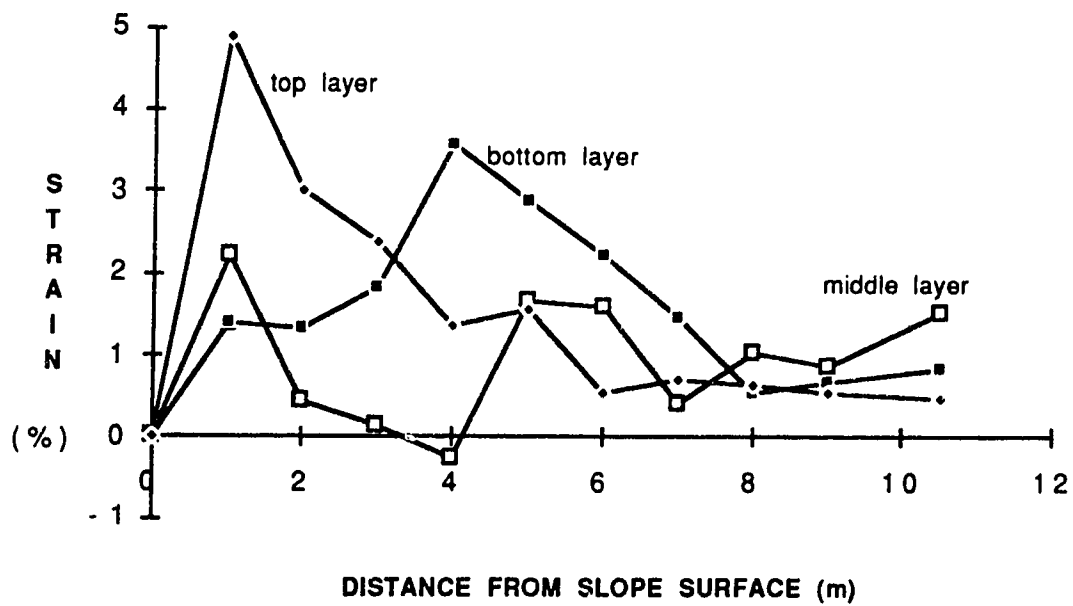


Figure 5.6 Strain Distribution (coil) in Paragrid Geogrid

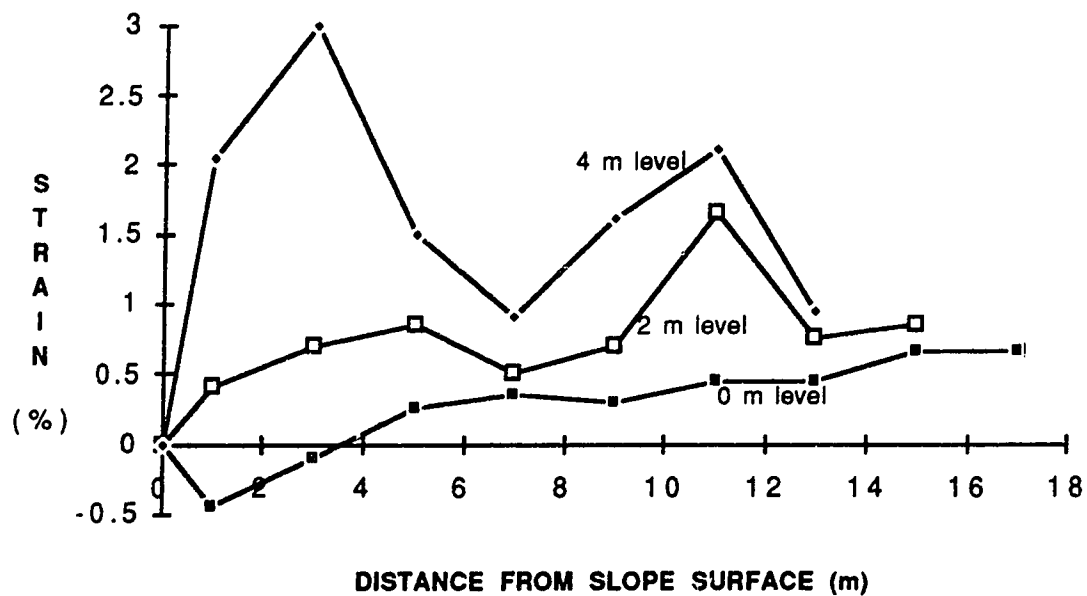


Figure 5.7 Distribution of Horizontal Strain of Fill Soil in Tensar Section

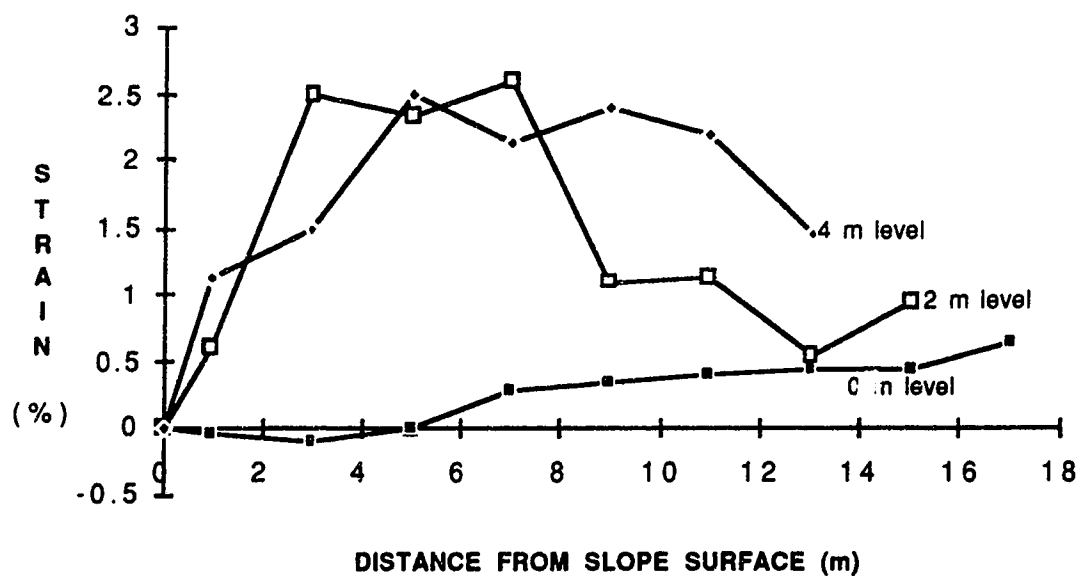


Figure 5.8 Distribution of Horizontal Strain of Fill Soil in Signode Section

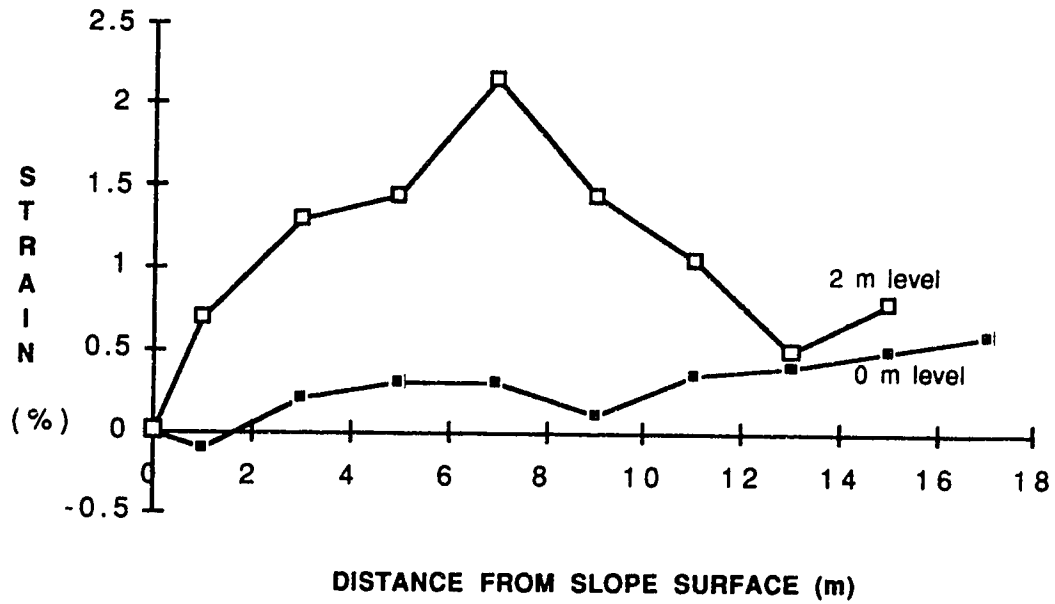


Figure 5.9 Distribution of Horizontal Strain of Fill Soil in Paragrid Section

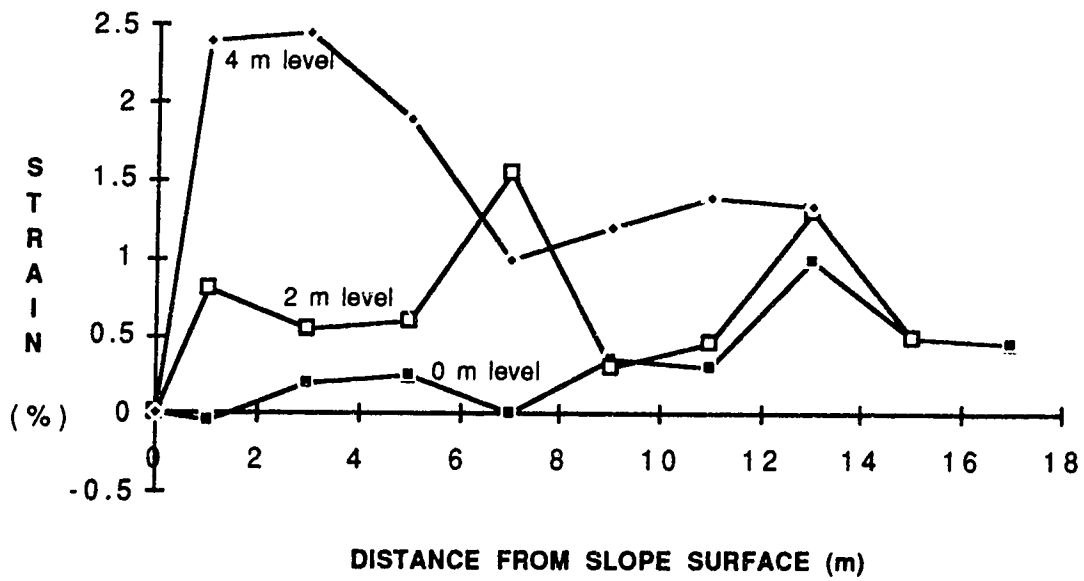


Figure 5.10 Distribution of Horizontal Strain of Fill Soil in Unreinforced Section

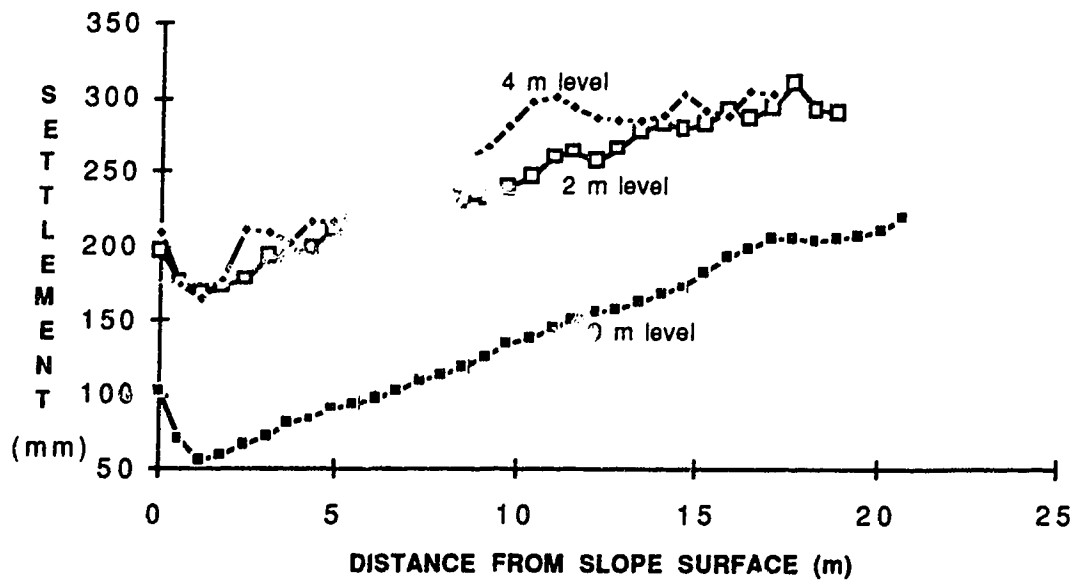


Figure 5.11 Settlement in Tensar Section

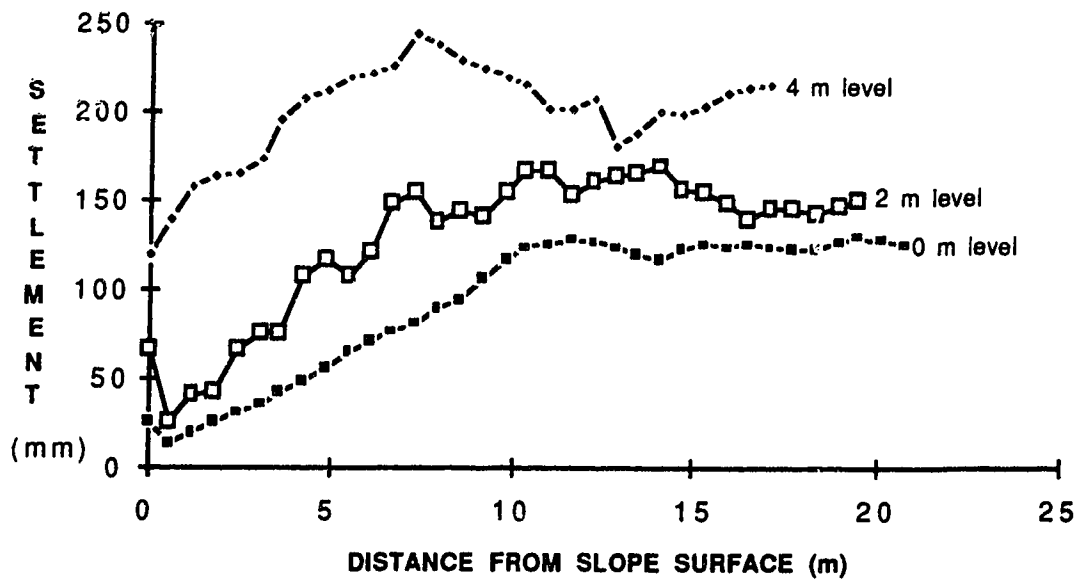


Figure 5.12 Settlement in Signode Section

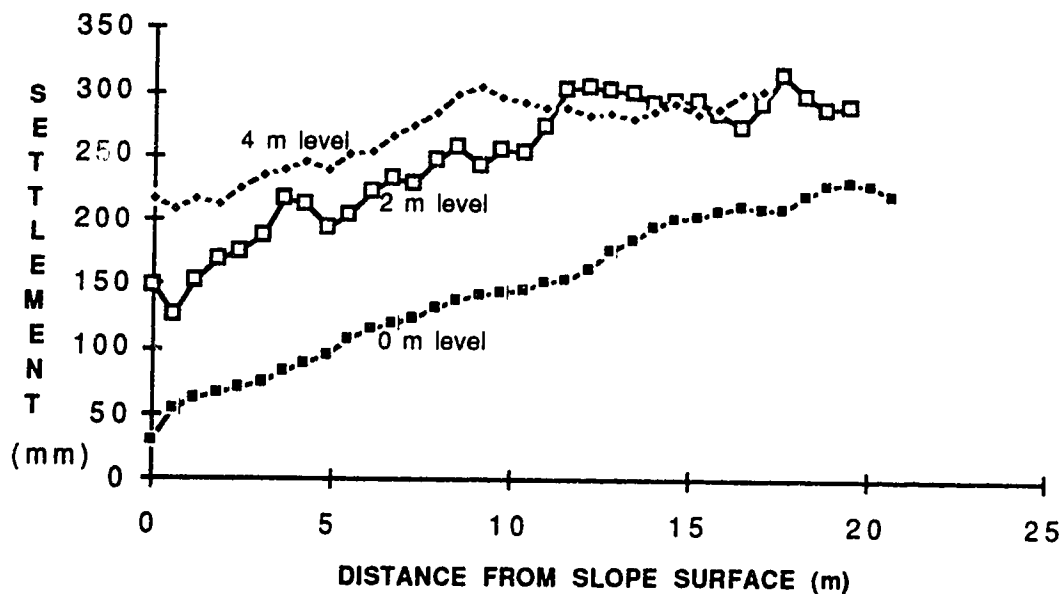


Figure 5.13 Settlement in Paragrid Section

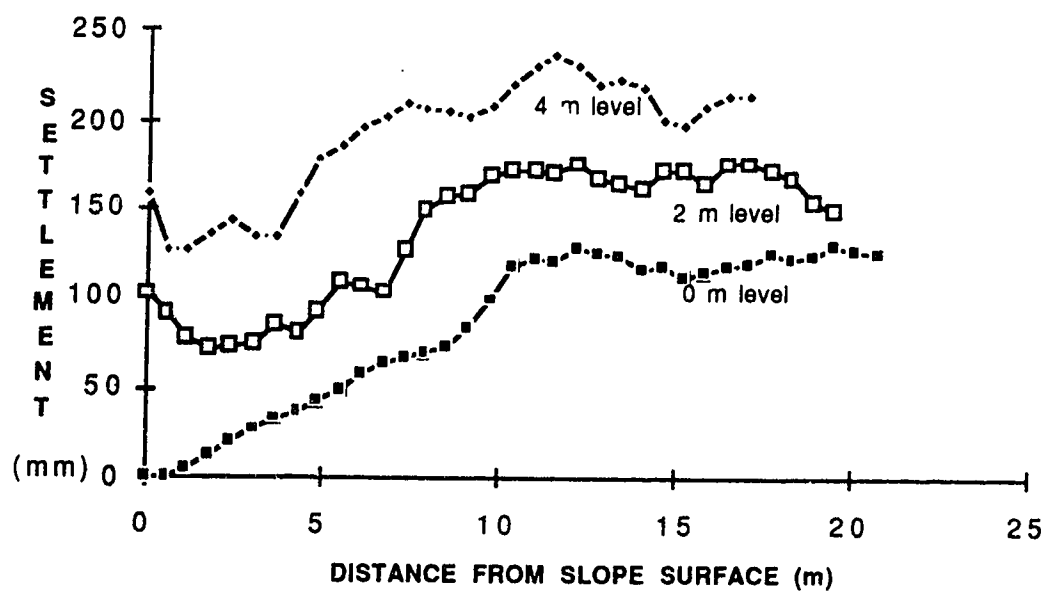
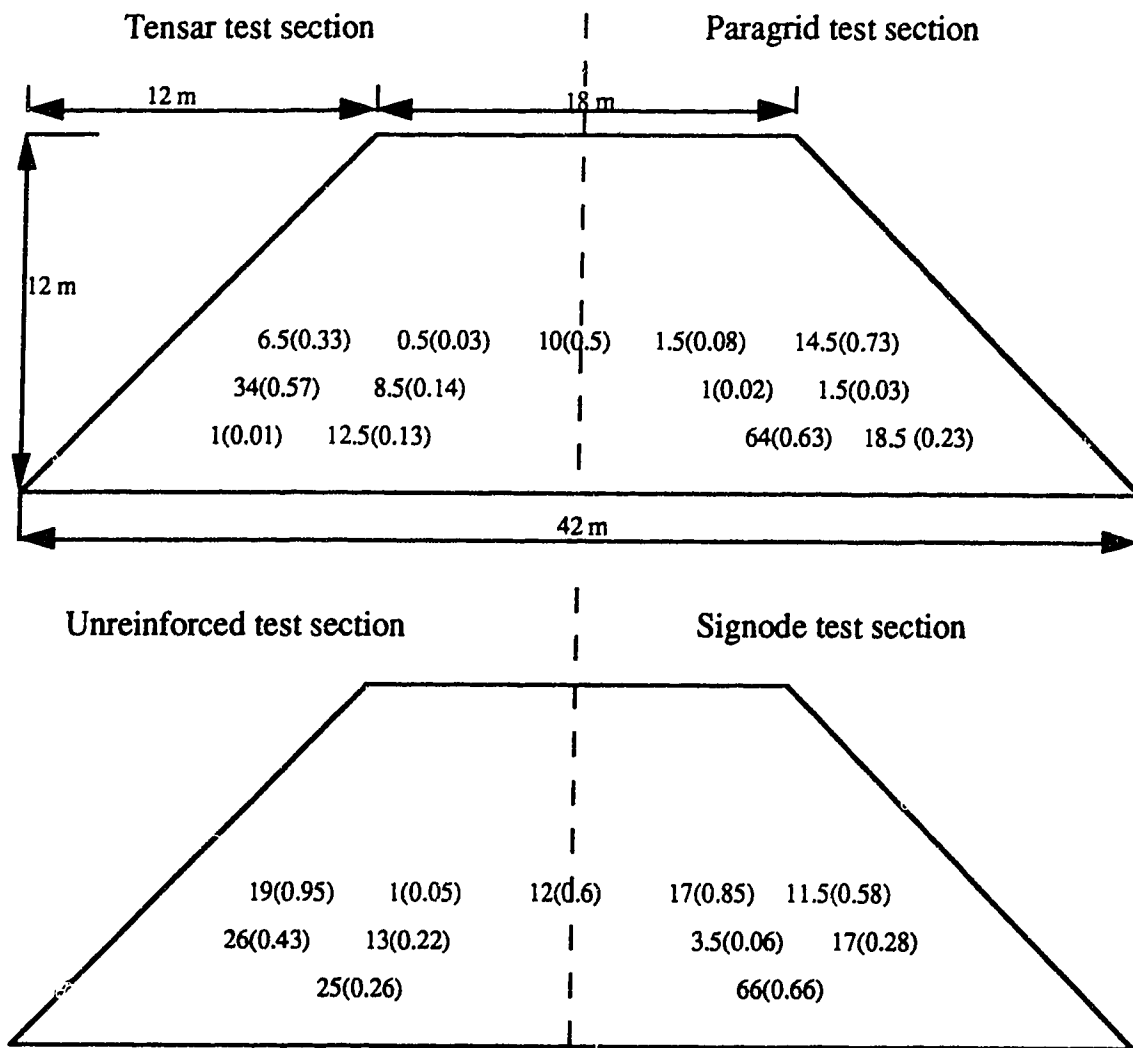
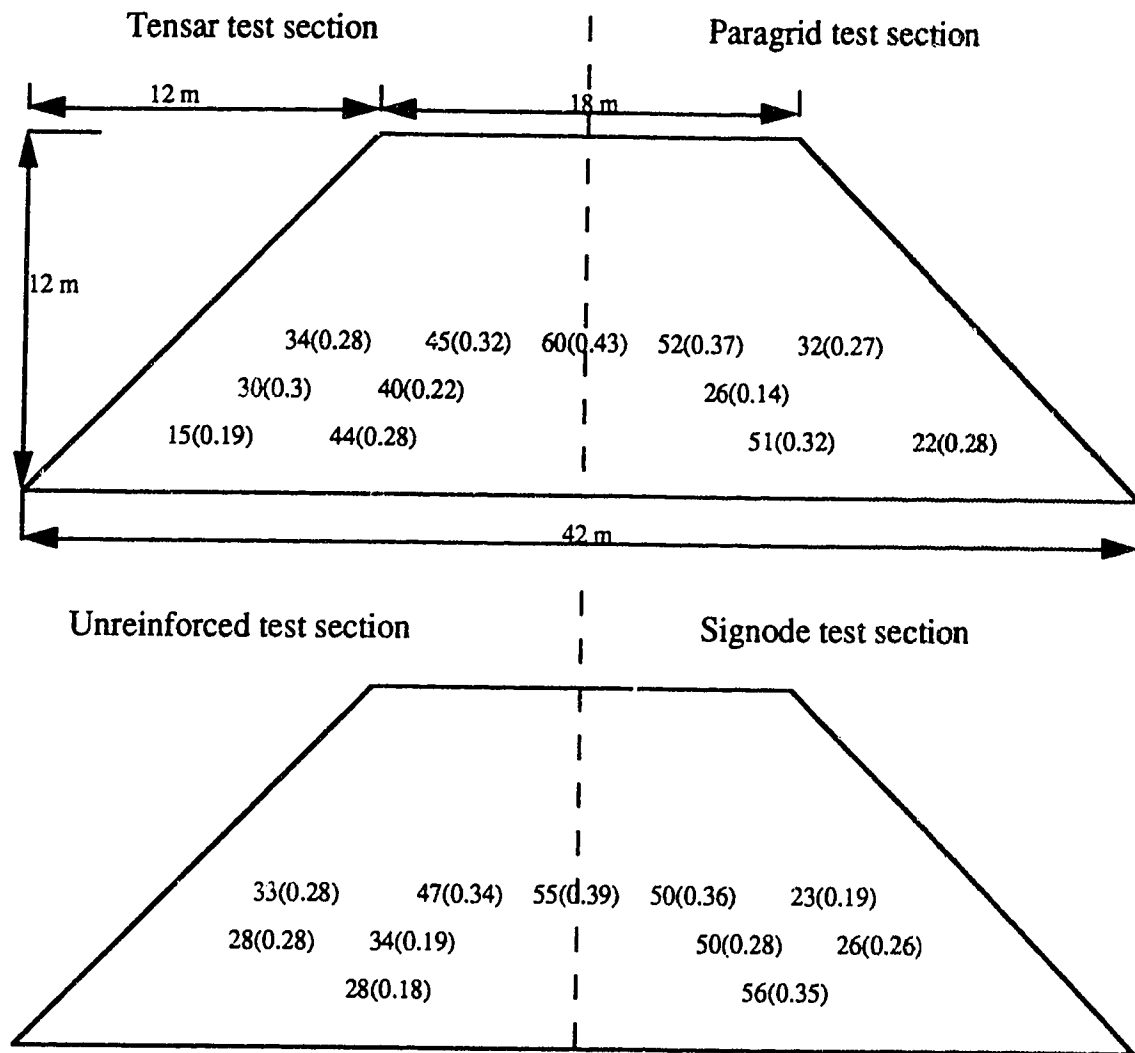


Figure 5.14 Settlement in Unreinforced Section



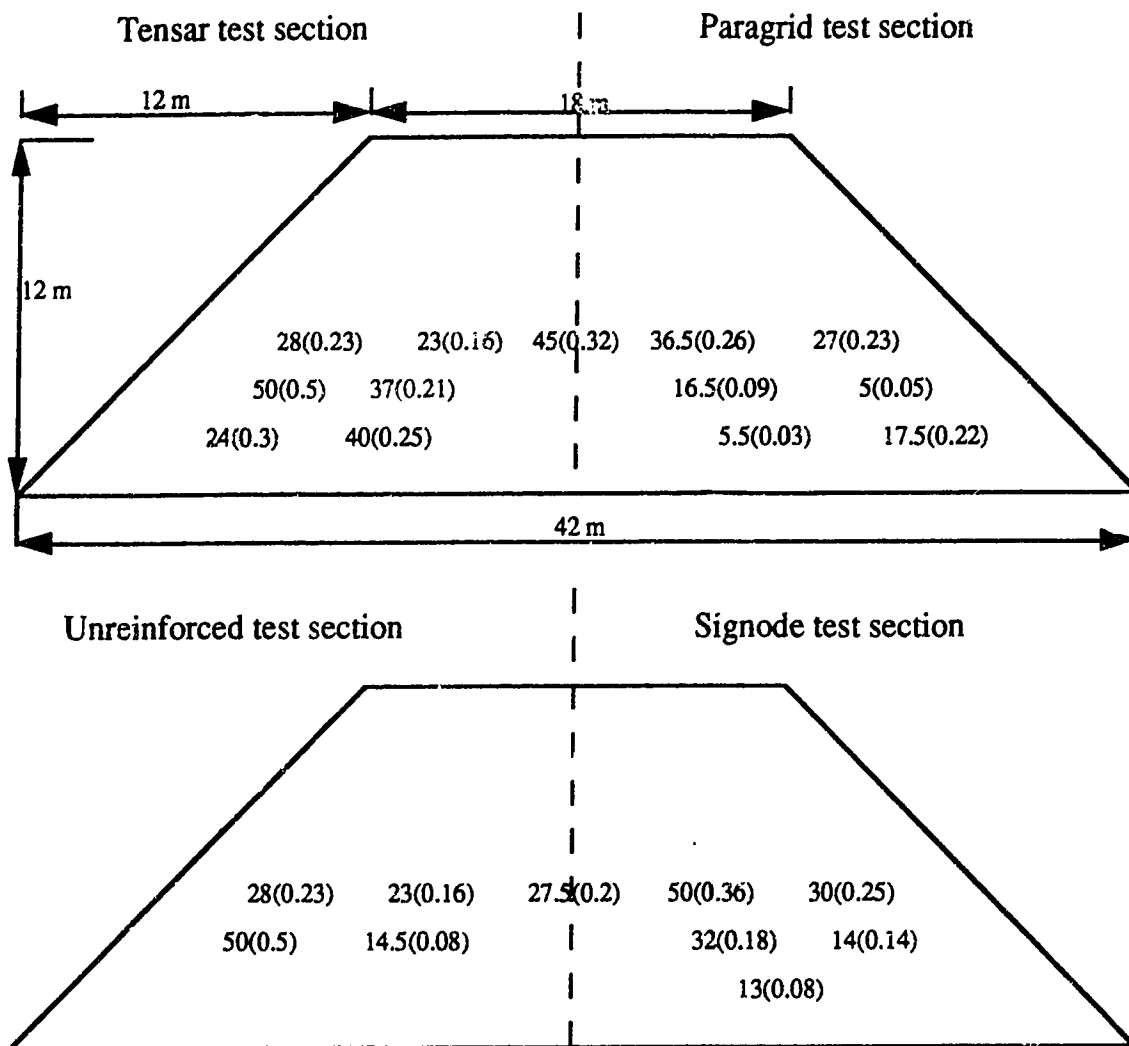
33: pore pressure (kPa); (): pore pressure ratio ru

Figure 5.15 Pore Pressure and Pore Pressure Ratio in Fill Soil at End of 1987 Construction Season



33: pore pressure (kPa); (): pore pressure ratio u

Figure 5.16 Pore Pressure and Pore Pressure Ratio in Fill Soil at End of 1988 Construction Season



33: pore pressure (kPa); (): pore pressure ratio u

Figure 5.17 Pore Pressure and Pore Pressure Ratio in Fill Soil One Year After 1988 Construction

Chapter 6. Limit Equilibrium Analyses

6.1 Introduction

Limit equilibrium analysis is still the most commonly used approach in design of soil slopes. Advantages and disadvantages of limit equilibrium methods have been well discussed in the geotechnical literature. The design of unreinforced slopes using limit equilibrium methods has proven successful and confidence in the methods exists in engineering practices. The use of limit equilibrium methods to design reinforced slopes, however, is relatively new with some uncertainties. Firstly, the failure modes of the reinforced slopes have to be assumed. Secondly, the concept of safety, defined in terms of the factor of safety, has not been clearly related to its conventional geotechnical engineering definition. Finally, the selection and use of design parameters for both the soil and reinforcement is still debated due to the complexity of the soil-reinforcement systems.

Various limit equilibrium methods have been proposed for use in analyzing the stability of reinforced soil slopes based upon differing assumptions about the failure modes and slip surfaces. This chapter analyzes the internal stability of the reinforced and unreinforced slopes of the Devon test fill using different limit equilibrium methods. (The external stability of the reinforced slopes can be analyzed using conventional limit equilibrium methods, as discussed in Chapter 2.) The dimensions and the soil profile of the test slopes are illustrated in Figure 6.1. The purpose of this chapter is to evaluate the validity of different design approaches, to compare the difference in the calculated factor of safety using various ways of incorporating the reinforcement and to examine the influences of factors such as the design working strains within the reinforcement and use of various parameters to represent both the soil and the reinforcement.

In the majority of the existing design approaches, only cohesionless fill materials are considered. When cohesive soils are considered, the shear resistance associated with the cohesion is usually neglected for long term stability considerations. Thus, another purpose of this research is to investigate the validity and the degree of conservatism associated with neglecting the cohesion. Various limit equilibrium methods are applied to the

reinforced slopes and the calculated factors of safety and potential slip surfaces are compared. These results for the reinforced slopes are compared with the results from the unreinforced slope to illustrate the effects of the reinforcement. The implications of the limit equilibrium analysis on design practices will be discussed in the following chapters.

As another comparison, the limit equilibrium methods are used to analyze Chalaturnyk's model embankment (Chalaturnyk, 1988). This model embankment, up to 18 m high with 1:1 side slope and built on a rigid foundation, was constructed using silty clay, $c'=33$ kPa and $\phi'=17^\circ$, and reinforced with an equivalent Tensar SR2 geogrid at 1 m vertical spacings. The results of the limit equilibrium analysis are compared with the results of the finite element analysis (non-linear elastic models), reported by Chalaturnyk (1988). The main purpose of the analysis and comparison is to investigate the validity and the accuracy of the limit equilibrium methods when applied to heavily reinforced slopes in contrast to the analysis of slopes, in the test fill which were lightly reinforced.

Properties of the fill and foundation soils have been reported by Hofmann (1988), as discussed in Chapter 3. Since the fill material shows strain hardening characteristics, the peak shear strength parameters, in terms of effective stresses, are used for the limit equilibrium analysis. The shear strength parameters of the fill soil were determined using laboratory consolidated undrained and consolidated drained triaxial compression tests conducted on compacted soil samples. The consolidated undrained tests, conducted on specimens with an average dry density of 1.59 g/cm^3 and a water content of 23.3%, gave $c'=10$ kPa and $\phi'=30^\circ$; the consolidated drained tests, carried out on samples with an average dry density of 1.65 g/cm^3 and a water content of 20.9%, yielded $c'=22$ kPa and $\phi'=27^\circ$. The strength parameters of the soil in the test fill were determined from the laboratory test results and the field measurements of dry density and water content at different locations in the test fill. The specimens in the laboratory tests were saturated using back pressures and the soil in the fill was unsaturated. However, the degree of saturation was greater than 90% for the fill soil. Therefore, the strength parameters from the laboratory tests were considered to be reasonably representative of the fill soil. As previously explained, there were no insitu

measurements taken in the top 6 m of the fill soil placed during 1988; the water content of the soil was significantly above the optimum water content according to field records. Hence the strength parameters of the top 6 m soil were estimated assuming that the water content is about 5% above the laboratory optimum. The related properties of the fill material are summarized in Table 6.1. Measured pore water pressures, in terms of average pore pressure ratio (Bishop and Morgenstern 1960), were incorporated into the stability analysis.

Tensile forces in the reinforcement, which were determined in two different ways, are incorporated into the limit equilibrium analysis. The forces were first determined based on the measured field tensile strains and the force-displacement diagrams obtained from laboratory tensile tests of the geogrids (designated as the measured reinforcement force). For most geotextile materials, the in-situ stiffness differs significantly from the stiffness in an unconfined laboratory tensile test. For geogrid materials, however, the differences between the in-situ stiffness and the unconfined stiffness are rather small. Therefore, it is reasonable to estimate the reinforcement forces using the field strains and the stiffness of the reinforcing materials in unconfined tensile tests (McGown 1984, Fannin and Hermann 1988). The maximum tensile forces in the top, middle and bottom primary reinforcing layers are 27.3, 16.4 and 9.9 kN/m for the Tensar section, 25.1, 29.9 and 23.7 kN/m for the Signode section and 6.8, 2.7 and 6.4 kN/m for the Paragrid section. The tensile forces in the reinforcement were also estimated based on the tensile strength obtained from laboratory tests (designated as the designed reinforcement force). Jewell and Greenwood (1988) and Jewell (1991) proposed that the allowable design tensile force equals the long term tensile strength of the reinforcement (obtained from isochronous load-extension curves) factored for mechanical damage f_d , environmental effects f_{env} , material uncertainty f_m and a reference factor, which reduces the average value from the laboratory tests to a value comparable to the characteristic value (achieved by 19 out of 20 samples). Christopher et al. (1990) suggested that the allowable design tensile force can be determined from the ultimate tensile strength (from wide strip tensile tests) reduced by durability factor of safety, construction damage factor of safety, creep reduction factor and an overall factor of safety, which is to account for

uncertainties of the structure geometry, fill and reinforcement properties and external loads. For this research purpose, the designed reinforcement forces were estimated from the peak laboratory tensile strength (wide strip tests) factored by $f_d=1.3$, $f_{env}=1.2$, $f_m=1.4$ and a reference factor 1.15 (creep was not accounted for based on the field measurements). For Tensar SR2 and Signode TNX5001 materials (peak tensile strength 78.8 and 87.5 kN/m respectively), the designed forces are estimated as 30 and 35 kN/m, which refer to a working strain range of 2-4% as recommended by other researchers. For Paragrid 50S material, the estimated force is 20 kN/m which refers to a working strain of about 6%. The purpose of using two reinforcement forces in the limit equilibrium analysis is to evaluate the influence on the factor of safety caused by the method used to determine the reinforcement force.

The meaning of the factor of safety for a reinforced slope is still a point of debate, as outlined in Chapter 2. Conceptually, the factor of safety for a reinforced slope represents the same degree of confidence in the safety as for a flatter unreinforced slope with the same factor of safety. The research by Cheng and Christopher (1991) shows that a reinforced slope would actually be safer than the unreinforced flatter slope when designed to the same factor of safety. Therefore, in this limit equilibrium analysis, the conventionally defined factor of safety (Bishop and Morgenstern 1960) is applied to the shear strength parameters of the fill soil. Partial factors of safety for the reinforcement materials will be discussed separately.

6.2 Bishop's Modified Methods

6.2.1 Introduction

Bishop's modified method (BMM) is a limit equilibrium method which analyzes the stability of reinforced slopes by incorporating reinforcement into Bishop's simplified method. Bishop's simplified method, which has been one of the most commonly used slope stability analysis methods in geotechnical engineering practice, is based on the method of slices. A slip circle is assumed to represent the failure surface. Vertical force equilibrium for each slice and overall moment equilibrium (around the center of slip circle) are satisfied, while the horizontal force equilibrium for each slice is neglected. Forces acting on a single slice are shown in Figure 6.2 and the full

derivation of equilibrium equations is given by Bishop and Morgenstern (1960). In spite of the fact that it does not satisfy all conditions of equilibrium, Bishop's simplified method has been found to be an accurate method of analysis for circular slip surfaces (Duncan and Wright, 1980).

In Bishop's simplified method, the factor of safety is defined as the factor by which the shear strength parameters in terms of effective stress, c' and ϕ' , can be reduced before the slope is brought into a state of limit equilibrium (Bishop and Morgenstern, 1960). The factor of safety for an unreinforced slope is expressed as:

$$F_s = \frac{1}{\sum W \sin \alpha} \sum \left[\{c'b + W(1 - r_u) \tan \phi'\} \frac{\sec \alpha}{1 + \frac{\tan \alpha \tan \phi'}{F_s}} \right] \quad (6.1)$$

Equation 6.1 is solved by iterating the term F_s on both sides until the error is reduced to an acceptable value.

6.2.2 Incorporation of reinforcement forces

There are two basic approaches to incorporate reinforcement into the limit equilibrium analysis. The common method is to treat the reinforcement force as a "free body" force, providing additional resisting force (or moment) against failure. The other approach divides the reinforcement force into two components, the component parallel to the slip surface, providing additional pseudo-cohesive resisting moment, and the component normal to the slip surface, thus increasing the shear resistance of the soil. In this case, by assuming that the reinforcement forces are oriented horizontally, the equation for the factor of safety becomes:

$$F_s = \frac{1}{\sum W \sin \alpha} \sum \left[\{c'b + W(1 - r_u) \tan \phi'\} \frac{\sec \alpha}{1 + \frac{\tan \alpha \tan \phi'}{F_s}} + T \sin \alpha \tan \phi' / F_s \right] \quad (6.2)$$

where T is the reinforcement force at the base of the individual soil slice. Since the reinforcement forces are a type of passive force which are mobilized only when the surrounding soil displaces, most researchers agree that the normal component of the reinforcement force should not be included in the stability analysis.

If the reinforcement force is considered as a free body force, it is applied to the sliding soil body at an angle to the assumed slip surface. The inclination of the reinforcement force affects the calculated resisting moment. In the case that the reinforcement is layered horizontally, which is the most common situation in practice, as the soil starts to displace along the slip circle, the reinforcement force acts nearly horizontally. After sufficient displacement, the force will act tangentially to the slip surface. Obviously, the resisting moment provided by the geogrid reinforcement ranges between the magnitudes corresponding to the horizontal force and the tangential force orientation.

If we express the stability equation of an unreinforced slope in terms of overall moment equilibrium, equation 6.1 becomes:

$$F_s = M_r / M_d \quad (6.3)$$

where M_r and M_d are resisting and disturbing moments of the soil. The resisting moment M_l provided by the reinforcement can be incorporated into equation 6.3 in various ways. It may be added to the numerator, as shown in equation 6.4,

$$F_s = (M_r + M_l) / M_d \quad (6.4)$$

assuming it increases the resisting moment. Equation 6.4 can also be expressed as $F_s = (M_r / M_d) + (M_l / M_d) = F_0 + \Delta F_r$, where F_0 is the factor of safety for unreinforced slope and ΔF_r is the increase in the factor of safety due to the reinforcement. The resisting moment may also be subtracted from the denominator, as shown in equation 6.5,

$$F_s = M_r / (M_d - M_l) \quad (6.5)$$

assuming it reduces the disturbing moment. In the former case, the same factor of safety is also applied to the reinforcement force as was applied to the soil strength parameters, whereas in the later, the full reinforcing effect is assumed. The choice depends upon the confidence in the reinforcement force mobilization and the philosophy used in applying the factors of safety during the analysis and design.

As mentioned previously, equation 6.1 is solved by iterating the term F_s on both sides of the equation until the error is small. However, for reinforced slopes, there are several different ways to solve equation 6.4 or 6.5 to determine the factor of safety. The simplest approach assumes that a reinforced slope slides along the same slip circle as without reinforcement. Hence, after M_r and M_d are determined for the most critical slip surface in the unreinforced case, the factor of safety is obtained simply by adding M_t to the equation 6.4 or 6.5. Due to the fact that the geogrid reinforcement changes the stress state within the slope, the failure surface of the reinforced slope differs from the unreinforced slope. Therefore, a more reasonable approach is to search for the most critical slip surface based on equation 6.4 or 6.5 instead of 6.1. Moreover, when the term M_t is involved in the equilibrium equation, it changes the iteration requirement to solve the equation and possibly yields a different factor of safety. Thus, another approach is to iterate equation 6.4 or 6.5 to obtain the factor of safety for the reinforced slope, rather than adding the additional factor of safety after the iteration, that is, in the form of $F_s = F_0 + \Delta F_r$. The differences in the factor of safety determined by these various approaches are governed by the relative magnitude of reinforcement forces with respect to the slope geometry and soil properties.

6.2.3 Results of Stability Analyses by Bishop's Modified Method

A computer program, RSSABM, has been written to analyze the stability of Devon test fill using Bishop's modified method. Comparing the results from similar computer programs, such as STABGM, in which the factor of safety is expressed as $F_s = (M_r + M_t) / M_d$ (Duncan et al., 1985), RSSABM has more capabilities to incorporate the reinforcement forces. Both equations 6.4 and 6.5 are used to solve the factor of safety. The assumption that the reinforcement force increases the soil shear strength is also examined using the program. Three ways of solving the equilibrium equation for the reinforced case, as discussed in the last section, are investigated. The main purpose of the program is to examine the differences in the factors of safety when the reinforcement forces are incorporated differently. Another purpose of the program is to investigate the different failure mechanism predicted by the various approaches of incorporating the effect of the

reinforcement. The failure mechanism of reinforced slopes, as discussed in the next chapter, has more significant and direct meaning than that of unreinforced slopes because the design of the reinforcement layout is based on the predicted failure mechanism. According to the fact that the measured horizontal movement of the foundation soils is small, it seems reasonable to assume that all potential slip circles pass through the toe of the slope. This assumption is also valid for Chalaturnyk's model embankment slopes (Chalaturnyk, 1988) because it is on a rigid foundation.

The program RSSABM is first applied to and tested on Chalaturnyk's model reinforced embankment slopes. The results from RSSABM are compared with the results from the finite element analysis (Chalaturnyk, 1988) and the results from the program STABGM. The factors of safety calculated for the unreinforced slope are shown in Table 6.2. The results from RSSABM match well with those from the finite element analysis. The factors of safety calculated for the reinforced slopes (with an estimated reinforcement force of 26 kN/m at each reinforcing layer) are summarized in Table 6.3. Some features of the analysis which can be observed from the results are:

1. The presence of reinforcing layers changes the critical slip surface. The factor of safety obtained by assuming that the slip surface is the same as for the unreinforced slope is not the minimum for most cases.
2. When the reinforcement forces are added to the equilibrium equation and the factor of safety is calculated by iterating equation 6.4 or 6.5, the F_s obtained is larger than the value determined by adding M_t to 6.4 or 6.5 after the iteration of 6.3, i.e., in the form of $F_s = F_0 + \Delta F_r$.
3. By assuming that the reinforcement forces improve the soil shear strength, the factor of safety obtained increases and it depends on the relative magnitude of the reinforcement forces.
4. When the fill height is small and the assumed reinforcement force remains unchanged (26 kN/m for each reinforcing layer), the differences caused by changing the orientation of the reinforcement forces become significant. As the fill height increases, the differences decrease. When the

overall factor of safety for the reinforced slope is around 1.3, even for a heavily reinforced slope, the differences are less than 10%.

By comparing the results to those of the finite element analysis, it is found that RSSABM gives reasonable estimates of the stability of the reinforced slope. The differences are less than 10% and are on the conservative side for the slope having a factor of safety less than 1.2 without reinforcement.

Bishop's Modified Method is also applied to the four test sections in the Devon test fill. Table 6.4 shows the factors of safety of the slopes in the four sections for the unreinforced case. As the fill was designed, the factor of safety at the end of the construction is close to unity. It was found that the factors of safety in the slopes were dominated by the pore pressure ratios within the embankment. Using the unreinforced slope as an example, when the pore water pressure ratio r_u decreases from 0.30 to 0.23 during the first year after completion of the fill, the factor of safety increases from 1.00 to 1.06. If the pore pressures dissipate completely, the factor of safety increases to 1.31. In other words, for the long term stability of the slope, no reinforcement is required to satisfy a general design.

The factors of safety of the reinforced slopes in the Tensar, Signode and Paragrid sections are presented in Table 6.5, 6.6 and 6.7 respectively. The effects of the different ways of incorporating the reinforcement force in the stability analysis are presented. The calculated factors of safety for the case of incorporating the designed reinforcement forces and the measured reinforcement forces are summarized in the tables. The coordinates of the centers of the most critical potential slip circles are also presented in the tables. From the tables, some important features can be observed:

1. The differences between the factors of safety calculated using the designed reinforcement forces and the measured reinforcement forces are significant for a fill height of 6 m. The differences become less as the fill height increases to 12 m. Since the reinforcement forces are passive forces which can only be mobilized with soil movement, the real forces in the geogrids depend significantly on the fill height. At a low height of fill, the reinforcement forces can easily be overestimated.

2. Even at a fill height of 12 m at which the factor of safety for the unreinforced case are around unity, and even for such lightly reinforced slopes, the designed factors of safety are larger than the most likely values. The errors are around 10% for the three different reinforced test sections.

3. Errors caused by the different ways of incorporating the reinforcement force in the analysis depend upon the relative magnitude of the force. For the case of the designed reinforcement forces, the errors are large (the maximum about 40%) when the fill height is 6 m. The errors then decrease as the fill height increases. When the fill height reaches 12 m, the errors are small because the resisting moment provided by the reinforcement is only a small fraction of the total resisting moment. For the case of the measured reinforcement forces, however, the errors are less than 10% for both $H=6$ m and $H=12$ m.

4. For slopes reinforced with relatively strong materials (Tensar and Signode), the predicted slip circles are usually slightly deeper than the slip circles for the unreinforced cases; for slopes reinforced with weak materials (Paragrid), the predicted slip circles are nearly identical to the circles for the unreinforced cases.

5. The improvement of the stability due to the reinforcement is controlled by the geogrid materials installed in the slopes. For instance, at the end of the final construction season in 1988, the increases in the factor of safety are 9.5, 11.6 and 1.9% for the Tensar, Signode and Paragrid sections respectively.

6. For the reinforced slopes in the test fill, the increases in the factors of safety due to the assumption that the reinforcement forces improve the shear strength of the soil and the assumption that the reinforcement forces act tangentially are insignificant.

7. The factors of safety calculated by iterating equation 6.4 or 6.5 are larger than the values from the other solutions. The estimated factors of safety assuming that the horizontal forces reduces the disturbing moment seem to be reasonable for the conditions evaluated. They also are close to the results of the finite element analysis presented by Chalaturnyk (1988).

8. Pore pressure ratio affects the calculated factor of safety. As the pore pressures decrease due to dissipation, the factor of safety increases significantly.

Where the long term behavior of a cohesive soil slope is concerned, it is sometimes suggested that cohesion of the soil should be neglected in the stability analysis. Table 6.8 illustrates the calculated factors of safety for the slopes in the three reinforced test sections when c' is set to zero. The results are significantly smaller than the factors of safety with c' considered. Obviously, the assumption of $c'=0$ is too conservative for reinforced slopes similar to the slopes constructed in the Devon test fill.

6.3 Spencer's Modified Method

6.3.1 Formulation

Spencer's modified method (SMM) is a limit equilibrium method which incorporates reinforcement into Spencer's stability method. Spencer's method, based on the method of slices and a circular sliding failure assumption, is considered as one of the most accurate slope stability methods. Similar to Janbu's and Morgenstern and Price's methods, Spencer's method satisfies all conditions of equilibrium. One assumption in Spencer's method is that the inter-slice forces are parallel. The same assumption is made in the formulation of SMM for analyzing reinforced slopes.

Forces acting on a single slice are illustrated in Figure 6.3. Resolving forces normal and parallel to the base of the slice for limit equilibrium (assuming horizontal reinforcement force), we have

$$N' + Q \sin(\alpha - \theta) - W \cos \alpha - T \sin \alpha + u \cdot b \cdot \sec \alpha = 0 \quad (6.6)$$

$$S - Q \cos(\alpha - \theta) - W \sin \alpha + T \cos \alpha = 0 \quad (6.7)$$

Based on Mohr-Coulomb criterion: (6.8)

$$S = c' \cdot b \cdot \sec \alpha / F_s + N' \cdot \tan \phi' / F_s$$

Solving equations 6.6, 6.7 and 6.8, we have:

$$Q = \frac{c'b \sin\alpha / Fs + \tan\phi'(W \cos\alpha + T \sin\alpha - ub \sec\alpha) / Fs - W \sin\alpha + T \cos\alpha}{\cos(\alpha - \theta) + \tan\phi' \sin(\alpha - \theta) / Fs} \quad (6.9)$$

If tangential reinforcement forces are assumed, the equation becomes:

$$Q = \frac{c'b \sin\alpha / Fs + \tan\phi'(W \cos\alpha - ub \sec\alpha) / Fs - W \sin\alpha + T}{\cos(\alpha - \theta) + \tan\phi' \sin(\alpha - \theta) / Fs} \quad (6.10)$$

If the external forces are in equilibrium, the sum of both the horizontal and vertical components of the inter-slice forces must be zero:

$$\sum [Q \cos\theta] = 0 \quad (6.11)$$

$$\sum [Q \sin\theta] = 0 \quad (6.12)$$

Since it is assumed that inter-slice forces are parallel, θ is a constant for all slices. Hence, equations 6.11 and 6.12 become:

$$\sum Q = 0 \quad (6.13)$$

Moreover, if the sum of the moments of the external forces about the center of rotation is zero, the sum of the moments of the inter-slice forces must also be zero:

$$\sum [Q \cos(\alpha - \theta)] = 0 \quad (6.14)$$

For a given slope, there is a unique combination of θ and Fs such that both equations 6.13 and 6.14 are satisfied. A trial and error method is generally used to calculate the factor of safety which satisfies both force and moment equilibrium.

6.3.2 Results of Stability Analyses by Spencer's Modified Method

A computer program, RSSASM, based on above formulation, has been written to analyze the stability of reinforced slopes using Spencer's modified method. Two reinforcement orientations, horizontal and tangential which are generally considered as the lower and upper bound estimations, are incorporated in the program. The assumption that reinforcement forces increase the shear strength of the surrounding soil is also accommodated by the program.

The program RSSASM is applied to the model embankment slope (Chalaturnyk, 1988) and the results are shown in Table 6.9. For the unreinforced case, the factors of safety are nearly identical to the results from Bishop's method and very close to the results of the finite element analysis. For the reinforced case, the factors of safety estimated by SMM are slightly larger than the values from the finite element analysis. The differences between the results of the two analyses decrease as the factors of safety of the slope decrease. Compared with the results of the finite element analysis, the tangential reinforcement force assumption in SMM overestimates the safety by 21.7, 8.4 and 2.6% for the fill height of 10, 15 and 18 m respectively. The assumption that reinforcement force acts horizontally and does not improve the soil shear strength yields the factors of safety which are closest to the finite element analysis results. The errors are estimated to be less than 5% for this type of slope with the factor of safety less than 1.2 without reinforcement.

The program RSSASM was used to analyze the stability of the reinforced slopes in the Devon test fill and the results are illustrated in Table 6.10, 6.11 and 6.12 for the Tensar, Signode and Paragrid sections respectively. The following observations can be made:

1. The factors of safety of the reinforced slopes based on the designed reinforcement forces are greater than the values based on the forces estimated from the field strain measurements. At a fill height of 6 m, the differences are up to 25%; at a fill height of 12 m, the differences are usually less than 10%.
2. The assumption that reinforcement forces improve soil shear strength does not significantly increase the factors of safety. In other words, treating the reinforcement force as a free body force in the stability analysis is reasonable and not too conservative.
3. By assuming that reinforcement forces are tangential, the safety of the reinforced slopes might be overestimated, especially when the designed reinforcement forces are relatively large for a low fill height. The errors are small for the lightly reinforced slopes in the test fill. For some heavily reinforced slopes, however, the assumption should be used with caution.

4. At a fill height of 6 m, the predicted slip circles vary with the magnitude and the orientation of the reinforcement forces, especially for the case of the designed reinforcement forces. At a fill height of 12 m, however, the predicted slip circles are similar for the three reinforced slopes and similar to the unreinforced case.

5. The angle of the inter-slice force increases as the fill height increases. In spite of this, the results of SMM are close to the results of BMM, which assumes that the inter-slice force acts horizontally.

6. The pore pressure ratio in the embankment significantly affects the factors of safety of the slopes.

6.4 Two Part Wedge Method

6.4.1 Formulation

The two-part wedge method is a slope stability analysis method based on force equilibrium. It has become a common method to analyze the stability of reinforced slopes (Jewell et al. 1984 and Schmertmann et al. 1987). Some details of using the two-part wedge method for design of reinforced slopes are discussed by Woods and Jewell (1990). Since only force equilibrium is considered in this method, the location of the reinforcing layers does not significantly affect the result of the stability analysis. This feature of the method makes the design of reinforced slopes simpler. The two-part wedge method assumes that failure of reinforced slopes occurs along two planar slip surfaces. The slip surfaces are defined by the coordinates of the nodal point, $A(x,y)$, and the inclination angles of the two slip surfaces, θ_1 and θ_2 , as shown in Figure 6.4.

Forces acting on the two wedges are illustrated in Figure 6.4. The two wedges are considered as separate soil bodies related by the interwedge force Q and the interwedge cohesion C_0 . Considering the equilibrium of wedge I, the forces acting on wedge I in the direction parallel and normal to the slip surface are:

$$U_{b1}\cos\theta_1 + C_{b1}\sin\theta_1 + Q_1\cos(\theta_1 - \delta) - W_1\sin\theta_1 + T_{1v}\sin\theta_1 + T_{1h}\cos\theta_1 + S_1 = 0 \quad (6.15)$$

$$U_{b1}\sin\theta_1 - C_{b1}\cos\theta_1 + Q_1\sin(\theta_1 - \delta) + W_1\cos\theta_1 - U_1 - T_{1v}\cos\theta_1 + T_{1h}\sin\theta_1 - N_1' = 0 \quad (6.16)$$

From the Mohr-Coulomb criterion, we have:

$$S_1 = (c_1' L_1 + N_1' \tan\phi_1') / F_s \quad (6.17)$$

Rearrange 6.16, gives:

$$N_1' = U_{b1}\sin\theta_1 - C_{b1}\cos\theta_1 + Q_1\sin(\theta_1 - \delta) + W_1\cos\theta_1 - U_1 - T_{1v}\cos\theta_1 + T_{1h}\sin\theta_1 \quad (6.18)$$

Substituting N_1' in equation 6.17 with equation 6.18, gives:

$$S_1 = c_1' L_1 / F_s + Q_1 \sin(\theta_1 - \delta) \tan\phi_1' / F_s + A_1 \quad (6.19)$$

where $A_1 = (U_{b1}\sin\theta_1 - C_{b1}\cos\theta_1 + W_1\cos\theta_1 - U_1 - T_{1v}\cos\theta_1 + T_{1h}\sin\theta_1) \tan\phi_1' / F_s$

Substituting the term S_1 in equation 6.15 with 6.19 and rearranging the equation, we have:

$$Q_1 = \frac{(W_1 - T_{1v} - C_{b1}) \sin\theta_1 - (U_{b1} + T_{1h}) \cos\theta_1 - A_1 - c_1' L_1 / F_s}{\cos(\theta_1 - \delta) + \tan\phi_1' \sin(\theta_1 - \delta) / F_s} \quad (6.20)$$

Similarly, considering the equilibrium of wedge II, produces:

$$Q_2 = \frac{(W_2 - T_{2v} + C_{b2}) \sin\theta_2 - (T_{2h} - U_{b2}) \cos\theta_2 - A_2 - c_2' L_2 / F_s}{\cos(\theta_2 - \delta) + \tan\phi_2' \sin(\theta_2 - \delta) / F_s} \quad (6.21)$$

where $A_2 = (C_{b2}\cos\theta_2 + W_2\cos\theta_2 - U_2 - U_{b2}\sin\theta_2 - T_{2v}\cos\theta_2 + T_{2h}\sin\theta_2) \tan\phi_2' / F_s$

For a given configuration of sliding wedge, defined by the nodal coordinates (x,y) and wedge angles (θ_1, θ_2), there is a unique F_s at which

$$Q_1 + Q_2 = 0 \quad (6.22)$$

The minimum F_s for a given nodal point is obtained by trying different combination of wedge angles θ_1 and θ_2 . This process determines the possible configuration of the sliding wedge for the given nodal point. Finally, the overall minimum F_s is achieved after searching at different nodal points, and the most critical failure mechanism for a given reinforced slope is then determined.

6.4.2 Uncertainties in Two-part Wedge Method

The two-part wedge method is not as widely used as Bishop's or Spencer's method for slope stability analysis in the geotechnical engineering practice. It is adopted for stability design of reinforced slopes mainly because of its simplicity and the separation between the stability and the reinforcement layout.

There are some uncertainties when using this method. The first uncertainty concerns the inter-wedge cohesion C_b . It could be assumed that the interwedge cohesion equals zero if one desires to be conservative. This assumption might be reasonable for granular soils, but may not be so for cohesive soils. The inter-wedge cohesion could also be assumed the same as the cohesion along the slip surface, that is, $C_b = C'/F_s$, where C' is the maximum available cohesive resistance of the soil along the interwedge surface. As a matter of fact, since the movement along the slip surface is much greater than that within the sliding soil body, the value of the inter-wedge cohesion most likely lies between zero and C'/F_s . The value of the inter-wedge cohesion directly affects the results of the stability analysis.

To solve equation 6.22, the inclination angle (δ) of the interwedge force has to be predetermined. This is another uncertainty in the two-part wedge method because the precise value of δ is unknown. The angle δ can be expressed in terms of the internal friction angle of the soil, that is, $\tan \delta = f_\delta \tan \phi'$, where f_δ is defined as the interwedge roughness factor (Woods and Jewell, 1990). For the same reason regarding the difference between the soil movement along the slip surface and the movement within the sliding body, f_δ obviously lies in the range of 0 to 1. Woods and Jewell (1990) discussed f_δ in detail and concluded that the adoption of $f_\delta = 0$ is prudent. Apparently, the assumption is conservative, but the use of $f_\delta > 0$ appears difficult to justify.

6.4.3 Results of Two-part Wedge Analysis

A computer program, RSSAWM, based on the formulation described earlier, has been written to analyze the stability of reinforced slopes using the two-part wedge method. Prepared for research purposes, the program is capable of examining the effects of the reinforcement force orientation, the interwedge cohesion and the inclination of the interwedge force. Since no significant horizontal movements were measured in the foundation soils, the

potential slip surfaces are assumed to occur within the slope and pass through the toe of the test embankment.

The program is first used to analyze the model embankment slope (Chalaturmyk, 1988) and the results are illustrated in Table 6.13, 6.14 and 6.15 for the cases of $C_b=0$, $C_b=C'/2F_s$ and $C_b=C'/F_s$ respectively, where C' is the maximum available cohesive resistance of the soil along the interwedge surface and F_s is the factor of safety applied to the soil strength parameters. The following important features can be seen observed in the summarized results:

1. The angle (δ) of the interwedge force inclination affects the calculated factor of safety. As shown in Figure 6.5 and 6.6, the factor of safety increases approximately linearly as the assumed angle of inclination increases. The rate of the increase reduces as the fill height becomes larger. For example, the increasing rate of F_s with δ for the case of $H=15$ m is larger than that for the case of $H=18$ m. In other words, as the slope approaches a limit equilibrium, the errors due to the assumed δ become smaller. At the fill height of 18 m for which the factor of safety in the unreinforced situation is slightly above unity, if it is assumed $f_\delta=0.5$ and $C_b=0$, the factors of safety will be 4.7% and 6.1% larger than the results of $f_\delta=0$ for the unreinforced and reinforced (horizontal reinforcement force) cases respectively; if f_δ is assumed to be 1.0, the factors of safety will be 8.6% and 11.5% larger for the two cases. If C_b is assumed equal to $C'/2F_s$, the errors will be 3.0% and 5.2% for the unreinforced and reinforced cases with $f_\delta=0.5$ and 5.6% and 9.6% for the two cases with $f_\delta=1.0$. It seems that the assumption of $\delta=0$ is not too conservative for practical design purposes.

2. The interwedge cohesion (C_b) significantly affects the magnitude of the calculated factor of safety. Comparing the results to those from the finite element analysis, the factor of safety is overestimated if C_b is assumed to have the same value as the cohesive resistance along the slip surface, i.e., $C_b=C'/F_s$. Even under the assumption of $C_b=C'/2F_s$, the factors of safety are still slightly overestimated for both the reinforced and the unreinforced cases in this model embankment slope. Therefore, it appears reasonable that C_b should be kept between 0 and $C'/2F_s$. It must be recognized, however, that the effects of both δ and C_b on the results of stability analysis vary with soil properties, pore

pressures, homogeneity and geometry of the slopes. A general conclusion can only be drawn when various types of slopes are investigated and compared. This comparison is beyond the scope of this thesis.

3. The estimated factor of safety assuming that the reinforcement forces act at the same inclination as the slip surface is larger than that by assuming the forces acting horizontally. The differences in these factors of safety decrease as the fill height increases. At a fill height of 18 m, the differences are within 5% for all cases.

4. Comparing Figure 6.5 with Figure 6.6, it is found that the differences between the factors of safety obtained from the finite element analysis and the factors of safety calculated using the two-part wedge method are larger in the reinforced slope than in the unreinforced slope for all cases of C_b and δ . This fact illustrates that the designed reinforcement forces might be larger than the mobilized forces in the finite element analysis. In other words, the reinforcement forces which are designed based on a factored tensile strength of the reinforcing material could be overestimated, especially for such a heavily reinforced slope.

Stability analyses of the slopes in the Devon test fill were carried out using the two-part wedge method. The factors of safety for the case of the designed reinforcement forces and the case of forces estimated from the field strain measurements were calculated. The effects of the interwedge cohesion (C_b) and the angle of interwedge force inclination (δ) were also examined. The results of the stability analysis of the slopes in three reinforced test sections of the test fill are shown in Table 6.16, 6.17 and 6.18. Some observations from the results are discussed in the following:

1. Comparing the calculated factors of safety with field observations, it was found that the two-part wedge method slightly underestimates the stability of both the reinforced and the unreinforced slopes in the test fill. In the unreinforced section, for example, the two-part wedge method (with assumptions of $C_b = C'/2F_s$ and $\delta = 0$) yields a factor of safety of 0.91 for the slope at the end of the 1988 construction season when the pore pressure ratio was 0.3. (The factors of safety of the reinforced slopes are also calculated to be less than unity even when the measured reinforcement forces are incorporated

into the calculation. All slopes in the test fill were predicted to fail.) Comparing these to the results of Bishop's method which is widely accepted as an accurate method, it was further found that, when the pore pressure ratio is greater than a certain value, the larger the pore pressure ratio, the more the underestimation; below a certain value, the differences between the results from the two methods are approximately the same. As shown in Figure 6.7, in the unreinforced section, when the pore pressure ratio decreases from 0.3 to 0.15, the difference in the factors of safety obtained from Bishop's and the two-part wedge ($C_b = C'/2Fs$ and $\delta = 0$) methods decreases from 0.097 to 0.033; below $ru = 0.15$, the difference is about 0.045 for different values of the pore pressure ratio. The same feature can be seen in the reinforced sections. In the Signode section, for example, the difference in the factor of safety (designed reinforcement forces) from the two methods decreases from 0.13 to 0.084 as the pore pressure ratio decreases from 0.31 in 1988 to 0.2 in 1989. The differences in the factors of safety from the two methods are also affected by the magnitude of the reinforcement forces. As a comparison to the Signode section where the designed reinforcement forces are 35 kN/m in each layer, the difference in the factors of safety in the Paragrid section (designed reinforcement forces 20 kN/m in each layer) changes from 0.109 to 0.054 as the pore pressure ratio decreases from 0.3 in 1988 to 0.17 in 1989. Nevertheless, the effects of the magnitude of the reinforcement forces are insignificant compared to the effects of the pore pressure ratio.

2. The factors of safety calculated by the two-part wedge method are affected by the value of the interwedge cohesion (C_b) and the angle of the interwedge force inclination (δ). The effects of C_b and δ are illustrated in Figure 6.8 for the unreinforced cases and in Figure 6.9, 6.10 and 6.11 for the reinforced cases. As discussed earlier, the calculated factors of safety increase as C_b and δ increase. For both the reinforced and the unreinforced cases, the interwedge cohesion influences the factors of safety more significantly than the interwedge force inclination does. In the cases of reinforced slopes in 1988, if the assumed interwedge cohesion increases from $C_b = 0$ to $C_b = C'/2Fs$, the calculated factors of safety (based on the measured reinforcement forces) increase about 8% on average for the three reinforced sections; if the assumed inclination angle of the interwedge force increases from 0 to 20° ($f_\delta = 0.8$), the increases in the Fs are less than 3%, which illustrates again that the

assumption of $\delta=0$ may not be too conservative in estimating F_s . Comparing to the field observation, the assumption of $C_b=C'/2F_s$ appears to yield a reasonable estimation of the factors of safety of the reinforced and the unreinforced slopes although the results are still slightly (less than 10%) on the conservative side. The effects of C_b and δ depend upon the pore pressure ratio. As shown in Figure 6.8 and 6.10, as the pore pressure ratio decreases, the variation of the factors of safety with C_b and δ becomes more obvious. The effects of C_b and δ also depend on the magnitude of the reinforcement forces, shown in Figure 6.9 and 6.11, but the influence (the magnitude of reinforcement forces) is rather insignificant for these lightly reinforced slopes.

3. As discussed in previous sections, the factors of safety calculated using the designed reinforcement forces are overestimated. The amount of overestimation depends not only upon the differences between the designed forces and the real mobilized forces, but also upon the pore pressure in the slopes. For example, in the Tensar section, the overestimations on F_s are 43.4%, 6.6% and 6.5% for the slope in 1987 ($H=6$ m, $r_u=0.33$), 1988 ($H=12$ m, $r_u=0.29$) and 1989 ($H=12$ m, $r_u=0.28$) respectively, whereas in the Signode section, the overestimations are 56.7%, 10.1% and 7.9% for the slope in 1987 ($r_u=0.53$), 1988 ($r_u=0.31$) and 1989 ($r_u=0.2$). This fact illustrates that attention and caution should be given to the anticipation of the strains (and consequently the tensile forces) in the reinforcing materials, especially when the pore water pressures in the slope are high, as occurred in the test fill during 1987 and 1988.

4. The assumption that the reinforcement forces act at the same inclination as the slip surface does not make a difference in the factor of safety for the slopes in the test fill when compared to the results of assuming that the forces act horizontally.

5. Pore pressure is an important factor in the stability analysis.

Comparing the results of the two-part wedge stability analysis of the model slope and the slopes in the Devon test fill with the results of the finite element analysis and the field observations and measurements, the assumption of $\delta=0$ and $C_b=C'/2F_s$ seems to yield reasonable estimations of the stability of

reinforced and unreinforced slopes. Moreover, the assumption that the reinforcement forces act horizontally appears appropriate. The results of the stability analysis of the slopes in the test fill are summarized in Table 6.19. It was found from the table that the geometry of the possible sliding soil body varies with the fill height, the magnitude of the reinforcement forces and the pore pressure ratio. Nevertheless, the analysis does give a general view of possible failure modes of the slopes, as discussed in the next chapter.

6.5 Summary and Discussion of Results of Limit Equilibrium Analyses

Bishop's modified method and the two-part wedge method, which are the most commonly used limit equilibrium stability analysis methods for reinforced slopes, together with Spencer's modified method, were applied to the model reinforced slope (Chalaturnyk, 1988) and the constructed slopes in the Devon test fill. The model slope is heavily reinforced, whereas the slopes in the test fill are lightly reinforced. The analyses performed on these two slopes should well represent the stability of reinforced slopes having similar geometrical configurations and soil properties.

The factors of safety of the model slopes, calculated using three different methods, are summarized in Table 6.20; the factors of safety of the slopes in the Devon test fill are shown in Table 6.21. The main purposes of the stability analyses were to evaluate the validity of different methods applied to reinforced slopes, to examine the effects of the assumptions employed in the methods and to investigate reasonable ways of incorporating reinforcement forces into the stability analysis. The analyses are performed through comparison between the results of the limit equilibrium methods and the results of the finite element method (for the model slopes) as well as the field observations and measurements (for the constructed slopes in the test fill). From the discussion in the previous sections, the following conclusions can be summarized:

1. Bishop's and Spencer's modified methods, which are based on the assumption of circular slip surface, provide good estimates of the stability of the reinforced slopes in both the model embankment (Chalaturnyk, 1988) and the Devon test fill. For the model slope, the differences between the results of the limit equilibrium analysis and the finite element analysis are less than 5%;

for the slopes in the test fill, the circular methods predict the factor of safety around unity for the unreinforced slope ($H=12$ m) and between 1.1 and 1.2 for the reinforced slopes, which matches well with the field observations and measurements. The results of Spencer's modified method appear to be closer to the actual factors of safety. However, due to the fact that Spencer's method is more complicated and needs much more computing time, Bishop's method has more advantages for use in practices. Bishop's modified method is slightly (less than 10%) on the conservative side for both the heavily and lightly reinforced slopes.

2. In using Bishop's modified method for the stability analysis of reinforced slopes, the resisting moment provided by the reinforcement should be added to the original equilibrium equation. The equation is then solved, using the technique of iteration, to obtain the factor of safety.

3. In the limit equilibrium analysis of reinforced slopes, the factor of safety should be only applied to the strength parameters of the soil, so that the concept of the safety margin will be the same as the traditional concept in geotechnical engineering. (In other words, being designed to the same factor of safety, the reinforced slope is as safe as the unreinforced but flatter or lower slope.) The magnitude of the reinforcement force should be estimated based on the anticipated strains in the geogrid and a partial factor of safety. (Strain compatibility in a reinforced slope will be discussed in the next chapter.) The equilibrium equation in Bishop's modified method could be expressed either as $F_s = M_r / (M_d - M_l)$ or as $F_s = (M_r + M_l) / M_d$ depending upon the confidence on the reinforcement force mobilization.

4. The results of the stability analysis using the two-part wedge method are affected by assumptions made about the interwedge cohesion and the interwedge force inclination. The calculated factors of safety under the assumption of $C_b = C'/2F_s$ and $\delta = 0$ appear to match the results of the finite element analysis and the field observation reasonably well for both the model slope and the slopes in the test fill.

5. The two-part wedge method provides reasonable estimates for the stability of the reinforced slopes. For the model slope, the two-part wedge method slightly overestimates the factor of safety; for the slopes in the test fill, the

factor of safety is a little underestimated. The error most likely comes from the assumed value of the interwedge cohesion. When a slope is heavily reinforced, only a small portion of the available interwedge cohesion might be mobilized. Therefore, $C_b = C'/4F_s$ would be more appropriate for a heavily reinforced slope. For most reinforced slopes, however, the assumption of $C_b = C'/2F_s$ should yield a reasonable result in geotechnical engineering design practice. Due to the simplicity and the special advantage that the location of the reinforcement layers does not affect the results of the stability analysis, the two part wedge method could be a useful approach for designing reinforced slopes although it may not be as accurate as Bishop's and Spencer's method in most cases.

6. If the reinforcement forces are assumed to act at the same inclination as the base of the sliding soil body rather than horizontally, the obtained factors of safety are slightly larger. However, to satisfy the assumption, sufficient movement in the reinforced slope must occur. Thus, assuming the reinforcement forces act horizontally seems more appropriate.

7. The assumption that reinforcement forces improve the shear strength of the soil is not supported on either theoretical or practical grounds. The increase in the factor of safety due to the assumption is insignificant, even for heavily reinforced slopes. Therefore, the reinforcement forces should be assumed to act only as free body forces.

8. The assumption of $c' = 0$ for long term stability purposes yields factors of safety considerably smaller than the real values. It leads to very conservative designs of reinforced cohesive soil slopes and, consequently, results in a large unnecessary expense. Thus, it is not appropriate to adopt the assumption in the stability analysis and design of reinforced slopes of silty clay or clay.

9. Pore water pressure in a slope significantly affects the stability. For the slopes in the Devon test fill, the factor of safety will reach about 1.3 even without reinforcement when the pore pressure fully dissipates. This fact illustrates a different philosophy in the design of reinforced cohesive soil slopes. In designing a reinforced granular soil slope, the resistance provided by the reinforcement is counted on for the design life of the structure. Hence, the long term behavior of the reinforcing material must be considered

as an important aspect during the design. For a cohesive soil slope, however, the resistance of the soil itself increases as the pore water pressure dissipates. In other words, the reinforcement may only be designed to provide additional resistance for the short term after the construction or initial loading. Therefore, the long term behavior of the reinforcing material may not be of major concern during the design. Moreover, it would be desirable that the reinforcing material have the capability of accelerating the pore water pressure dissipation by providing additional drainage paths within the reinforced fill.

Elevation	Dry Density (g/cm ³)	w (%) in Laboratory	w (%) in Field		c' (kPa)	ϕ' (°)
			range	average		
0-3 m	1.67	20.9%	18.6-24.1	20.6 (1.8)*	27	28
3-6 m	1.64	23.1%	20.0-25.3	22.7 (1.5)	13	30
6-12 m	---	---	---	---	10	20

* (1.8): standard deviation

Table 6.1 Soil Properties in Devon Test fill

Method	H = 5 m	H = 10 m	H = 15 m	H = 18 m
RSSABM	2.63	1.60	1.26	1.13
STABGM	2.62	1.59	1.24	1.11
Finite Element Method	2.78	1.67	1.30	1.16

Table 6.2 Factors of Safety of Model Slope (Unreinforced) from BMM

method and reinforcement force incorporation			H = 5 m	H = 10 m	H = 15 m	H = 18 m
R S S A B M	assuming the same slip circle as the unreinforced slope	H*, $F_s = (M_r + M_t)/M_d$	3.10	1.86	1.46	1.27
		H, $F_s = M_r/(M_d - M_t)$	4.97	2.16	1.57	1.32
		T#, $F_s = (M_r + M_t)/M_d$	3.30	1.96	1.52	1.30
		T, $F_s = M_r/(M_d - M_t)$	7.92	2.50	1.69	1.37
	M _t added in searching for the minimum F _s	H, $F_s = (M_r + M_t)/M_d$	3.11	1.86	1.41	1.23
		H, $F_s = M_r/(M_d - M_t)$	M _t > M _d	2.15	1.46	1.26
		T, $F_s = (M_r + M_t)/M_d$	3.32	1.93	1.43	1.26
		T, $F_s = M_r/(M_d - M_t)$	6.35	2.36	1.50	1.28
	M _t added in iterating for F _s	H, $F_s = (M_r + M_t)/M_d$	3.20	1.89	1.44	1.24
		H, $F_s = M_r/(M_d - M_t)$	M _t > M _d	2.22	1.49	1.28
		T, $F_s = (M_r + M_t)/M_d$	3.35	1.97	1.46	1.27
		T, $F_s = M_r/(M_d - M_t)$	6.49	2.46	1.50	1.28
	M _t in iterating, improving soil shear strength	H, $F_s = M_r/(M_d - M_t)$	5.41	2.24	1.48	1.27
	STABGM, $F_s = (M_r + M_t)/M_d$		3.01	1.82	1.41	1.26
	Finite Element Method		3.12	1.96	1.55	1.35

* H-- assuming reinforcement forces horizontal

T-- assuming reinforcement forces tangential

Table 6.3 Factors of Safety of Model Slope (Reinforced) from BMM

Test Section	H=6 m (87)		H=12 m (88)		H=12 m (89)	
	r_u	E_s	r_u	E_s	r_u	E_s
Tensar section	0.33	1.688	0.29	1.001	0.28	1.009
Signode section	0.53	1.424	0.31	0.981	0.20	1.096
Paragrid section	0.42	1.437	0.30	1.002	0.17	1.128
Unreinforced section	0.28	1.638	0.30	1.002	0.23	1.064

Table 6.4 Factors of Safety of Slopes in Test Fill (Unreinforced)
from BMM

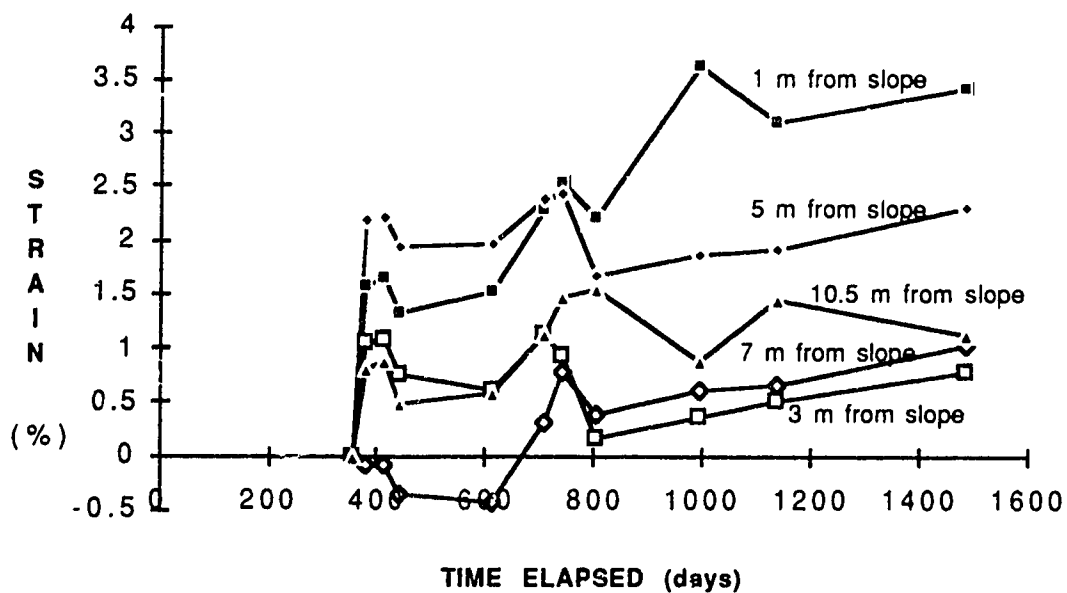


Figure A11. Strain Development (coil) in Paragrid Middle Layer

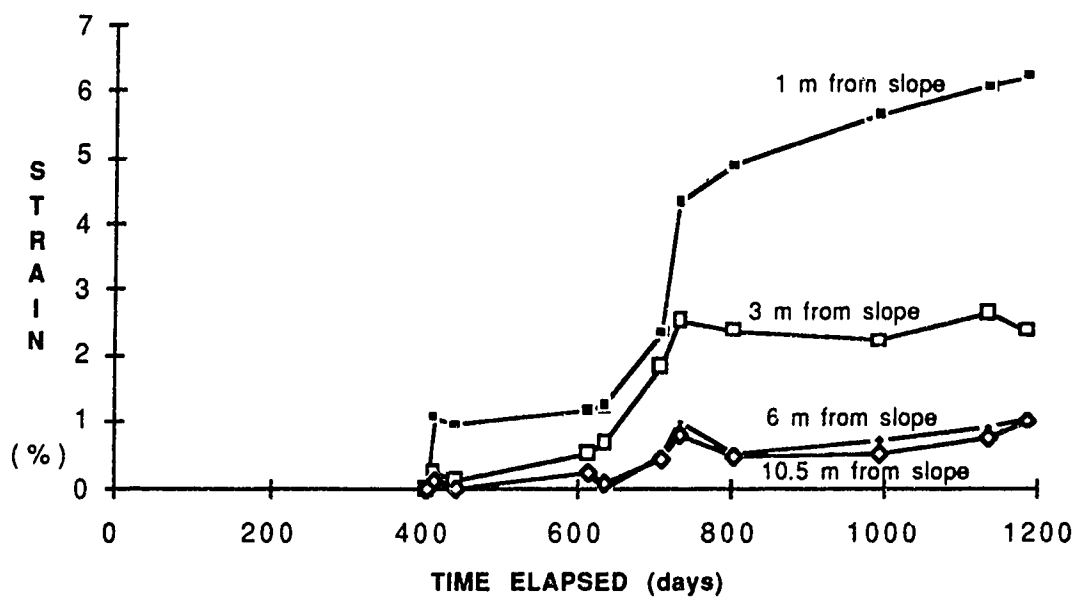


Figure A12. Strain Development (coil) in Paragrid Top Layer

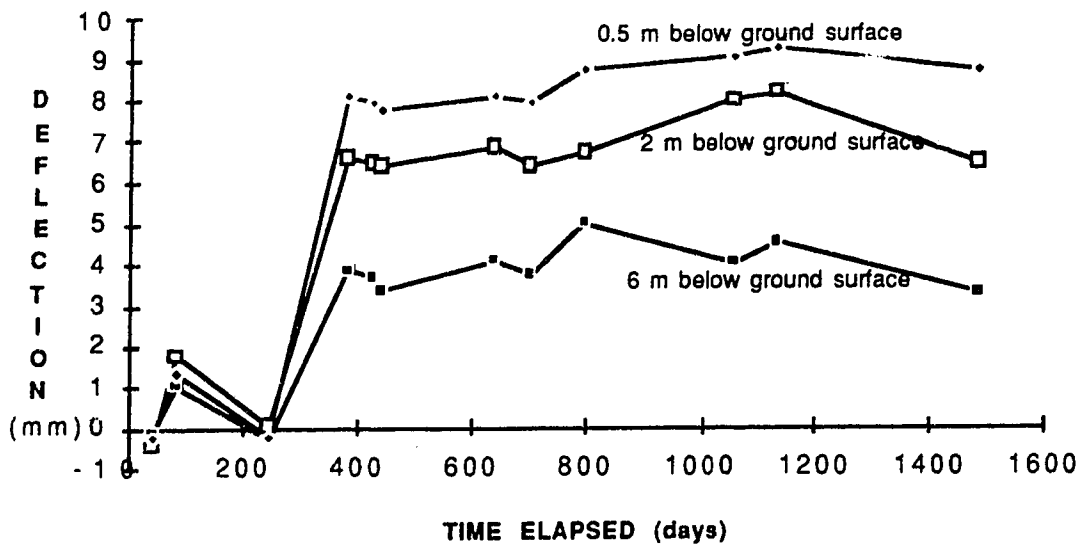


Figure A13. Development of Horizontal Deflection (B) of Soils beneath Toe of Slope in Tensar Section

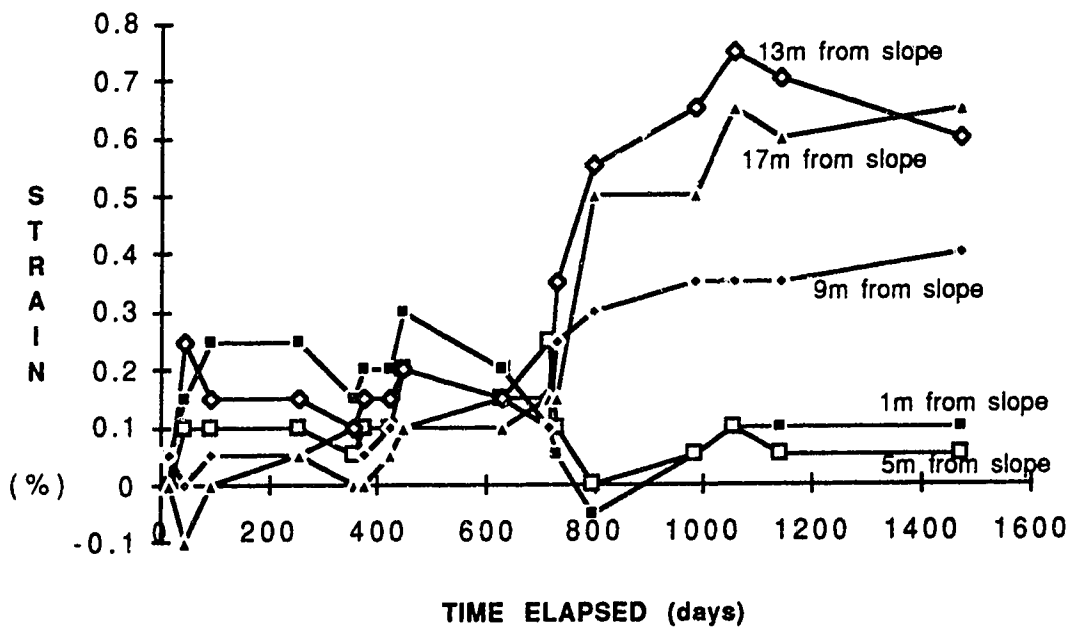


Figure A14. Development of Horizontal Strain of Soil at 0 m Level in Signode Section

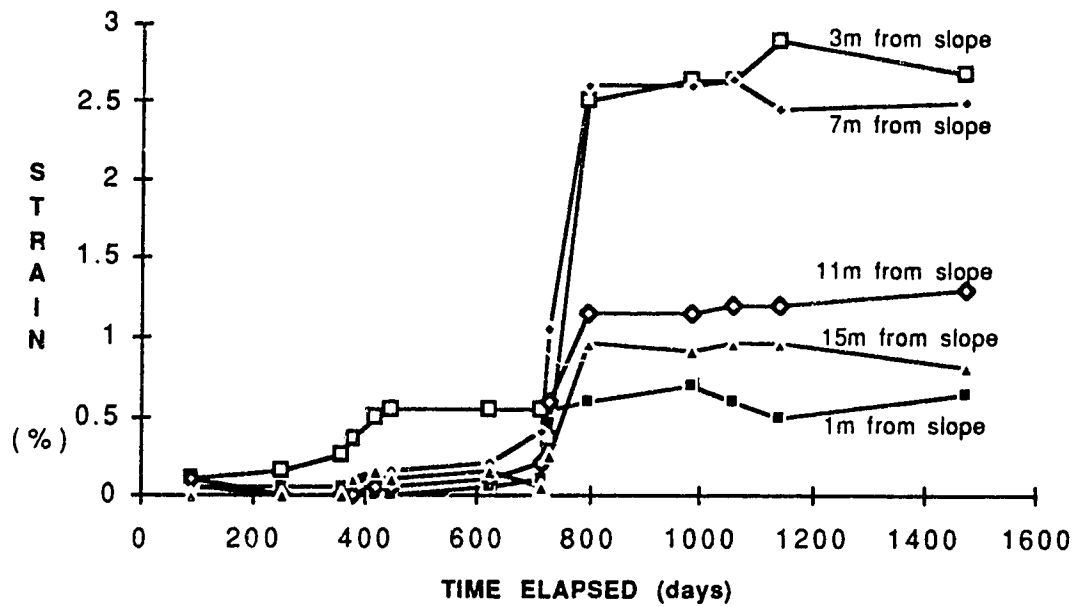


Figure A15. Development of Horizontal Strain of Soil at 2 m Level in Signode Section

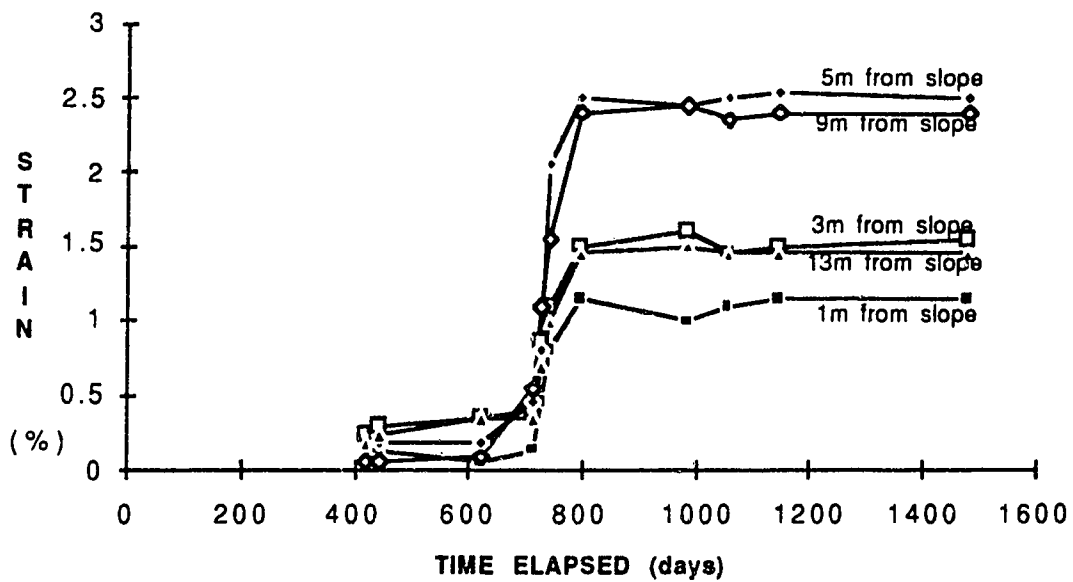


Figure A16. Development of Horizontal Strain of Soil at 4 m Level in Signode Section

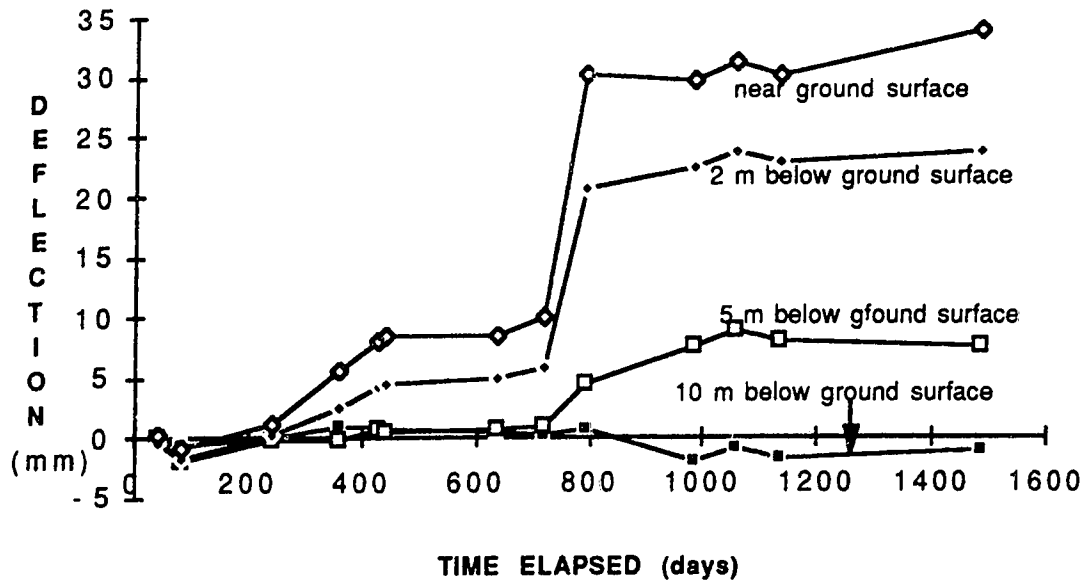


Figure A17. Development of Horizontal Deflection (A) of Soils beneath Toe of Slope in Signode Section

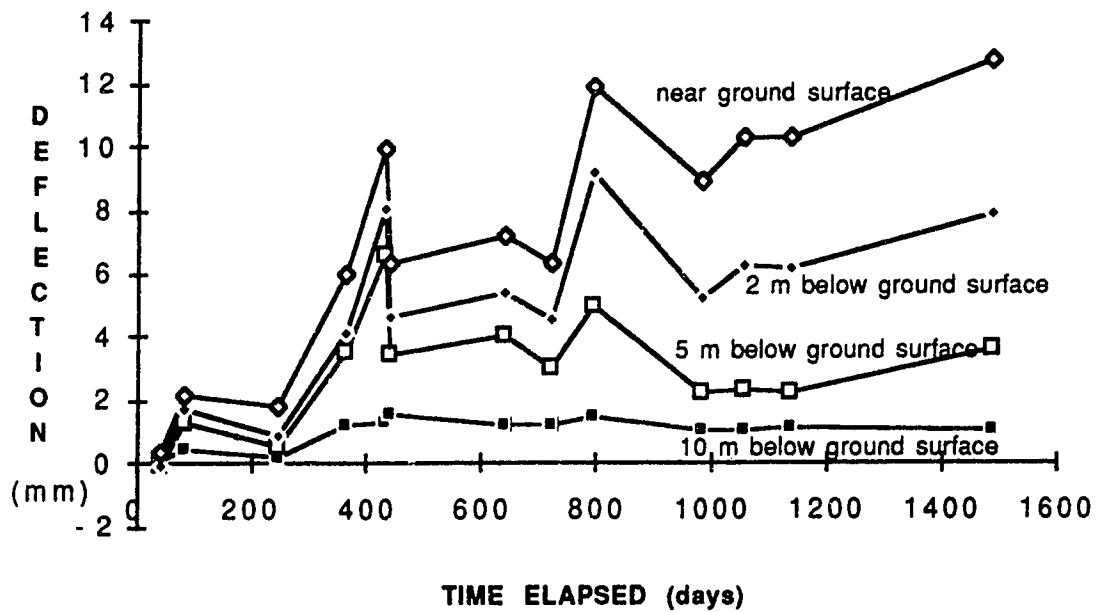


Figure A18. Development of Horizontal Deflection (B) of Soils beneath Toe of Slope in Signode Section

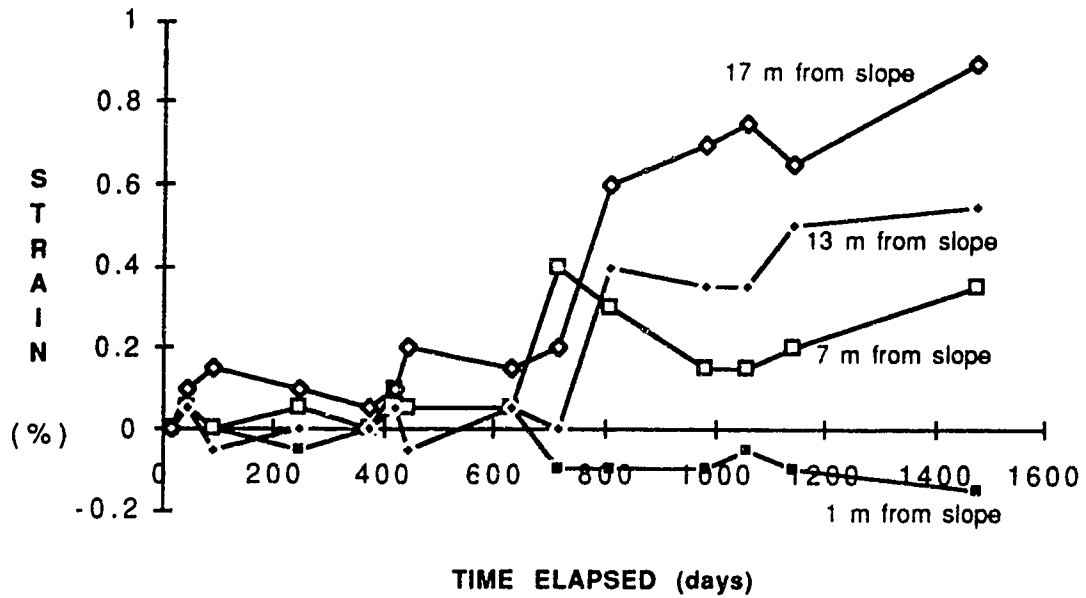


Figure A19. Development of Horizontal Strain of Soil at 0 m Level in Paragrid Section

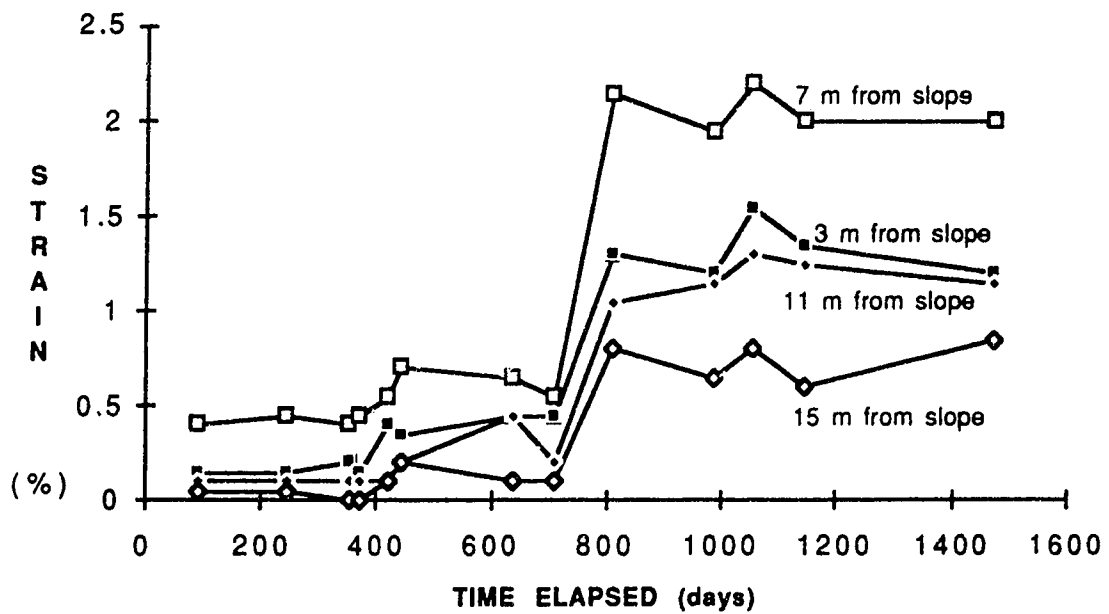


Figure A20. Development of Horizontal Strain of Soil at 2 m Level in Paragrid Section

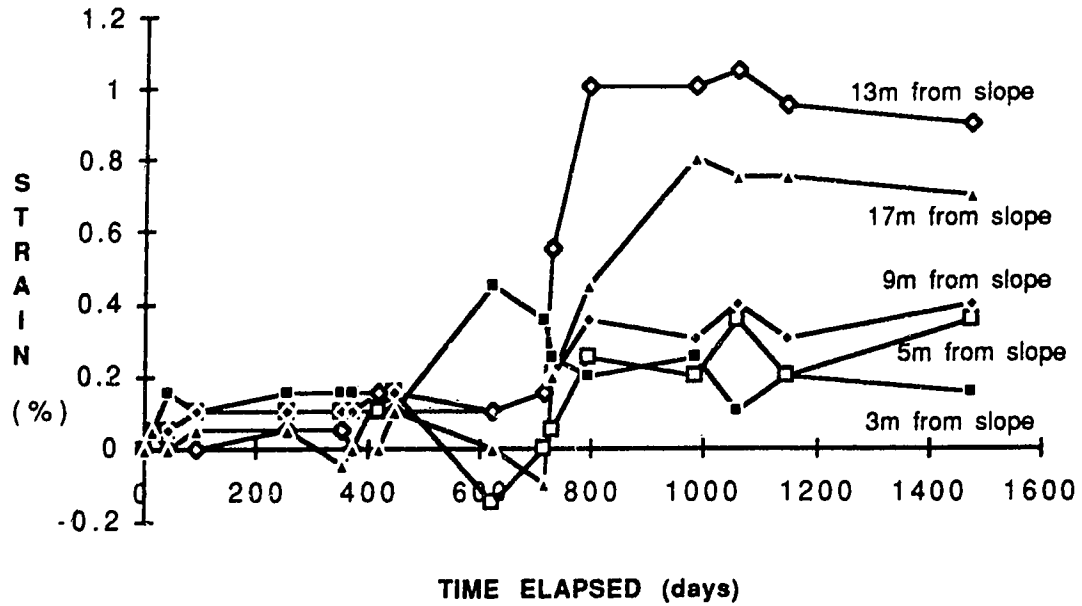


Figure A21. Development of Horizontal Strain of Soil at 0 m Level in Unreinforced Section

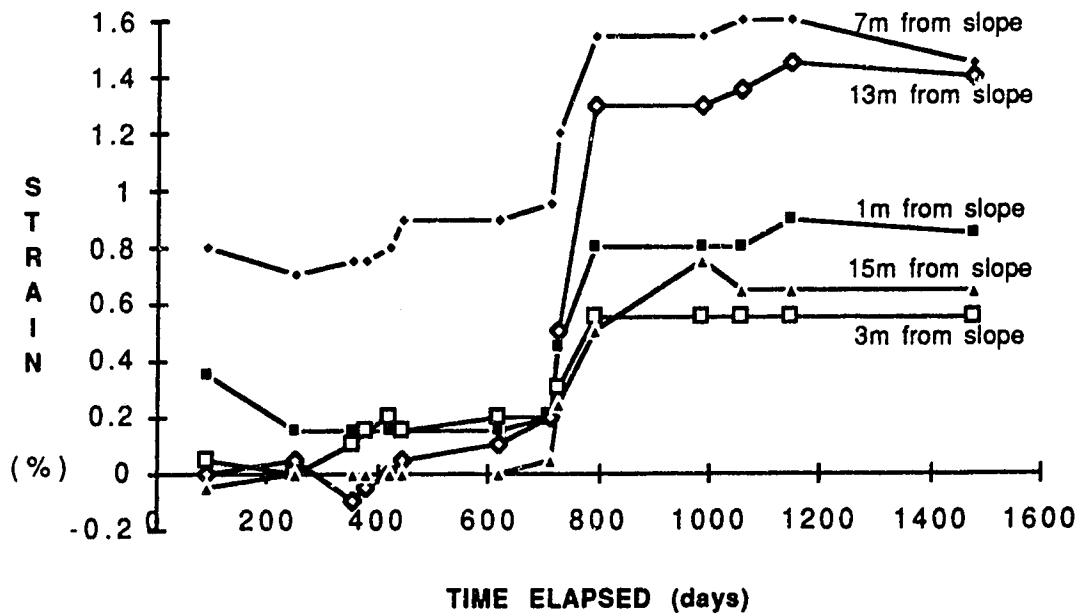


Figure A22. Development of Horizontal Strain of Soil at 2 m Level in Unreinforced Section

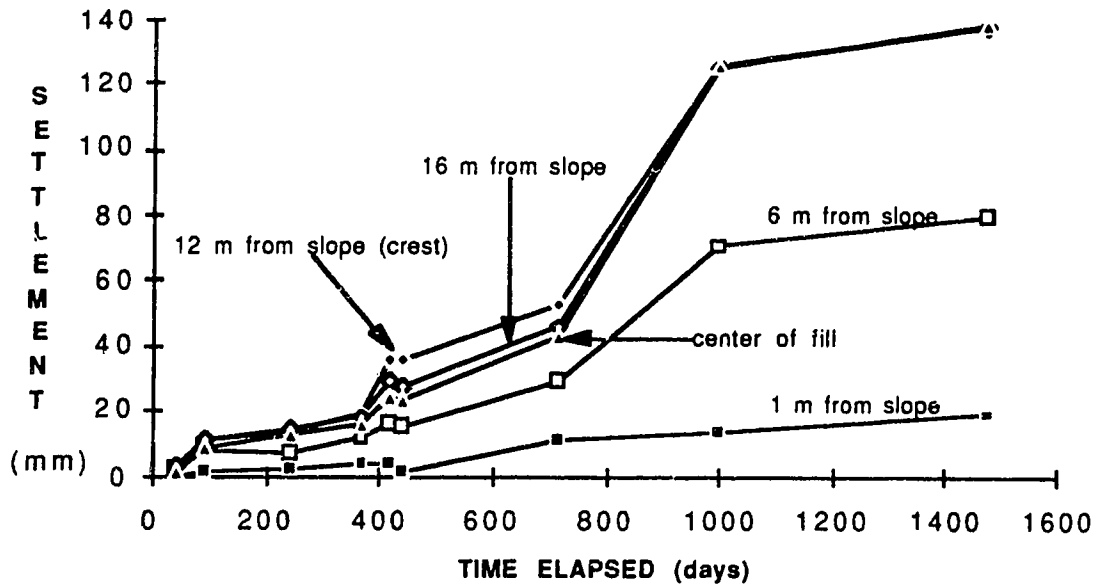


Figure A23. Development of Settlement at 0 m Level in Signode Section

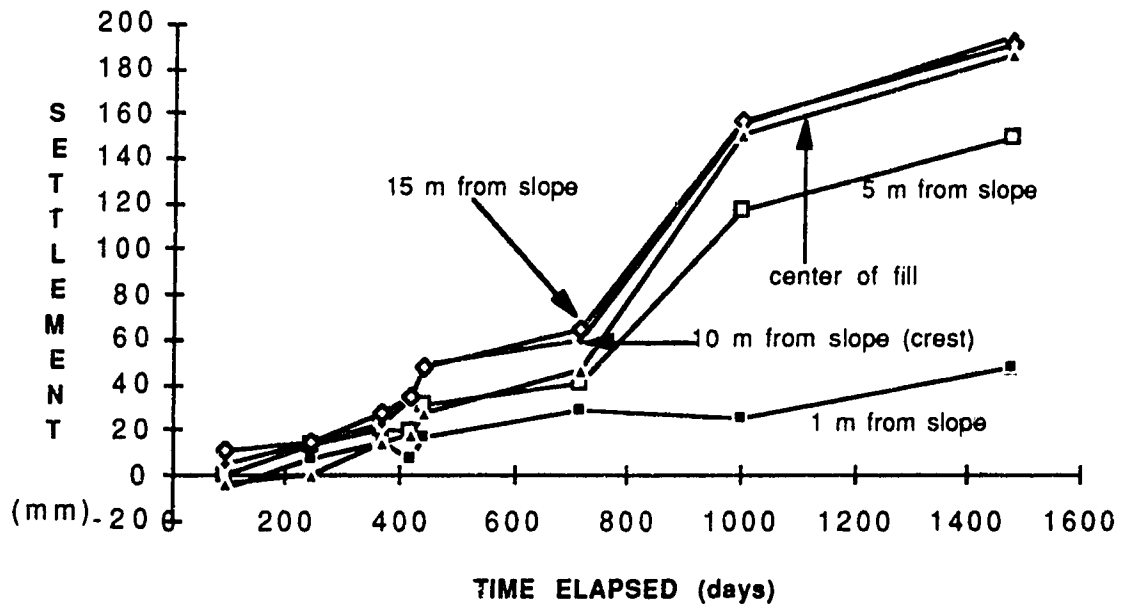


Figure A24. Development of Settlement at 2 m Level in Signode Section

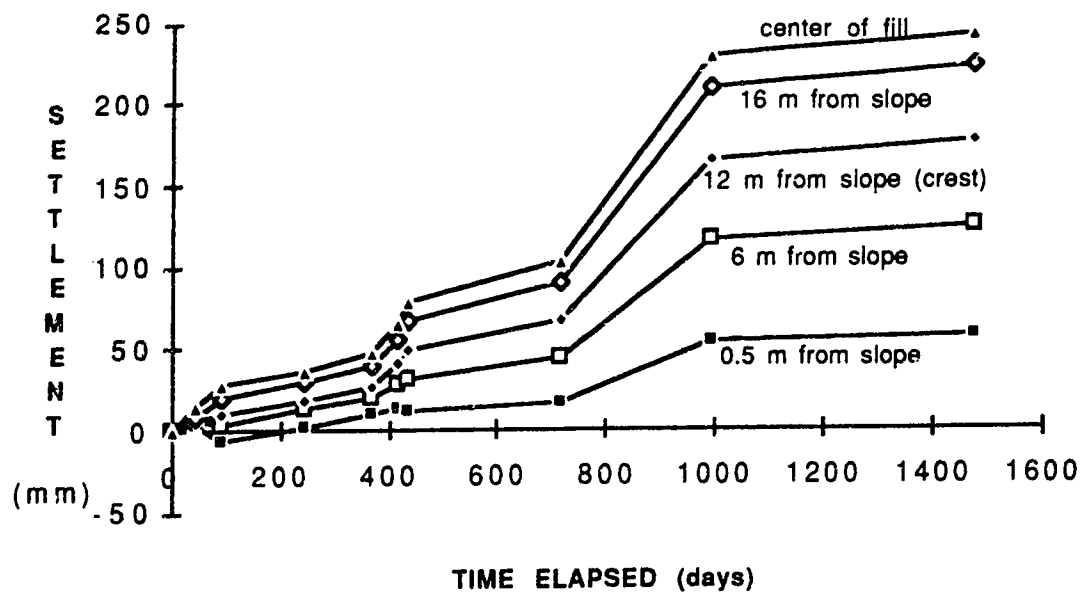


Figure A25. Development of Settlement at 0 m Level in Paragrid Section

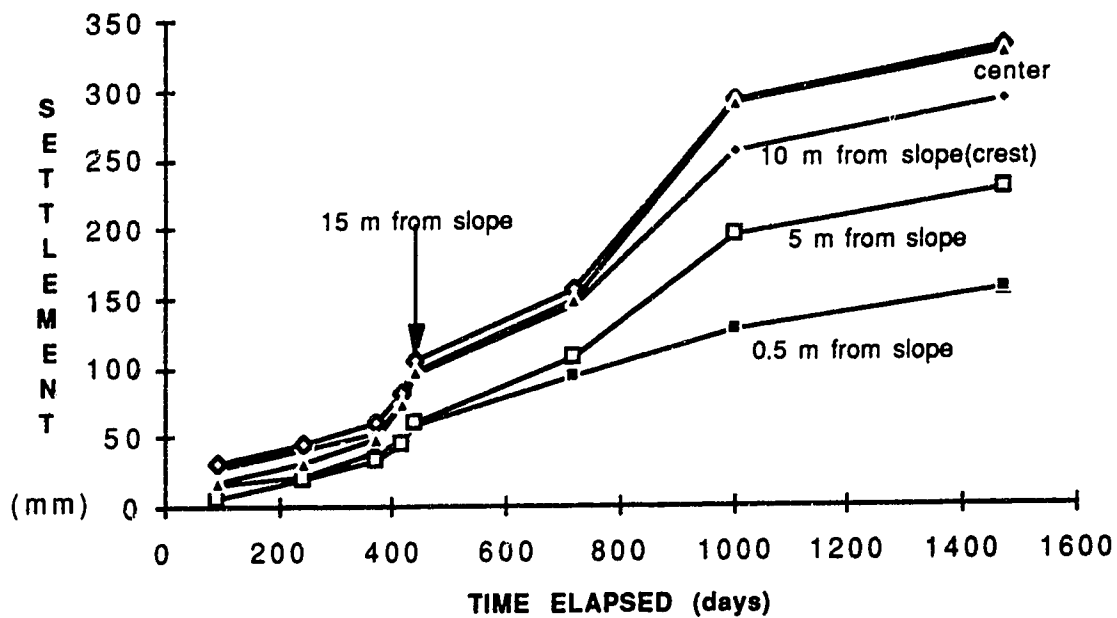


Figure A26. Development of Settlement at 2 m Level in Paragrid Section

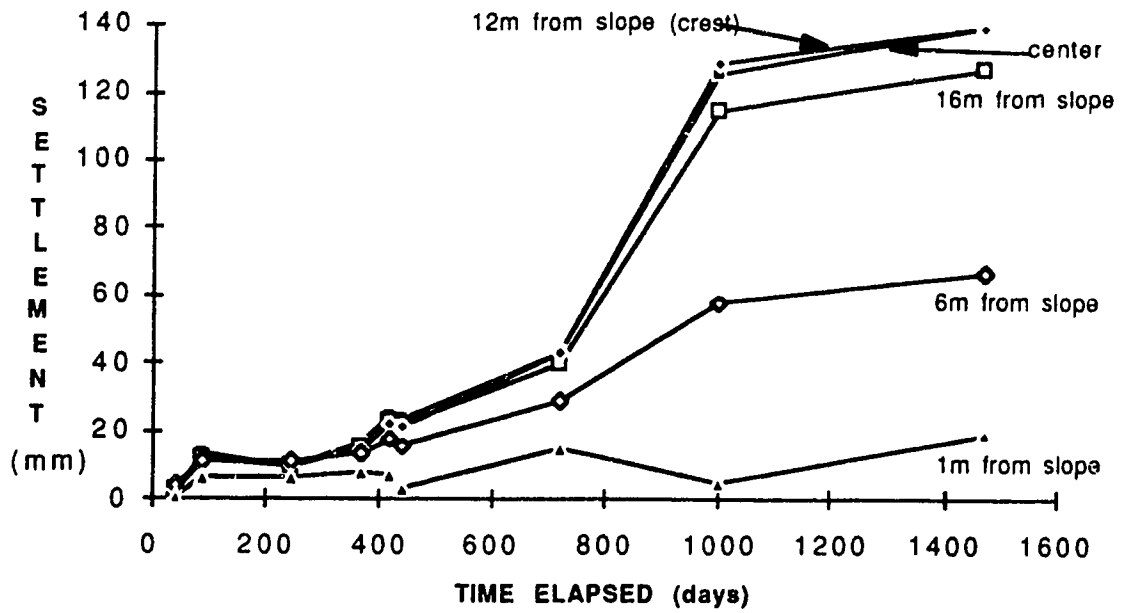


Figure A27. Development of Settlement at 0 m Level in Unreinforced Section

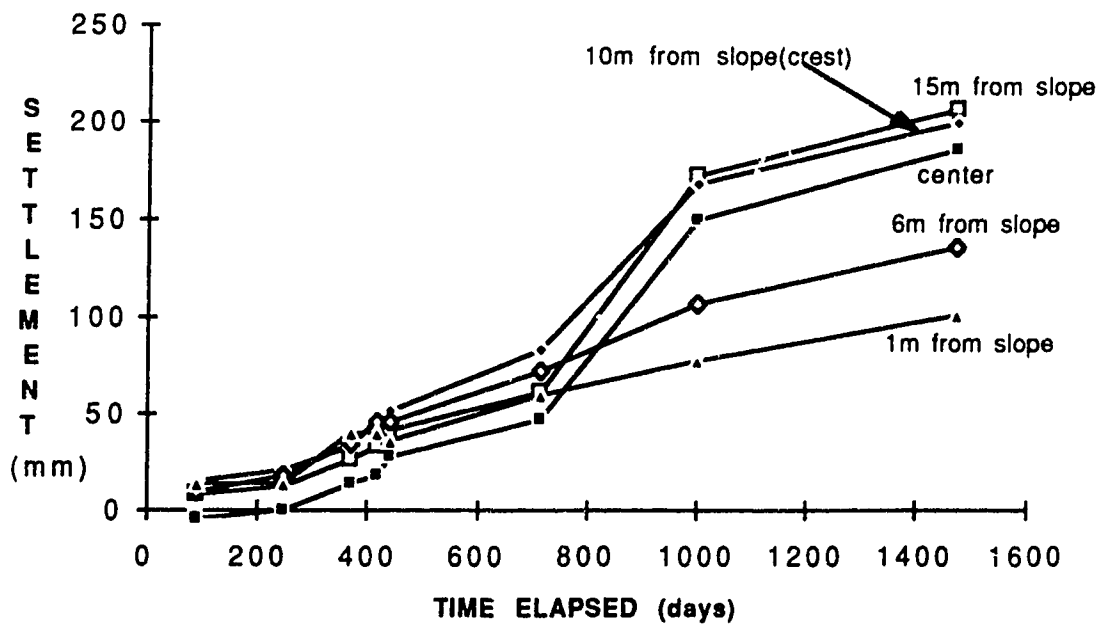


Figure A28. Development of Settlement at 2 m Level in Unreinforced Section

Appendix B. Description and Source Code of RSSABM

This appendix presents the source code of the computer program RSSABM which analyzes stability of reinforced slopes using modified Bishop's method. This program was written in standard FORTRAN 77 and can be run with a Microsoft FORTRAN Compiler 3.2 or a FORTRAN compiler of higher version. This program can be easily changed to fit other types of computers.

A typical profile of a reinforced slope is shown in Figure 6.1. The geometry of the slope is characterized by the coordinates of the toe and the crest of the slope. A soil layer in the foundation or within the slope is defined by the coordinates of the upper boundary of the layer. The tensile forces in a reinforcement layer are controlled by the coordinates of sampling points along the layer and the magnitude of the force at the sampling points.

Some assumptions were made:

- 1) Slip circle passes through the toe of the slope.
- 2) Reinforcement force does not improve the shear strength of the soil.
- 3) Reinforcement force acts horizontally.
- 4) Reinforcement force reduces the disturbing moment.

The following is an example of input data for the program RSSABM (corresponding to the slope configuration in Figure 6.1):

Tensor Reinforced Section, H=12m at 1988
4,3,4,5,
22.0,19.0,9.0,14.0,21.0,2.0,0.0,1.0,0.29,
0.0,2.0,30.0,2.0,23.0,0.419,20.0,
0.0,5.0,18.0,5.0,27.0,0.488,20.2,
0.0,8.0,15.0,8.0,13.0,0.524,20.2,
0.0,14.0,9.0,14.0,10.0,0.349,20.0,
3.0,20.0,0.0,19.0,30.0,10.0,30.0,9.0,0.0,
5.0,18.0,0.0,17.0,30.0,6.0,30.0,5.0,0.0,
7.0,16.0,0.0,15.0,30.0,3.0,30.0,2.0,0.0,

```

C      Program RSSABM for stability analysis of reinforced slopes by Bishop
C      modified method, written by Liu Yixin (Bill), June 1991.
C      Assume reinforcement force:
C          1) doesn't improve soil strength;
C          2) horizontal
C          3) reduce disturbing moment
C      Explanation:
C          NSL-- number of soil layers, in slope and foundation
C          NRFL-- number of reinforcement layers
C          NSST-- numbers of searching steps of the minimum Fs
C          NSP-- number of sampling points at each reinforcement layer
C          X0,Y0-- coordinate of the center of first circle to be analysed
C          XC,YC-- coordinate of crest
C          XT,YT-- coordinate of toe
C          DC-- designed final spacing of grid in searching
C          AFA-- slope angle of top surface
C          N-- number of slices
C          SP(I,J)-- coordinate(upper boundary of the soil layers) and
C          properties of soil layers (from bottom to top),i.e. (x1,y1,
C          x2,y2,C,Fi,Gama)
C          YH(I)-- boundary of horizontal layers (interpolation)
C          YS-- coordinate of slope and top surface
C          R-- radius of slip circle
C          SW-- width of slices
C          WT(I)-- weight of slices
C          MOMT,MOT(I)-- moment by reinforcement force horizontal
C          CO(I),FI(I)-- cohesion and friction angle at base of each slice
C          RU-- pore pressure coefficient
C          H(I)-- Y-coordinate of reinforcement layers
C          XCO(I,J)-- X-coordinate of sampling points at each reinforcement layer
C          F(I,J)-- reinforcement force at sampling points
C          RF(I)-- reinforcement force at intersection with slip circle
C
C      CHARACTER FIN*14,FOUT*14,TITLE*72
C      COMMON/GERN/NSL,NRFL,NSP,NSST,DC,N,RU
C      COMMON/GEOMT/X0,Y0,XC,YC,XT,YT,AFA,R,SW,YH(10),YS
C      COMMON/PROP/SP(20,8),H(20),XCO(20,20),F(20,20)
C      REAL MOMT,MOT(20)
C      DIMENSION FM(4),XM(4),YM(4),RF(20),XX(20)
C      DIMENSION WT0(50),WT(50),BT0(50),BT(50)
C
C
C      WRITE(*,910)
910  FORMAT(5X,'slope stability analysis of reinforced slopes')
      WRITE(*,915)
915  FORMAT(5X,'by Bishop modified method, written by Liu Yixin(Bill)')
      WRITE(*,920)
920  FORMAT(5X,'input the number of slices')
      READ(*,930)N
930  FORMAT(I2)
      WRITE(*,935)

```

```

935  FORMAT(5X,'input the name of data file')
      READ(*,940)FIN
940  FORMAT(A14)
      WRITE(*,945)
945  FORMAT(5X,'input the name of output file ')
      READ(*,950)FOUT
950  FORMAT(A14)
      WRITE(*,960)
960  FORMAT(5X,'input the partial Fs for reinforcement force')
      READ(*,970) FP
970  FORMAT(F4.2)
C
      OPEN (6,FILE=FOUT,STATUS='NEW',ACCESS='SEQUENTIAL')
      OPEN (5,FILE=FIN,STATUS='OLD',ACCESS='SEQUENTIAL')
      WRITE(6,1000)
1000  FORMAT(5X,'Slope Stability Analysis by Bishop Modified Method')
      WRITE(6,1002)
1002  FORMAT(5X,'Assuming reinforcement force: 1) horizontal')
      WRITE(6,1003)
1003  FORMAT(7X,'2) reducing resisting moment; 3) not improving soil')
      WRITE(6,1004)N
1004  FORMAT(5X,'Number of slices:',I2)
C
C      input and output data
C
      READ(5,1050) TITLE
1050  FORMAT(A72)
      WRITE(6,1050) TITLE
C
C      input control data
C
      READ(5,*)NSL,NRFL,NSP,NSST
      WRITE(6,1060) NSL,NRFL,NSP,NSST
1060  FORMAT(5X,4(I5,3X))
C
C      input geometry and pore pressure data
C
      READ(5,*) X0,Y0,XC,YC,XT,YT,AFA,DC,RU
      WRITE(6,1070) X0,Y0,XC,YC,XT,YT,AFA,DC,RU,FP
1070  FORMAT(5X,9(F6.2,1X),'FP:',F4.2)
C
C      input soil parameters by layers
C
      DO 1080 I=1,NSL
      READ(5,*) (SP(I,J),J=1,7)
      WRITE(6,1085) (SP(I,J),J=1,7)
1085  FORMAT(5X,7(F8.3,2X))
1080  CONTINUE
C
      IF(NRFL.EQ.0) GOTO 1100
C
C      input reinforcement force data by layers
C
      DO 1055 I=1,NRFL

```

```

      READ(5,*) H(I),(XCO(I,J),F(I,J),J=1,NSP)
C      from the point closest to slope surface, where X at maximum
      WRITE(6,1065) H(I),(XCO(I,J),F(I,J),J=1,NSP)
1065  FORMAT(5X,30(F7.2,1X))
1055  CONTINUE
C
C      control the calculation
C
1001  WRITE(*,1053)
1053  FORMAT(3X,'input your choice: unreinforced-0;reinforced-1;
      * stop-2')
      READ(*,1057)NC
1057  FORMAT(I2)
      IF(NC.EQ.0) GOTO 1100
      IF(NC.EQ.1) GOTO 1150
      IF(NC.EQ.2) GOTO 1270
      WRITE(*,1058)
1058  FORMAT(3X,'wrong input, choose again')
      GOTO 1001
C
C      calculate Fs of unreinforced slope at first trial circle
C
1100  CALL BISHOP(FS,WT,BT)
C
C      searching for the slip circle with minimum Fs in unreinforced slope
C
1105  FS1=FS
      DO 1107 II=1,N
      WT0(II)=WT(II)
      BT0(II)=BT(II)
1107  CONTINUE
      X00=X0
      Y00=Y0
C
      DO 1110 I=1,NSST
      DO 1115 J=1,2
      DO 1115 K=1,2
      X0=X00+DC*I*(-1)**J
      Y0=Y00+DC*I*(-1)**K
C      control the center of slip circle to be above toe
      IF(YT.GT.Y0) GOTO 1115
C      restrain the slip circle within the slope
      D1=SQRT((X0-XT)**2+(Y0-YT)**2)
      D2=SQRT((X0-XC)**2+(Y0-YC)**2)
      IF(D2.GT.D1) GOTO 1115
C      prevent the center of circle within the slope
      YS0=(X0-XT)*(YC-YT)/(XC-XT)+YT
      IF(Y0.LE.YS0) GOTO 1115
C
      CALL BISHOP(FS,WT,BT)
      IF((FS+0.01).LT.FS1) GOTO 1105
1115  CONTINUE
1110  CONTINUE
C

```

```

C      calculate the radius of the most possible slip circle
      R0=SQRT((X00-XT)**2+(Y00-YT)**2)
C
C
C      print the result for unreinforced slope stability analysis
C
1120 WRITE(6,1210)
1210 FORMAT(5X,'stability analysis of unreinforced slope')
      WRITE(6,1212) X00,Y00,R0
1212 FORMAT(5X,'center of slip circle: X0=',F8.3,5X,'Y0=',F8.3,5X,
+ 'R0=',F10.3)
      WRITE(6,1215) FS1
1215 FORMAT(5X,'factor of safety=',F8.3)
      WRITE(6,1220) SW
1220 FORMAT(5X,'WIDTH OF SLICE:',F10.3)
      WRITE(6,1226)(WT0(I),BT0(I),I=1,N)
1226 FORMAT(5X,'WT:',F10.3,5X,'BT:',F10.5)
C
      GOTO 1001
C
C      calculate Fs for reinforced slope
C
1150 CALL BMMR(FS,WT,BT,MOMT,FP)
C
1155 FS1=FS
      DO 1157 II=1,N
          WT0(II)=WT(II)
          BT0(II)=BT(II)
1157 CONTINUE
      X00=X0
      Y00=Y0
C
      DO 1160 I=1,NSST
          DO 1165 J=1,2
              DO 1165 K=1,2
                  X0=X00+DC*I*(-1)**J
                  Y0=Y00+DC*I*(-1)**K
C          control the center of slip circle to be above toe
          IF(YT.GT.Y0) GOTO 1165
C          restrain the slip circle within the slope
          D1=SQRT((X0-XT)**2+(Y0-YT)**2)
          D2=SQRT((X0-XC)**2+(Y0-YC)**2)
          IF(D2.GT.D1) GOTO 1165
C          prevent the center of circle within the slope
          YS0=(X0-XT)*(YC-YT)/(XC-XT)+YT
          IF(Y0.LE.YS0) GOTO 1165
C
          CALL BMMR(FS,WT,BT,MOMT,FP)
          IF((FS+0.01).LT.FS1) GOTO 1155
1165 CONTINUE
1160 CONTINUE
C
C      calculate the radius of the most possible slip circle
      R0=SQRT((X00-XT)**2+(Y00-YT)**2)

```

```

C
C
C   print the result for reinforced slope stability analysis
C
      WRITE(6,1211)
1211  FORMAT(3X,'stability analysis of reinforced slope')
      WRITE(6,1212) X00,Y00,R0
      WRITE(6,1215) FS1
      WRITE(6,1220) SW
      WRITE(6,1226)(WT0(I),BT0(I),I=1,N)
C
      GOTO 1001
C
1270  STOP
      END
C
C
      SUBROUTINE BISHOP(FS,WT,BT)
C
      COMMON/GERN/NSL,NRFL,NSP,NSST,DC,N,RU
      COMMON/GEOMT/X0,Y0,XC,YC,XT,YT,AFA,R,SW,YH(10),YS
      COMMON/PROP/SP(20,8),H(20),XCO(20,20),F(20,20)
      DIMENSION CO(50),FI(50),BT(50),WT(50)
C
C   determine strength parameters at base of each slice
C
      CALL GEOMETRY(BT,WT)
      DO 800 I=1,N
        X=XT-(1-0.5)*SW
        Y=Y0-SQRT(R**2-(X-X0)**2)
        DO 810 J=1,NSL
          YH(J)=(X-SP(J,1))*(SP(J,4)-SP(J,2))/(SP(J,3)-SP(J,1))+SP(J,2)
          IF(Y.GT.YH(J)) GOTO 810
          CO(I)=SP(J,5)
          FI(I)=SP(J,6)
        GOTO 800
      810  CONTINUE
      800  CONTINUE
C
C   iterate and calculate Fs
C
      FS=1.2
      840  A=0.0
          B=0.0
          C=0.0
          F0=FS
          DO 830 I=1,N
            A=A+WT(I)*SIN(BT(I))
            C=COS(BT(I))*(1+TAN(BT(I))*TAN(FI(I))/F0)
            B=B+(CO(I)*SW+WT(I)*(1-RU)*TAN(FI(I)))/C
          830  CONTINUE
          FS=B/A
          IF(ABS(FS-F0).GT.0.01) GOTO 840
C

```

```

      RETURN
      END
C
C
C
      SUBROUTINE BMMR(FS,WT,BT,MOMT,FP)
C
      COMMON/GERN/NSL,NRFL,NSP,NSST,DC,N,RU
      COMMON/GEOMT/X0,Y0,XC,YC,XT,YT,AFA,R,SW,YH(10),YS
      COMMON/PROP/SP(20,8),H(20),XCO(20,20),F(20,20)
      DIMENSION CO(50),FI(50),BT(50),WT(50),T(50)
      REAL MOMT,MOT(20)
C
C      determine strength parameters at base of each slice
C
      CALL GEOMETRY(BT,WT)
      DO 600 I=1,N
        X=XT-(I-0.5)*SW
        Y=Y0-SQRT(R**2-(X-X0)**2)
        DO 610 J=1,NSL
          YH(J)=(X-SP(J,1))*(SP(J,4)-SP(J,2))/(SP(J,3)-SP(J,1))+SP(J,2)
          IF(Y.GT.YH(J)) GOTO 610
          CO(I)=SP(J,5)
          FI(I)=SP(J,6)
          GOTO 600
610      CONTINUE
600      CONTINUE
C
C      iterate and calculate Fs
C
      CALL REINF(MOMT,FP,XX)
      FS=1.2
640      A=0.0
          B=0.0
          C=0.0
          F0=FS
          DO 630 I=1,N
            A=A+WT(I)*SIN(BT(I))
            C=COS(BT(I))*(1+TAN(BT(I))*TAN(FI(I))/F0)
            B=B+(CO(I)*SW+WT(I)*(1-RU)*TAN(FI(I)))/C
630      CONTINUE
          FS=(B*R)/(A*R-MOMT)
          IF(ABS(FS-F0).GT.0.01) GOTO 640
C
C
C
      RETURN
      END
C
C
C
      SUBROUTINE GEOMETRY(BT,WT)
C
      COMMON/GERN/NSL,NRFL,NSP,NSST,DC,N,RU

```



```

COMMON/GEOMT/X0,Y0,XC,YC,XT,YT,AFA,R,SW,YH(10),YS
COMMON/PROP/SP(20,8),H(20),XCO(20,20),F(20,20)
DIMENSION BT(50),WT(50)
C   calculate width of slices
C
R=SQRT((X0-XT)**2+(Y0-YT)**2)
X1=X0-SQRT(R**2-(YC-Y0)**2)
DY=(XC-X1)*TAN(AFA)
Y1=YC+DY
XS=X0-SQRT(R**2-(Y1-Y0)**2)
SW=(XT-XS)/N
C
C   calculate weight and base angle (BT(I)) of each slice
C
DO 500 I=1,N
X=XT-(I-0.5)*SW
Y=Y0-SQRT(R**2-(X-X0)**2)
BT(I)=ATAN((X0-X)/SQRT(R**2-(X-X0)**2))
WT(I)=0.0
AB=0.0
C
DO 510 J=1,NSL
YH(J)=(X-SP(J,1))*(SP(J,4)-SP(J,2))/(SP(J,3)-SP(J,1))+SP(J,2)
IF(Y.GE.YH(J)) GOTO 510
IF(XC.GE.X) GOTO 520
YS=(X-XC)*(YT-YC)/(XT-XC)+YC
IF(YH(J).GE.YS) GOTO 525
W=SW*(YH(J)-Y-AB)*SP(J,7)
AB=YH(J)-Y
WT(I)=WT(I)+W
GOTO 510
525 W=SW*(YS-Y-AB)*SP(J,7)
WT(I)=WT(I)+W
GOTO 500
520 YS=(XC-X)*TAN(AFA)+YC
IF(YH(J).GE.YS) GOTO 540
W=SW*(YH(J)-Y-AB)*SP(J,7)
AB=YH(J)-Y
WT(I)=WT(I)+W
GOTO 510
540 W=SW*(YS-Y-AB)*SP(J,7)
WT(I)=WT(I)+W
GOTO 500
C
510 CONTINUE
C
500 CONTINUE
C
RETURN
END
C
C
SUBROUTINE REINF(MOMT,FP,XX)
C

```

```

C      calculate reinforcement force and moment
C
      REAL MOT(20),RF(20),MOMT,XX(20)
      COMMON/GERN/NSL,NRFL,NSP,NSST,DC,N,RU
      COMMON/GEOMT/X0,Y0,XC,YC,XT,YT,AFA,R,SW,YH(10),YS
      COMMON/PROP/SP(20,8),H(20),XCO(20,20),F(20,20)

C
      MOMT=0.0
      DO 700 I=1,NRFL
        XX(I)=X0-SQRT(R**2-(H(I)-Y0)**2)
        MOT(I)=0.0

C
C      jump over the case that circle doesn't insect reinforcement
C
      IF(XX(I).GT.XCO(I,1)) GOTO 715
      IF(XX(I).LT.XCO(I,NSP)) GOTO 715

C
      DO 710 J=1,NSP
        IF(XCO(I,J).GT.XX(I)) GOTO 710
        RF(I)=(XX(I)-XCO(I,J-1))*(F(I,J)-F(I,J-1))/(XCO(I,J)-XCO(I,J-1))
        * +F(I,J-1)
        MOT(I)=RF(I)*(Y0-H(I))/FP
        MOMT=MOMT+MOT(I)
        GOTO 700
710      CONTINUE
715      RF(I)=0.0
700      CONTINUE

C
      RETURN
      END

```

Appendix C. Description and Source Code of RSSASM

This appendix presents the source code of the computer program RSSASM which analyzes stability of reinforced slopes using modified Spencer's method. This program was written in standard FORTRAN 77 and can be run with a Microsoft FORTRAN Compiler 3.2 or a FORTRAN compiler of higher version. However, it may take considerable long time if it is run in a PC type computer. This program can be easily changed to fit other types of computers.

A typical profile of a reinforced slope is shown in Figure 6.1. The geometry of the slope is characterized by the coordinates of the toe and the crest of the slope. A soil layer in the foundation or within the slope is defined by the coordinates of the upper boundary of the layer. The tensile forces in a reinforcement layer are controlled by the coordinates of sampling points along the layer and the magnitude of the force at the sampling points.

Some assumptions were made:

- 1) Slip circle passes through the toe of the slope.
- 2) Reinforcement force does not improve the shear strength of the soil.
- 3) Reinforcement force acts horizontally.

The following is an example of input data for the program RSSASM (corresponding to the slope configuration in Figure 6.1):

Tensar Reinforced Section, H=12m at 1988

4,3,4,5,
22.0,19.0,9.0,14.0,21.0,2.0,0.0,1.0,0.29,
0.0,2.0,30.0,2.0,23.0,0.419,20.0,
0.0,5.0,18.0,5.0,27.0,0.488,20.2,
0.0,8.0,15.0,8.0,13.0,0.524,20.2,
0.0,14.0,9.0,14.0,10.0,0.349,20.0,
3.0,20.0,0.0,19.0,30.0,10.0,30.0,9.0,0.0,
5.0,18.0,0.0,17.0,30.0,6.0,30.0,5.0,0.0,
7.0,16.0,0.0,15.0,30.0,3.0,30.0,2.0,0.0,

```

C   Program RSSASM for stability analysis of reinforced slopes by Spencer
C   modified method, written by Liu Yixin (Bill), July 1990.
C   Assume reinforcement force: 1) horizontal
C                               2) not improve soil strength.
C   Assume circular slip surface pass through the toe of slope
C   Explanation:
C   NSL-- number of soil layers, in slope and foundation
C   NRFL-- number of reinforcement layers
C   NSST-- numbers of searching steps of the minimum Fs
C   NSP-- number of sampling points at each reinforcement layer
C   X0,Y0-- coordinate of the center of first circle to be analysed
C   XC,YC-- coordinate of crest
C   XT,YT-- coordinate of toe
C   DC-- designed final spacing of grid in searching
C   DST-- degree of searching angle of interslice force inclination
C   DSTF-- maximum expected angle of interslice force inclination
C   AFA-- slope angle of top surface
C   N-- numner of slices
C   SP(I,J)-- coordinate(upper boundary of the soil layers) and
C   properties of soil layers (from bottom to top),i.e. (x1,y1,
C   x2,y2,C,Fi,Gama)
C   YH(I)-- boundary of horizontal layers (interpolation)
C   YS-- coordinate of slope and top sueface
C   R-- radius of slip circle
C   SW-- width of slices
C   WT(I)-- weight of slices
C   CO(I),FI(I)-- cohesion and friction angle at base of each slice
C   RU-- pore pressure coefficient
C   H(I)-- Y-coordinate of reinforcement layers (from bottom to top)
C   XCO(I,J)-- X-coordinate of sampling points at each reinforcement layer
C   F(I,J)-- reinforcement force at sampling points
C   RF(I)-- reinforcement force at intersection with slip circle
C   FS,FM,FF-- factor of safety in terms of overall, moment and force
C               equilibrium
C
C   CHARACTER TITLE*72,FIN*14,FOUT*14
C   COMMON/GERN/NSL,NRFL,NSP,DC,N,RU,DST,DSTF
C   COMMON/GEOMT/X0,Y0,XC,YC,XT,YT,AFA,R,SW,YH(10),YS
C   COMMON/PROP/SP(20,8),H(20),XCO(20,20),F(20,20)
C   DIMENSION FM(4),XM(4),YM(4),RF(20),XX(20)
C   DIMENSION WT0(50),WT(50),BT0(50),BT(50),T(50)
C
C   WRITE(*,910)
910  FORMAT(5X,'internal stability analysis of reinforced slopes')
C   WRITE(*,905)
905  FORMAT(5X,'assuming circular slip surface passing through toe')
C   WRITE(*,915)
915  FORMAT(5X,'by Spencer Modified Method, written by Liu Yixin(Bill)')
C   WRITE(*,920)
920  FORMAT(5X,'input the number of slices')
C   READ(*,930)N

```

```

930  FORMAT(I2)
      WRITE(*,935)
935  FORMAT(5X,'input the name of data file')
      READ(*,940)FIN
940  FORMAT(A14)
      WRITE(*,945)
945  FORMAT(5X,'input the name of output file ')
      READ(*,950)FOUT
950  FORMAT(A14)
      WRITE(*,953)
953  FORMAT(3X,'input the degree of searching angle for interslice
* force inclination')
      READ(*,952)DST
952  FORMAT(F8.2)
      WRITE(*,956)
956  FORMAT(3X,'input the expecting maximum angle of interslice
* force inclination')
      READ(*,957)DSTF
957  FORMAT(F8.2)
      WRITE(*,960)
960  FORMAT(5X,'input the partial Fs for reinforcement force')
      READ(*,970) FP
970  FORMAT(F4.2)
C
      OPEN (6,FILE=FOUT,STATUS='NEW',ACCESS='SEQUENTIAL')
      OPEN (5,FILE=FIN,STATUS='OLD',ACCESS='SEQUENTIAL')
C
C
      WRITE(6,1000)
1000  FORMAT(5X,'stability analysis of reinforced slopes by')
      WRITE(6,1002)
1002  FORMAT(5X,'Spencer modified method, written by Liu Yixin(Bill)')
      WRITE(6,1003)
1003  FORMAT(5X,'horizontal rein-force and not improving soil strength')
      WRITE(6,1004)N,DST,FP
1004  FORMAT(5X,'Number of slices:',I2,5X,'DST & FP:',2F8.3)
C
      DST=DST*3.14/180.0
      DSTF=DSTF*3.14/180.0
C
      input and output data
C
      READ(5,1050) TITLE
1050  FORMAT(A72)
      WRITE(6,1050) TITLE
C
      READ(5,*)NSL,NRFL,NSP,NSST
      WRITE(6,1060) NSL,NRFL,NSP,NSST
1060  FORMAT(5X,4(I5,3X))
C
      READ(5,*) X0,Y0,XC,YC,XT,YT,AFA,DC,RU
      WRITE(6,1070) X0,Y0,XC,YC,XT,YT,AFA,DC,RU,FP
1070  FORMAT(5X,9(F6.2,1X),'FP:',F4.2)
C
      DO 1100 I=1,NSL

```

```

      READ(5,*) (SP(I,J),J=1,7)
      WRITE(6,1110) (SP(I,J),J=1,7)
1110  FORMAT(5X,7(F8.3,2X))
1100  CONTINUE
C
      IF(NRFL.EQ.0) GOTO 1150
C
      DO 1140 I=1,NRFL
      READ(5,*) H(I),(XCO(I,J),F(I,J),J=1,NSP)
C      from the point closest to slope surface, where X at maximum
      WRITE(6,1120) H(I),(XCO(I,J),F(I,J),J=1,NSP)
1120  FORMAT(5X,30(F7.3,2X))
1140  CONTINUE
C
C      calculate Fs of unreinforced slope at first trial circle
C
1150  CALL SPR(FS,WT,BT,ST0,FT0)
C
      IF(FS.EQ.0.0) GOTO 1270
C      searching for the slip circle with minimum Fs in unreinforced slope
C
1125      FS1=FS
      ST1=ST0
      FT1=FT0
      DO 1127 II=1,N
      WT0(II)=WT(II)
      BT0(II)=BT(II)
1127  CONTINUE
      X00=X0
      Y00=Y0
C
      DO 1155 I=1,NSST
      DO 1160 J=0,7
      X0=X00+DC*I*SIN(J*3.1416/4)
      Y0=Y00+DC*I*COS(J*3.1416/4)
C      control the center of slip circle to be above toe
      IF(YT.GT.Y0) GOTO 1160
C      restrain the slip circle within the slope
      D1=SQRT((X0-XT)**2+(Y0-YT)**2)
      D2=SQRT((X0-XC)**2+(Y0-YC)**2)
      IF(D2.GT.D1) GOTO 1160
C      prevent the center of circle within the slope
      YS0=(X0-XT)*(YC-YT)/(XC-XT)+YT
      IF(Y0.LE.YS0) GOTO 1160
C
      CALL SPR(FS,WT,BT,ST0,FT0)
      IF((FS+0.01).LT.FS1) GOTO 1125
1160  CONTINUE
1155  CONTINUE
C
C      calculate the radius of the most possible slip circle
      R0=SQRT((X00-XT)**2+(Y00-YT)**2)
C
C

```

```

C      print the result for unreinforced slope stability analysis
C
1200  WRITE(6,1210)
1210  FORMAT(5X,'stability analysis of unreinforced slope')
      WRITE(6,1212) X00,Y00,R0
1212  FORMAT(5X,'center of slip circle: X0=',F8.3,5X,'Y0=',F8.3,5X,
+ 'R0=',F10.3)
      WRITE(6,1215) FS1,ST1
1215  FORMAT(5X,'factor of safety,Fs=',F8.3,'angle of in-force',F10.3)
      WRITE(6,1220) SW,FT1
1220  FORMAT(5X,'WIDTH OF SLICE:',F10.3,5X,'error of Ff and Fm:',F10.3)
      WRITE(6,1226)(WT0(I),BT0(I),I=1,N)
1226  FORMAT(5X,'WT:',F10.3,5X,'BT:',F10.5)
C
C      calculate Fs for reinforced slope
      IF(NRFL.EQ.0) GOTO 1270
C
      X0=X00
      Y0=Y00
C      first try
1250  CALL SPRRF(FS,ST0,FT0,FP)
C      searching minimum Fs for reinforced slope
C
1300  FS1=FS
      ST1=ST0
      FT0=FT1
      X00=X0
      Y00=Y0
C
      DO 1310 I=1,NSST
        DO 1320 J=1,2
          X0=X00+DC*I*SIN(J*3.1416/4)
          Y0=Y00+DC*I*COS(J*3.1416/4)
C          control the center of slip circle to be above toe
          IF(YT.GT.Y0) GOTO 1320
C          restrain the slip circle within the slope
          D1=SQRT((X0-XT)**2+(Y0-YT)**2)
          D2=SQRT((X0-XC)**2+(Y0-YC)**2)
          IF(D2.GT.D1) GOTO 1320
C          prevent the center of circle within the slope
          YS0=(X0-XT)*(YC-YT)/(XC-XT)+YT
          IF(Y0.LE.YS0) GOTO 1320
C
          CALL SPRRF(FS,ST0,FT0,FP)
          IF((FS+0.01).LT.FS1) GOTO 1300
1320  CONTINUE
1310  CONTINUE
C
C      print results of reinforced slope stability analysis
C
      WRITE(6,1206)
1206  FORMAT(5X,'STABILITY OF REINFORCED SLOPE')
      WRITE(6,1330)X00,Y00
1330  FORMAT(5X,'center of slip circle, X0=',F10.3,'Y0=',F10.3)

```

```

WRITE(6,1340)FS1,ST1
1340 FORMAT(5X,'factor of safety, Fs=',F8.3,'angle of in-force',F10.5)
WRITE(6,1345)FT1
1345 FORMAT(5X,'error between Ff amd Fm:',f10.5)
1270 STOP
END

C
C
SUBROUTINE SPR(FS,WT,BT,ST0,FT0)
C
C stability analysis for unreinforced slope
COMMON/GERN/NSL,NRFL,NSP,DC,N,RU,DST,DSTF
COMMON/GEOMT/X0,Y0,XC,YC,XT,YT,AFA,R,SW,YH(10),YS
COMMON/PROP/SP(20,8),H(20),XCO(20,20),F(20,20)
DIMENSION CO(50),FI(50),BT(50),WT(50),T(50)

C
C determine strength parameters at base of each slice
C
FS=0.0
CALL GEOMETRY(BT,WT)
DO 800 I=1,N
X=XT-(I-0.5)*SW
Y=Y0-SQRT(R**2-(X-X0)**2)
DO 810 J=1,NSL
YH(J)=(X-SP(J,1))*(SP(J,4)-SP(J,2))/(SP(J,3)-SP(J,1))+SP(J,2)
IF(Y.GT.YH(J)) GOTO 810
CO(I)=SP(J,5)
FI(I)=SP(J,6)
GOTO 800
810 CONTINUE
800 CONTINUE

C
C try at different angle of interal force inclination
C
NN=INT(DSTF/DST)
FT0=10.0
DO 802 I=0,NN
ST=I*DST

C
C working for Fs in terms of force equilibrium
C searching Sum(Q)=0 at large steps
C
F0=4.0
Q=0.0
DO 815 II=0,18
FB=F0-II*0.2
Q0=Q
Q=0.0
DO 805 J=1,N
A=CO(J)*SW/FB/COS(BT(J))+TAN(FI(J))*(WT(J)*COS(BT(J))-
@ RU*WT(J)/COS(BT(J)))/FB-WT(J)*SIN(BT(J))
B=COS(BT(J)-ST)*(1+TAN(FI(J))*TAN(BT(J)-ST)/FB)
Q=Q+A/B
805 CONTINUE

```



```

C      solving Sum(Q)=0
      TES=Q*Q0
      IF(TES.LT.0.0) GOTO 816
815    CONTINUE
      FS=4.0
      GOTO 850

C
C      searching Sum(Q)=0 at small steps
C
816    F0=FB+0.2
      Q=0.0
      DO 817 II=0,20
      FB=F0-II*0.01
      Q0=Q
      Q=0.0
      DO 807 J=1,N
      A=CO(J)*SW/FB/COS(BT(J))+TAN(FI(J))*(WT(J)*COS(BT(J))-
@    RU*WT(J)/COS(BT(J)))/FB-WT(J)*SIN(BT(J))
      B=COS(BT(J)-ST)*(1+TAN(FI(J))*TAN(BT(J)-ST)/FB)
      Q=Q+A/B
807    CONTINUE
C      solving Sum(Q)=0
      TES=Q*Q0
      IF(TES.LT.0.0) GOTO 819
817    CONTINUE
819    FF=FB+0.005

C
C      working for Fs in terms of moment equilibrium
C
C      searching Sum(Q)=0 at large steps
C
      F0=4.0
      Q=0.0
      DO 835 II=0,18
      FB=F0-II*0.2
      Q0=Q
      Q=0.0
      DO 825 J=1,N
      A=CO(J)*SW/FB/COS(BT(J))+TAN(FI(J))*(WT(J)*COS(BT(J))-
@    RU*WT(J)/COS(BT(J)))/FB-WT(J)*SIN(BT(J))
      B=COS(BT(J)-ST)*(1+TAN(FI(J))*TAN(BT(J)-ST)/FB)
      Q=Q+A*COS(BT(J)-ST)/B
825    CONTINUE
C      solving Sum(Q)=0
      TES=Q*Q0
      IF(TES.LT.0.0) GOTO 836
835    CONTINUE
      FS=4.0
      GOTO 850

C
C      searching Sum(Q)=0 at small steps
C
836    F0=FB+0.2
      Q=0.0

```

```

DO 837 II=0,20
FB=F0-II*0.01
Q0=Q
Q=0.0
DO 827 J=1,N
A=CO(J)*SW/FB/COS(BT(J))+TAN(FI(J))*(WT(J)*COS(BT(J))-
@ RU*WT(J)/COS(BT(J)))/FB-WT(J)*SIN(BT(J))
B=COS(BT(J)-ST)*(1+TAN(FI(J))*TAN(BT(J)-ST)/FB)
Q=Q+A*COS(BT(J)-ST)/B
827 CONTINUE
C solving Sum(Q)=0
TES=Q*Q0
IF(TES.LT.0.0) GOTO 839
837 CONTINUE
839 FM=FB+0.005
C
C searching for minimum difference between Fs in force and Fs in moment
C
IF(FM.EQ.FF) GOTO 849
FT=ABS(FM-FF)
IF(FT.GT.FT0) GOTO 802
C
FT0=FT
FS=(FF+FM)/2.0
ST0=ST*180.0/3.14
802 CONTINUE
GOTO 850
849 FT0=FT
FS=FM
ST0=ST*180.0/3.14
850 RETURN
END
C
C
SUBROUTINE SPRRF(FS,ST0,FT0,FP)
C
C stability analysis of reinforced slopes
COMMON/GERN/NSL,NRFL,NSP,DC,N,RU,DST,DSTF
COMMON/GEOMT/X0,Y0,XC,YC,XT,YT,AFA,R,SW,YH(10),YS
COMMON/PROP/SP(20,8),H(20),XCO(20,20),F(20,20)
DIMENSION CO(50),FI(50),BT(50),WT(50),T(50),RF(20),XX(20)
C
C determine reinforcement force at the base of each slice
C
C calculate reinforcement force at intersection of the circle
R0=SQRT((X0-XT)**2+(Y0-YT)**2)
DO 700 I=1,NRFL
XX(I)=X0-SQRT(R0**2-(H(I)-Y0)**2)
C
C jump over the case that circle doesn't insect reinforcement
C
IF(XX(I).GT.XCO(I,1)) GOTO 715
IF(XX(I).LT.XCO(I,NSP)) GOTO 715
C

```

```

DO 710 J=1,NSP
IF(XCO(I,J).GT.XX(I)) GOTO 710
RF(I)=(XX(I)-XCO(I,J-1))*(F(I,J)-F(I,J-1))/(XCO(I,J)-XCO(I,J-1))
@ +F(I,J-1)
GOTO 700
710 CONTINUE
715 RF(I)=0.0
700 CONTINUE
C
C search for reinforcement force at base of each slice
C
CALL GEOMETRY(BT,WT)
N00=1
DO 720 I=1,N
X=XT-SW*I
T(I)+0.0
IF(N00.GT.NRFL)GOTO 720
DO 730 J=N00,NRFL
IF(X.GT.XX(J)) GOTO 730
T(I)=T(I)+RF(J)/FP
N00=N00+1
730 CONTINUE
720 CONTINUE
C determine strength parameters at base of each slice
C
FS=0.0
DO 740 I=1,N
X=XT-(I-0.5)*SW
Y=Y0-SQRT(R**2-(X-X0)**2)
DO 745 J=1,NSL
YH(J)=(X-SP(J,1))*(SP(J,4)-SP(J,2))/(SP(J,3)-SP(J,1))+SP(J,2)
IF(Y.GT.YH(J)) GOTO 745
CO(I)=SP(J,5)
FI(I)=SP(J,6)
GOTO 740
745 CONTINUE
740 CONTINUE
C
C try at different angle of internal force inclination
C
NN=INT(DSTF/DST)
FT0=10.0
DO 750 I=0,NN
ST=I*DST
C
C working for Fs in terms of force equilibrium
C searching Sum(Q)=0 at large steps
C
F0=4.0
Q=0.0
DO 753 II=0,18
FB=F0-II*0.2
Q=Q
Q=0.0

```

```

DO 756 J=1,N
A=CO(J)*SW/FB/COS(BT(J))+TAN(FI(J))*(WT(J)*COS(BT(J))-
@ RU*WT(J)/COS(BT(J)))/FB-WT(J)*SIN(BT(J))+T(J)*COS(BT(J))
B=COS(BT(J)-ST)*(1+TAN(FI(J))*TAN(BT(J)-ST)/FB)
Q=Q+A/B
756 CONTINUE
C solving Sum(Q)=0
TES=Q*Q0
IF(TES.LT.0.0) GOTO 760
753 CONTINUE
FS=4.0
GOTO 799

C
C searching Sum(Q)=0 at small steps
C
760 F0=FB+0.2
Q=0.0
DO 763 II=0,20
FB=F0-II*0.01
Q0=Q
Q=0.0
DO 766 J=1,N
A=CO(J)*SW/FB/COS(BT(J))+TAN(FI(J))*(WT(J)*COS(BT(J))-
@ RU*WT(J)/COS(BT(J)))/FB-WT(J)*SIN(BT(J))+T(J)*COS(BT(J))
B=COS(BT(J)-ST)*(1+TAN(FI(J))*TAN(BT(J)-ST)/FB)
Q=Q+A/B
766 CONTINUE
C solving Sum(Q)=0
TES=Q*Q0
IF(TES.LT.0.0) GOTO 769
763 CONTINUE
769 FF=FB+0.005

C
C working for Fs in terms of moment equilibrium
C
C searching Sum(Q)=0 at large steps
C
F0=4.0
Q=0.0
DO 770 II=0,18
FB=F0-II*0.2
Q0=Q
Q=0.0
DO 773 J=1,N
A=CO(J)*SW/FB/COS(BT(J))+TAN(FI(J))*(WT(J)*COS(BT(J))-
@ RU*WT(J)/COS(BT(J)))/FB-WT(J)*SIN(BT(J))+T(J)*COS(BT(J))
B=COS(BT(J)-ST)*(1+TAN(FI(J))*TAN(BT(J)-ST)/FB)
Q=Q+A*COS(BT(J)-ST)/B
773 CONTINUE
C solving Sum(Q)=0
TES=Q*Q0
IF(TES.LT.0.0) GOTO 780
770 CONTINUE
FS=4.0

```

```

      GOTO 799
C
C      searching Sum(Q)=0 at small steps
C
780  F0=FB+0.2
      Q=0.0
      DO 783 II=0,20
      FB=F0-II*0.01
      Q0=Q
      Q=0.0
      DO 786 J=1,N
      A=CO(J)*SW/FB/COS(BT(J))+TAN(FI(J))*(WT(J)*COS(BT(J))-
@  RU*WT(J)/COS(BT(J)))/FB-WT(J)*SIN(BT(J))+T(J)*COS(BT(J))
      B=COS(BT(J)-ST)*(1+TAN(FI(J))*TAN(BT(J)-ST)/FB)
      Q=Q+A*COS(BT(J)-ST)/B
786  CONTINUE
C      solving Sum(Q)=0
      TES=Q*Q0
      IF(TES.LT.0.0) GOTO 789
783  CONTINUE
789  FM=FB+0.005
C
C      searching for minimum difference between Fs in force and Fs in moment
C
      IF(FF.EQ.FM) GOTO 790
      FT=ABS(FM-FF)
      IF(FT.GT.FT0) GOTO 750
C
      FT0=FT
      FS=(FF+FM)/2.0
      ST0=ST*180.0/3.14
750  CONTINUE
      GOTO 799
790  FS=FM
      FT0=0.0
      ST0=ST*180.0/3.14
799  RETURN
      END

C
      SUBROUTINE GEOMETRY(BT,WT)
C
      COMMON/GERN/NSL,NRFL,NSP,DC,N,RU,DST,DSTF
      COMMON/GEOMT/X0,Y0,XC,YC,XT,YT,AFA,R,SW,YH(10),YS
      COMMON/PROP/SP(20,8),H(20),XCO(20,20),F(20,20)
      DIMENSION BT(50),WT(50)
C      calculate width of slices
C
      R=SQRT((X0-XT)**2+(Y0-YT)**2)
      X1=X0-SQRT(R**2-(YC-Y0)**2)
      DY=(XC-X1)*TAN(AFA)
      Y1=YC+DY
      XS=X0-SQRT(R**2-(Y1-Y0)**2)
      SW=(XT-XS)/N

```

```

C
C      calculate weight and base angle (BT(I)) of each slice
C
      DO 500 I=1,N
      X=XT-(I-0.5)*SW
      Y=Y0-SQRT(R**2-(X-X0)**2)
      BT(I)=ATAN((X0-X)/SQRT(R**2-(X-X0)**2))
      WT(I)=0.0
      AB=0.0
C
      DO 510 J=1,NSL
      YH(J)=(X-SP(J,1))*(SP(J,4)-SP(J,2))/(SP(J,3)-SP(J,1))+SP(J,2)
      IF(Y.GE.YH(J)) GOTO 510
      IF(XC.GE.X) GOTO 520
      YS=(X-XC)*(YT-YC)/(XT-XC)+YC
      IF(YH(J).GE.YS) GOTO 525
      W=SW*(YH(J)-Y-AB)*SP(J,7)
      AB=YH(J)-Y
      WT(I)=WT(I)+W
      GOTO 510
525   W=SW*(YS-Y-AB)*SP(J,7)
      WT(I)=WT(I)+W
      GOTO 500
520   YS=(XC-X)*TAN(AFA)+YC
      IF(YH(J).GE.YS) GOTO 540
      W=SW*(YH(J)-Y-AB)*SP(J,7)
      AB=YH(J)-Y
      WT(I)=WT(I)+W
      GOTO 510
540   W=SW*(YS-Y-AB)*SP(J,7)
      WT(I)=WT(I)+W
      GOTO 500
C
510   CONTINUE
C
500   CONTINUE
C
      RETURN
      END

```

Appendix D. Description and Source Code of RSSAWM

This appendix presents the source code of the computer program RSSAWM which analyzes stability of reinforced slopes using the two-part wedge method. This program was written in standard FORTRAN 77 and can be run with a Microsoft FORTRAN Compiler 3.2 or a FORTRAN compiler of higher version. This program can be easily changed to fit other types of computers.

A typical profile of a reinforced slope is shown in Figure 6.1. The geometry of the slope is characterized by the coordinates of the toe and the crest of the slope and the bilinear failure surface is characterized by the coordinates of the nodal point A and the inclination angle θ_1 along the base of wedge I (Fig. 6.4). A soil layer in the foundation or within the slope is defined by the coordinates of the upper boundary of the layer. The tensile forces in a reinforcement layer are controlled by the coordinates of sampling points along the layer and the magnitude of the force at the sampling points. It was assumed that the slip surface passed through the toe of the slope.

The following is an example of input data for the program RSSAWM (corresponding to the slope configuration in Figure 6.1 and 6.4):

Tensar Reinforced Section, H=12m at 1988

4,3,4,5,

5.3,3.3,9.0,14.0,21.0,2.0,0.0,0.19,0.29,

-30.0,2.0,30.0,2.0,23.0,0.419,20.0,

-30.0,5.0,18.0,5.0,27.0,0.488,20.2,

-30.0,8.0,15.0,8.0,13.0,0.524,20.2,

-30.0,14.0,9.0,14.0,10.0,0.349,20.0;

3.0,20.0,0.0,19.0,30.0,10.0,30.0,9.0,0.0,

5.0,18.0,0.0,17.0,30.0,6.0,30.0,5.0,0.0,

7.0,16.0,0.0,15.0,30.0,3.0,30.0,2.0,0.0,

```

C      Program RSSAWM for stability analysis of reinforced slopes by
C      two-part wedge method, written by Liu Yixin (Bill), July 1991.
C      Explanation:
C      NSL-- number of soil layers, in slope and foundation
C      NRFL-- number of reinforcement layers
C      NSST-- numbers of searching steps of the minimum Fs
C      NSP-- number of sampling points at each reinforcement layer
C      X0,Y0-- coordinate of the node in the first searching effort
C      XC,YC-- coordinate of crest
C      XT,YT-- coordinate of toe
C      DC-- designed final spacing of grid in searching
C      AFA-- slope angle of top surface
C      SP(I,J)-- coordinate(upper boundary of the soil layers) and
C      properties of soil layers (from bottom to top),i.e. (x1,y1,
C      x2,y2,C,Fi,Gama)
C      YH(I)-- boundary of horizontal layers (interpolation)
C      YS-- coordinate of slope and top surface
C      RU-- pore pressure coefficient
C      H(I)-- Y-coordinate of reinforcement layers
C      XCO(I,J)-- X-coordinate of sampling points at each reinforcement layer
C      F(I,J)-- reinforcement force at sampling points
C      RF(I)-- reinforcement force at intersection with slip surface
C      DTA-- inclination angle of interwedge force
C      CB-- cohesive force along the interwedge boundary
C      Q-- reduction factor of cohesive force along the interwedge boundary
C      varying between 0.0 and 1.0
C      UB-- pore pressure (force) in the interwedge boundary
C      W1,W2-- weight of two wedges
C      Rh1,Rh2,RV1,RV2-- horizontal and vertical component of
C      reinforcement forces in two wedges
C      TFI1,TFI2-- weighted average coefficients of internal friction
C      C1,C2-- total cohesive resistant along slip surface in two wedges
C      L1,L2-- length of slip surface in two wedges
C      CT1,CT2-- inclination of two parts of slip surface
C
C      CHARACTER FIN*14,FOUT*14,TITLE*72
C      COMMON/GERN/NSL,NRFL,NSP,NSST,DC,RU,ATA,FP,NCON,NSIGN
C      COMMON/GEOMT/X0,Y0,XC,YC,XT,YT,BT,CT2,W1,W2
C      COMMON/PROP/SP(20,8),H(20),XCO(20,20),F(20,20)
C      COMMON/AVPROP/GMA,C1,C2,TFI1,TFI2,CB,Q,UB,U1,U2
C      REAL L1,L2
C
C      WRITE(*,910)
910  FORMAT(5X,'Stability analysis of reinforced slopes')
C      WRITE(*,915)
915  FORMAT(5X,'by two-part wedge method, written by Liu Yixin(Bill)')
C      WRITE(*,935)
935  FORMAT(5X,'input the name of data file')
C      READ(*,940) FIN
940  FORMAT(A14)
C      WRITE(*,945)
945  FORMAT(5X,'input the name of output file ')

```



```

      READ(*,950) FOUT
950  FORMAT(A14)
      WRITE(*,952)
952  FORMAT(3X,'input the reduction factor of the cohesive force')
      WRITE(*,953)
953  FORMAT(3X,'along the interwedge boundary,i.e.  $CB=Q \cdot C$ ')
      READ(*,957) Q
957  FORMAT(F8.4)
      WRITE(*,960)
960  FORMAT(5X,'input the partial  $F_s$  for reinforcement force')
      READ(*,970) FP
970  FORMAT(F4.2)
C
      OPEN (6,FILE=FOUT,STATUS='NEW',ACCESS='SEQUENTIAL')
      OPEN (5,FILE=FIN,STATUS='OLD',ACCESS='SEQUENTIAL')
      WRITE(6,1000)
1000 FORMAT(5X,'stability analysis of reinforced slopes by')
      WRITE(6,1002)
1002 FORMAT(5X,' two-part wedge method, written by Liu Yixin(Bill)')
      WRITE(6,1003) Q
1003 FORMAT(5X,'reduction factor of interwedge cohesion',F8.4)
C
C   input and output data
C
      READ(5,1050) TITLE
1050 FORMAT(A72)
      WRITE(6,1050) TITLE
C
C   input controlling and geometric data
      READ(5,*)NSL,NRFL,NSP,NSST
      WRITE(6,1060) NSL,NRFL,NSP,NSST
1060 FORMAT(5X,'NSL,NRFL,NSP,NSST:',4(I5,3X))
C
      READ(5,*) X0,Y0,XC,YC,XT,YT,AFA,DC,RU
      WRITE(6,1070) XC,YC,XT,YT,RU,FP
1070 FORMAT(5X,'XC,YC,XT,YT:',4(F6.2,1X),'RU,FP:',2(F4.2,1X))
C
C   input soil property data and calculate average unit weight GMA
      GMA=0.0
      DO 1075 I=1,NSL
      READ(5,*) (SP(I,J),J=1,7)
      GMA=GMA+SP(I,7)
      WRITE(6,1080) (SP(I,J),J=1,7)
1080 FORMAT(5X,7(F8.3,2X))
1075 CONTINUE
      GMA=GMA/NSL
      WRITE(6,1077) GMA
1077 FORMAT(5X,'average unit weight:',F8.3)
C
      IF(NRFL.EQ.0) GOTO 800
C   input reinforcement force data
C
      DO 1090 I=1,NRFL
      READ(5,*) H(I),(XCO(I,J),F(I,J),J=1,NSP)

```

```

C      from the point closest to slope surface, where X at maximum
      WRITE(6,1085) H(I),(XCO(I,J),F(I,J),J=1,NSP)
1085  FORMAT(5X,30(F7.3,2X))
1090  CONTINUE
C
C      finish data input
C
800   WRITE(*,1100)
1100  FORMAT(5X,'make your choice, input control numbers')
      WRITE(*,1105)
1105  FORMAT(5X,'stop--0; unreinforced--1; reinforced--2')
      READ(*,1110) NCON
1110  FORMAT(I2)
C
      IF(NCON.EQ.0) GOTO 899
      IF(NCON.EQ.1) GOTO 810
      IF(NCON.EQ.2) GOTO 850
      WRITE(*,1115)
1115  FORMAT(5X,'invalid input, please make your choice again')
      GOTO 800
C
C      calculate Fs of unreinforced slopes, starting at the given node
C
810   WRITE(*,1140)
1140  FORMAT(5X,'input the inclining angle of interwedge force')
      READ(*,1145) ATA
1145  FORMAT(F8.3)
      ATA=ATA*3.14/180
      CT2=ATAN((Y0-YT)/(XT-X0))
      BT=ATAN((YC-YT)/(XT-XC))
      CALL WEDGE(FS,CT1,0.0,0.0,0.0,0.0)
      NNN=1
820   FS1=FS
      X00=X0
      Y00=Y0
      CT10=CT1
      CT20=CT2
      C10=C1
      C20=C2
      TFI10=TFI1
      TFI20=TFI2
      W10=W1
      W20=W2
      CB0=CB
      UB0=UB
      U10=U1
      U20=U2
C
      IF(NNN.EQ.2) GOTO 840
C      searching the node having minimum Fs, at big (five times) steps
      DO 830 I=1,NSST
        DO 835 J=0,7
          X0=X00+DC*5*I*SIN(J*3.1416/4)
          Y0=Y00+DC*5*I*COS(J*3.1416/4)

```

```

      IF(X0.LT.0.0) GOTO 835
      IF(X0.GE.XT) GOTO 835
      IF(X0.EQ.XC) X0=X0+0.3
C     control the node below the crest
      IF(Y0.GE.YC) GOTO 835
C     control the node above the toe
      IF(Y0.LE.YT) GOTO 835
C     control the node below slope surface
      YY=(XT-X0)*TAN(BT)+YT
      IF(Y0.GE.YY) GOTO 835
C
      CT2=ATAN((Y0-YT)/(XT-X0))
      CALL WEDGE(FS,CT1,0.0,0.0,0.0,0.0)
      IF((FS+0.003).LE.FS1) GOTO 820
835   CONTINUE
830   CONTINUE
C
c     searching the node having minimum Fs, at small steps
      NNN=2
840   DO 842 I=1,NSST
      DO 844 J=0,7
      X0=X00+DC*I*SIN(J*3.1416/4)
      Y0=Y00+DC*I*COS(J*3.1416/4)
      IF(X0.LT.0.0) GOTO 844
      IF(X0.GE.XT) GOTO 844
      IF(X0.EQ.XC) X0=X0+0.3
C     control the node below the crest
      IF(Y0.GE.YC) GOTO 844
C     control the node above the toe
      IF(Y0.LE.YT) GOTO 844
C     control the node below slope surface
      YY=(XT-X0)*TAN(BT)+YT
      IF(Y0.GE.YY) GOTO 844
C
      CT2=ATAN((Y0-YT)/(XT-X0))
      CALL WEDGE(FS,CT1,0.0,0.0,0.0,0.0)
      IF((FS+0.003).LE.FS1) GOTO 820
844   CONTINUE
842   CONTINUE
C
C     finishing searching
c
      X0=X00
      Y0=Y00
      CT1=CT10*180/3.14
      CT2=CT20*180/3.14
      ATA=ATA*180/3.14
C     print the result for unreinforced slope stability analysis
C
      WRITE(6,1120)
1120  FORMAT(5X,'Stability of unreinforced slope')
      WRITE(6,1125) X0,Y0,CT1,CT2
1125  FORMAT(5X,'X0,Y0:',2(F8.3,3X),'CTA1,CTA2:',2(F8.3,3X))
      WRITE(6,1130) FS1,ATA

```

```

1130 FORMAT(5X,'Fs=',F8.3,3X,'interwedge force inclication', F8.3)
      WRITE(6,1135) W10,W20,C10,C20,TFI10,TFI20
1135 FORMAT(5X,'W1,W2,C1,C2,TFI1,TFI2:',4(F9.2,2X),2(F7.4,2X))
      WRITE(6,1137) CB0,UB0,U10,U20
1137 FORMAT(5X,'BC,UB,U1,U2:',4(F9.2,2X))
C
      GOTO 800
C
C      calculate Fs of reinforced slopes
C
850  WRITE(*,1150)
1150  FORMAT(5X,'input the inclining angle of interwedge force')
      READ(*,1155) ATA
1155  FORMAT(F8.3)
      ATA=ATA*3.14/180
      WRITE(*,1185)
1185  FORMAT(5X,'choice of reinforcement force orientation')
      WRITE(*,1188)
1188  FORMAT(5X,'horizontal--0; same inclination as slip surface--1')
      READ(*,1190) NSIGN
1190  FORMAT(I2)
      CT2=ATAN((Y0-YT)/(XT-X0))
      BT=ATAN((YC-YT)/(XT-XC))
      CALL WEDGE(FS,CT1,RV1,RV2,RH1,RH2)
      NNN=1
855  FS1=FS
      X00=X0
      Y00=Y0
      CT10=CT1
      CT20=CT2
      C10=C1
      C20=C2
      TFI10=TFI1
      TFI20=TFI2
      W10=W1
      W20=W2
      RV10=RV1
      RV20=RV2
      RH10=RH1
      RH20=RH2
      CB0=CB
      UB0=UB
      U10=U1
      U20=U2
C
C      searching the node having minimum Fs, at big steps
      IF(NNN.EQ.2) GOTO 870
C
      DO 860 I=1,NSST
      DO 865 J=0,7
      X0=X00+DC*5*I*SIN(J*3.1416/4)
      Y0=Y00+DC*5*I*COS(J*3.1416/4)
      IF(X0.GE.XT) GOTO 865
      IF(X0.LT.0.0) GOTO 865

```

```

      IF(X0.EQ.XC) X0=X0+0.3
C      control the node below the crest
      IF(Y0.GE.YC) GOTO 865
C      control the node above the toe
      IF(Y0.LE.YT) GOTO 865
C      control the node below slope surface
      YY=(XT-X0)*TAN(BT)+YT
      IF(Y0.GE.YY) GOTO 865
C
      CT2=ATAN((Y0-YT)/(XT-X0))
      CALL WEDGE(FS,CT1,RV1,RV2,RH1,RH2)
      IF((FS+0.003).LE.FS1) GOTO 855
865  CONTINUE
860  CONTINUE
C
C      searching the node having minimum Fs, at small steps
      NNN=2
870  DO 872 I=1,NSST
      DO 874 J=0,7
      X0=X00+DC*I*SIN(J*3.1416/4)
      Y0=Y00+DC*I*COS(J*3.1416/4)
      IF(X0.GE.XT) GOTO 874
      IF(X0.LT.0.0) GOTO 874
      IF(X0.EQ.XC) X0=X0+0.3
C      control the node below the crest
      IF(Y0.GE.YC) GOTO 874
C      control the node above the toe
      IF(Y0.LE.YT) GOTO 874
C      control the node below slope surface
      YY=(XT-X0)*TAN(BT)+YT
      IF(Y0.GE.YY) GOTO 874
C
      CT2=ATAN((Y0-YT)/(XT-X0))
      CALL WEDGE(FS,CT1,RV1,RV2,RH1,RH2)
      IF((FS+0.003).LE.FS1) GOTO 855
874  CONTINUE
872  CONTINUE
c      finishing searching
      X0=X00
      Y0=Y00
      CT1=CT10*180/3.14
      CT2=CT20*180/3.14
      ATA=ATA*180/3.14
C
C      print the result for reinforced slope stability analysis
C
      WRITE(6,1160)
1160  FORMAT(5X,'Stability of Rreinforced slope')
      WRITE(6,1165) X0,Y0,CT1,CT2
1165  FORMAT(5X,'X0,Y0:',2(F8.3,3X),'CTA1,CTA2:',2(F8.3,3X))
      WRITE(6,1170) FS1,ATA
1170  FORMAT(5X,'Fs=',F8.3,3X,'interwedge force inclination',F8.3)
      WRITE(6,1175) W10,W20,C10,C20,TFI10,TFI20
1175  FORMAT(5X,'W1,W2,C1,C2,TFI1,TFI2:',4(F9.2,2X),2(F7.4,2X))

```

```

WRITE(6,1178) CB0,UB0,U10,U20
1178 FORMAT(5X,'CB,UB,U1,U2:',4(F9.3))
WRITE(6,1180) RV10,RV20,RH10,RH20
1180 FORMAT(5X,'RV1,RV2,RH1,RH2:',4(F12.3,2X))
C
GOTO 800
C
899 STOP
END
C
C
C
SUBROUTINE WEDGE(FS,CT1,RV1,RV2,RH1,RH2)
C
COMMON/GERN/NSL,NRFL,NSP,NSST,DC,RU,ATA,FP,NCON,NSIGN
COMMON/GEOMT/X0,Y0,XC,YC,XT,YT,BT,CT2,W1,W2
COMMON/PROP/SP(20,8),H(20),XCO(20,20),F(20,20)
COMMON/AVPROP/GMA,C1,C2,TFI1,TFI2,CB,Q,UB,U1,U2
REAL L1,L2
C
C      determin the most critical surface for a given node
C      searching in big steps
C
DD0=-100000.0
DO 600 I=2,25
CT1=3.14/2-I*3*3.14/180
IF(CT1.LT.CT2) GOTO 600
IF(CT1.EQ.BT) CT1=CT1-0.035
CALL GEOMETRY(L1,L2,CT1)
CALL PROPERTIES(L1,L2,CT1)
IF(NCON.EQ.1) GOTO 603
IF(NRFL.EQ.0) GOTO 603
CALL REINF(CT1,RV1,RV2,RH1,RH2)
603 FS=1.2
C
A1=(UB+RH1)*SIN(CT1)+(W1-RV1-CB*Q/FS)*COS(CT1)-U1
B1=COS(CT1-ATA)+SIN(CT1-ATA)*TFI1/FS
T1=((W1-RV1-CB*Q/FS)*SIN(CT1)-(UB+RH1)*COS(CT1)
@ -C1/FS-TFI1*A1/FS)/B1
IF(T1.LT.DD0) GOTO 600
DD0=T1
CT0=CT1
600 CONTINUE
C
C      searching in small steps
C
DD0=-100000.0
DO 610 I=0,6
CT1=CT0-(I-3)*3.14/180
IF(CT1.LT.CT2) GOTO 610
IF(CT1.EQ.BT) CT1=CT1-0.035
CALL GEOMETRY(L1,L2,CT1)
CALL PROPERTIES(L1,L2,CT1)
IF(NCON.EQ.1) GOTO 613

```

```

        IF(NRFL.EQ.0) GOTO 613
        CALL REINF(CT1,RV1,RV2,RH1,RH2)
613    FS=1.2
C
        A1=(UB+RH1)*SIN(CT1)+(W1-RV1-CB*Q/FS)*COS(CT1)-U1
        B1=COS(CT1-ATA)+SIN(CT1-ATA)*TFI1/FS
        T1=((W1-RV1-CB*Q/FS)*SIN(CT1)-(UB+RH1)*COS(CT1)
@      -C1/FS-TFI1*A1/FS)/B1
        IF(T1.LT.DD0) GOTO 610
        DD0=T1
        CT10=CT1
610    CONTINUE
C
C      iterate to obtain the actual Fs about the most critical slip surface
C
        CT1=CT10
        CALL GEOMETRY(L1,L2,CT1)
        CALL PROPERTIES(L1,L2,CT1)
        IF(NCON.EQ.1) GOTO 623
        IF(NRFL.EQ.0) GOTO 623
        CALL REINF(CT1,RV1,RV2,RH1,RH2)
C      searching in big steps for the unique minimum Fs
623    DD1=0
        DO 620 I=1,20
        FS=3.5-I*0.15
        A1=(UB+RH1)*SIN(CT1)+(W1-RV1-CB*Q/FS)*COS(CT1)-U1
        A2=(-UB+RH2)*SIN(CT2)+(W2-RV2+CB*Q/FS)*COS(CT2)-U2
        B1=COS(CT1-ATA)+SIN(CT1-ATA)*TFI1/FS
        B2=COS(CT2-ATA)+SIN(CT2-ATA)*TFI2/FS
        T1=((W1-RV1-CB*Q/FS)*SIN(CT1)-(UB+RH1)*COS(CT1)
@      -C1/FS-TFI1*A1/FS)/B1
        T2=((W2-RV2+CB*Q/FS)*SIN(CT2)-(-UB+RH2)*COS(CT2)
@      -C2/FS-TFI2*A2/FS)/B2
        DD1=T1+T2
        IF(DD1.GT.0.0) GOTO 620
        FS0=FS+0.15
        GOTO 622
620    CONTINUE
C      searching in small steps for the unique minimum Fs
622    DD1=0
        DO 640 I=1,25
        FS=FS0-I*0.006
        A1=(UB+RH1)*SIN(CT1)+(W1-RV1-CB*Q/FS)*COS(CT1)-U1
        A2=(-UB+RH2)*SIN(CT2)+(W2-RV2+CB*Q/FS)*COS(CT2)-U2
        B1=COS(CT1-ATA)+SIN(CT1-ATA)*TFI1/FS
        B2=COS(CT2-ATA)+SIN(CT2-ATA)*TFI2/FS
        T1=((W1-RV1-CB*Q/FS)*SIN(CT1)-(UB+RH1)*COS(CT1)
@      -C1/FS-TFI1*A1/FS)/B1
        T2=((W2-RV2+CB*Q/FS)*SIN(CT2)-(-UB+RH2)*COS(CT2)
@      -C2/FS-TFI2*A2/FS)/B2
        DD1=T1+T2
        IF(DD1.LT.0.0) GOTO 670
640    CONTINUE
C

```

```

C
670  FS=FS+0.003
      RETURN
      END

C
C
      SUBROUTINE GEOMETRY(L1,L2,CT1)
C
      COMMON/GERN/NSL,NRFL,NSP,NSST,DC,RU,ATA,FP,NCON,NSIGN
      COMMON/GEOMT/X0,Y0,XC,YC,XT,YT,BT,CT2,W1,W2
      COMMON/PROP/SP(20,8),H(20),XCO(20,20),F(20,20)
      COMMON/AVPROP/GMA,C1,C2,TFI1,TFI2,CB,Q,UB,U1,U2
      REAL L1,L2

C
      L2=SQRT((X0-XT)**2+(Y0-YT)**2)
      IF(XC.GT.X0) GOTO 500
      CT0=ATAN((YC-Y0)/(X0-XC))

C
      YB=TAN(BT)*(XT-X0)+YT
C
      weight of wedge 2
      SS1=YB-Y0
      SS2=SQRT((X0-XT)**2+(YB-YT)**2)
      PP=(SS1+SS2+L2)/2
      W2=GMA*SQRT(PP*(PP-SS1)*(PP-SS2)*(PP-L2))

C
      pore pressure U2
      XM2=(X0+XT)/2
      HM2=(XT-XM2)*(TAN(BT)-TAN(CT2))
      U2=HM2*GMA*RU*L2

C
C
      weight of wedge 1
      IF(CT1.GT.CT0) GOTO 510
      L1=(YC-Y0)/SIN(CT1)
      YN=TAN(CT1)*(X0-XC)+Y0
      XN=X0-(YC-Y0)/TAN(CT1)
      W1=GMA/2.0*((X0-XC)*(YB-Y0+YC-YN)+(XC-XN)*(YC-YN))

C
      pore pressure U1
      XM1=(XN+X0)/2
      HM1=(XT-XM1)*TAN(BT)+YT-(X0-XM1)*TAN(CT1)-Y0
      IF(XM1.LE.XC) HM1=YC-(X0-XM1)*TAN(CT1)-Y0
      U1=HM1*GMA*RU*L1
      GOTO 530

C
510  XM=(X0*TAN(CT1)-XT*TAN(BT)+Y0-YT)/(TAN(CT1)-TAN(BT))
      YM=TAN(CT1)*(X0-XM)+Y0
      L1=SQRT((XM-X0)**2+(YM-Y0)**2)
      SS2=SQRT((XM-X0)**2+(YM-YB)**2)
      PP=(SS1+SS2+L1)/2
      W1=GMA*SQRT(PP*(PP-SS1)*(PP-SS2)*(PP-L1))

C
      pore pressure U1
      XM1=(XM+X0)/2
      HM1=(XT-XM1)*TAN(BT)+YT-(X0-XM1)*TAN(CT1)-Y0
      U1=HM1*GMA*RU*L1
      GOTO 530

C

```



```

500  YM=TAN(CT2)*(XT-XC)+YT
      L1=(YC-Y0)/SIN(CT1)
      SS1=YC-YM
      SS2=SQRT((XC-XT)**2+(YC-YT)**2)
      SS3=SQRT((XC-XT)**2+(YM-YT)**2)
      PP=(SS1+SS2+SS3)/2
      W2=GMA*(SQRT(PP*(PP-SS1)*(PP-SS2)*(PP-SS3))+(XC-X0)*(SS1+YC-
@   Y0)/2)
      W1=GMA*(YC-Y0)**2/TAN(CT1)/2
C   pore pressure U1 and U2
      XM2=(X0+XT)/2
      HM2=(XT-XM2)*(TAN(BT)-TAN(CT2))
      IF(XM2.LE.XC) HM2=YC-(XT-XM2)*TAN(CT2)-YT
      HM1=(YC-Y0)/2
      U1=HM1*GMA*RU*L1
      U2=HM2*GMA*RU*L2
C
530  RETURN
      END
C
C
      SUBROUTINE PROPERTIES(L1,L2,CT1)
C
      COMMON/GERN/NSL,NRFL,NSP,NSST,DC,RU,ATA,FP,NCON,NSIGN
      COMMON/GEOMT/X0,Y0,XC,YC,XT,YT,BT,CT2,W1,W2
      COMMON/PROP/SP(20,8),H(20),XCO(20,20),F(20,20)
      COMMON/AVPROP/GMA,C1,C2,TFI1,TFI2,CB,Q,UB,U1,U2
      REAL L1,L2,LJ
C
C   calculate pore water pressure along interwedge boundary
C
      YB=TAN(BT)*(XT-X0)+YT
      IF(X0.LE.XC) YB=YC
      UB=(YB-Y0)**2*GMA*RU/2
C
C   calculate average friction coefficient and cohesion
C   along slip surface 1, 2 and interwedge boundary
C
      AA=0.0
      BB=XT
      C1=0.0
      C2=0.0
      TFI1=0.0
      TFI2=0.0
      CB=0.0
      EE=Y0
      DD=0.0
C
      DO 400 I=1,NSL
      IF(SP(I,2).LE.YT) GOTO 400
      IF(SP(I-1,2).GT.Y0) GOTO 410
C   average properties of the second wedge
C   XX--x coordinate of intersection between slip surface and soil
c   upper boundary

```

```

C      XA--x coordinate of middle of vertical slice cut by slip surface
c      and soil upper & lower boundaries
C
      XX=XT-(SP(I,2)-YT)/TAN(CT2)
      IF(XX.LE.X0) GOTO 420
      LL=SQRT((XX-XT)**2+(SP(I,2)-YT)**2)
      C2=C2+SP(I,5)*(LL-AA)
      XA=(XX+BB)/2
      HA=(XT-XA)*(TAN(BT)-TAN(CT2))
      IF(XA.LT.XC) HA=YC-(XT-XA)*TAN(CT2)-YT
      TFI2=TFI2+HA*TAN(SP(I,6))
      AA=LL
      BB=XX
      DD=DD+HA
      GOTO 400

C
420   C2=SP(I,5)*(L2-AA)+C2
      XA=(X0+BB)/2
      HA=(XT-XA)*(TAN(BT)-TAN(CT2))
      IF(XA.LT.XC) HA=YC-(XT-XA)*TAN(CT2)-YT
      TFI2=(TFI2+HA*TAN(SP(I,6)))/(DD+HA)

C
C      average properties of the first wedge
C
      AA=0.0
      BB=X0
      DD=0.0
410   IF(XC.GT.X0) GOTO 413
      CT0=ATAN((YC-Y0)/(X0-XC))
      IF(CT1.LT.CT0) GOTO 413
      XN=(X0*TAN(CT1)-XT*TAN(BT)+Y0-YT)/(TAN(CT1)-TAN(BT))
      YN=TAN(CT1)*(X0-XN)+Y0
      IF(SP(I-1,2).GT.YN) GOTO 400
      IF(SP(I,2).LT.YN) GOTO 413
      XX=XN
      GOTO 416
413   XX=X0-(SP(I,2)-Y0)/TAN(CT1)
416   LL=SQRT((XX-X0)**2+(SP(I,2)-Y0)**2)
      C1=C1+SP(I,5)*(LL-AA)
      XA=(XX+BB)/2
      HA=(XT-XA)*TAN(BT)+YT-(X0-XA)*TAN(CT1)-Y0
      IF(XA.LT.XC) HA=YC-(X0-XA)*TAN(CT1)-Y0
      TFI1=TFI1+HA*TAN(SP(I,6))
      AA=LL
      BB=XX
      DD=DD+HA

C      calculate total cohesion along the interwedge boundary
C
      CB=CB+SP(I,5)*(SP(I,2)-EE)
      EE=SP(I,2)

C
400   CONTINUE
C
      TFI1=TFI1/DD

```

```

C      RETURN
C      END
C
C      SUBROUTINE REINF(CT1,RV1,RV2,RH1,RH2)
C
C      COMMON/GERN/NSL,NRFL,NSP,NSST,DC,RU,ATA,FP,NCON,NSIGN
C      COMMON/GEOMT/X0,Y0,XC,YC,XT,YT,BT,CT2,W1,W2
C      COMMON/PROP/SP(20,8),H(20),XCO(20,20),F(20,20)
C      COMMON/AVPROP/GMA,C1,C2,TFI1,TFI2,CB,Q,UB,U1,U2
C
C      RF1=0.0
C      RF2=0.0
C      DO 700 I=1,NRFL
C      IF(H(I).GT.Y0) GOTO 710
C      total reinforcement force in the second wedge
C      XX-- x coordinate of intersection between slip surface and
C      reinforcement
C      XX=XT-(H(I)-YT)/TAN(CT2)
C      jump over the case that slip surface doesn't intersect reinforcement
C
C      IF(XX.GT.XCO(I,1)) GOTO 705
C      IF(XX.LT.XCO(I,NSP)) GOTO 705
C
C      DO 720 J=1,NSP
C      IF(XCO(I,J).GT.XX) GOTO 720
C      RF=(XX-XCO(I,J-1))*(F(I,J)-F(I,J-1))/(XCO(I,J)-XCO(I,J-1))
C      @ +F(I,J-1)
C      GOTO 730
720  CONTINUE
705  RF=0.0
730  RF2=RF2+RF
C      GOTO 700
C      total reinforcement force in the first wedge
710  XX=X0-(H(I)-Y0)/TAN(CT1)
C      jump over the case that slip surface doesn't intersect reinforcement
C
C      IF(XX.GT.XCO(I,1)) GOTO 735
C      IF(XX.LT.XCO(I,NSP)) GOTO 735
C
C      DO 740 J=1,NSP
C      IF(XCO(I,J).GT.XX) GOTO 740
C      RF=(XX-XCO(I,J-1))*(F(I,J)-F(I,J-1))/(XCO(I,J)-XCO(I,J-1))
C      @ +F(I,J-1)
C      GOTO 750
740  CONTINUE
735  RF=0.0
750  RF1=RF1+RF
C
C      700  CONTINUE
C
C      IF(NSIGN.EQ.1) GOTO 760
C      IF(NSIGN.EQ.0) GOTO 755

```

```

      WRITE(*,780)
780  FORMAT(5X,'invalid reinforcement force orientation')
      RV1=0.0
      RV2=0.0
      RH1=0.0
      RH2=0.0
      GOTO 790
C     horizontal reinforcement forces
C
755  RV1=0.0
      RV2=0.0
      RH1=RF1/FP
      RH2=RF2/FP
      GOTO 790
C     assuming reinforcement force inclined at same angles as slip surfaces
C
760  RV1=RF1*SIN(CT1)/FP
      RV2=RF2*SIN(CT2)/FP
      RH1=RF1*COS(CT1)/FP
      RH2=RF2*COS(CT2)/FP
C
790  RETURN
      END

```